NASA Technical Memorandum 100527

High Reynolds Number Transonic Tests of an NACA 0012 Airfoil in the Langley 0.3-Meter Transonic Cryogenic Tunnel

Charles L. Ladson and Acquilla S. Hill

DECEMBER 1987

National Aeronautics and Space Administration

Langley Research Center
Hampton, Virginia 23665

SUMMARY

Tests were conducted in the two dimensional test section of the Langley 0.3 meter Transonic Cryogenic Tunnel on an NACA 0012 airfoil to obtain aerodynamic data as a part of the Advanced Technology Airfoil Test (ATAT) program. The test program covered a Mach number range of 0.30 to 0.82 and a Reynolds number range of 3.0×10^6 to 45.0×10^6. The stagnation pressure was varied between 1.2 and 6.0 atmospheres and the stagnation temperature was varied between 300 K and 90 K to obtain these test conditions.

Plots of the spanwise variation of drag coefficient as a function of normal force coefficient and the variation of the basic aerodynamic characteristics with angle of attack are shown. The data are presented uncorrected for wall interference effects and without analysis. This data adds to the existing data base to be used for tunnel comparison purposes as well as assessment of wall interference and correction procedures.

INTRODUCTION

A comprehensive test program has been undertaken in the Langley Research Center 0.3 meter transonic cryogenic tunnel (0.3-m TCT) to obtain the static aerodynamic characteristics of a series of two dimensional airfoils at transonic speeds and flight equivalent Reynolds numbers. This program, known as the Advanced Technology Airfoil Test program (ATAT), was sponsored by the Langley Aircraft Energy Efficiency Project Office and the Transonic Aerodynamics Division. A description and status report on this program was first presented in reference 1.

The primary objectives of this program, as stated in this reference, were to provide the U. S. transport industry the opportunity to test and compare their most advanced airfoils to the latest

NASA design at high Reynolds numbers in the same facility and to provide experience in the design and construction of models for testing in a cryogenic environment as well as testing techniques unique to this environment. Included in this test program were four series of tests: (1) Correlation airfoils, (2) Advanced NASA supercritical airfoil, (3) Industry airfoils, and (4) Foreign technology airfoils.

This report presents results obtained from tests of the NACA 0012 airfoil which was tested as a part of the Correlation series of airfoils. Tests were conducted at Mach numbers from 0.30 to about 0.82 at chord Reynolds numbers from 3×10^6 to 45×10^6. To obtain these conditions, the stagnation pressure varied from 1.2 to 6.0 atmospheres and the stagnation temperature from 300 K to about 90 K. Model surface pressures, wake survey pressures, and tunnel wall pressures were obtained during the test program.

Plots and tabulated values of model surface pressure distributions as well as tabulated values of the integrated force and moment coefficients obtained in this test program are presented in reference 2. This paper contains plots of the spanwise variation of drag coefficient as a function of normal force coefficient and the variation of basic aerodynamic coefficients with angle of attack. Normal force and pitching moment coefficients were obtained from integration of the surface pressure distributions and the drag coefficient was obtained from integration of the wake survey data. The data are uncorrected for wall effects and are presented without analysis. In this format, the data should be useful for tunnel comparison purposes as well as extending the existing data base for use in evaluating wall interference and correction procedures.

SYMBOLS

All measurements and calculations were made in U.S. Customary Units; however, the

measurements are presented with the International System of Units (SI) in parentheses.

a	angle of attack,deg
b	airfoil model span, 8.00 in (20.32 cm)
c	airfoil model chord, 6.00 in (15.24 cm)
c_d	section drag coefficient ($c_{d,corr2}$ if valid data exist, otherwise, $c_{d,corr1}$)
$c_{d,corr1}$	section drag force coefficient from integration of wake total head profile for probe located at y/(b/2) = 0.125
$c_{d,corr2}$	section drag force coefficient from integration of wake total head profile for probe located at y/(b/2) = 0.0
$c_{d,corr3}$	section drag force coefficient from integration of wake total head profile for probe located at y/(b/2) = -0.125
$c_{d,corr4}$	section drag force coefficient from integration of wake total head profile for probe located at y/(b/2) = -0.375
$c_{d,corr5}$	section drag force coefficient from integration of wake total head profile for probe located at y/(b/2) = -0.500
c_m	section pitching moment coefficient about model 25-percent chord point from integration of model surface pressure coefficients
c_n	section normal force coefficient from integration of model surface pressure coefficients
M	average free stream Mach number
p_t	free stream stagnation pressure
R	Reynolds number based on model chord
T_t	free stream stagnation temperature, K
y	spanwise distance from tunnel centerline, (positive toward right hand side)

APPARATUS

The test program was conducted in the 8 in by 24 in (20.32 cm by 60.96 cm) two dimensional test section of the Langley 0.3-meter transonic cryogenic tunnel. This facility is a continuous flow,

fan driven, pressure tunnel which uses nitrogen gas as the test medium. The test section is rectangular in cross section, has solid sidewalls, and slotted top and bottom walls. Two slots are located in each of these walls with a spacing of 4.0 in (10.16 cm) and a total open area ratio of 0.05. Further details of this tunnel and test section are contained in reference 3.

Data were recorded on a shared, remote central data acquisition system. This system is referred to as the original data acquisition system for the two dimensional test section of the 0.3-m TCT in reference 3 and further details of the capability of the system are given in this reference.

MODEL

The model tested was a two dimensional model of the NACA 0012 airfoil with a chord of 6.00 in (15.24 cm) and a span of 8.00 in (20.32 cm). The equation for the ordinates of this airfoil shape was first presented in reference 4 and the ordinates for this model were obtained from the computer program of reference 5.

The model was constructed of A286 stainless steel which is an acceptable material for cryogenic test conditions. To locate all pressure instrumentation tubes internally in the model, it was constructed in two halves, the tubing installed, and then these two halves were bonded together. By locating the tubes internally, the model surface can be maintained in a very smooth condition which is required for high Reynolds number testing. One longitudinal row of pressure orifices was located on each surface of the model near the mid-span location and three spanwise rows were located on the upper surface. The ordinates for each orifice location are presented in the tabulated data. An orifice diameter of 0.010 in (0.25 mm) was used for all locations.

Upon completion of model construction and after several cryogenic temperature cycles, the model

ordinates were measured and compared to the design values. The maximum deviation from design was found to be 0.003 in (0.076 mm) with most of the model surface being within the manufacturing tolerance of 0.001 in (0.025 mm).

TESTS

The tests of this airfoil covered a Mach number range from 0.30 to 0.82 and a Reynolds number range of 3.0×10^6 to 45.0×10^6. To obtain these test conditions, the tunnel stagnation pressure varied between 1.2 atm and 6.0 atm and the stagnation temperature varied between 300 K and 90 K. Measurements of model surface pressure, wake total head surveys, sidewall pressures at the wake survey station, tunnel floor and ceiling pressures, and various tunnel parameters were made during the tests.

For these tests, the wake surveys were made at a station 1.2 model chords downstream of the model trailing edge. Data were obtained with both free and fixed locations of boundary layer transition. For the fixed transition tests, data were obtained only at Reynolds numbers of 3.0×10^6 and 9.0×10^6. The angle of attack range for all tests was from zero degrees to that for drag divergence. Limited data were also obtained at negative angles of attack as a check for asymmetry which could result from flow angularity, model inaccuracies, or incorrect angle of attack setting.

For the fixed transition data, transition strips were located on both the upper and lower surfaces of the model at the 5-percent chord station. These strips were about 1-percent chord in length and consisted of #240 carborundum grit applied with an acrylic spray.

TEST PROCEDURES

Model Pressures

All model surface and tunnel floor and ceiling pressures were measured using 48-port scanni-valves connected to high precision variable capacitance type pressure transducers. Three samples of data, taken at 0.25 second intervals, were recorded for each port. These readings were averaged during the data reduction process. To provide for lag in the response time of the pressure tubing and transducer, a delay time was invoked after each port change before the data were recorded. This delay time varied from 2.0 seconds near the model leading edge where large changes in pressure occurred between ports to 0.5 seconds for the aft portion of the model.

Wake Pressures

Surveys of the total pressure in the model wake were made using a traversing rake cantilevered from one of the tunnel sidewalls. This rake contained five individual probes such that a spanwise survey could also be obtained. The drive mechanism consisted of an electric stepper motor which was synchronized with the scannivalve system so that the rake would advance one step in distance with each scannivalve step. For these tests, approximately 75 steps were made as the rake traversed the model wake region. Tunnel sidewall static pressure data was obtained at the same tunnel station as the rake probes for use in data reduction. Individual pressure transducers were connected to each of the probes as well as the sidewall pressure taps to keep response time to a minimum. For this test program, the survey probes were located approximately 1.1 model chords downstream of the model trailing edge.

Corrections

All data and tunnel parameters were corrected for real gas effects by the method of reference 6. No corrections have been made for wall interference effects on the data presented herein; however, these corrections have been made for some of this data and the results presented in reference 7. These corrections reduce the test angle of attack for all conditions and the free stream Mach number, mainly at supercritical conditions.

PRESENTATION OF RESULTS

The results of this investigation are presented in this paper as plots of integrated force and moment coefficients obtained from surface pressure distribution data and wake surveys. These data are presented for reference purposes only and no analysis of the results is presented. An index to the various figures for both free and fixed transition data follows.

I. Effects of normal force coefficient on the spanwise variation of drag coefficient for various Mach and Reynolds numbers. Transition free.

Mach number	Figure
0.30	1
0.40	2
0.50	3
0.60	4
0.65	5
0.70	6
0.74	7
0.76	8
0.78	9
0.80	10
0.82	11

II. Effects of normal force coefficient on the spanwise variation of drag coefficient for various Mach and Reynolds numbers. Transition fixed.

0.30	12
0.50	13
0.70	14
0.74	15
0.76	16
0.78	17
0.80	18

III. Variation of basic aerodynamic characteristics with angle of attack for various Mach and Reynolds numbers. Transition free.

0.30	19
0.40	20
0.50	21
0.60	22
0.65	23
0.70	24
0.74	25
0.76	26
0.78	27
0.80	28
0.82	29

IV. Effects of fixing transition on the variation of basic aerodynamic characteristics with angle of attack for various Mach and Reynolds numbers.

0.30	30
0.50	31
0.70	32
0.74	33
0.76	34
0.78	35
0.80	36

V. Comparison of the effects of Reynolds number on the basic aerodynamic characteristics for various Mach numbers. Transition free.

0.30	37
0.40	38
0.50	39
0.60	40
0.65	41
0.70	42
0.74	43
0.76	44
0.78	45
0.80	46
0.82	47

VI. Comparison of the effects of Reynolds number on the basic aerodynamic characteristics for various Mach numbers. Transition fixed.

0.30	48
0.50	49
0.70	50

REFERENCES

1. **Ladson, Charles L. and Ray, Edward J.:** Status of Advanced Airfoil Tests in the Langley 0.3-Meter Transonic Cryogenic Tunnel. NASA CP-2208, 1981.

2. **Ladson, Charles L.; Hill, Acquilla S.; and Johnson, William G., Jr.:** Pressure Distributions From High Reynolds Number Tests of an NACA 0012 Airfoil in the Langley 0.3-Meter Transonic Cryogenic Tunnel. NASA TM-100526, 1987.

3. **Ladson, Charles L. and Ray, Edward E.:** Evolution, Calibration, and Operational Characteristics of the Two-Dimensional Test Section of the Langley 0.3 Meter Transonic Cryogenic Tunnel. NASA TP-2749, 1987.

4. **Jacobs, Eastman N.; Ward, Kenneth E.; and Pinkerton, Robert M.:** The Characteristics of 78 Related Airfoil Sections From Tests in the Variable-Density Wind Tunnel. NACA Rep. 460, 1933.

5. **Ladson, Charles L.; and Brooks, Cuyler W., Jr.:** Development of A Computer Program To Obtain Ordinates for NACA 4-Digit, 4-Digit Modified, 5-Digit, and 16-Series Airfoils. NASA TM X-3284, 1975.

6. **Adcock, Jerry B.:** Real-Gas Effects Associated With One-Dimensional Transonic Flow of Cryogenic Nitrogen. NASA TN D-8274, 1976.

7. **Gumbert, Clyde R., and Newman, Perry A.:** Validation of A Wall Interference Assessment/Correction Procedure for Airfoil Tests in the Langley 0.3-m Transonic Cryogenic Tunnel. AIAA-84-2151, 1984.

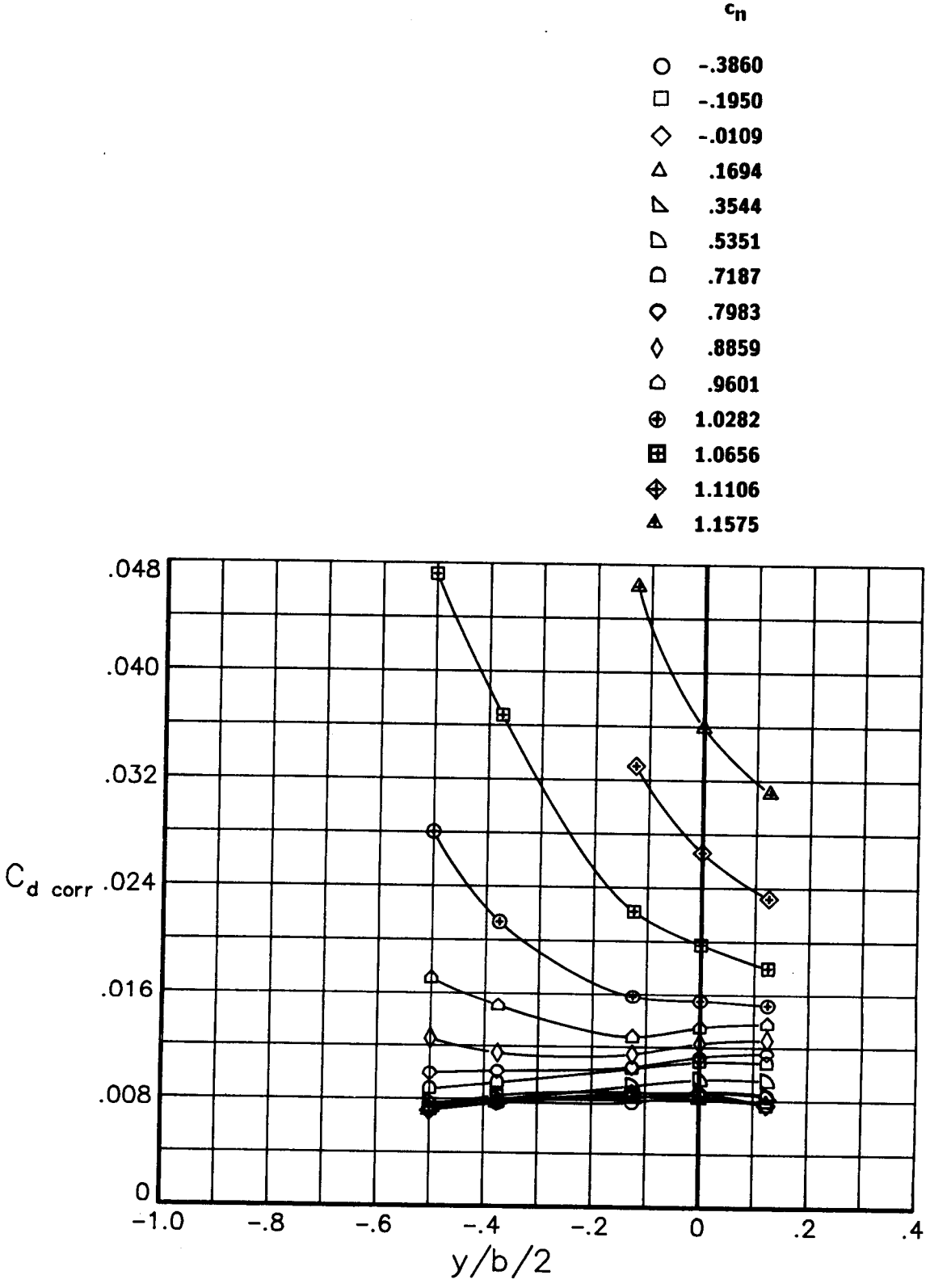

(a) $R = 3.0 \times 10^6$

Figure 1.- Effects of normal force coefficient on the spanwise variation of drag coefficient for various Reynolds numbers at a Mach number of 0.30. Transition free.

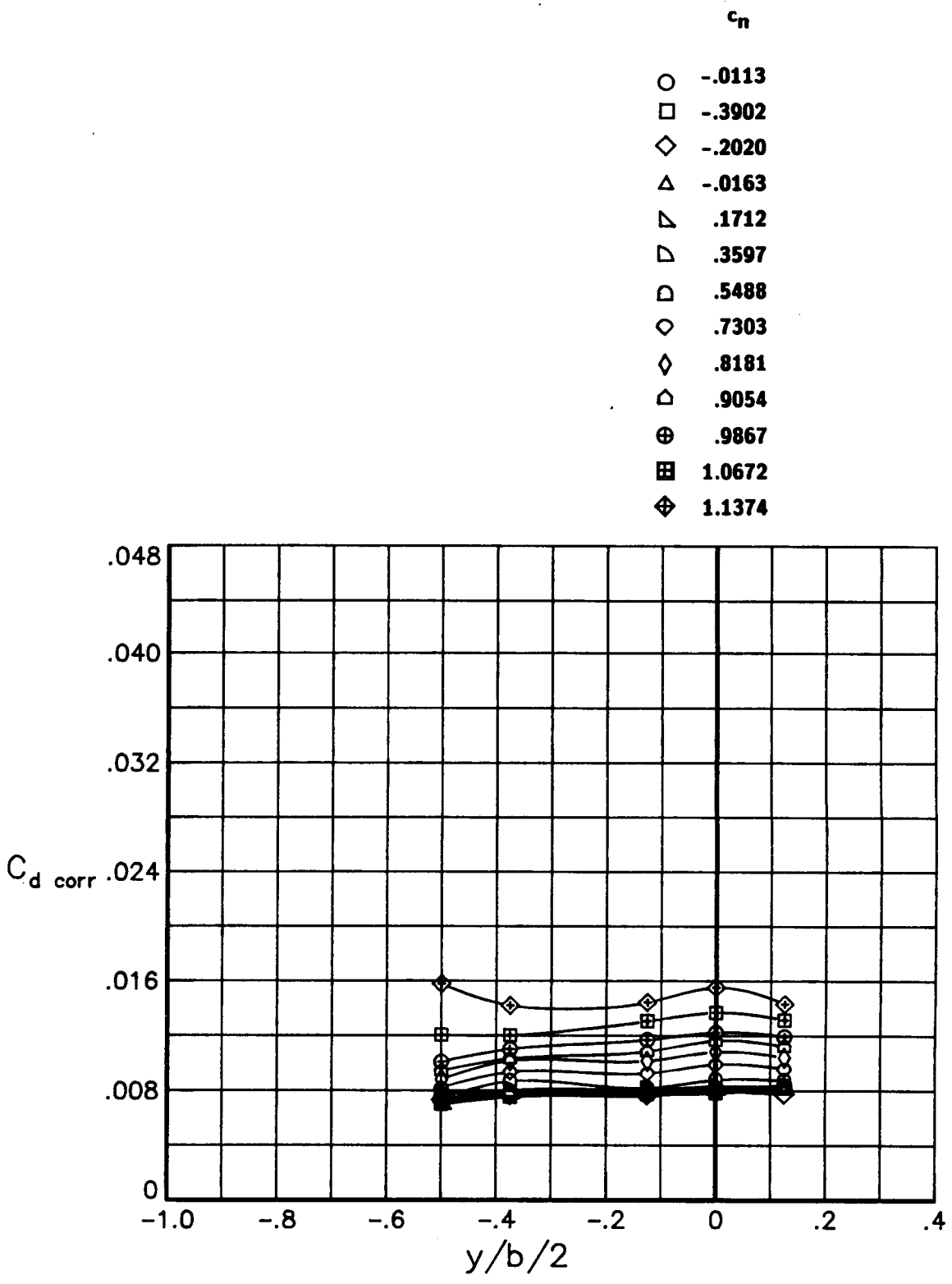

(b) R = 6.0 x 10^6

Figure 1.- Continued.

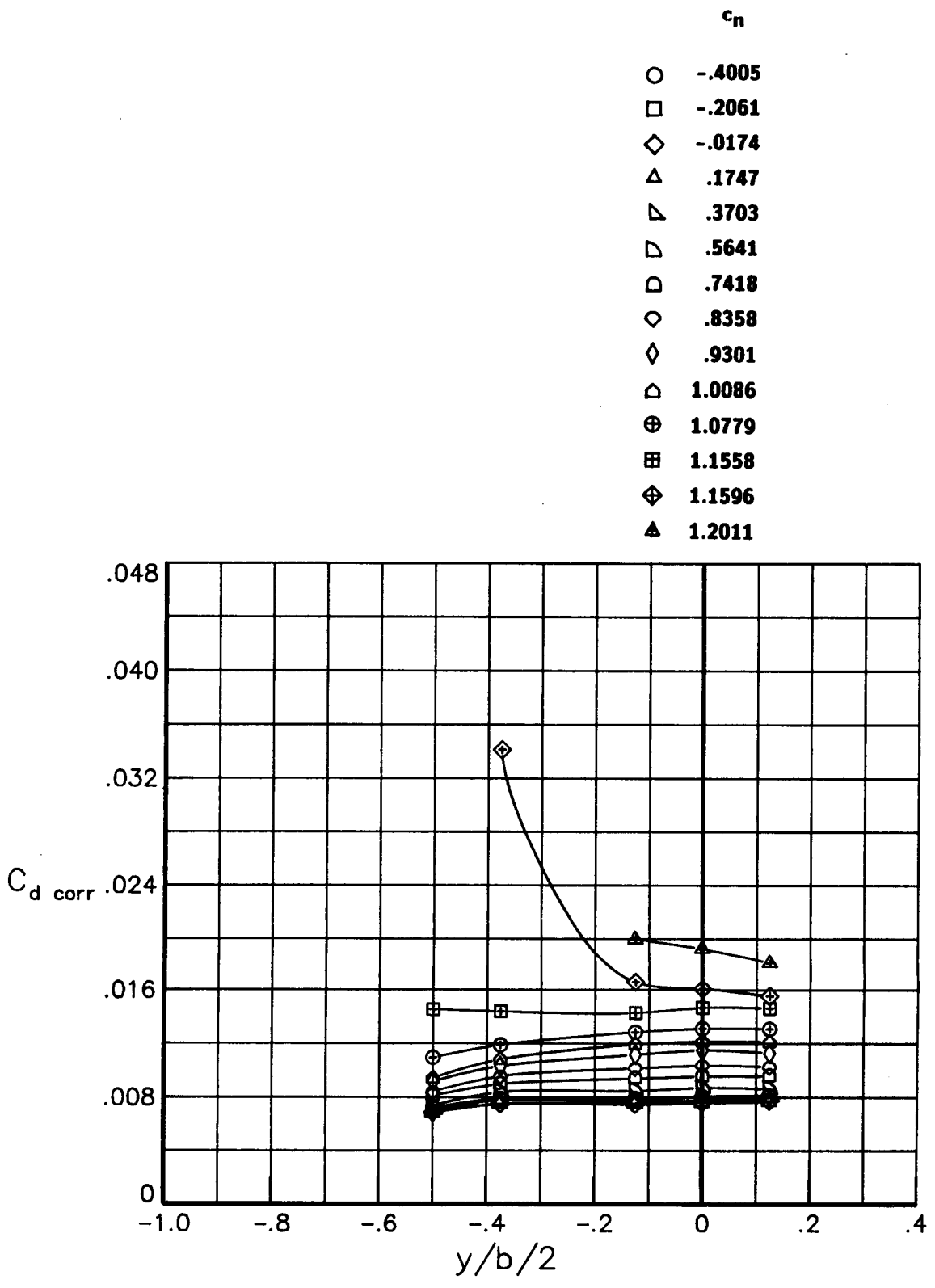

(c) R = 9.0 x 10^6

Figure 1.- Continued.

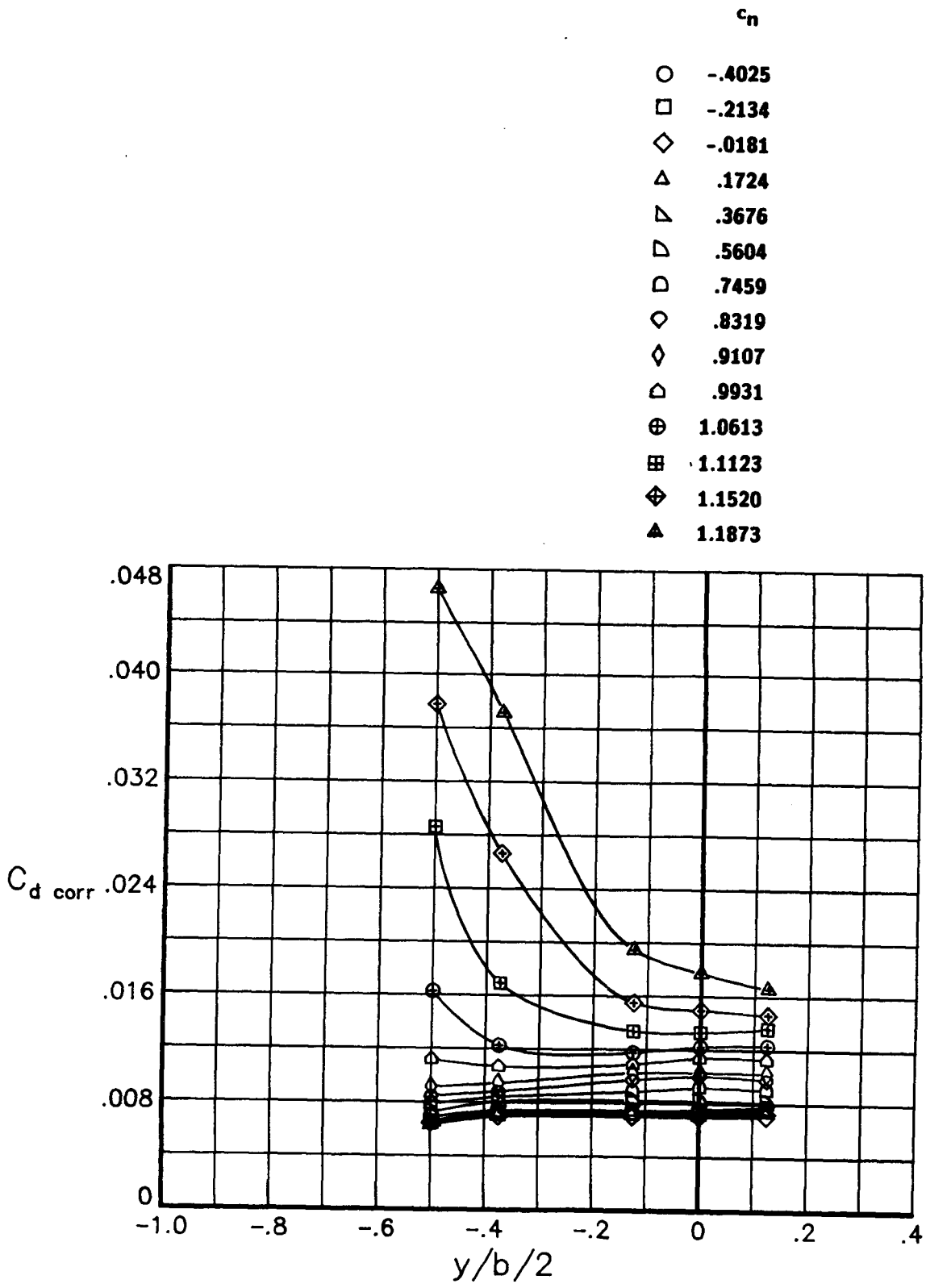

(d) R = 15.0 x 10^6

Figure 1.- Concluded.

23

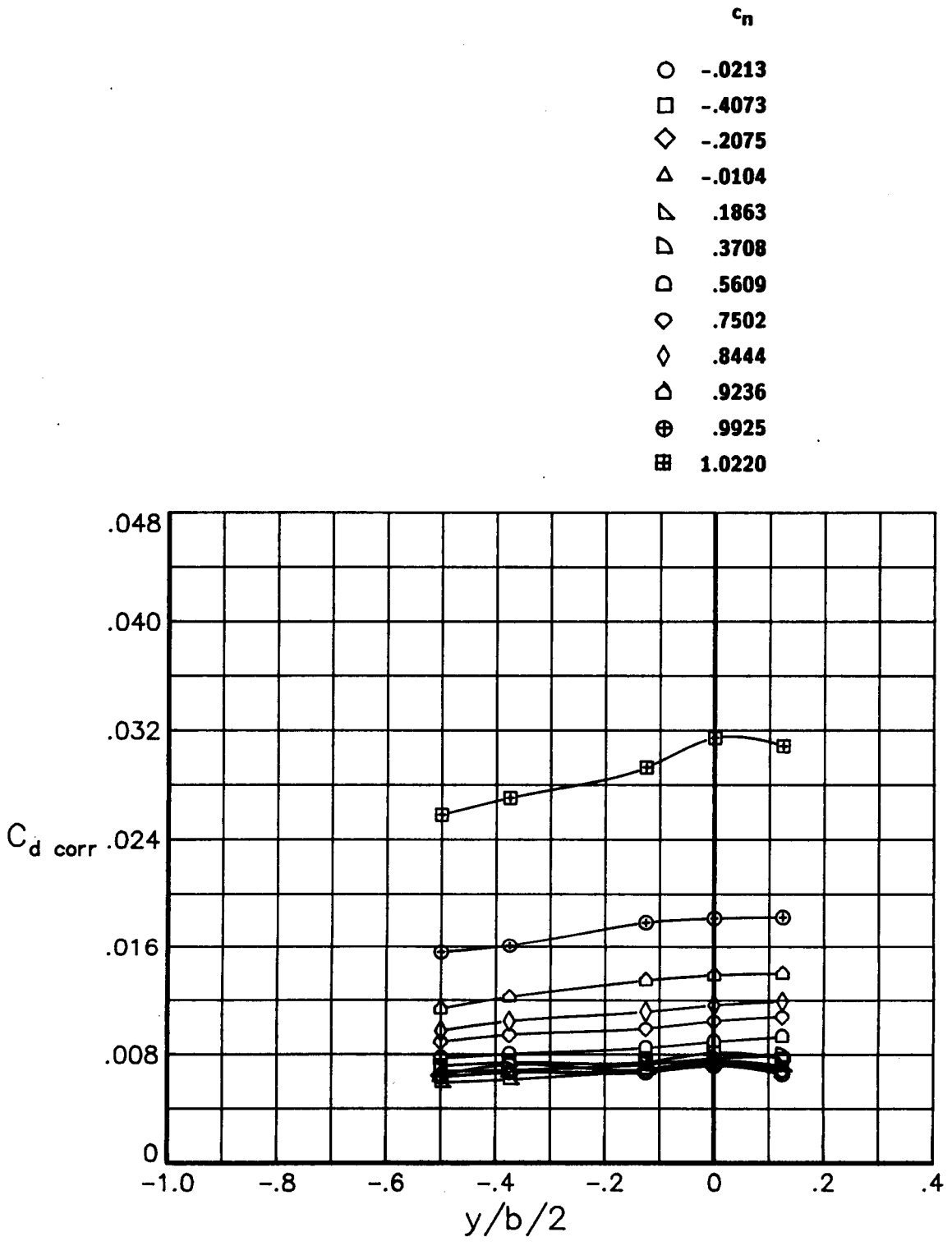

(a) $R = 3.0 \times 10^6$

Figure 2.- Effects of normal force coefficient on the spanwise variation of drag coefficient for various Reynolds numbers at a Mach number of 0.40. Transition free.

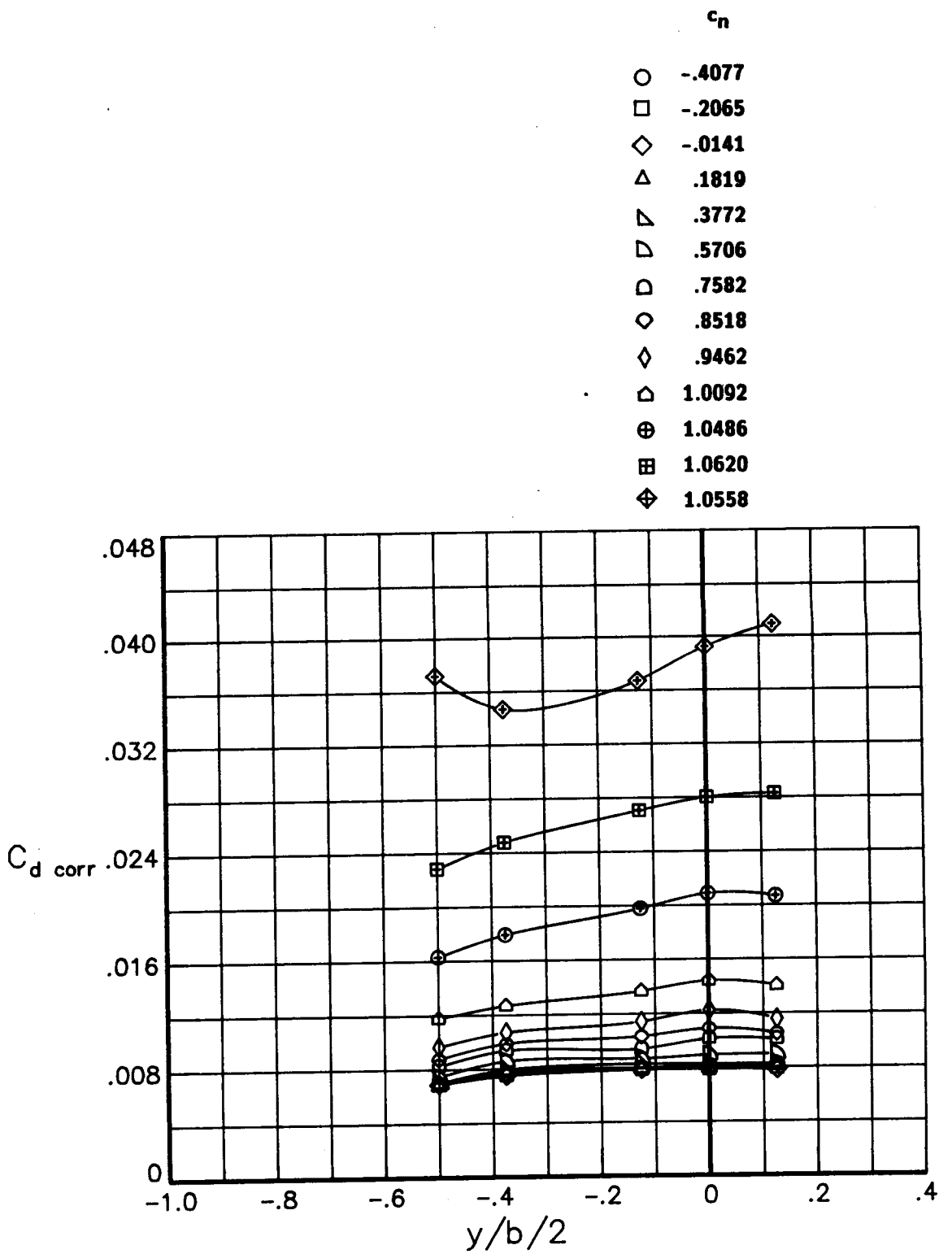

(b) R = 6.0 x 10^6

Figure 2.- Continued.

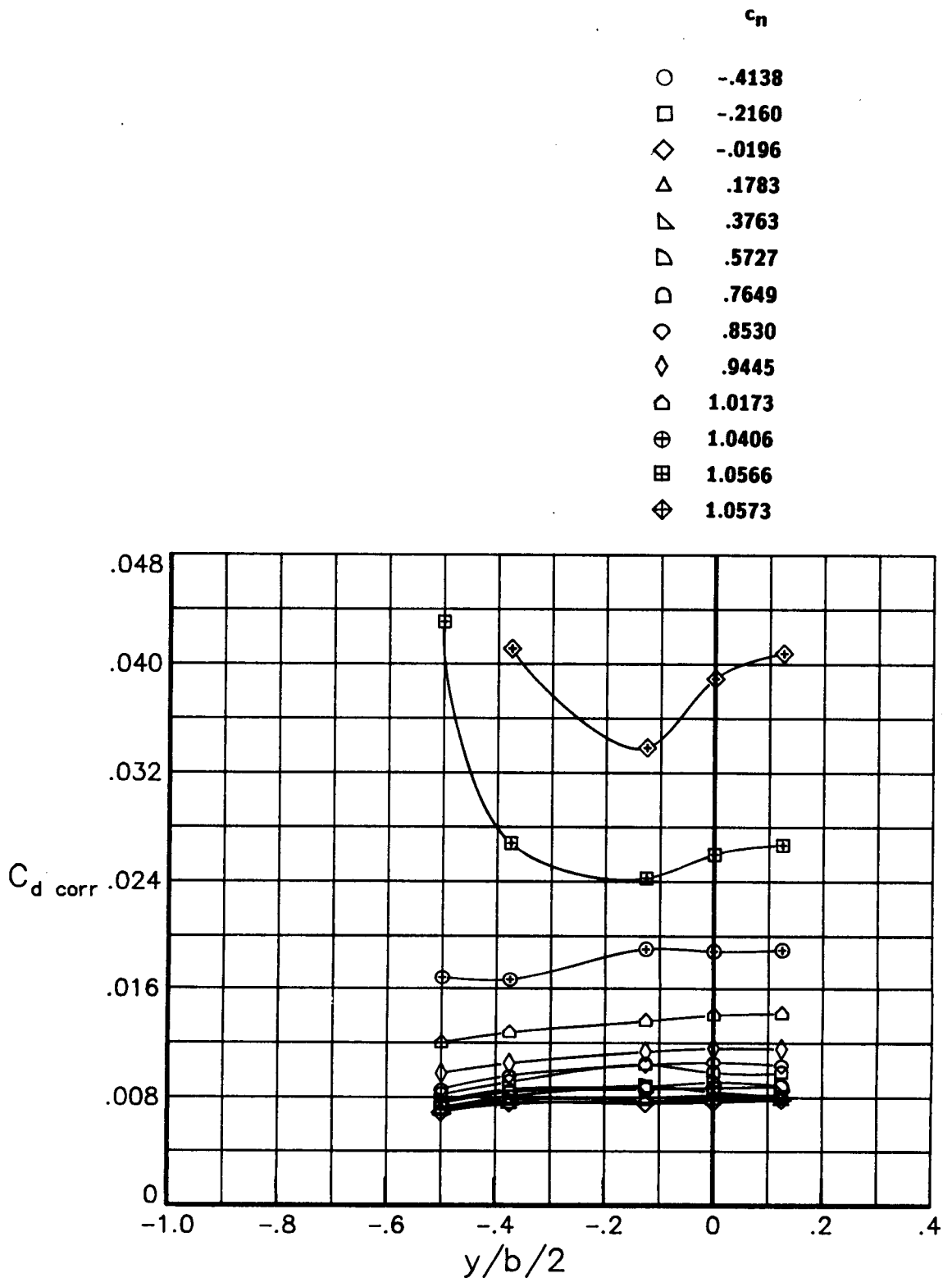

(c) R = 9.0 x 10^6

Figure 2.- Continued.

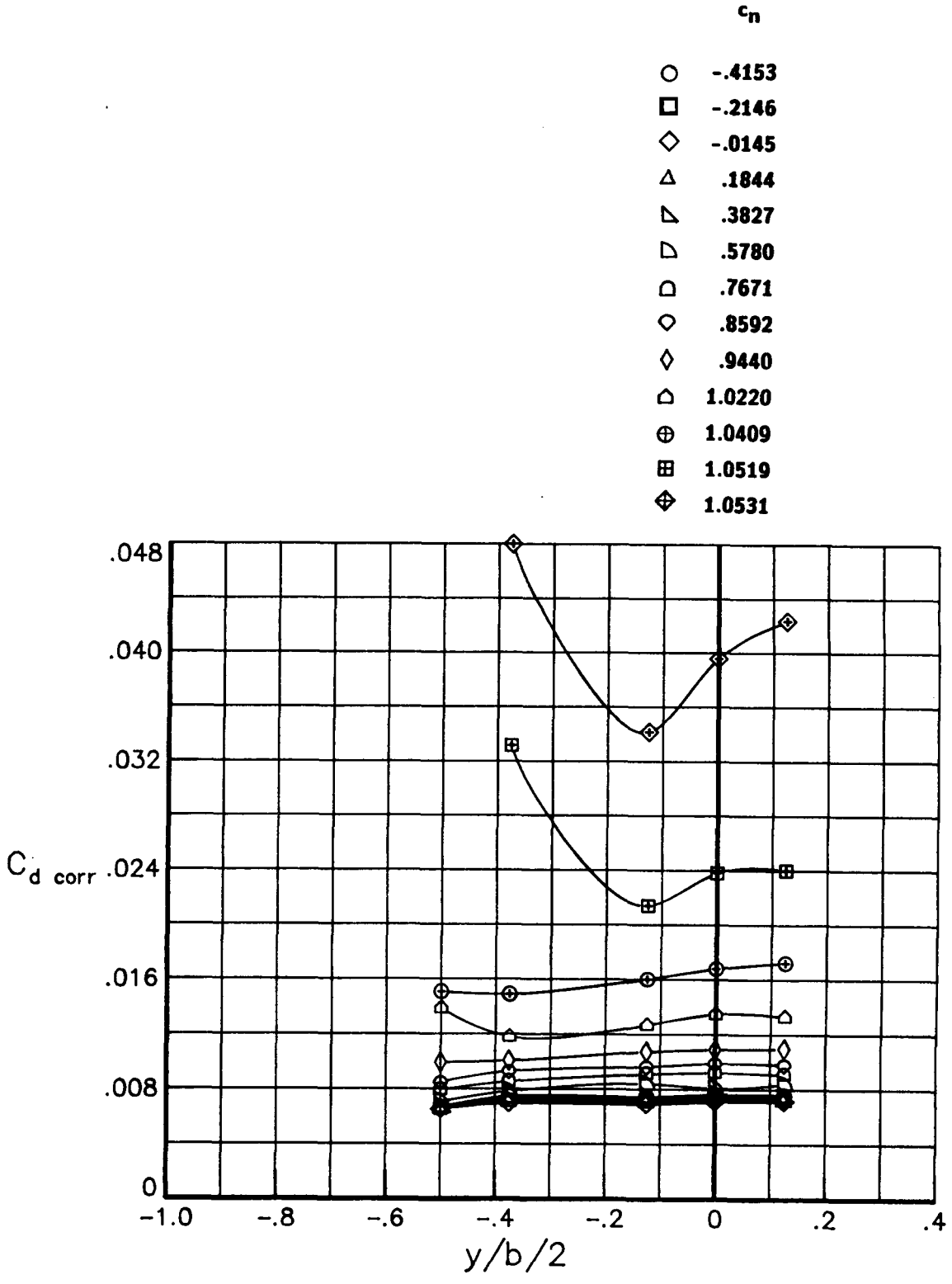

(d) R = 15.0 x 10^6

Figure 2.- Concluded.

24

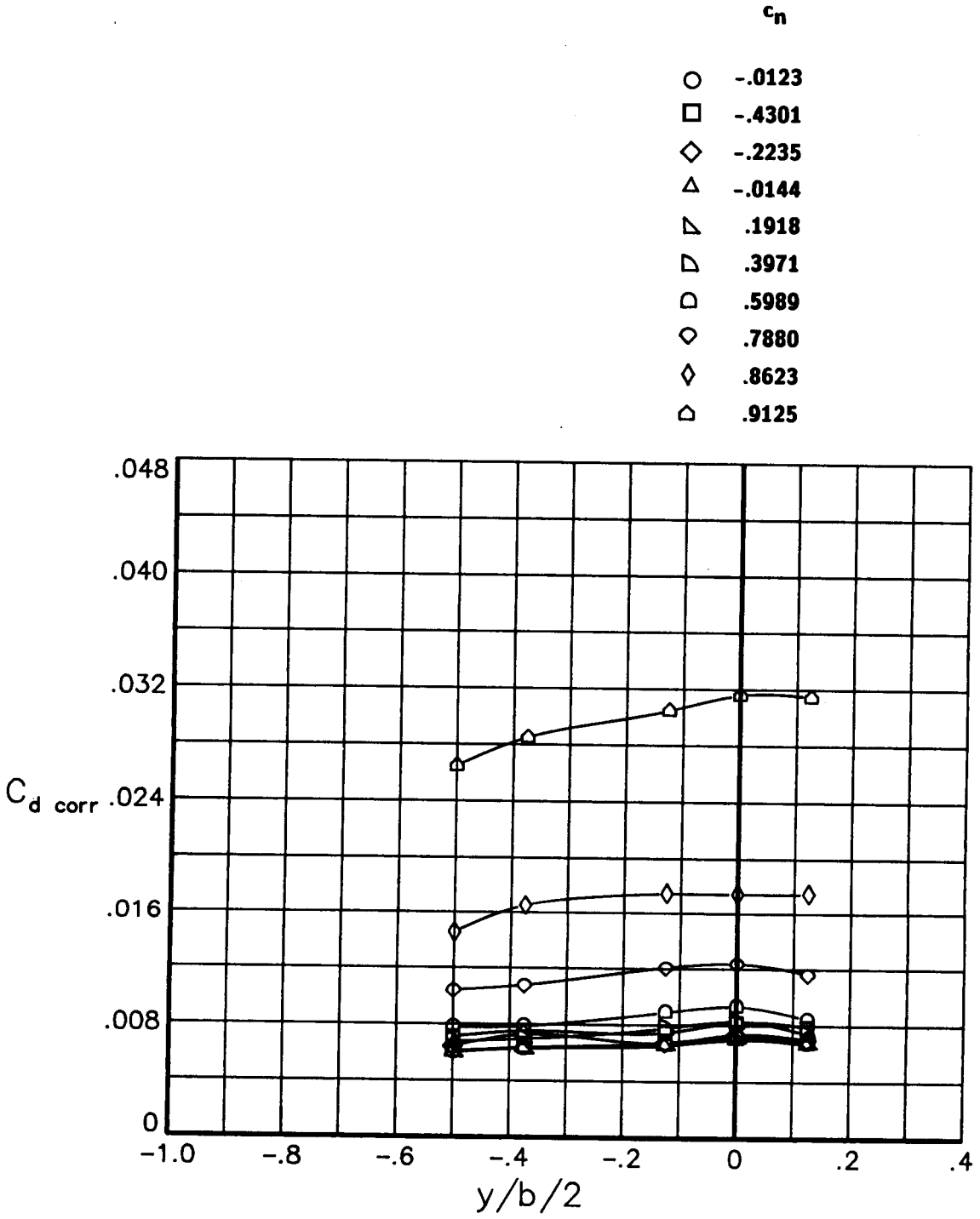

(a) R = 3.0 x 10^6

Figure 3.- Effects of normal force coefficient on the spanwise variation of drag coefficient for various Reynolds numbers at a Mach number of 0.50. Transition free.

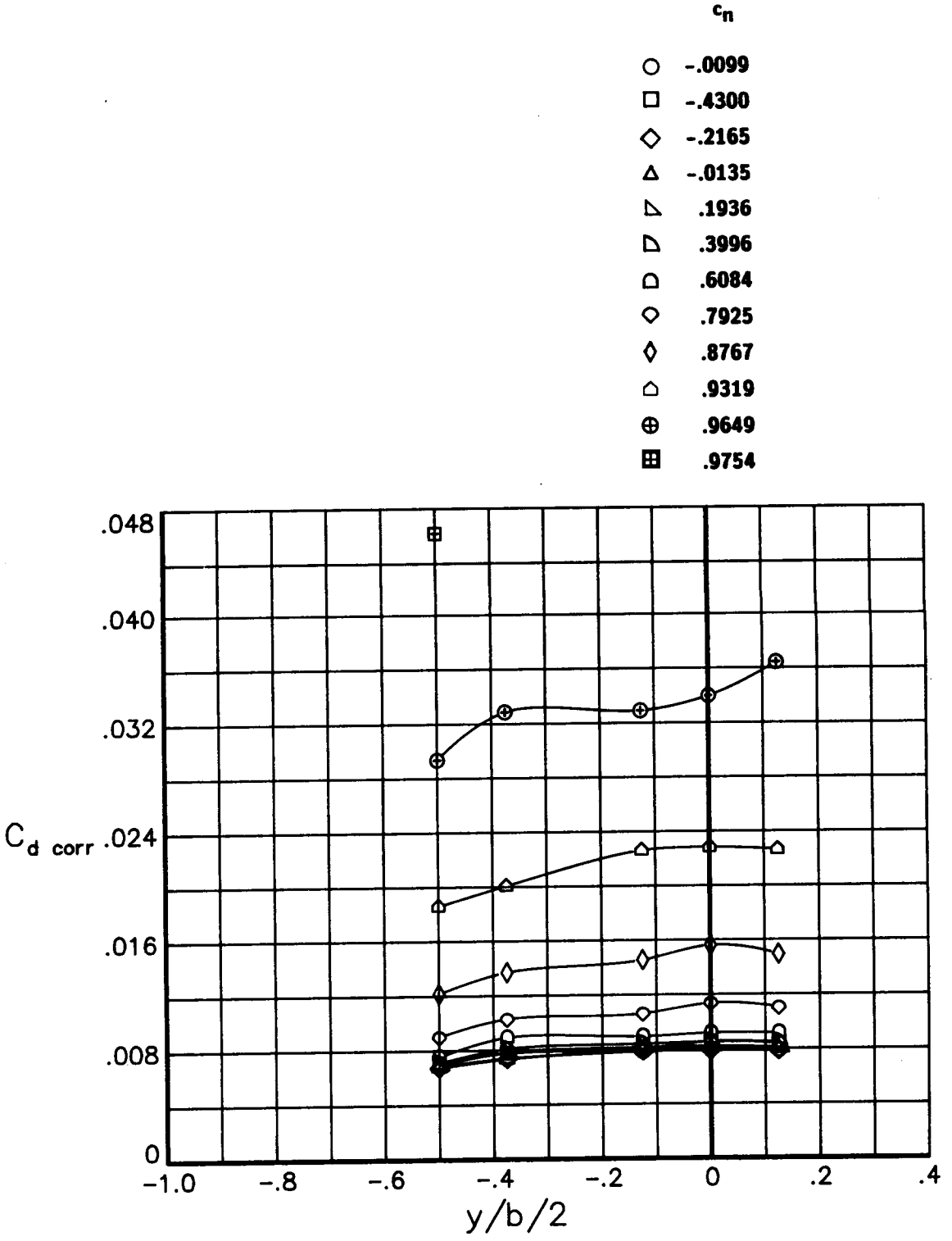

(b) R = 6.0 x 10^6

Figure 3.- Continued.

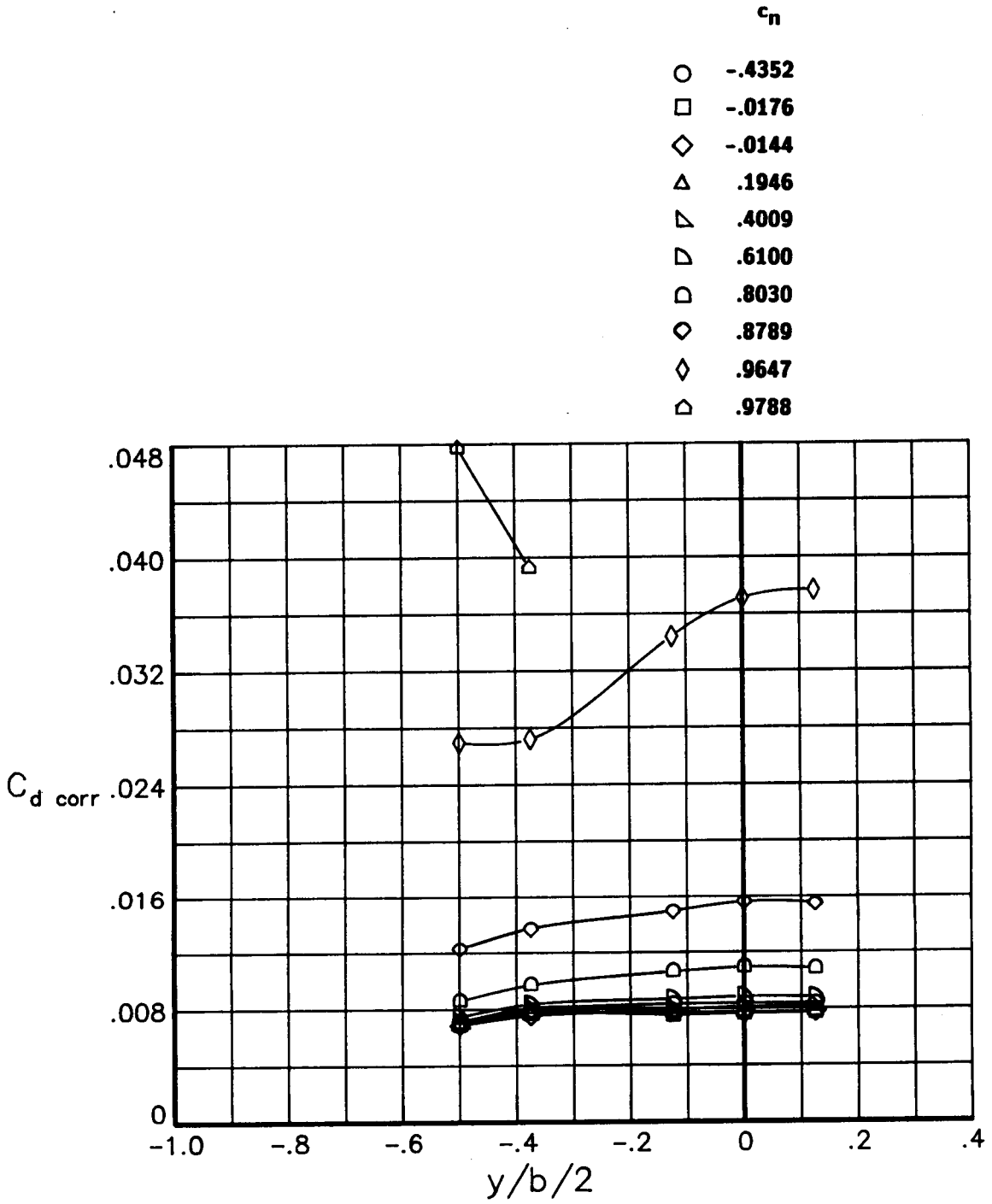

(c) R = 9.0 x 10^6

Figure 3.- Continued.

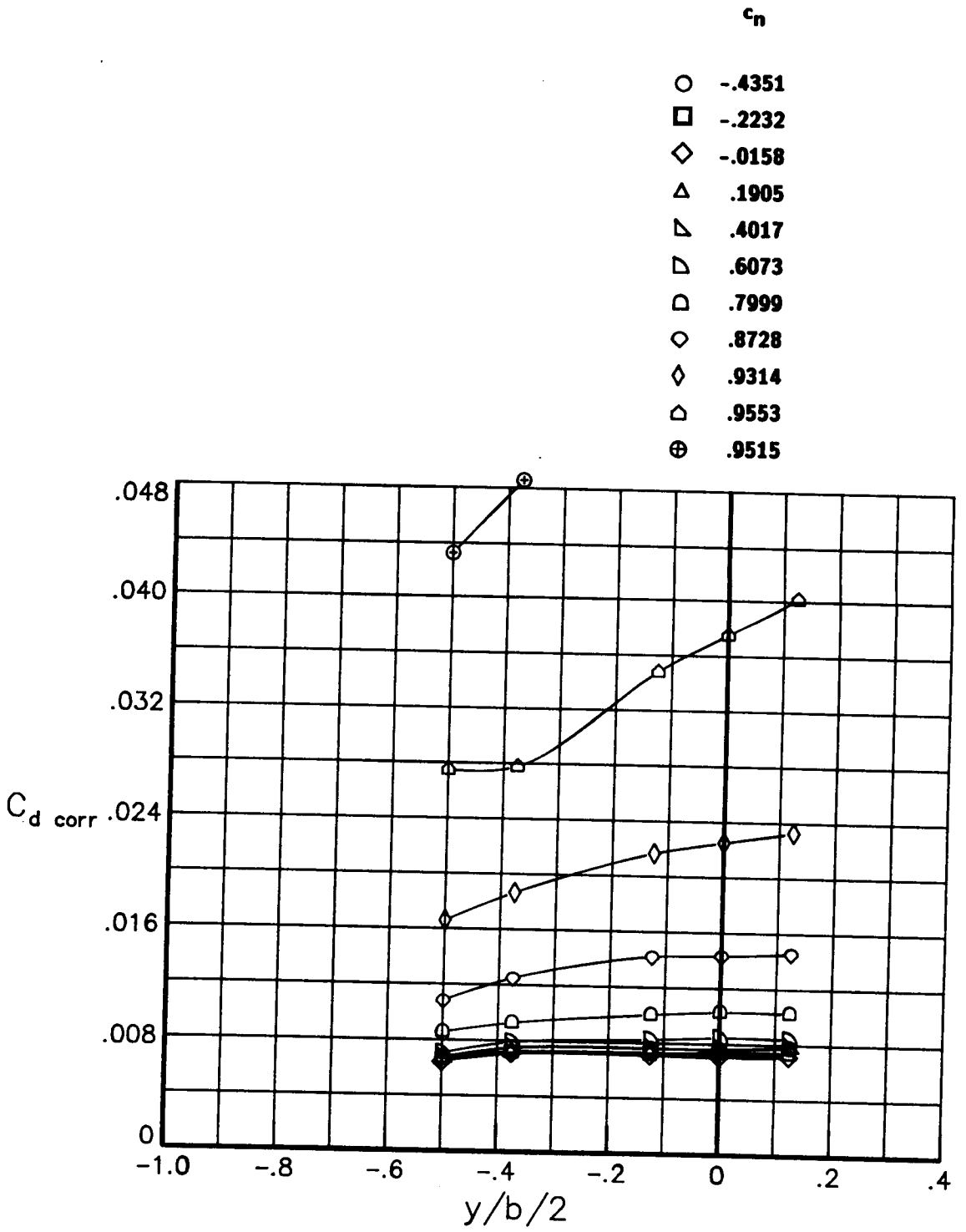

(d) R = 15.0 x 10^6

Figure 3.- Continued.

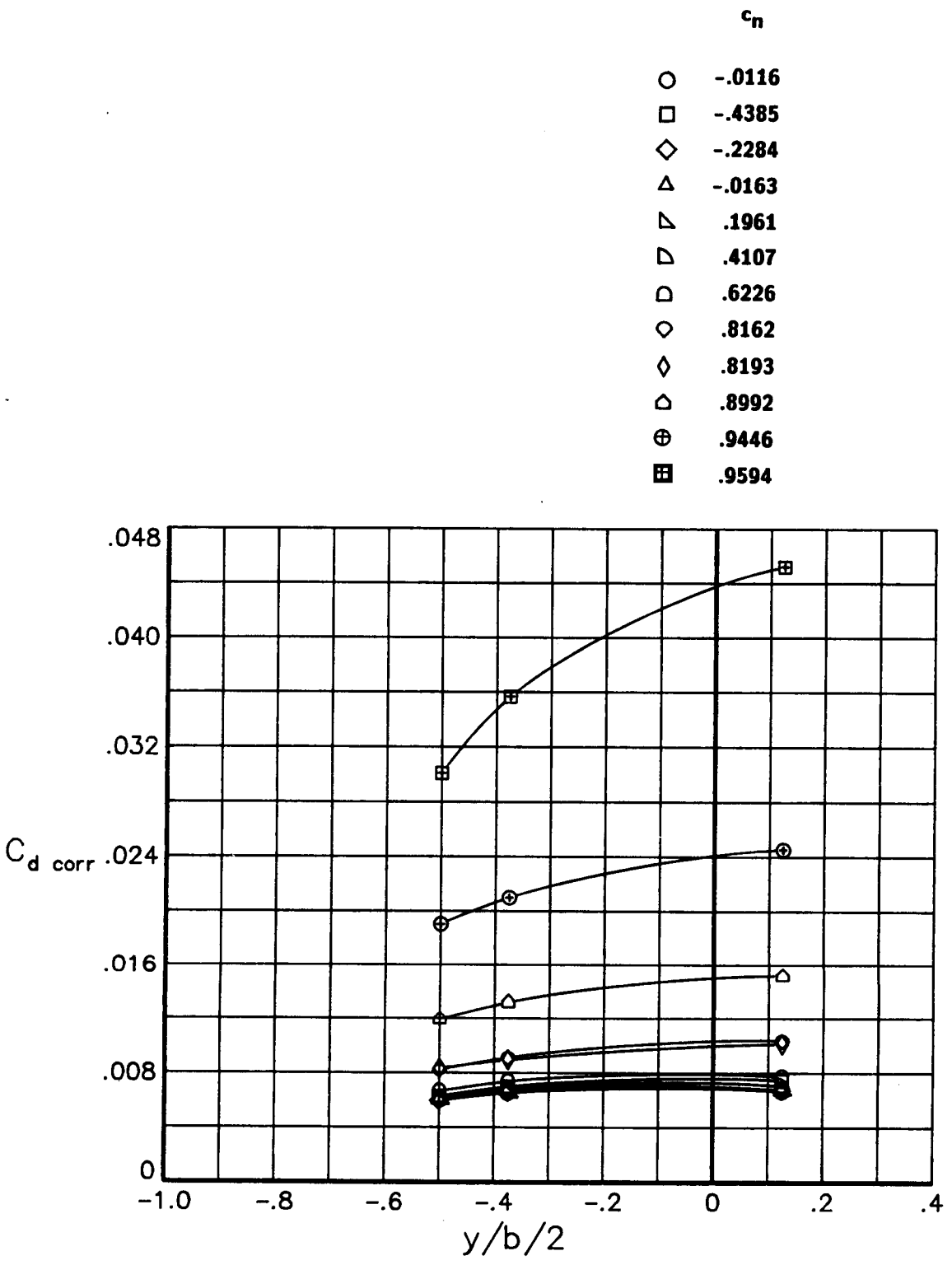

(e) R = 30.0 x 10^6

Figure 3.- Concluded.

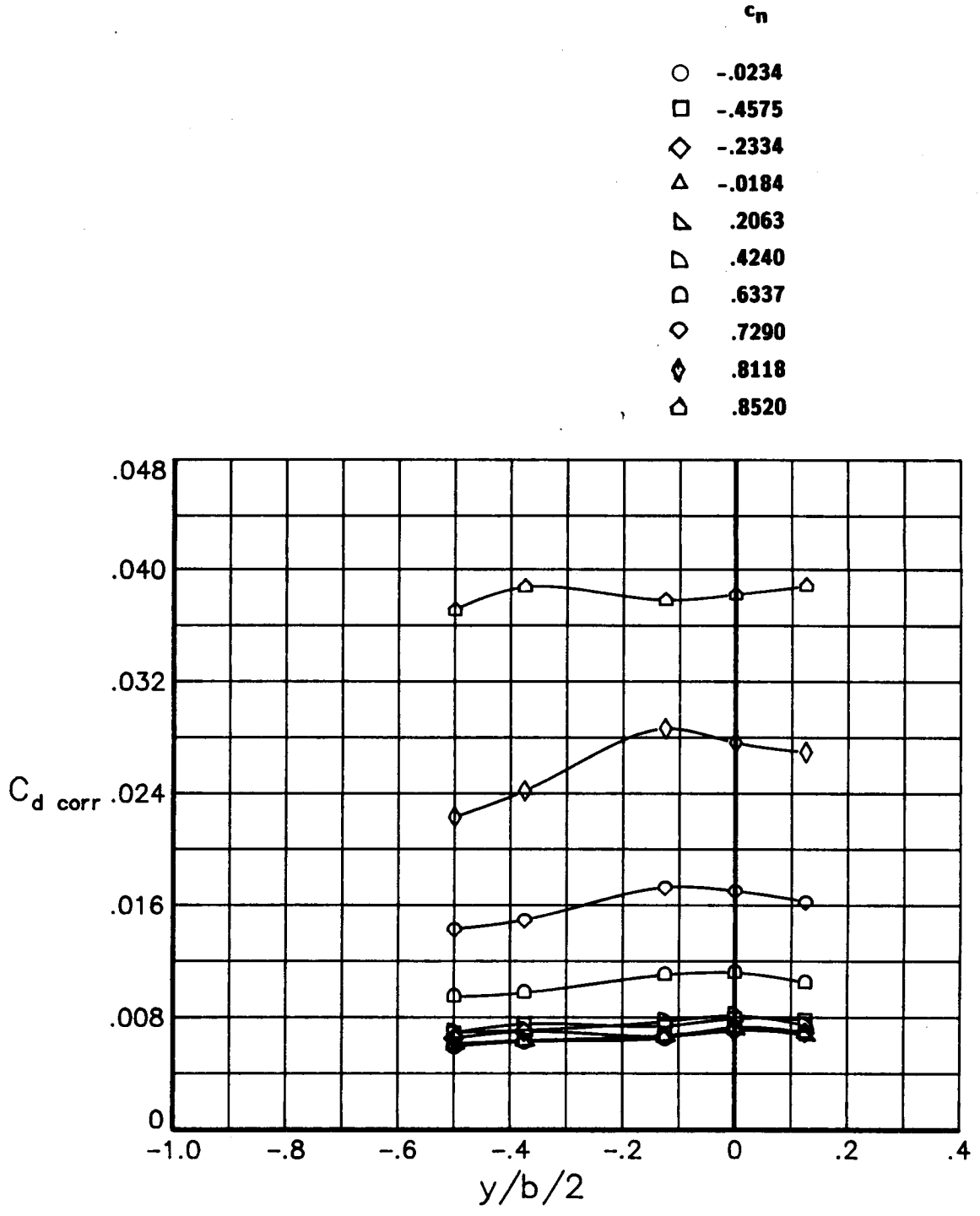

(a) $R = 3.0 \times 10^6$

Figure 4.- Effects of normal force coefficient on the spanwise variation of drag coefficient for various Reynolds numbers at a Mach number of 0.60. Transition free.

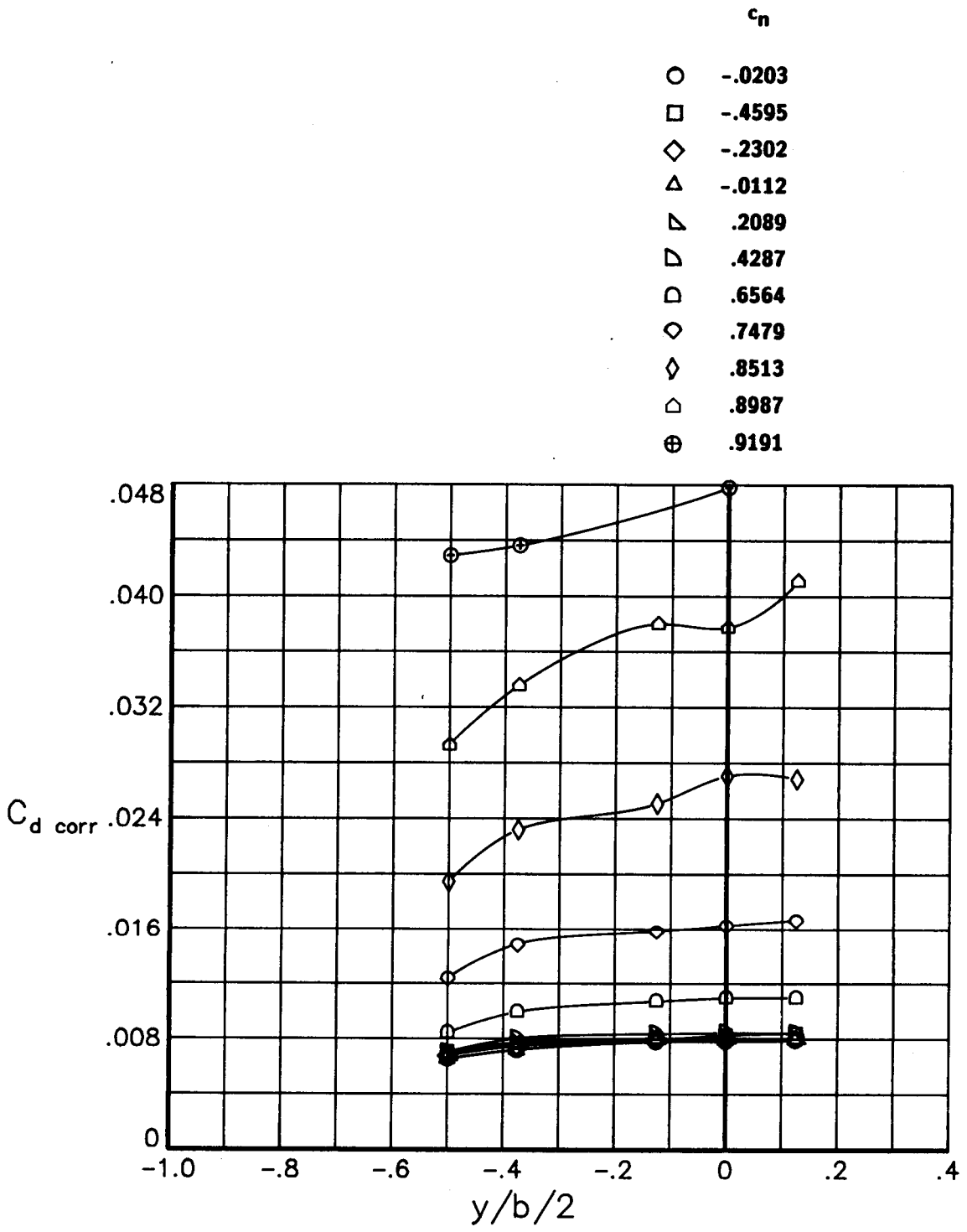

(b) R = 6.0 x 10^6

Figure 4.- Continued.

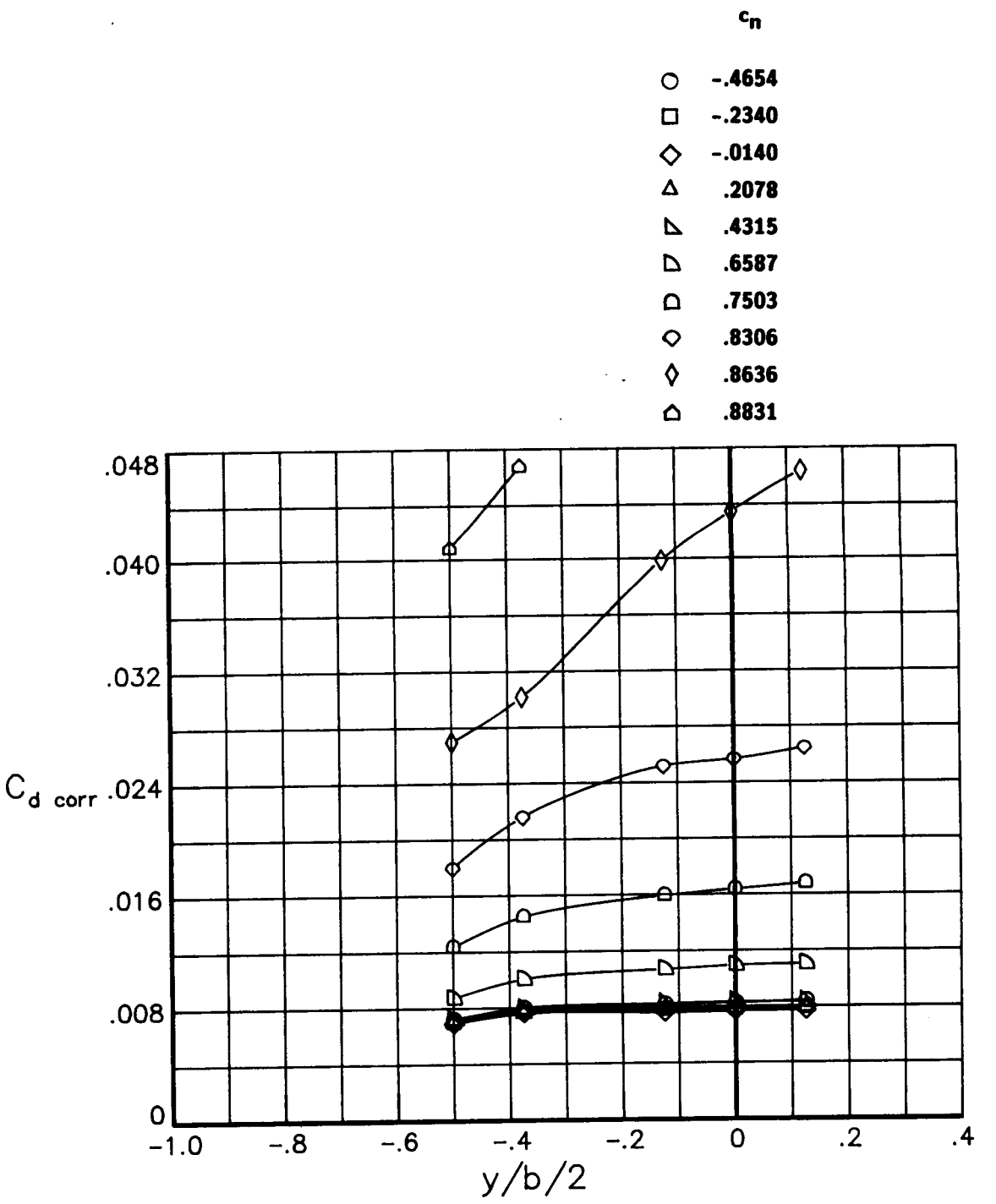

(c) R = 9.0 x 10^6

Figure 4.- Continued.

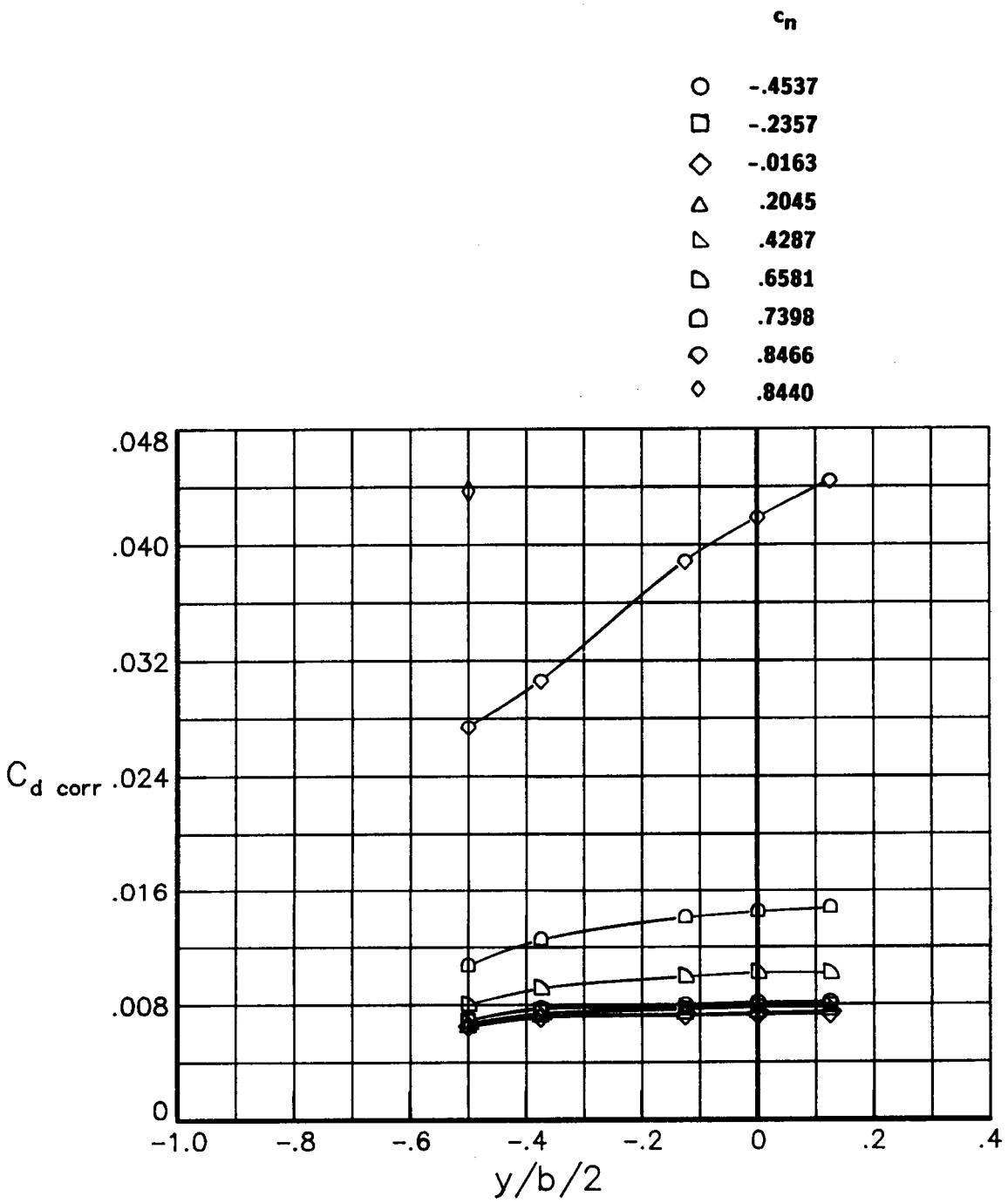

(d) R = 15.0 x 10^6

Figure 4.- Continued.

34

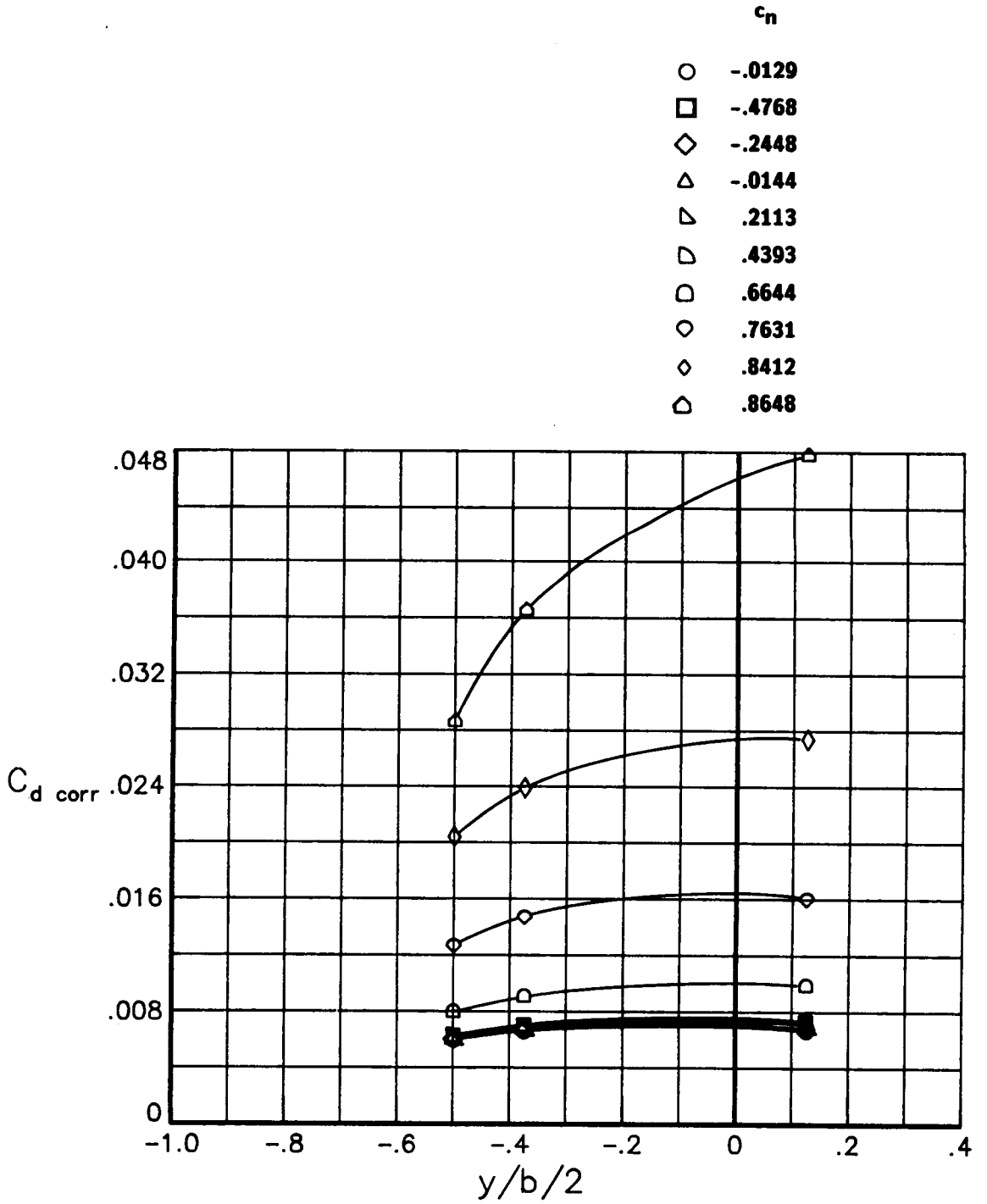

(e) R = 30.0 x 10^6

Figure 4.- Concluded.

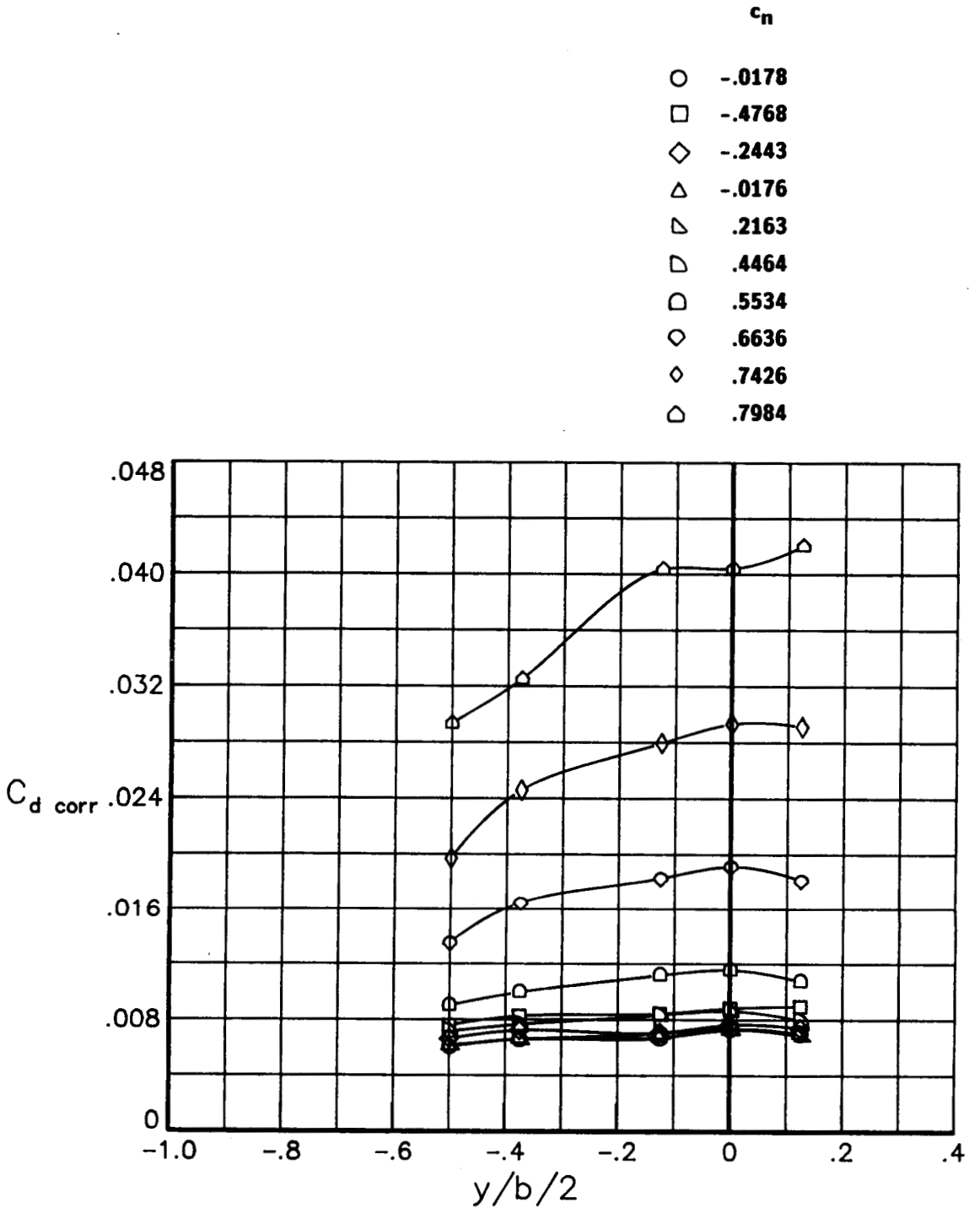

(a) R = 3.0 x 10^6

Figure 5.- Effects of normal force coefficient on the spanwise variation of drag coefficient for various Reynolds numbers at a Mach number of 0.65. Transition free.

48

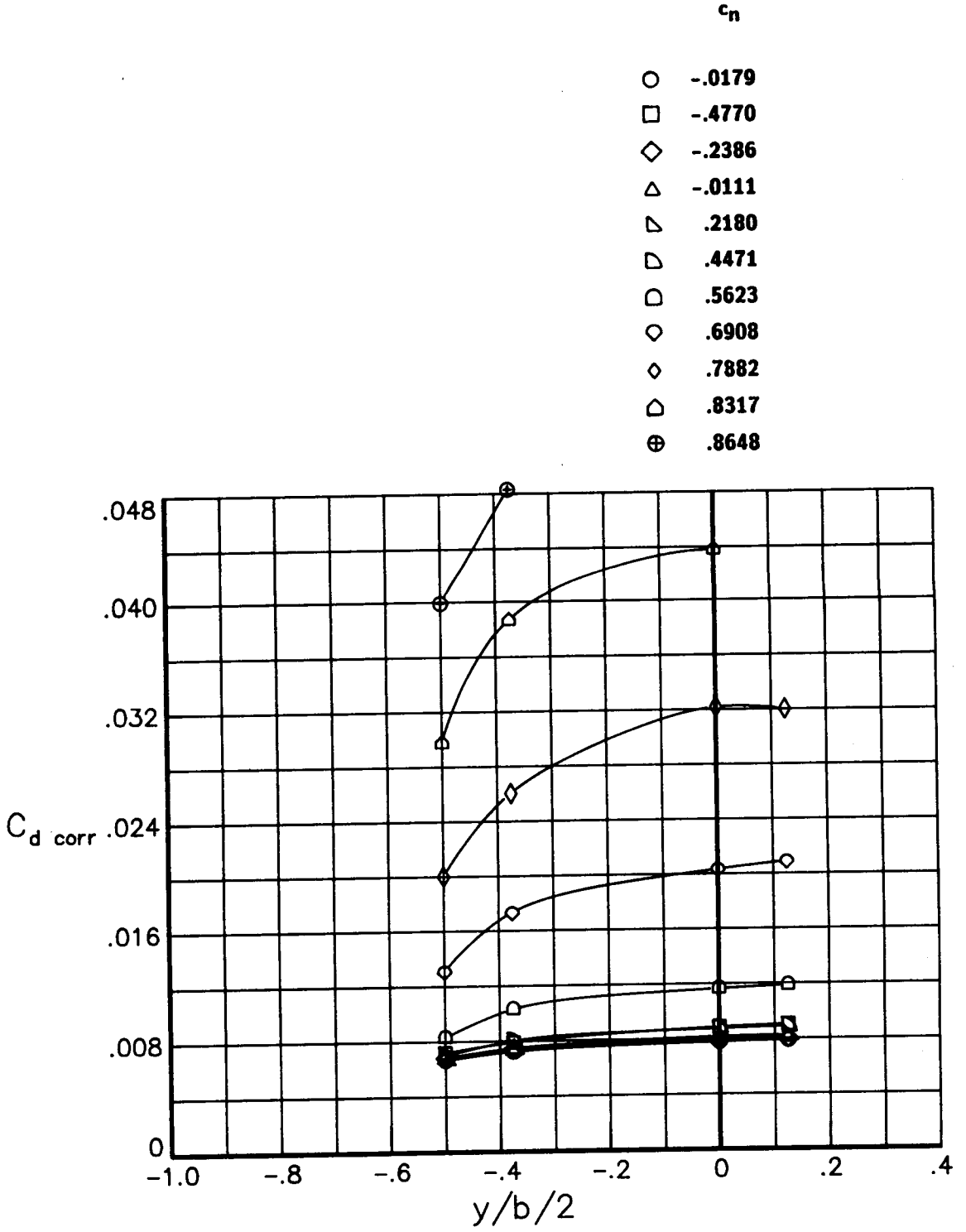

(b) R = 6.0 x 10^6

Figure 5.- Continued.

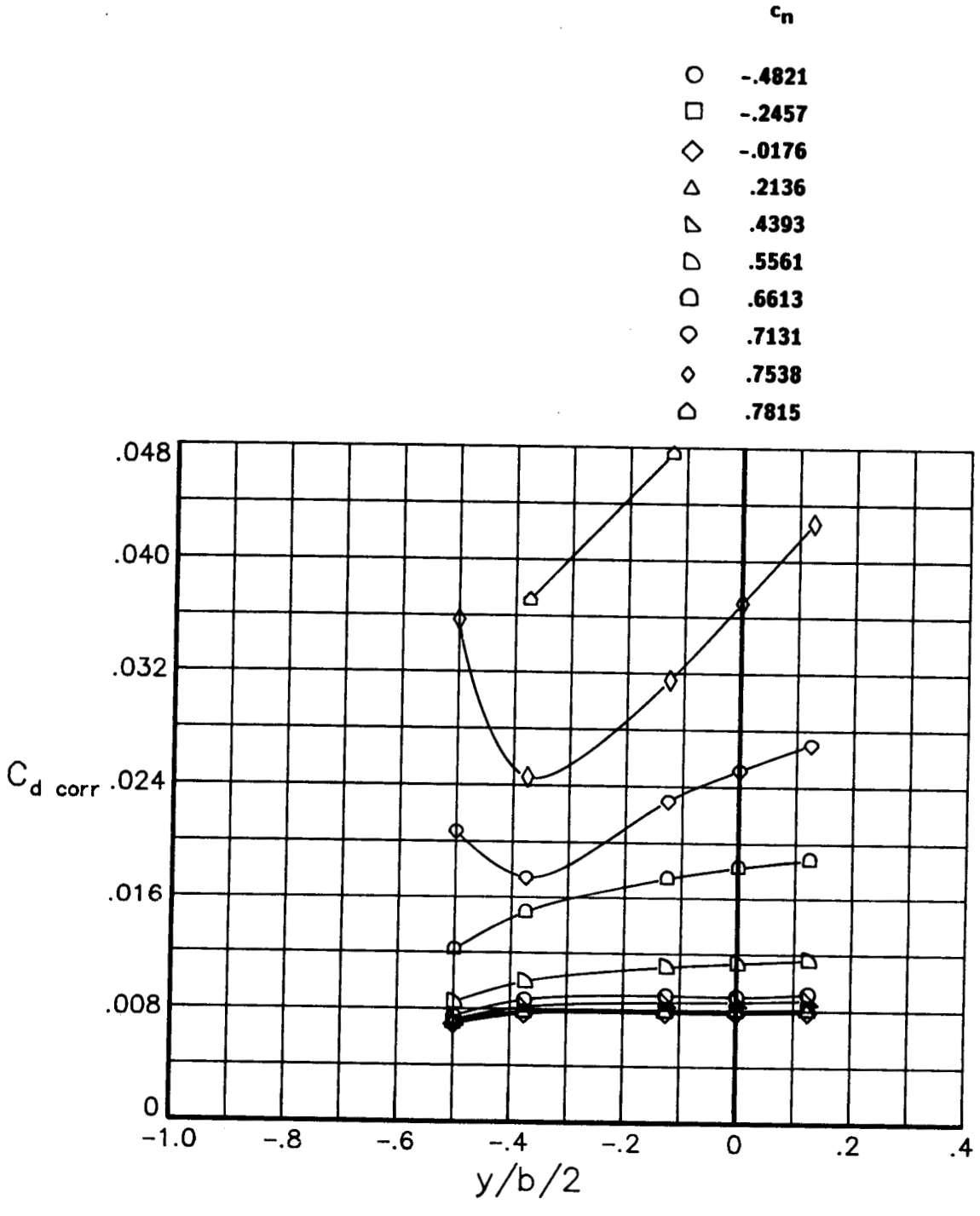

(c) $R = 9.0 \times 10^6$

Figure 5.- Continued.

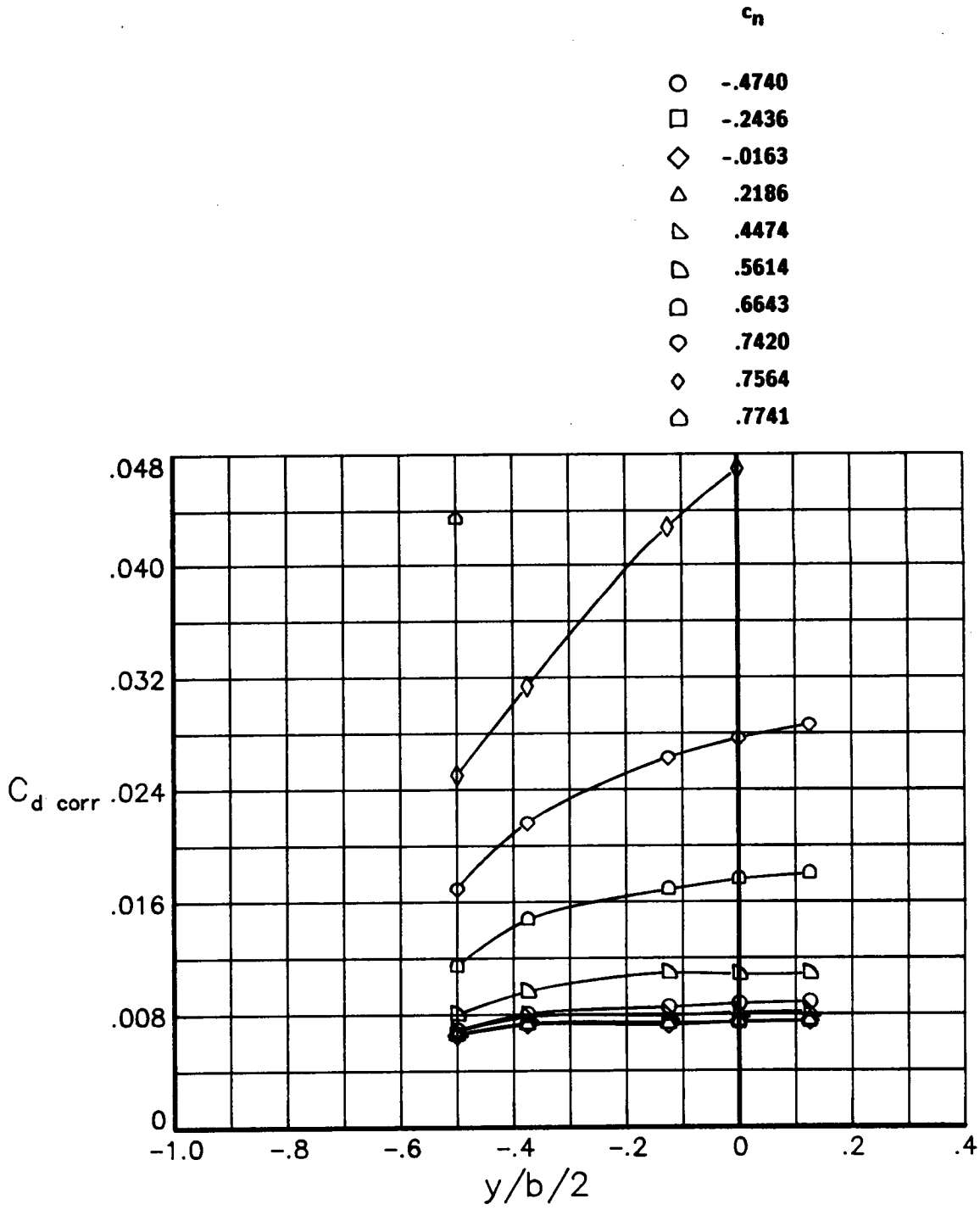

(d) $R = 15.0 \times 10^6$

Figure 5.- Continued.

35

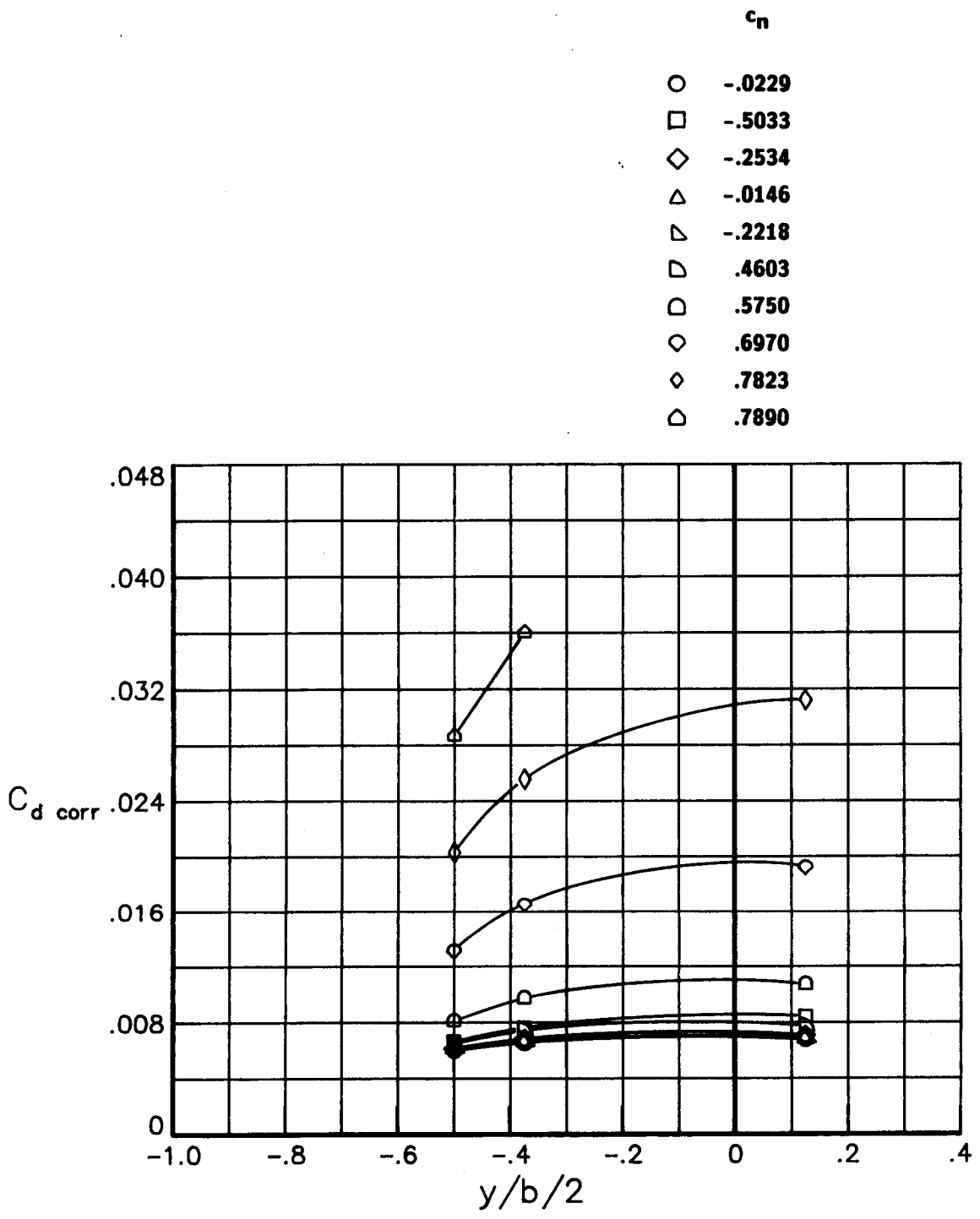

(e) R = 30.0 x 10^6

Figure 5.- Concluded.

27

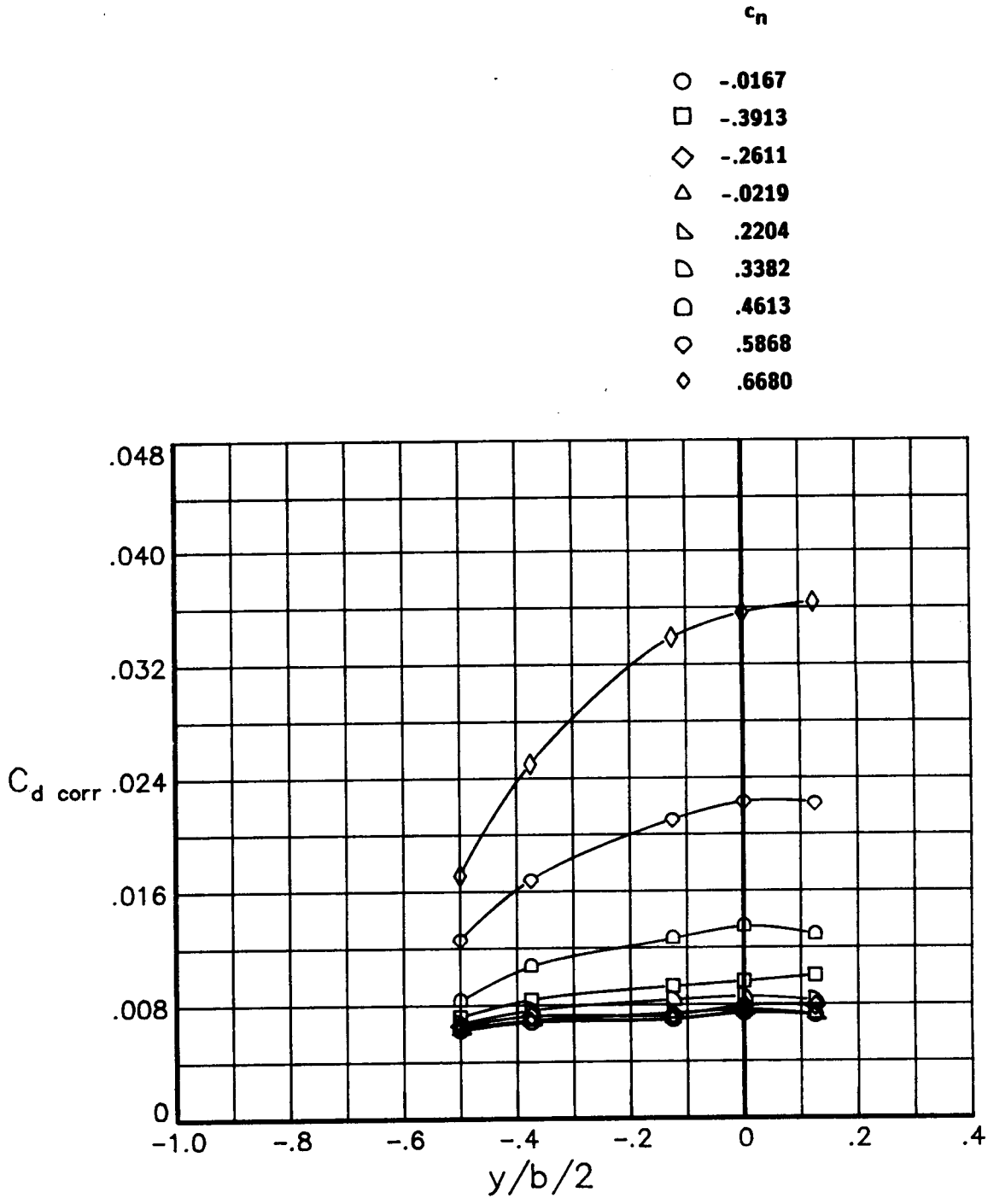

(a) $R = 3.0 \times 10^6$

Figure 6.- Effects of normal force coefficient on the spanwise variation of drag coefficient for various Reynolds numbers at a Mach number of 0.70. Transition free.

49

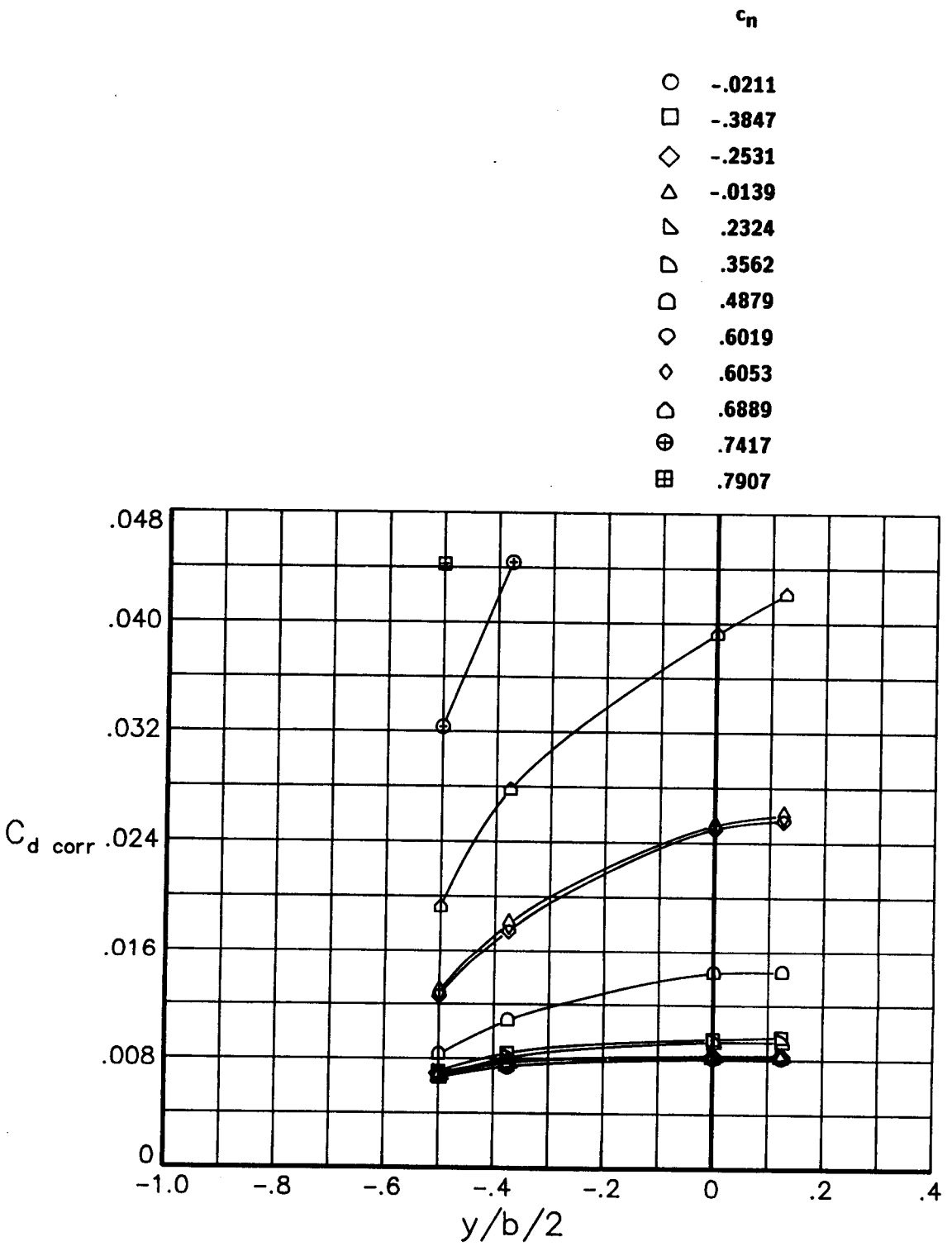

(b) R = 6.0 x 10^6

Figure 6.- Continued.

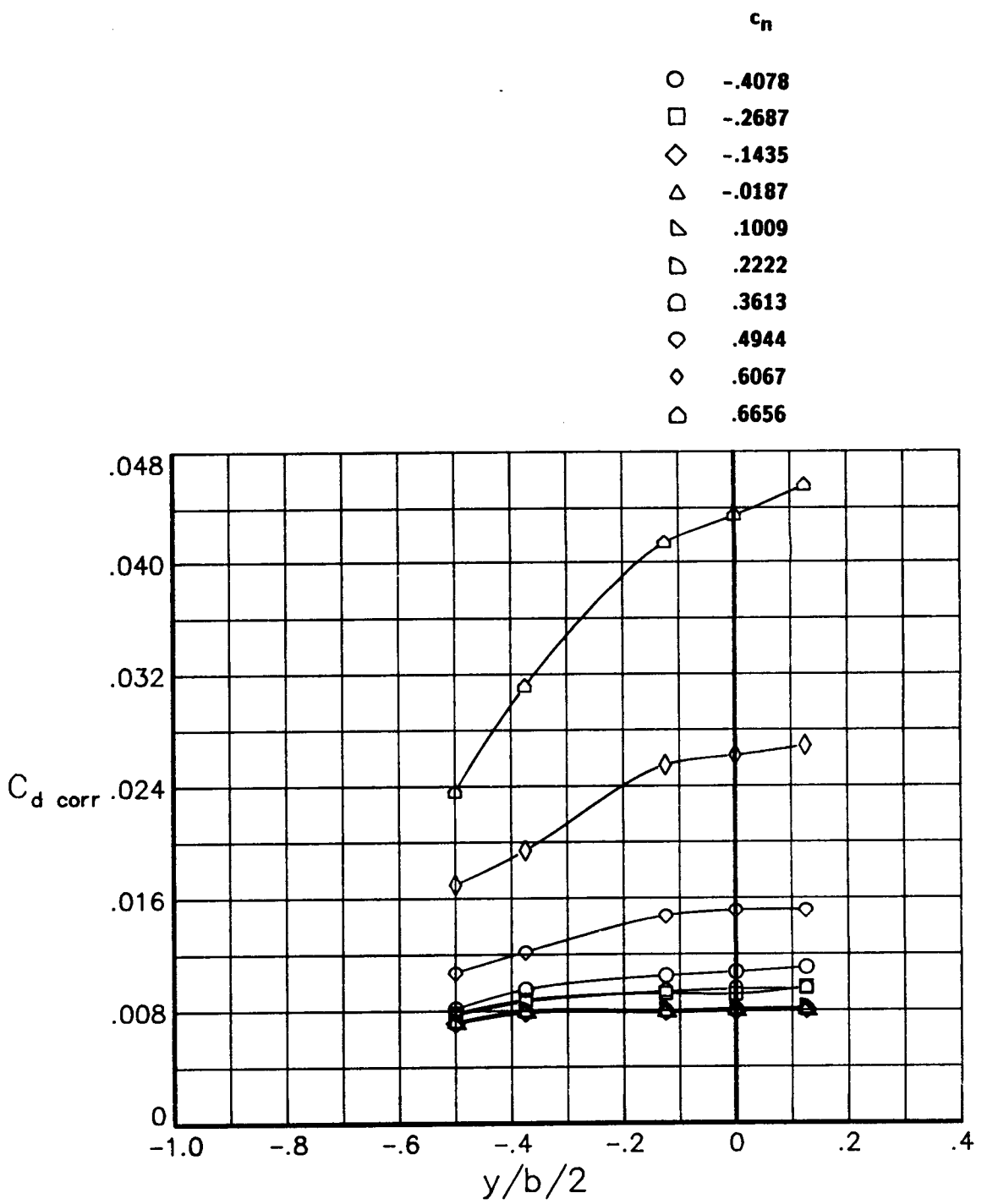

(c) R = 9.0 x 10^6

Figure 6.- Continued.

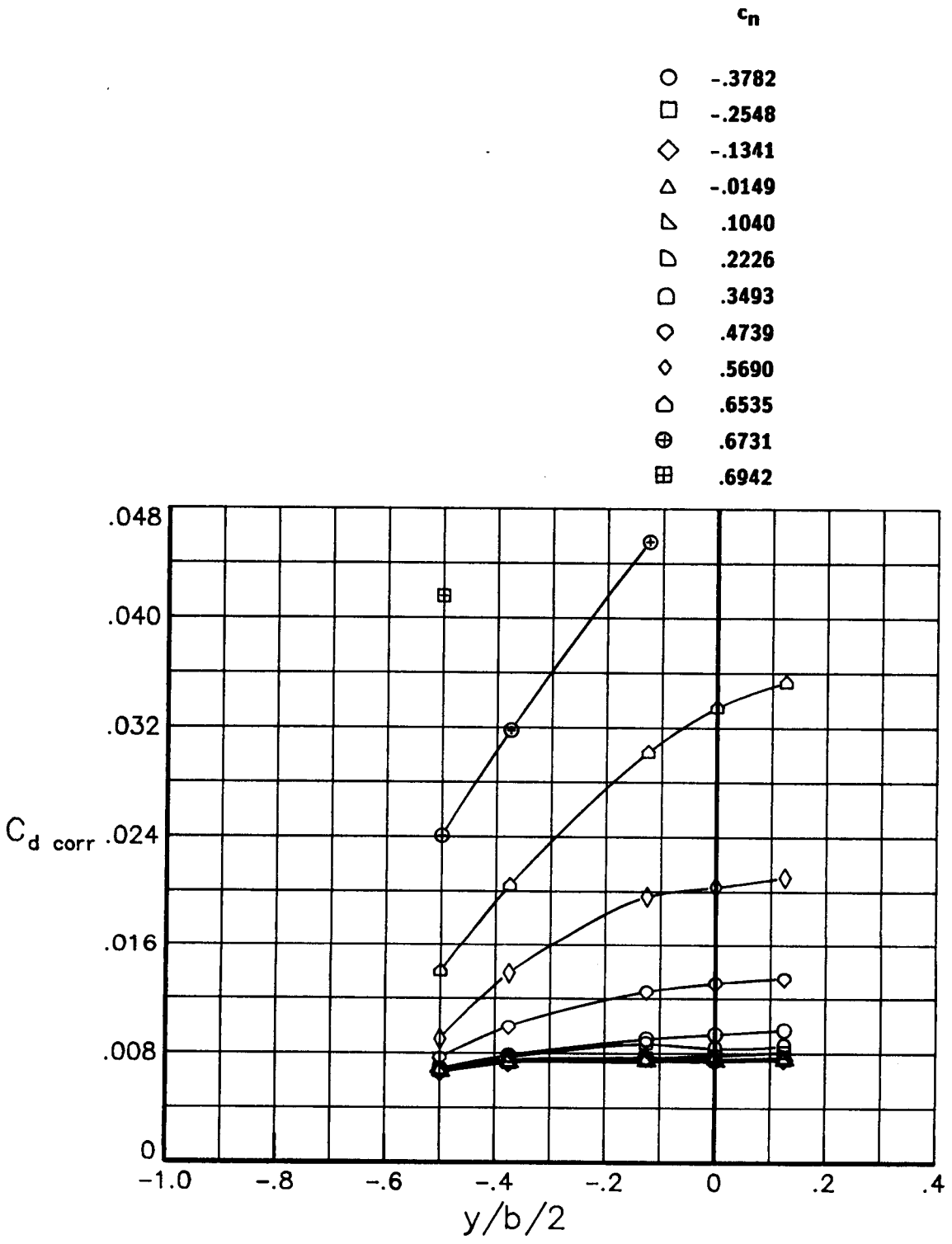

(d) R = 15.0 x 10^6

Figure 6.- Continued.

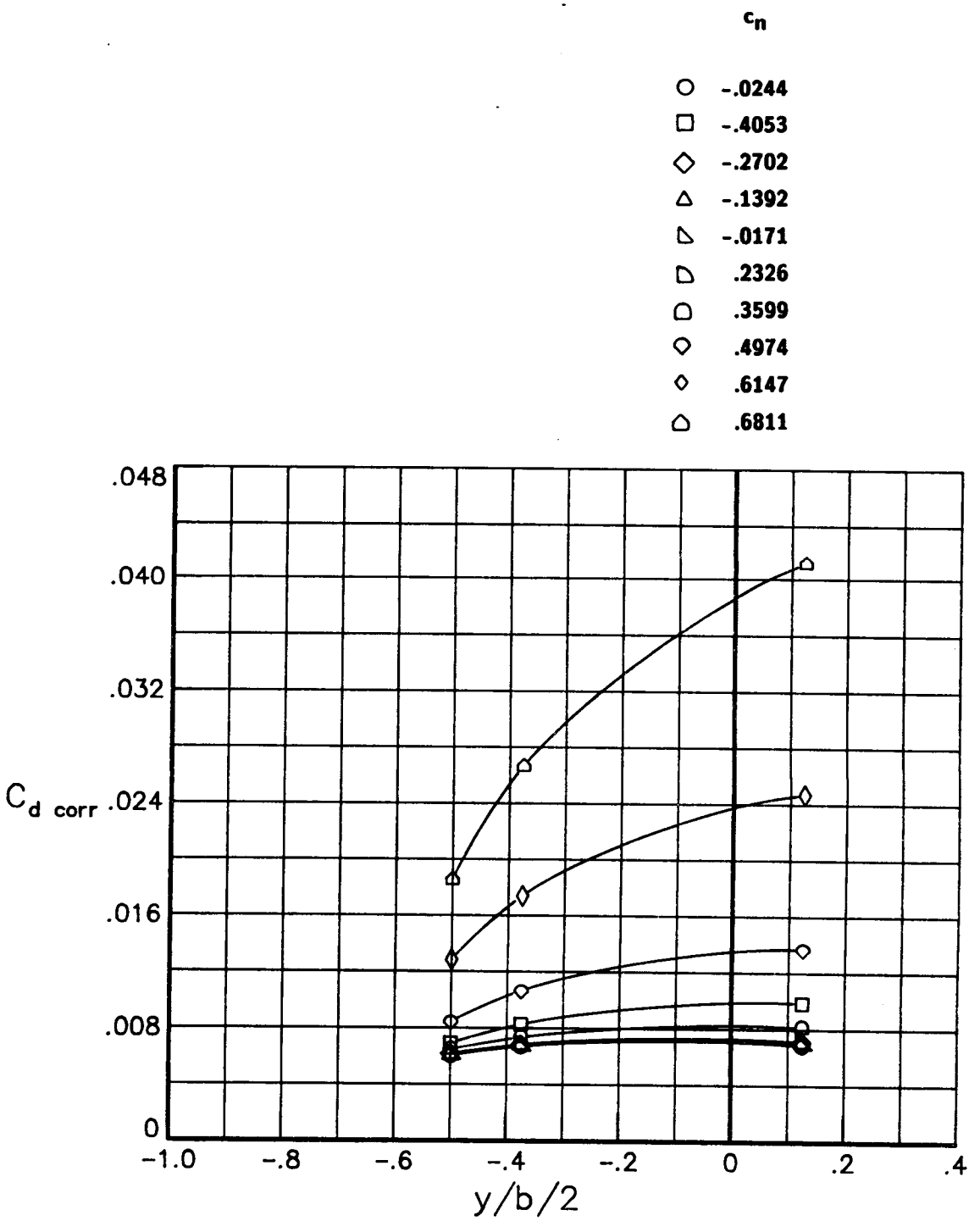

(e) R = 30.0 x 10^6

Figure 6.- Concluded.

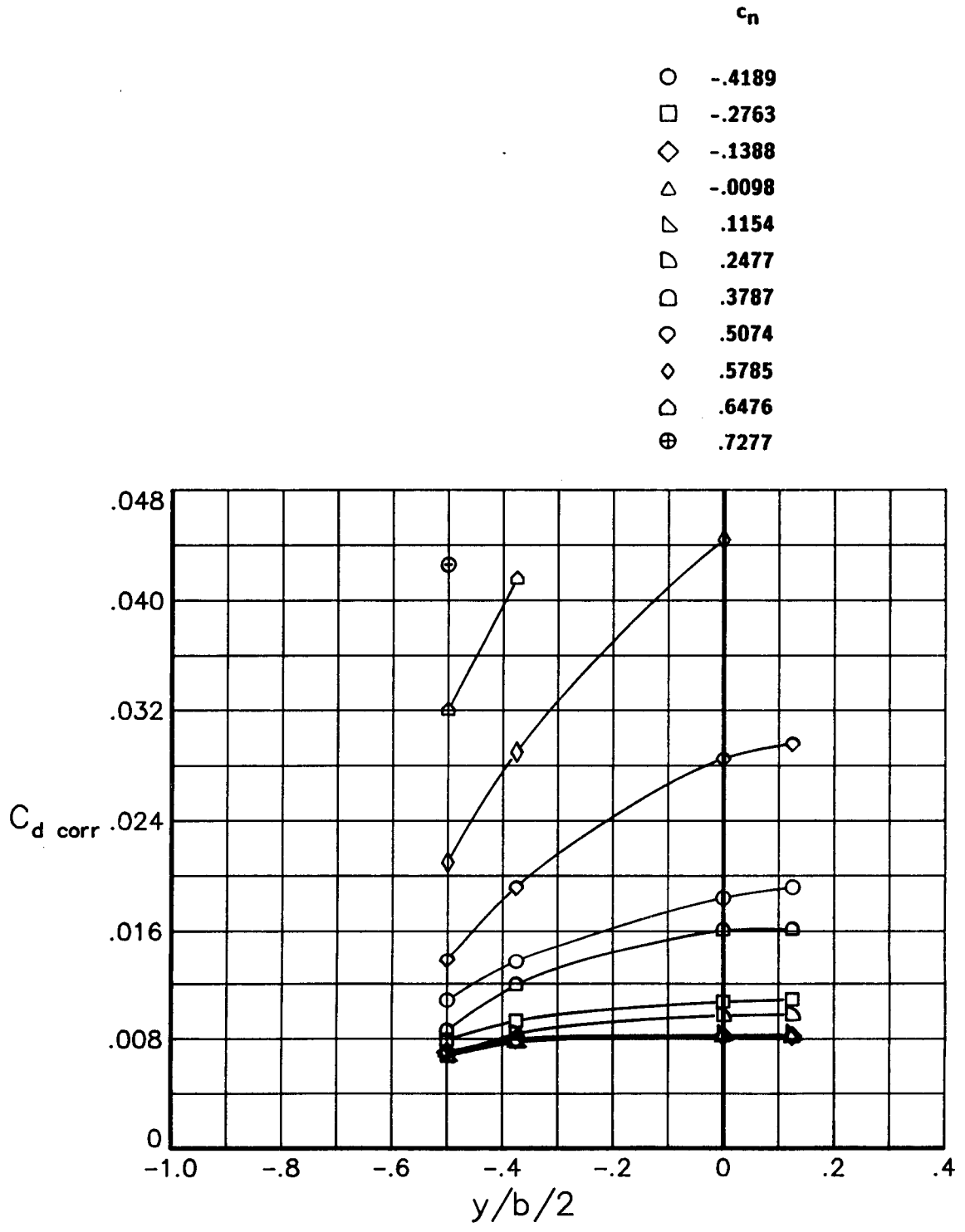

(a) $R = 6.0 \times 10^6$

Figure 7.- Effects of normal force coefficient on the spanwise variation of drag coefficient for various Reynolds numbers at a Mach number of 0.74. Transition free.

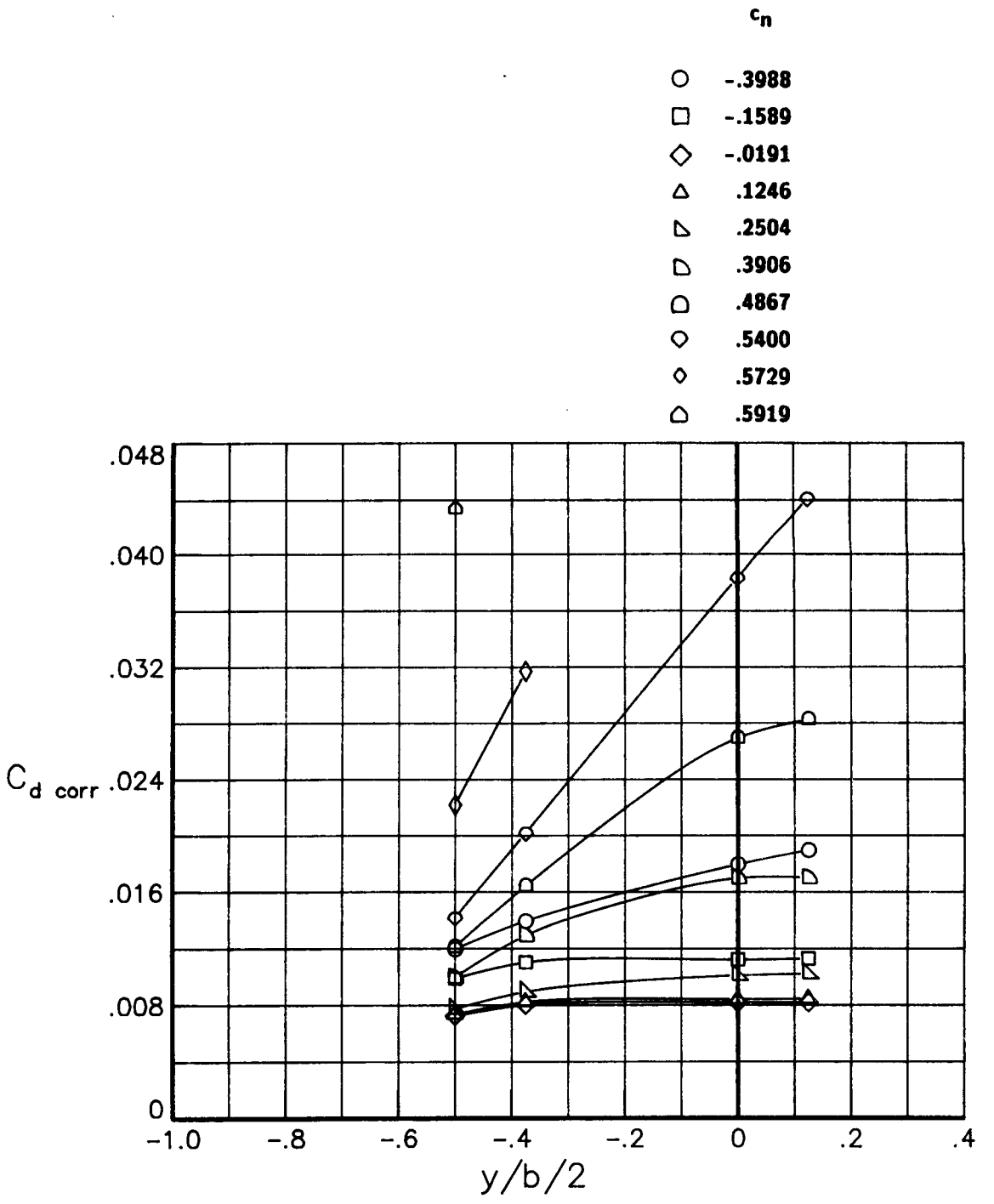

(b) R = 9.0 x 10^6

Figure 7.- Continued.

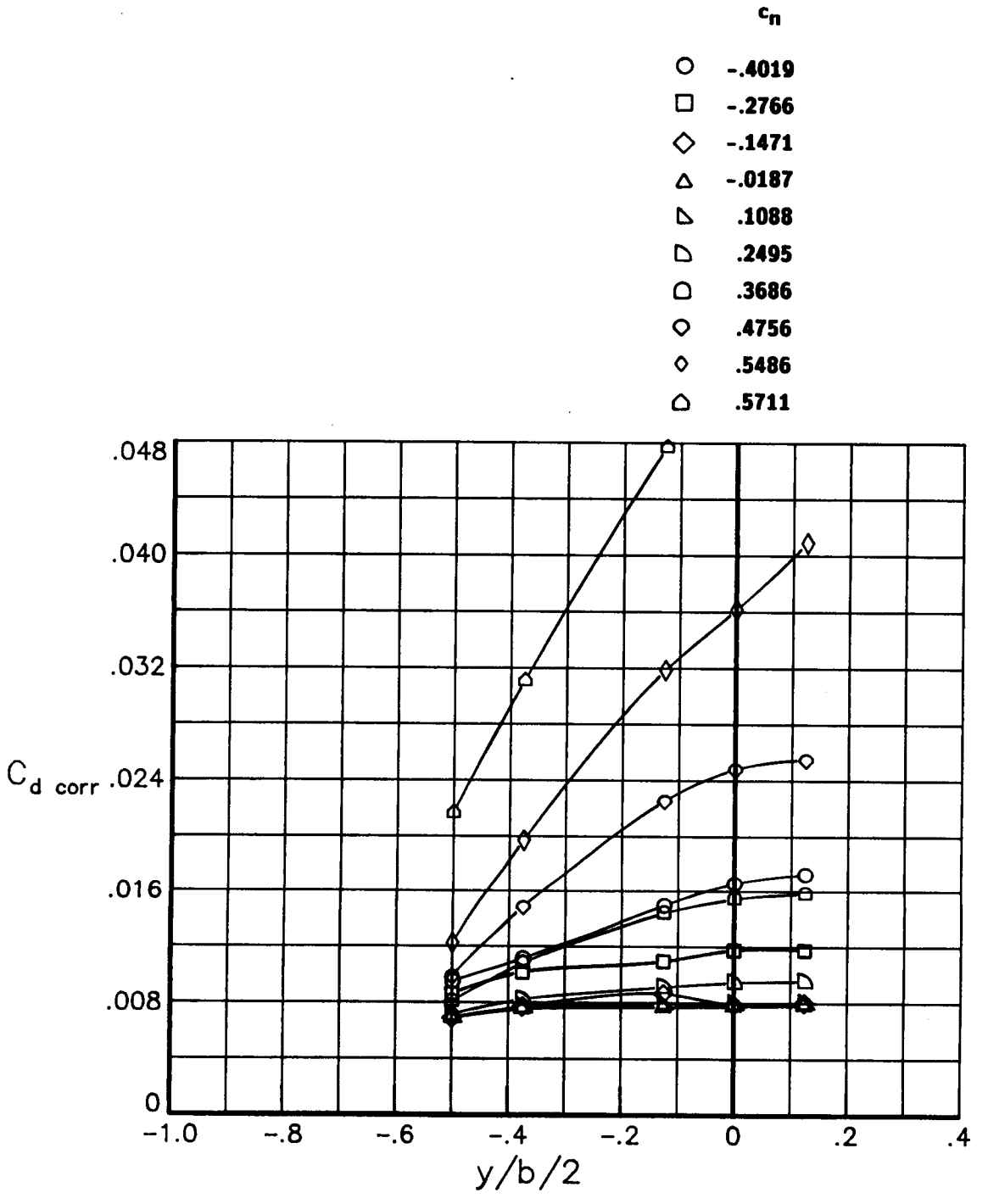

(c) R = 15.0 x 10^6

Figure 7.- Continued.

37

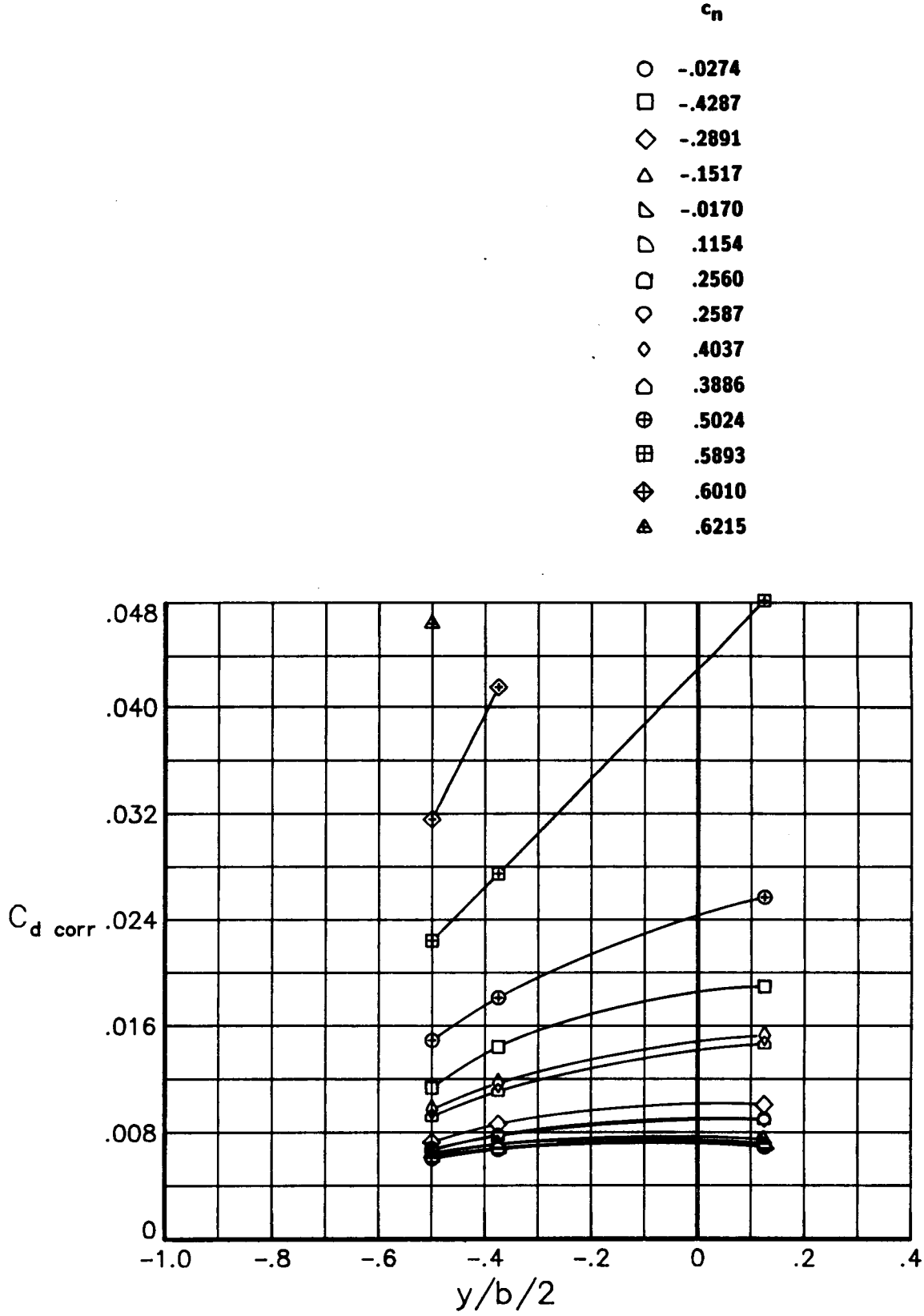

(d) R = 30.0 x 10^6

Figure 7.- Concluded.

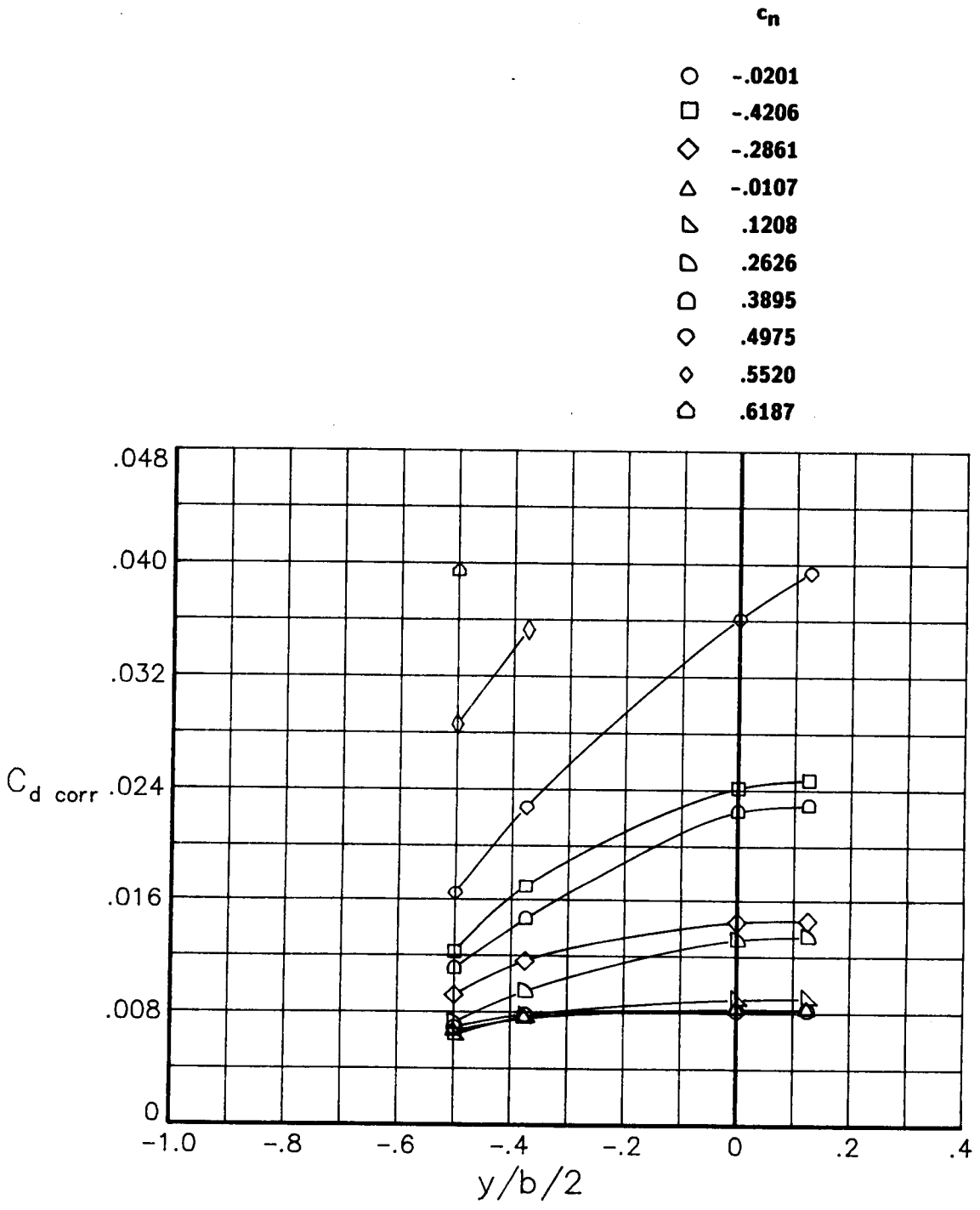

(a) R = 6.0 x 10^6

Figure 8.- Effects of normal force coefficient on the spanwise variation of drag coefficient for various Reynolds numbers at a Mach number of 0.76. Transition free.

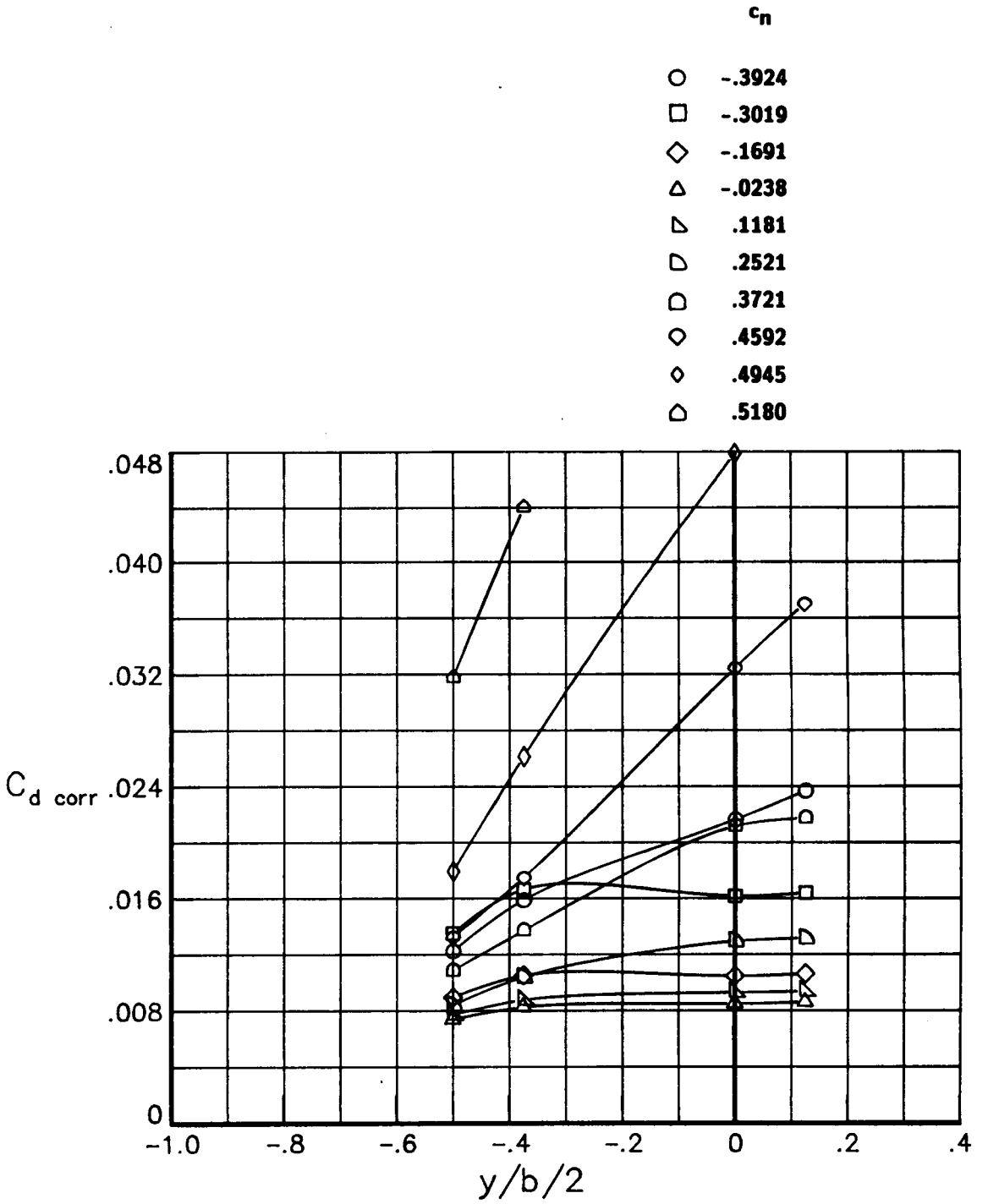

(b) $R = 9.0 \times 10^6$

Figure 8.- Continued.

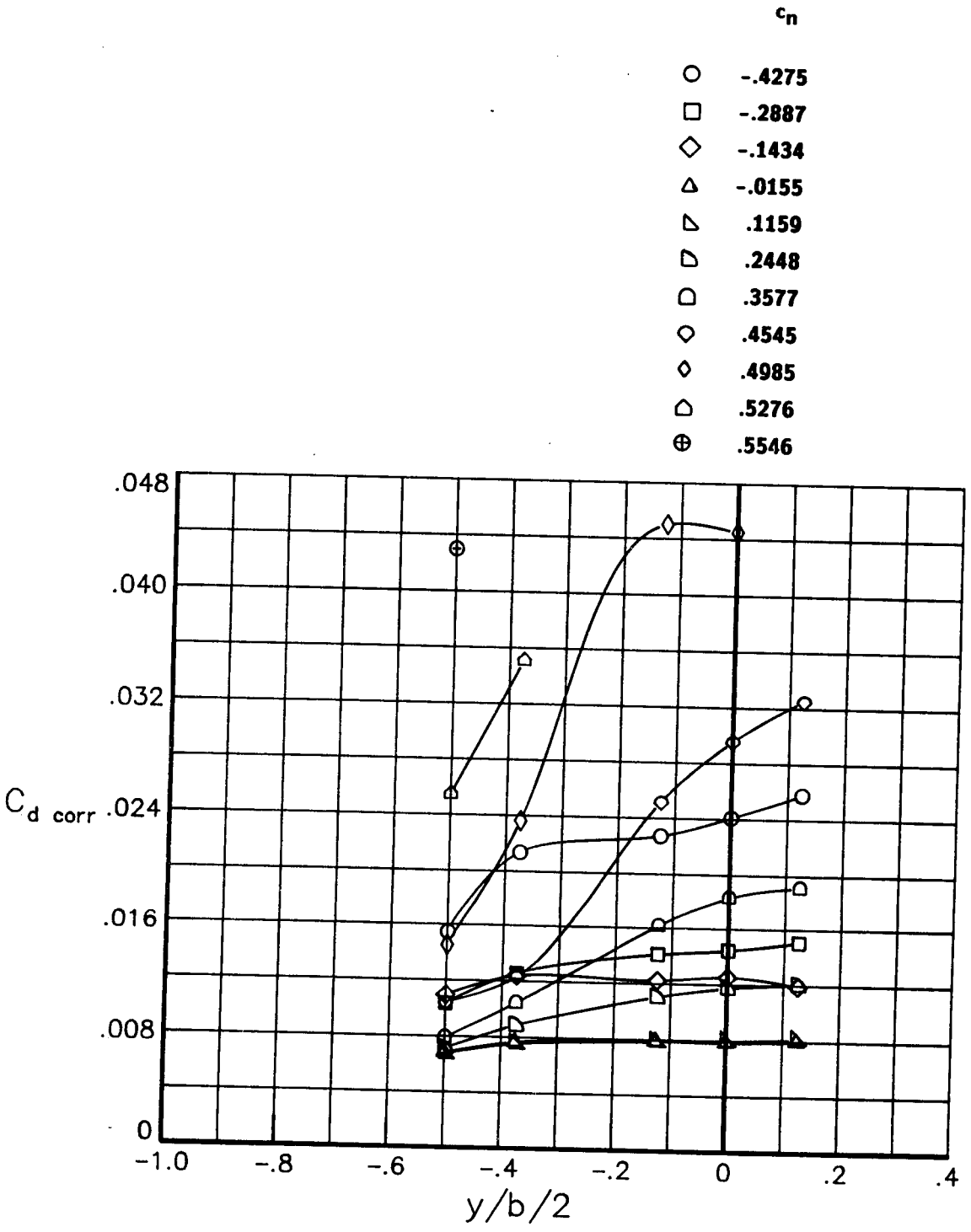

(c) R = 15.0 x 10^6

Figure 8.- Continued.

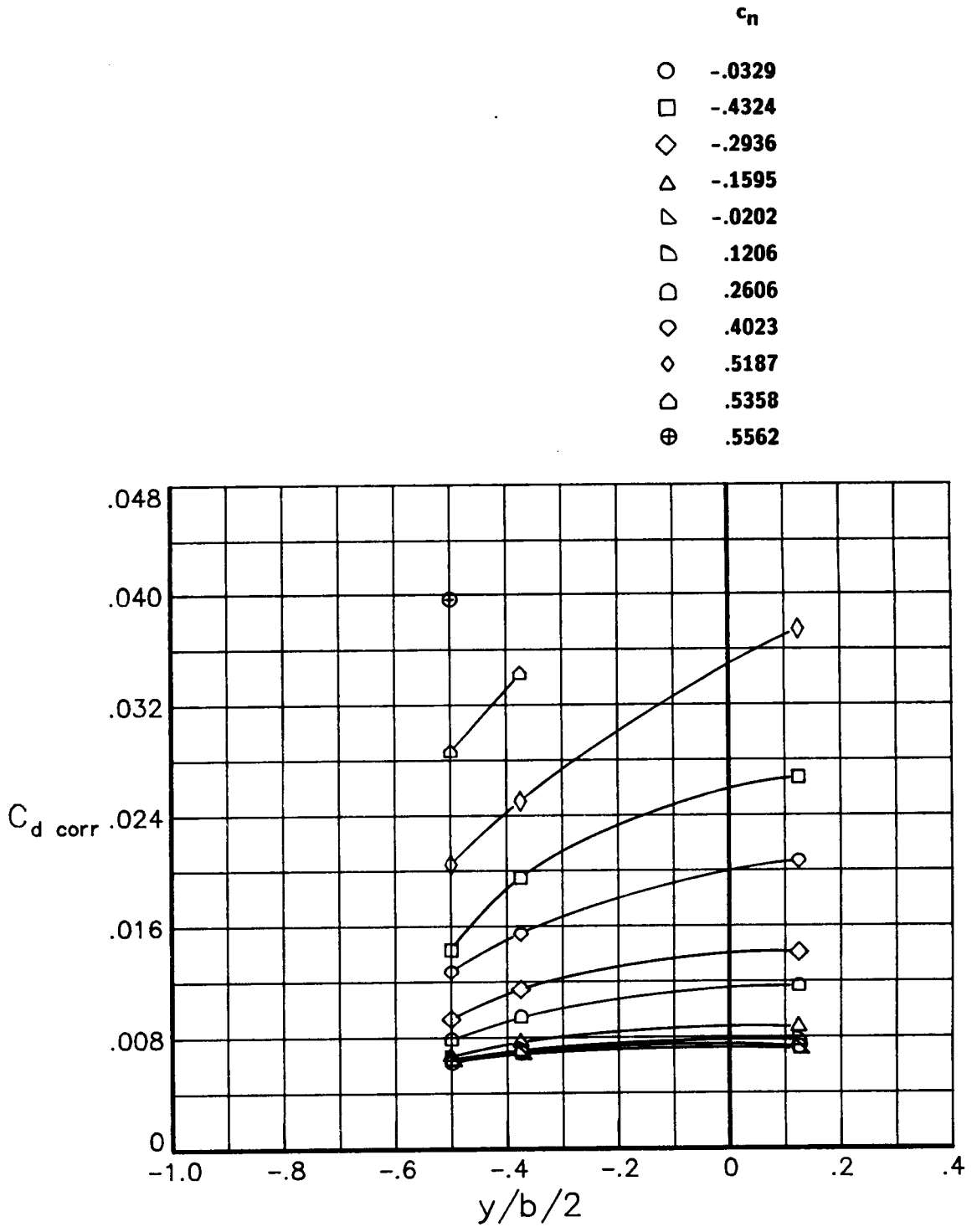

(d) R = 30.0 x 10^6

Figure 8.- Continued.

28

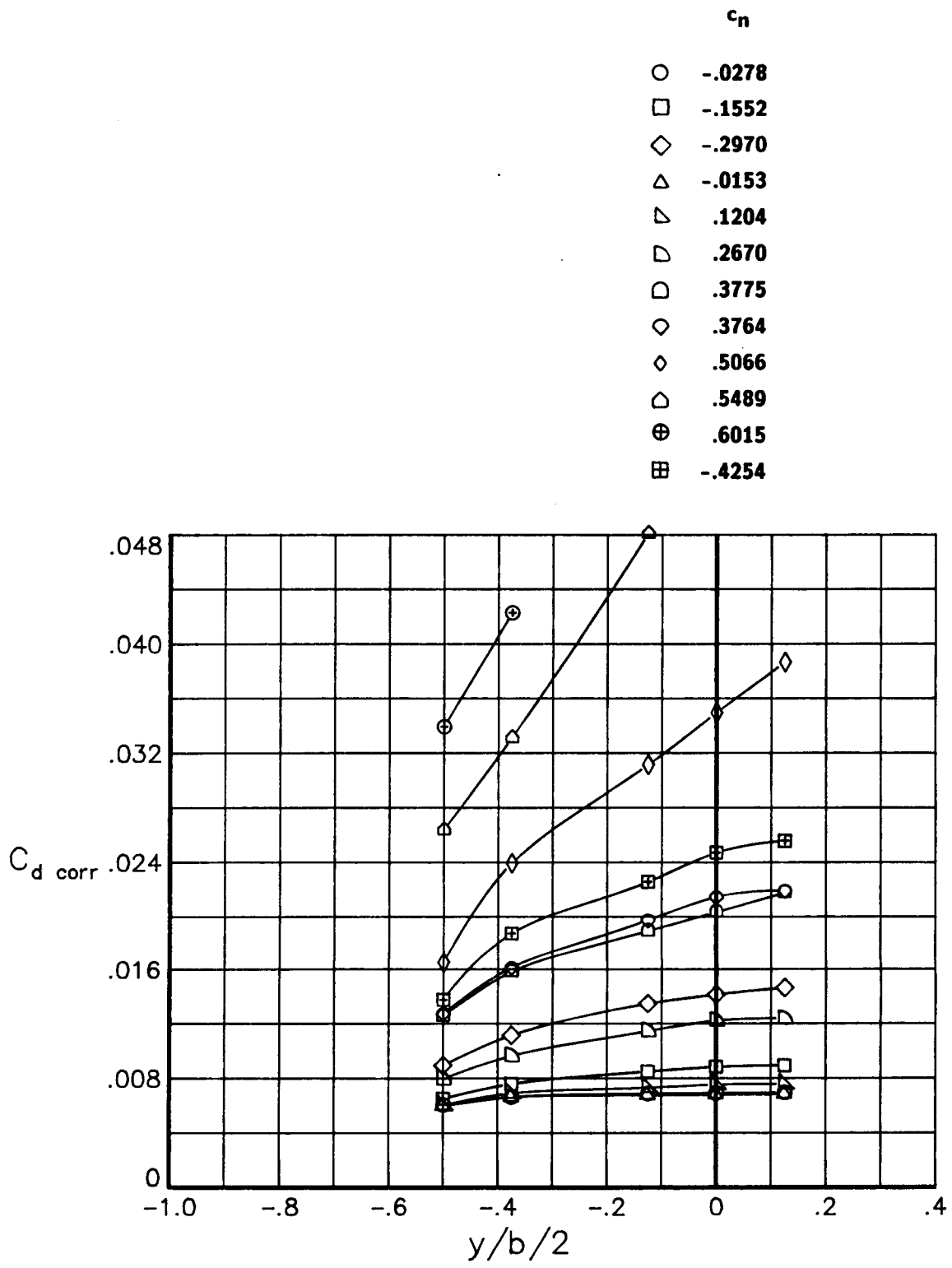

(e) R = 45.0 x 10^6

Figure 8.- Concluded.

52

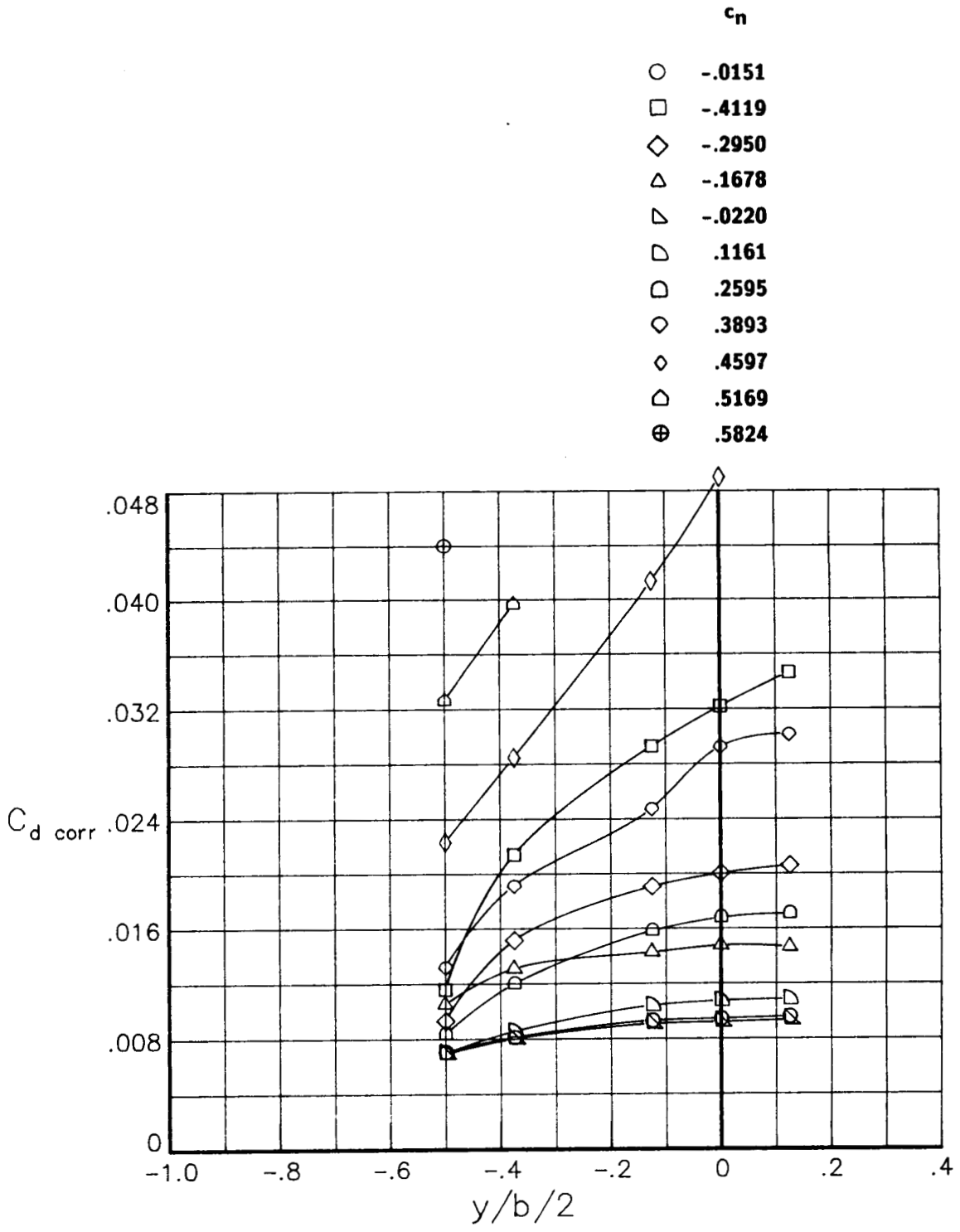

(a) R = 6.0 x 10^6

Figure 9.- Effects of normal force coefficient on the spanwise variation of drag coefficient for various Reynolds numbers at a Mach number of 0.78. Transition free.

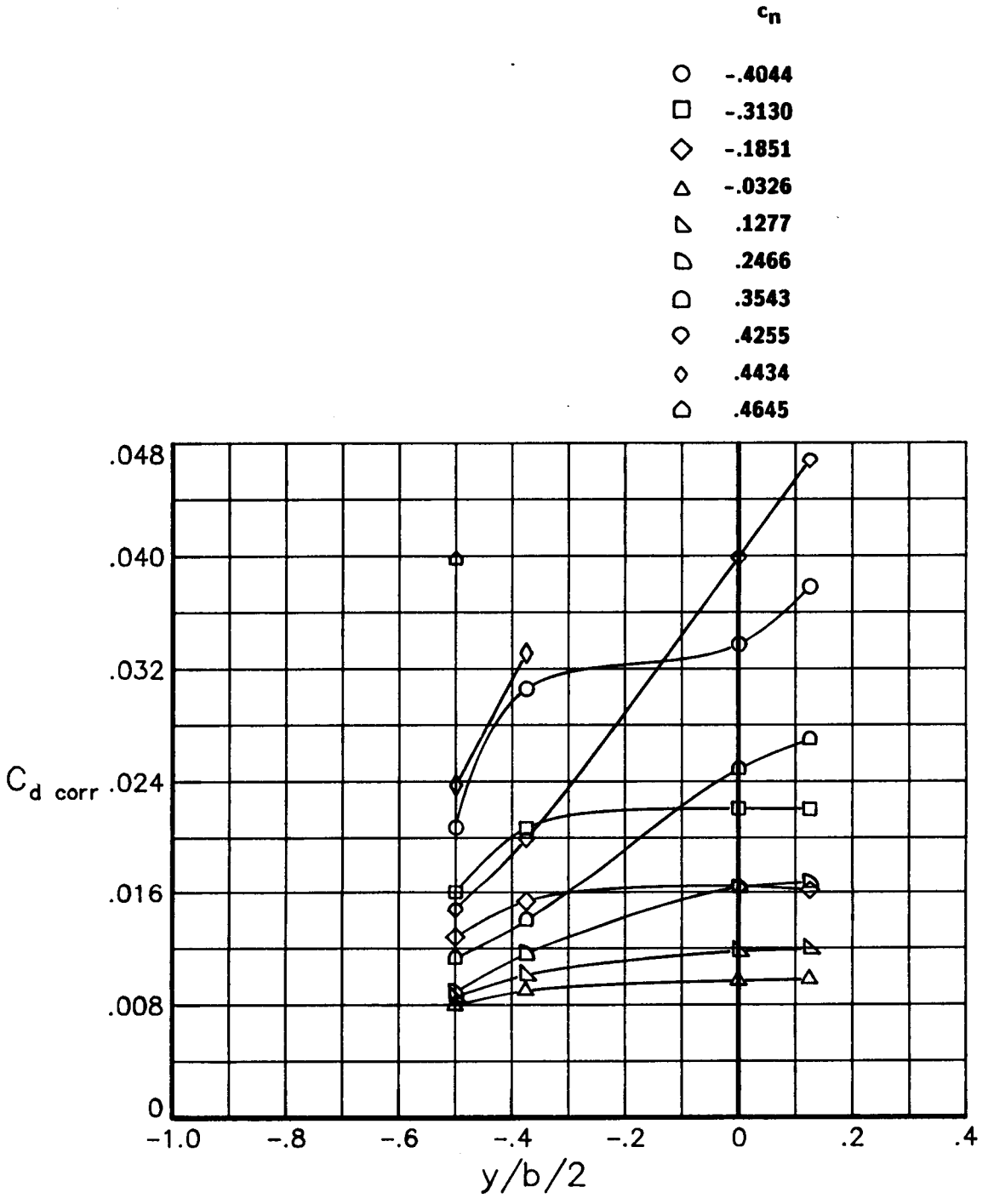

(b) R = 9.0 x 10^6

Figure 9.- Continued.

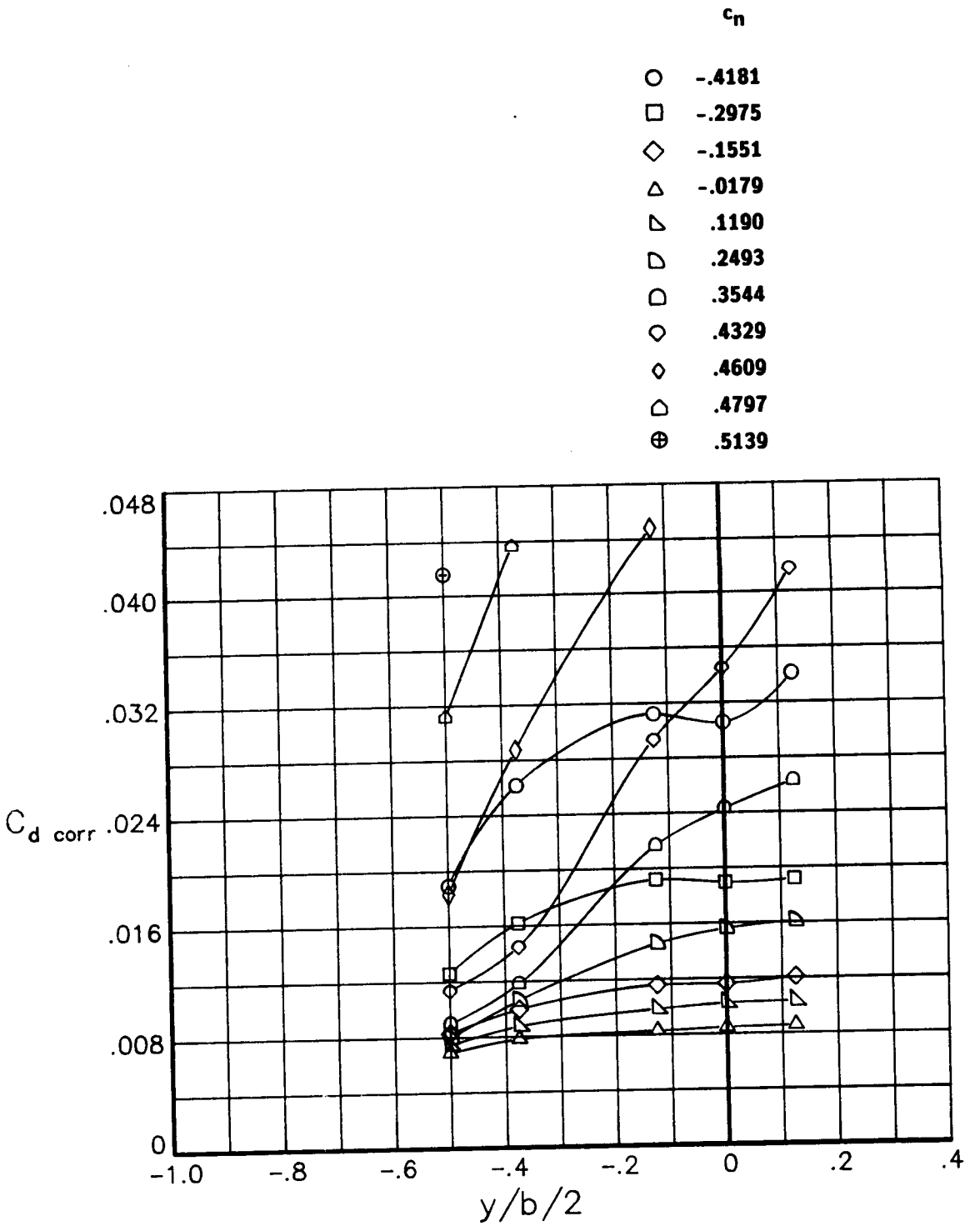

(c) R = 15.0 x 10^6

Figure 9.- Continued.

39

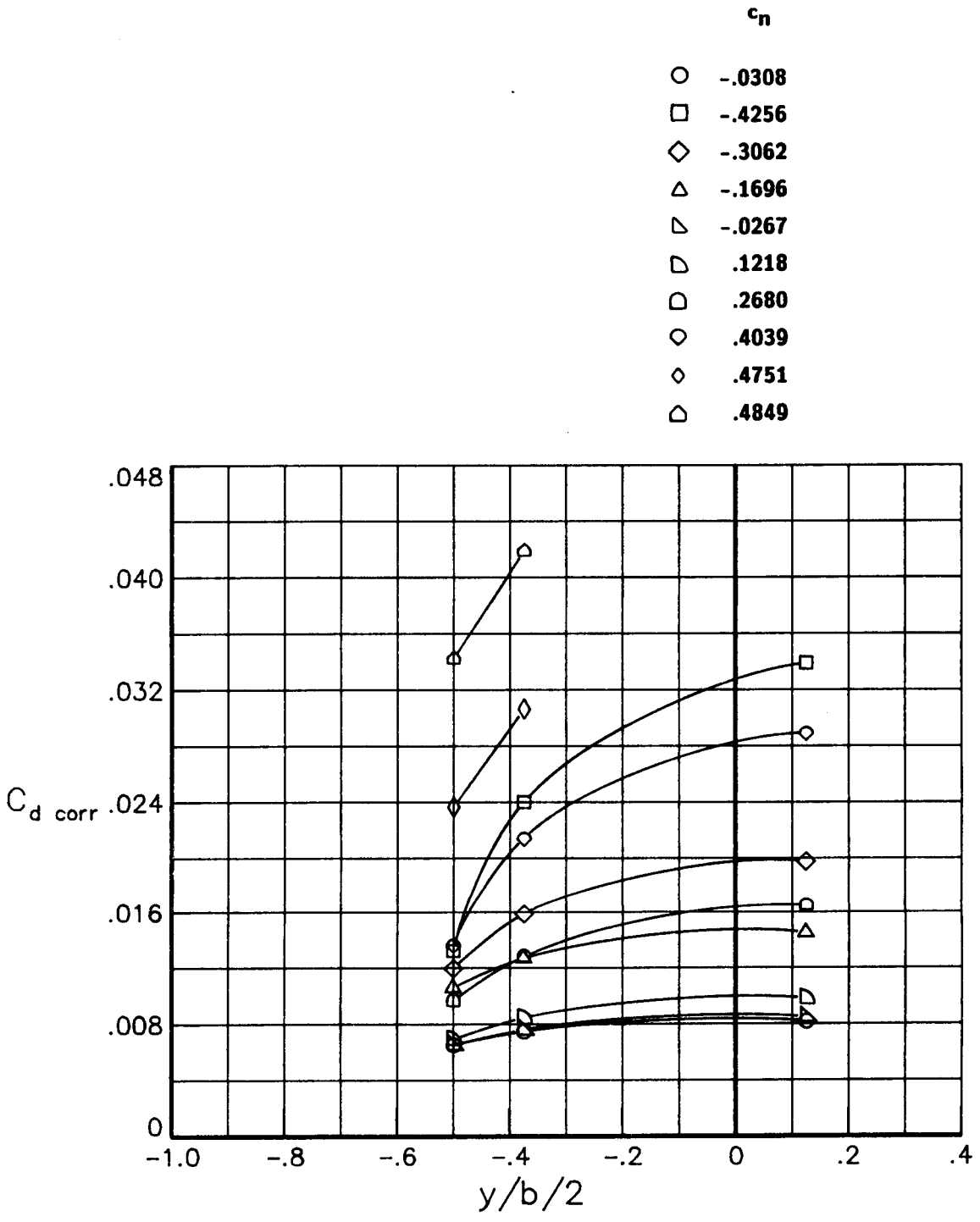

(d) R = 30.0 x 10^6

Figure 9.- Continued.

29

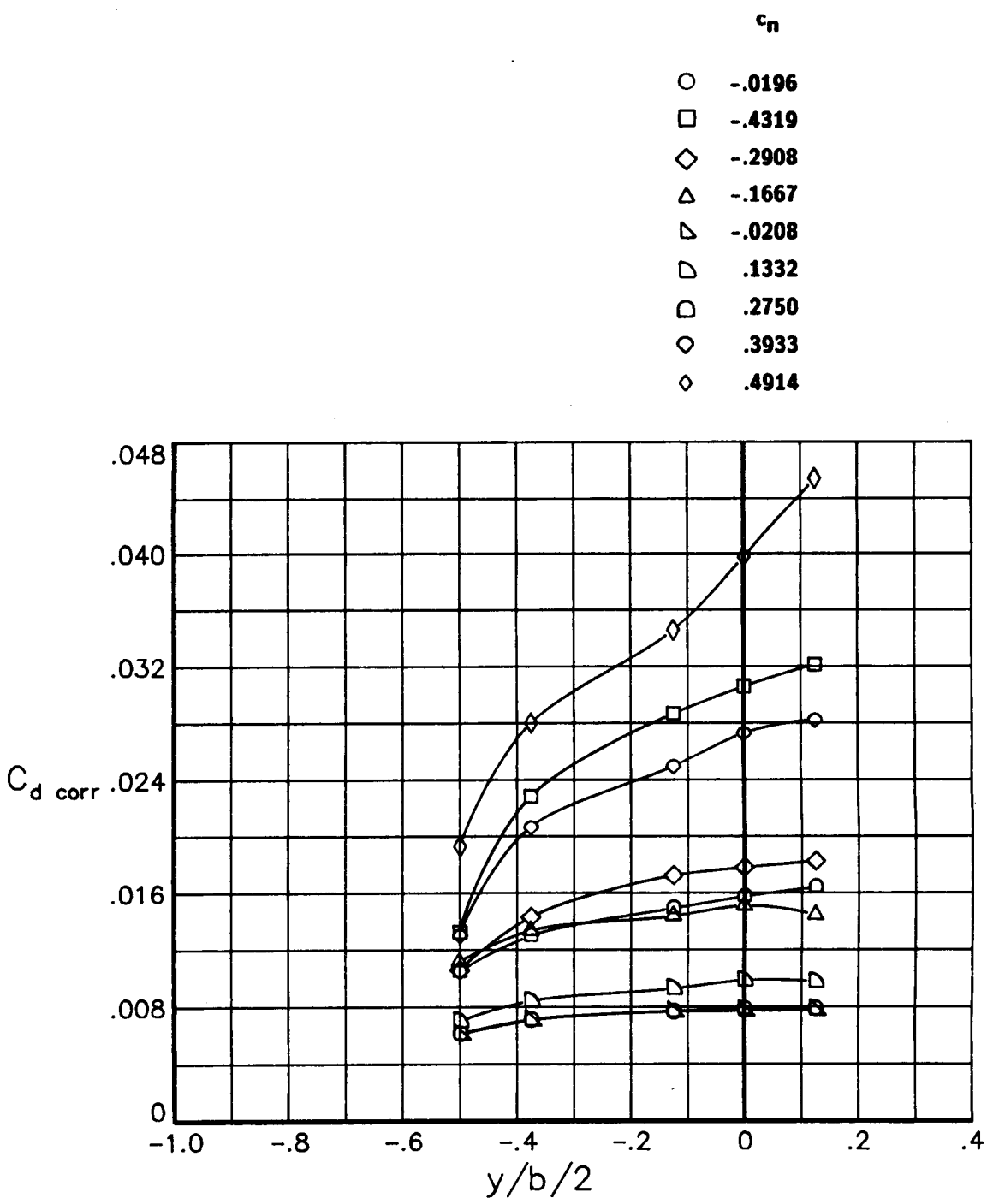

(e) R = 45.0 x 10^6

Figure 9.- Concluded.

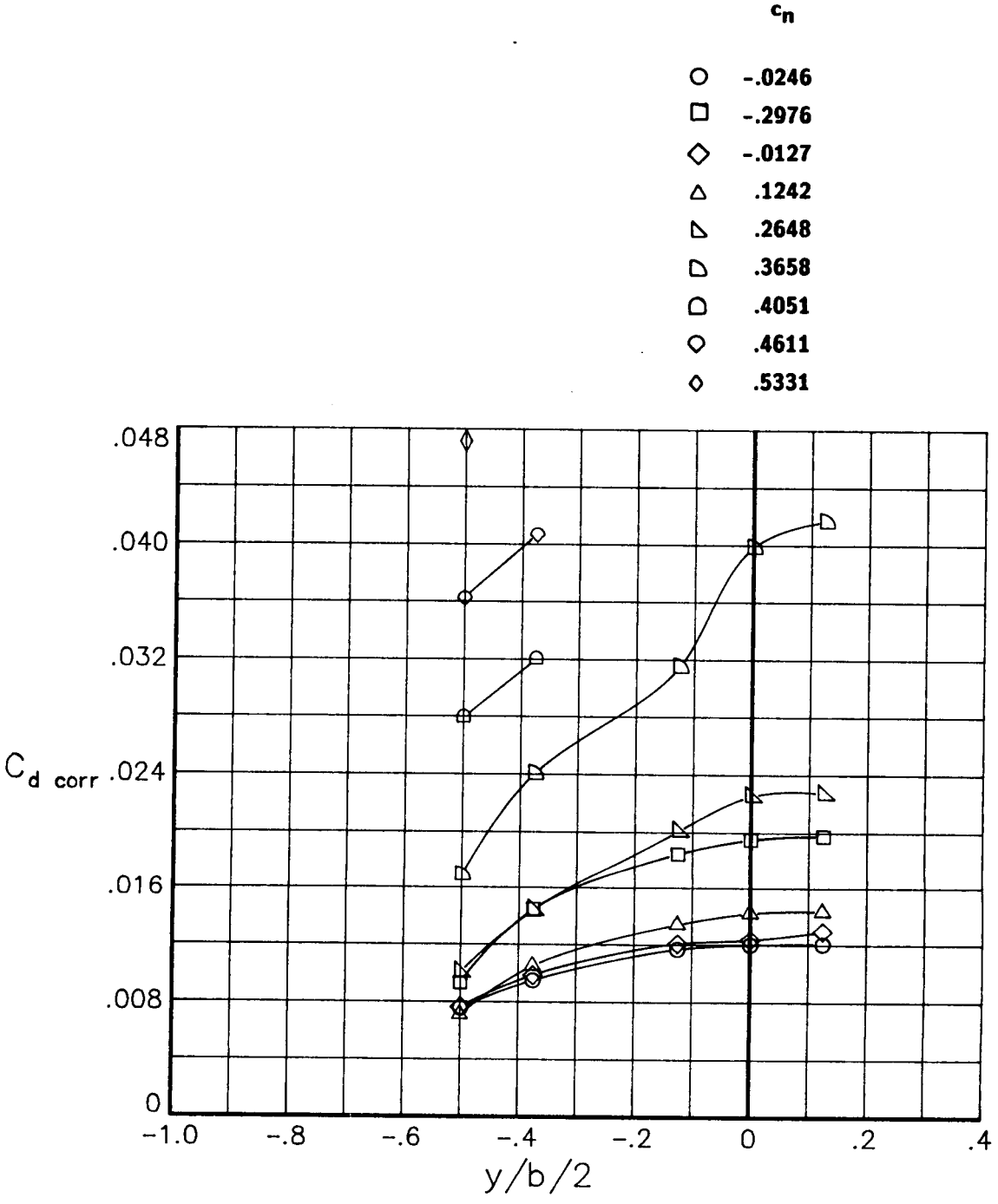

(a) $R = 6.0 \times 10^6$

Figure 10.- Effects of normal force coefficient on the spanwise variation of drag coefficient for various Reynolds numbers at a Mach number of 0.80. Transition free.

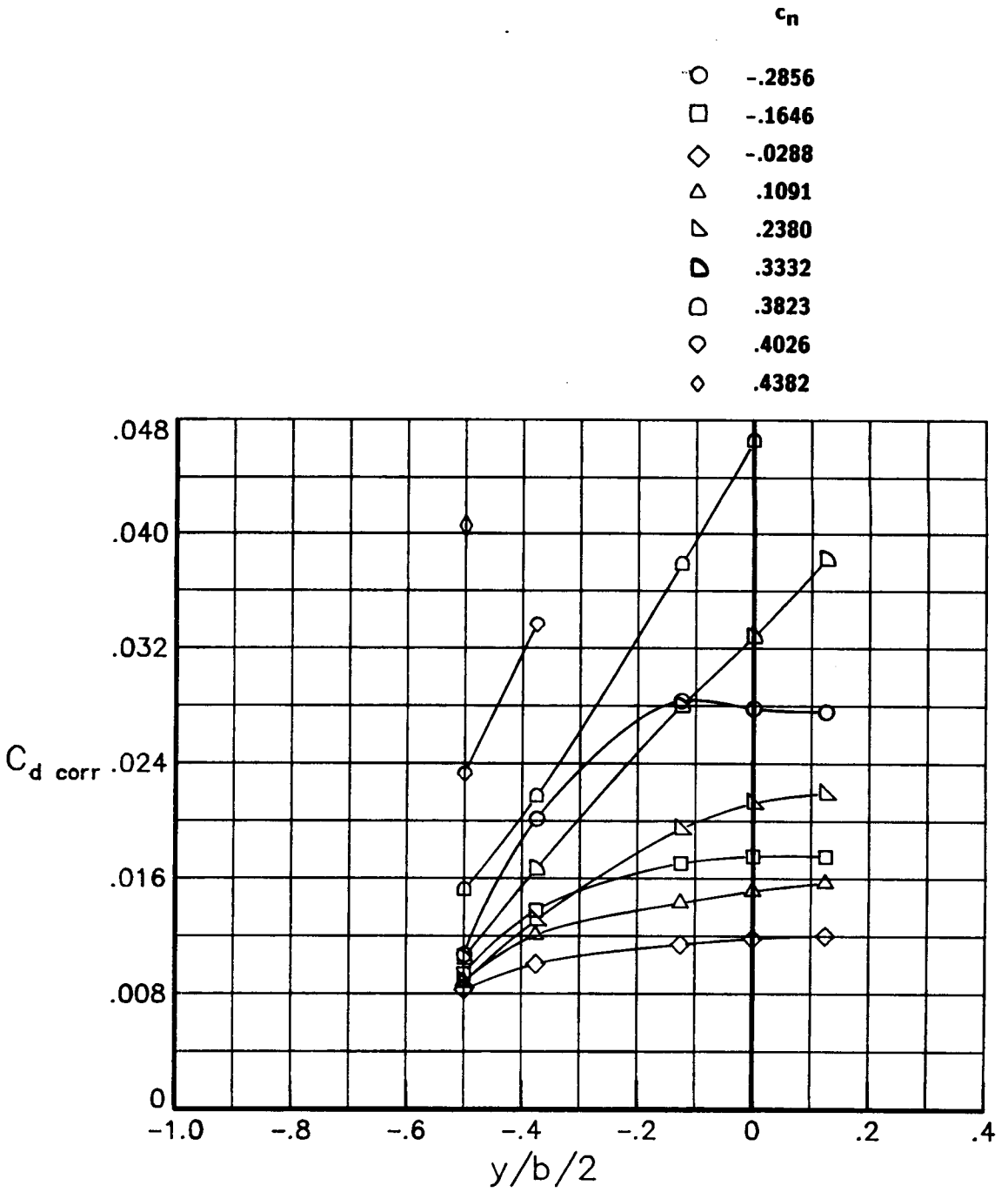

(b) $R = 9.0 \times 10^6$

Figure 10.- Continued.

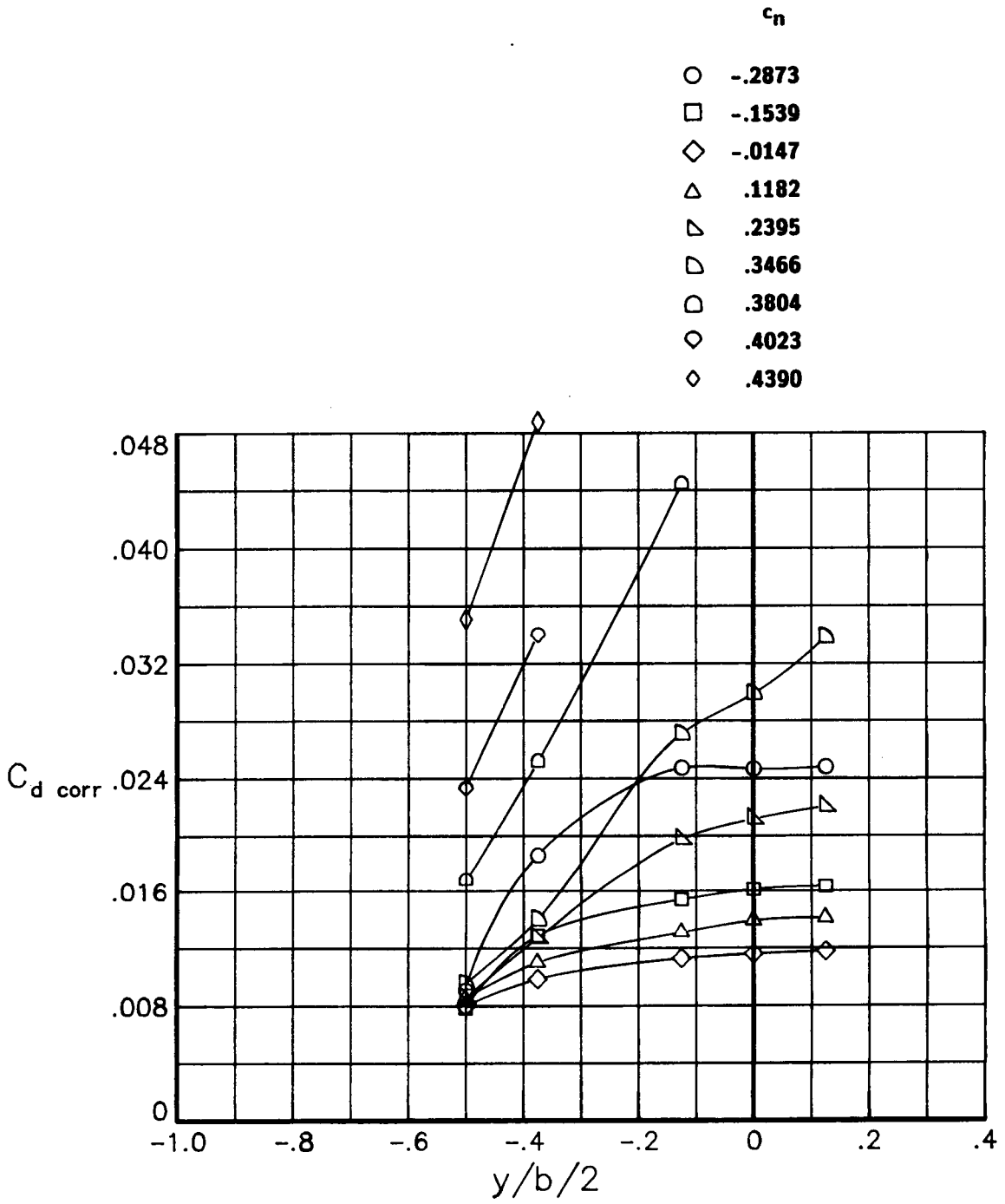

(c) R = 15.0 x 10^6

Figure 10.- Continued.

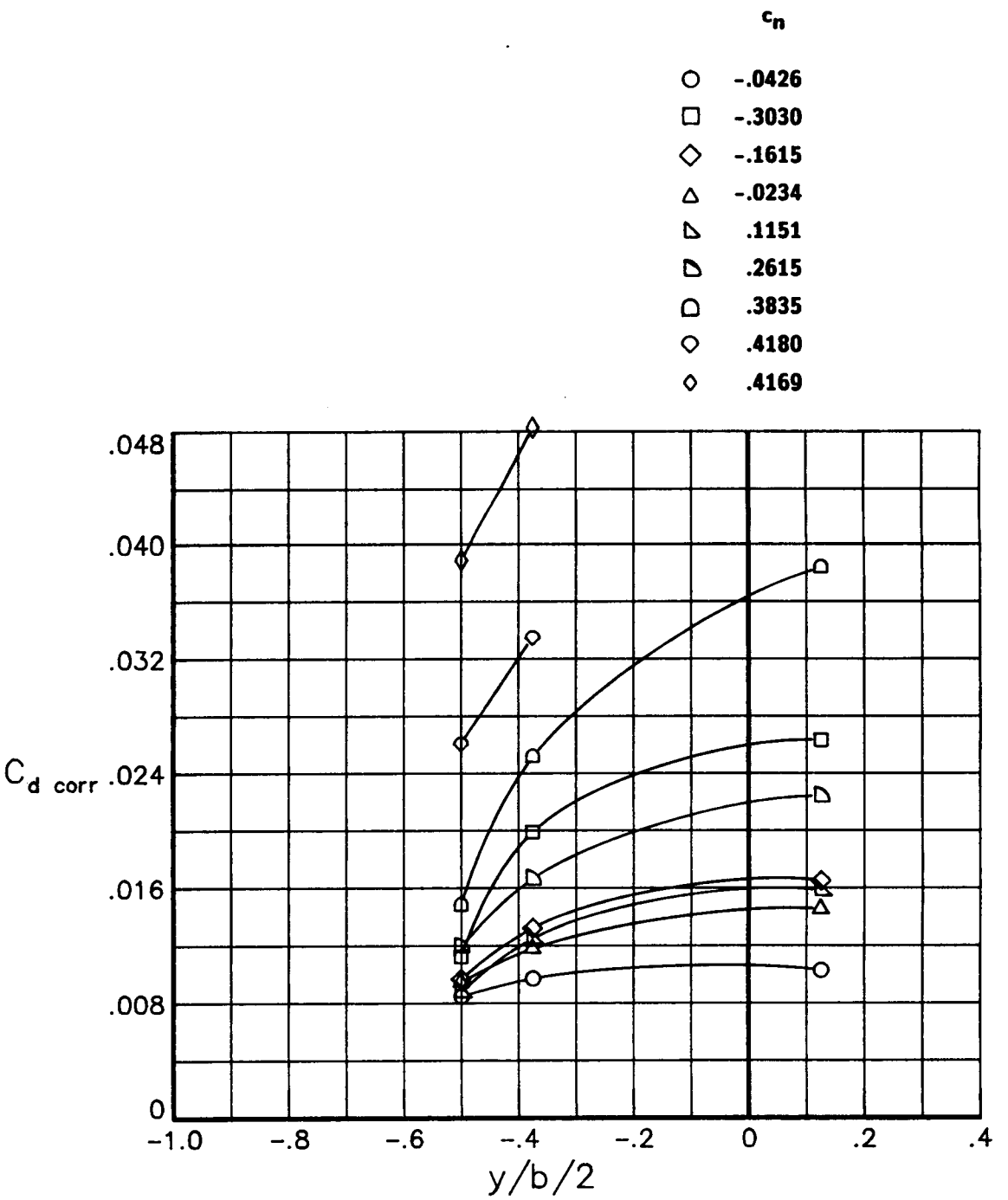

(d) $R = 30.0 \times 10^6$

Figure 10.- Continued.

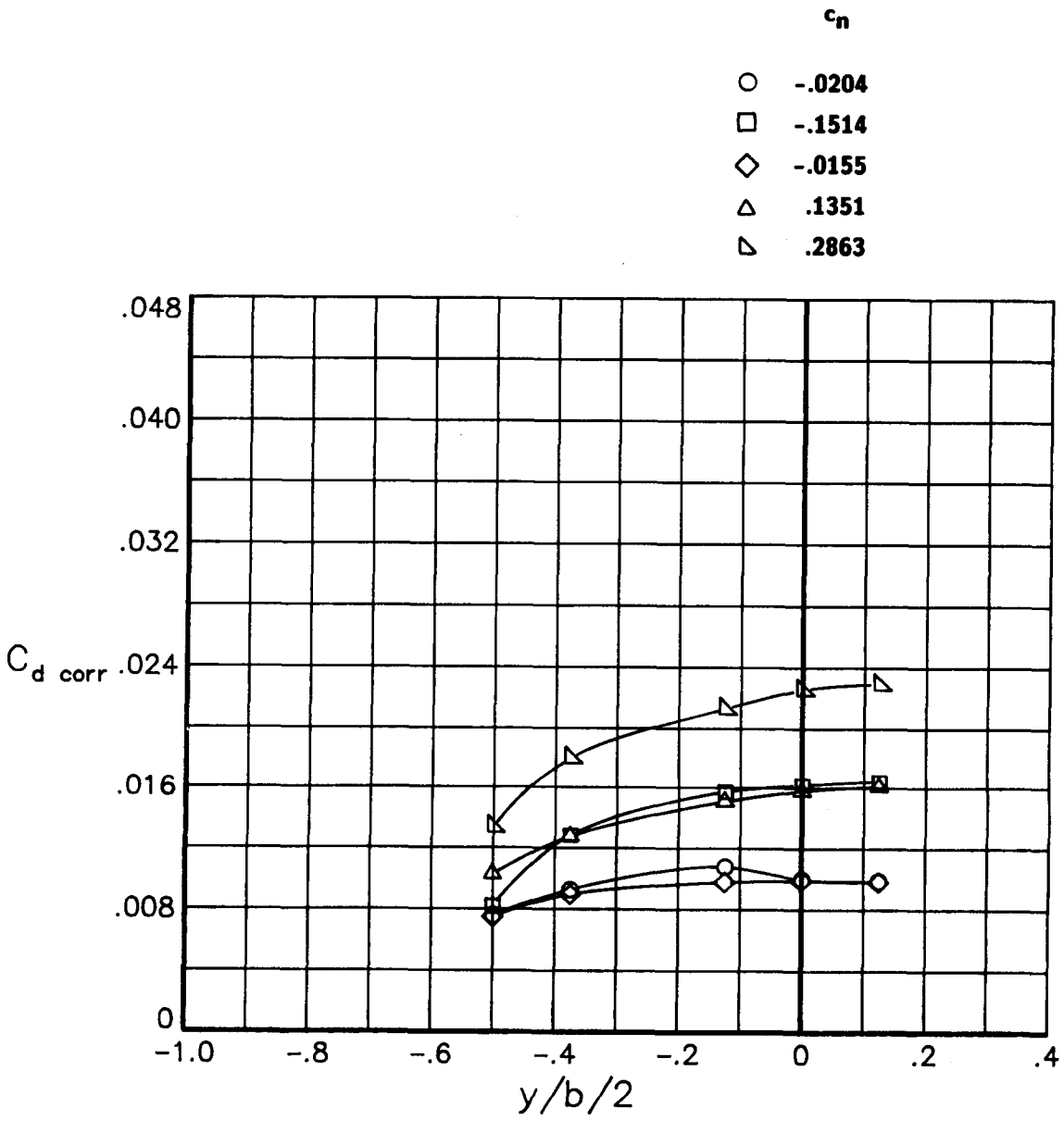

(e) R = 45.0 x 10^6

Figure 10.- Concluded.

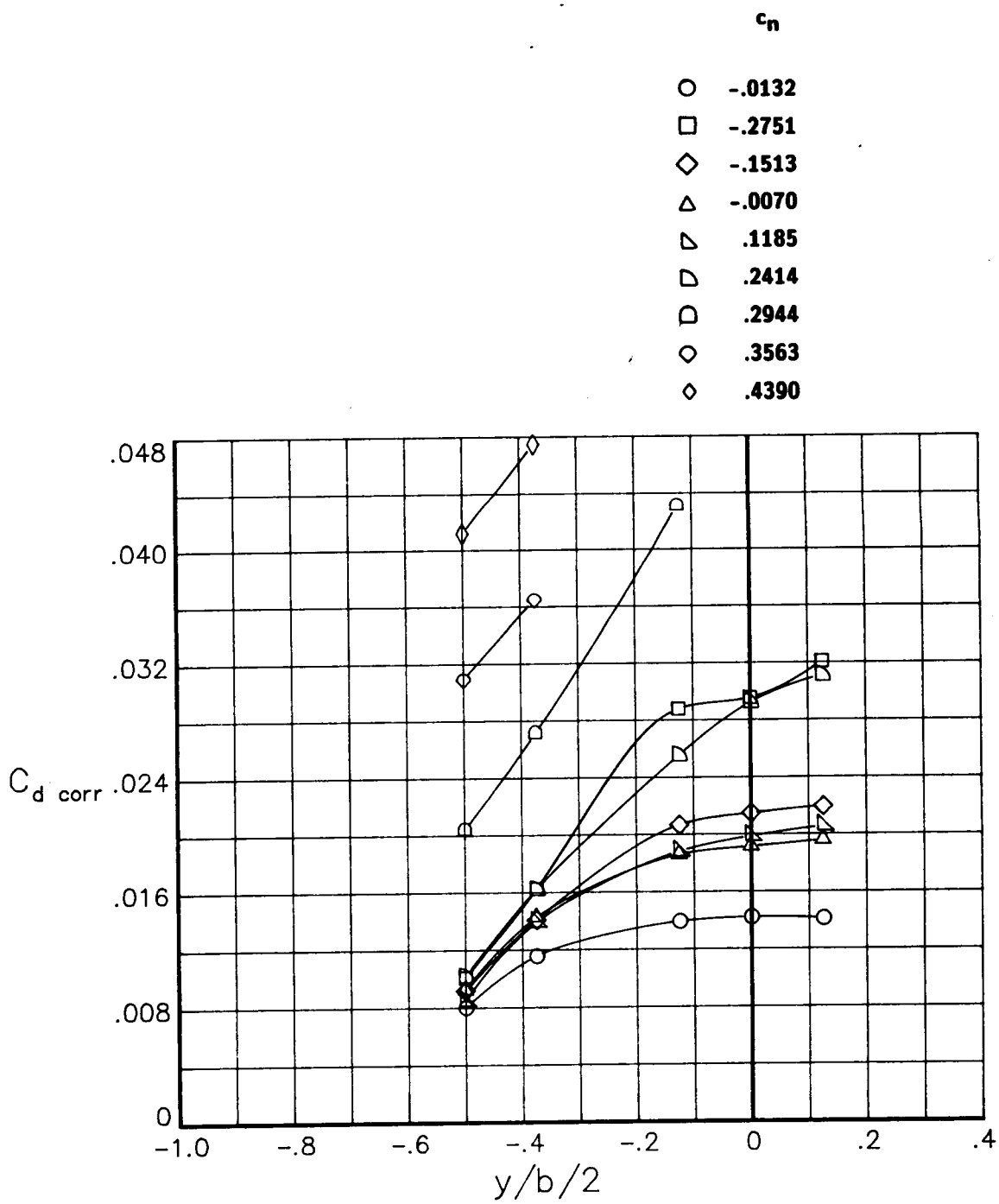

(a) $R = 6.0 \times 10^6$

Figure 11.- Effects of normal force coefficient on the spanwise variation of drag coefficient for various Reynolds numbers at a Mach number of 0.82. Transition free.

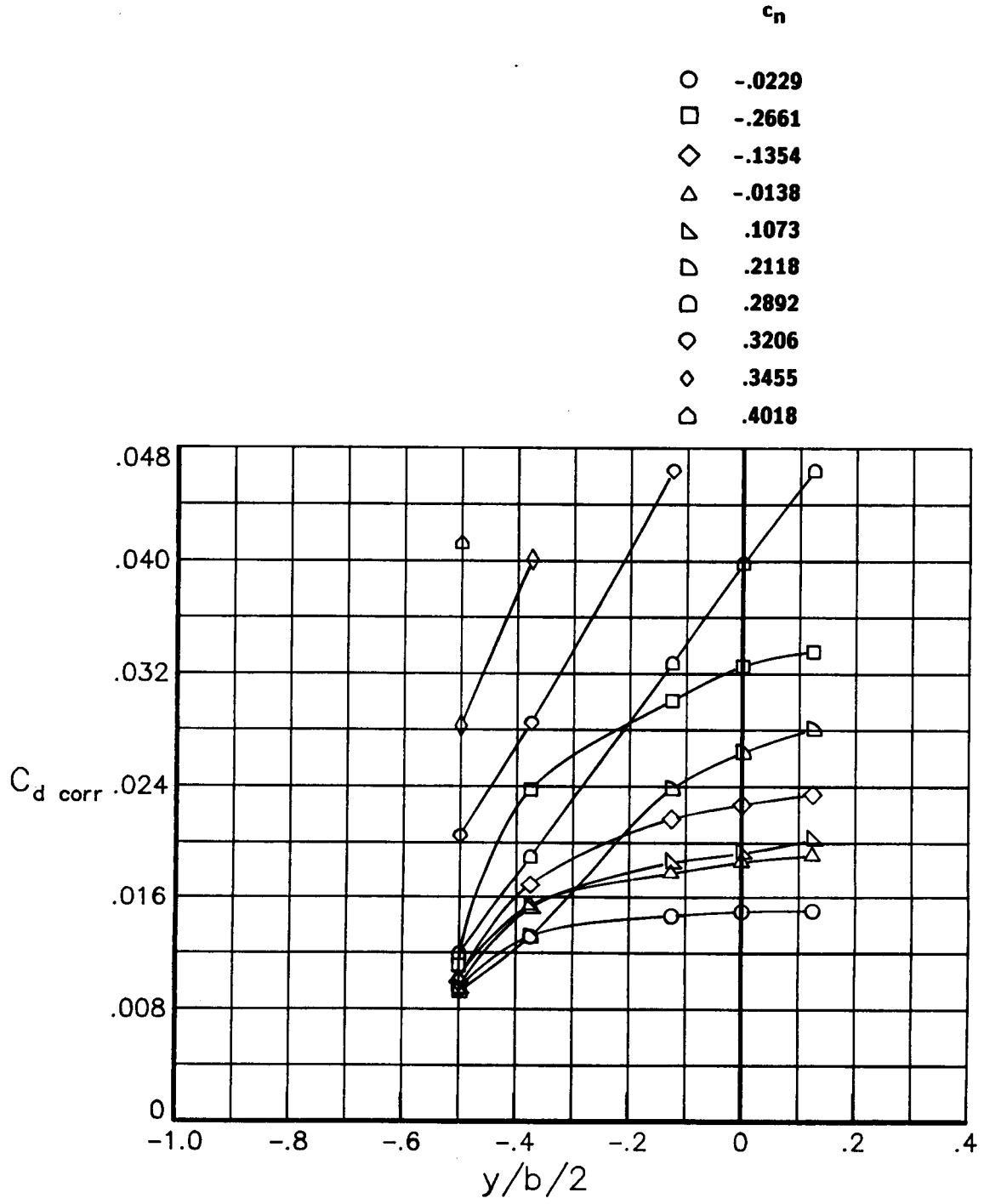

(b) R = 9.0 x 10^6

Figure 11.- Continued.

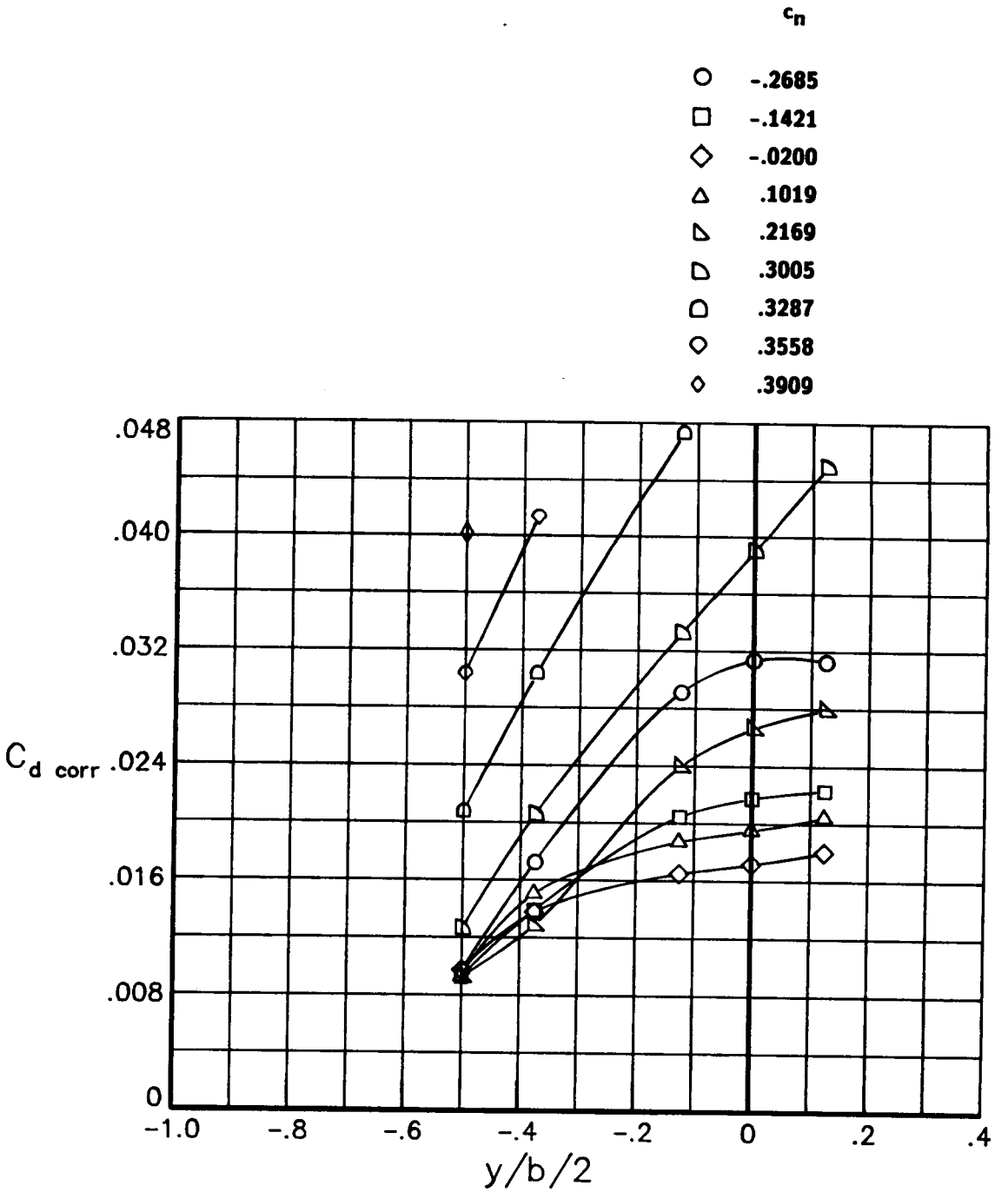

(c) R = 15.0 x 10^6

Figure 11.- Continued.

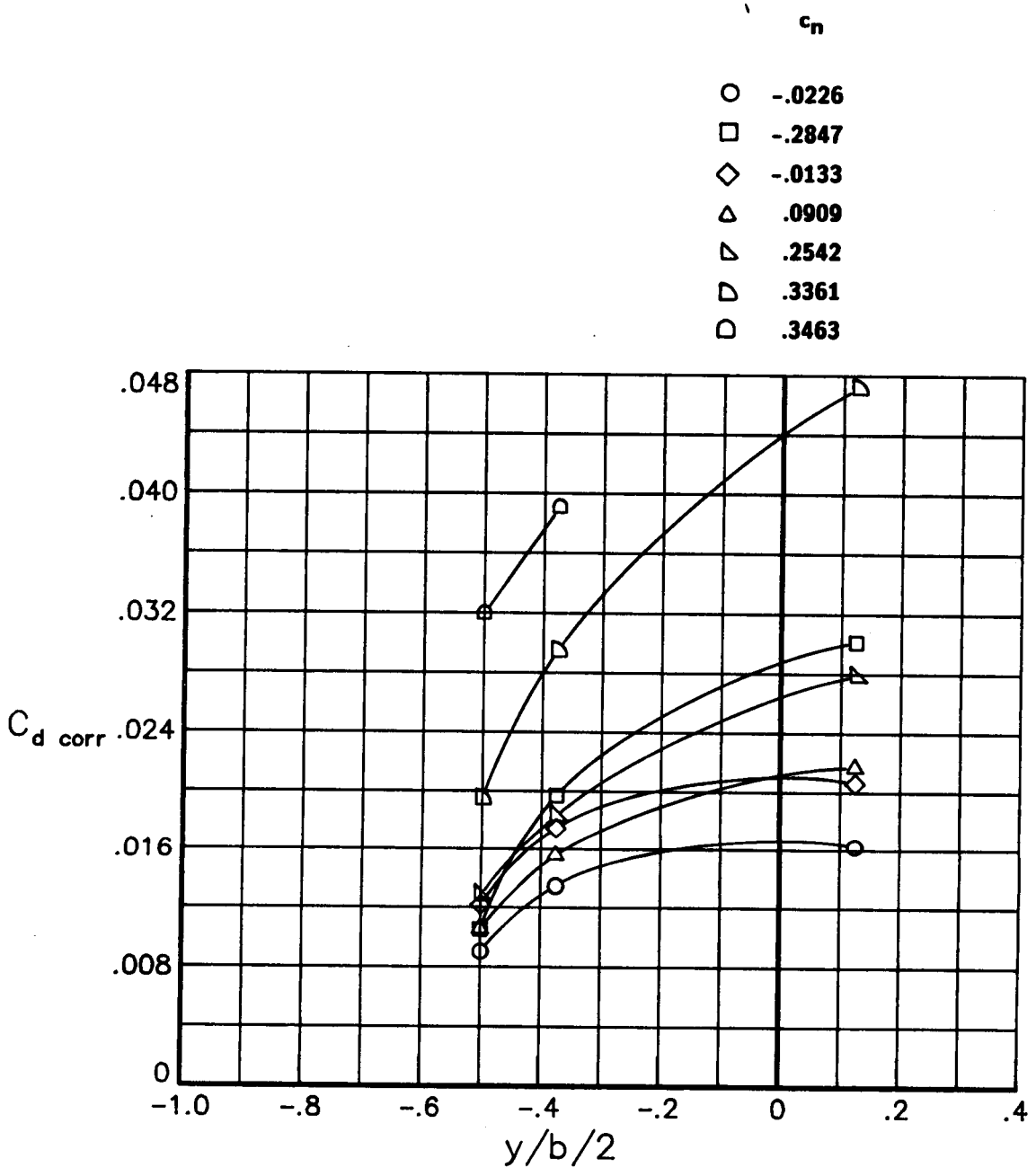

(d) R = 30.0 x 10^6

Figure 11.- Continued.

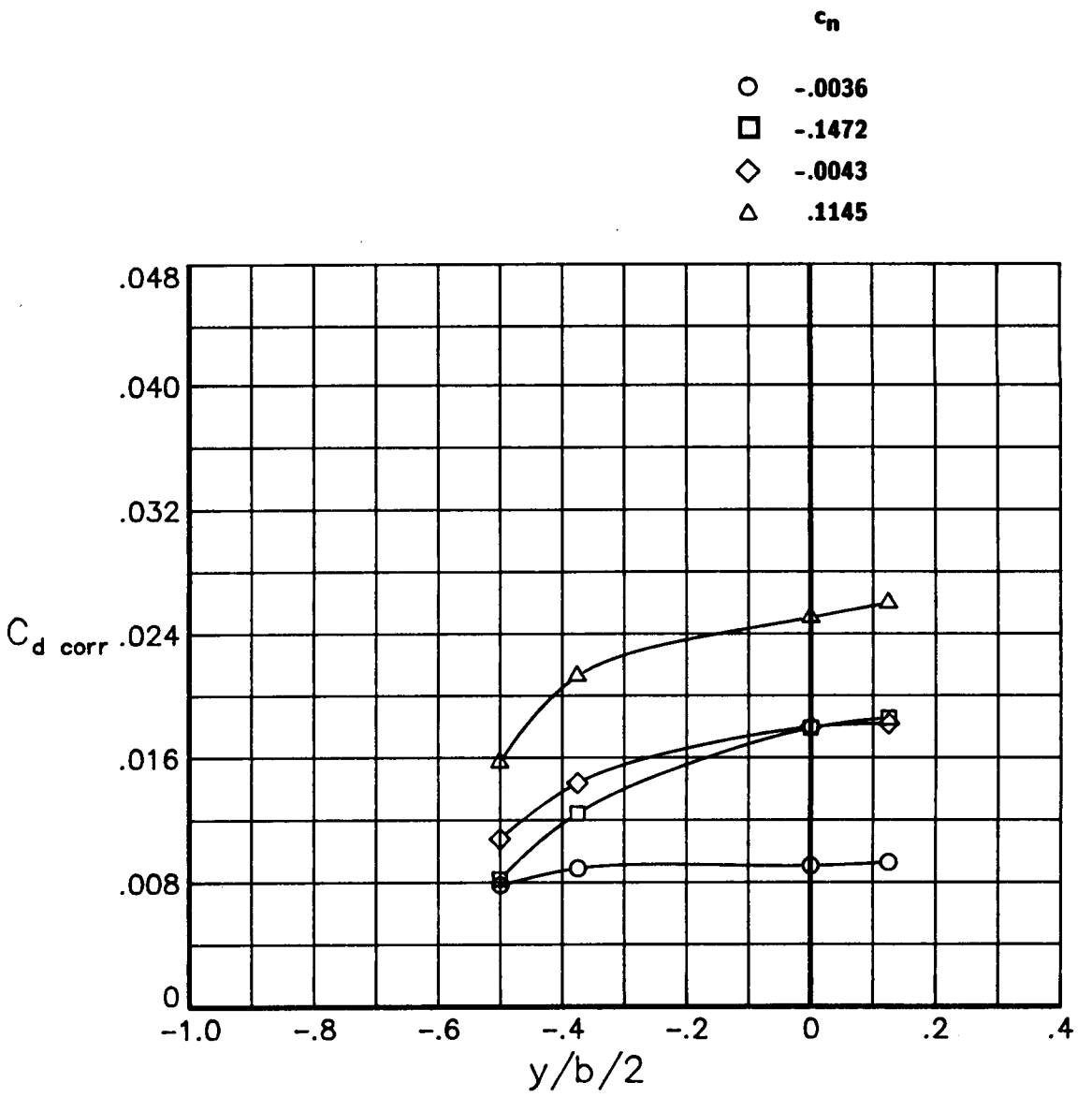

(e) R = 45.0 x 10^6

Figure 11.- Concluded.

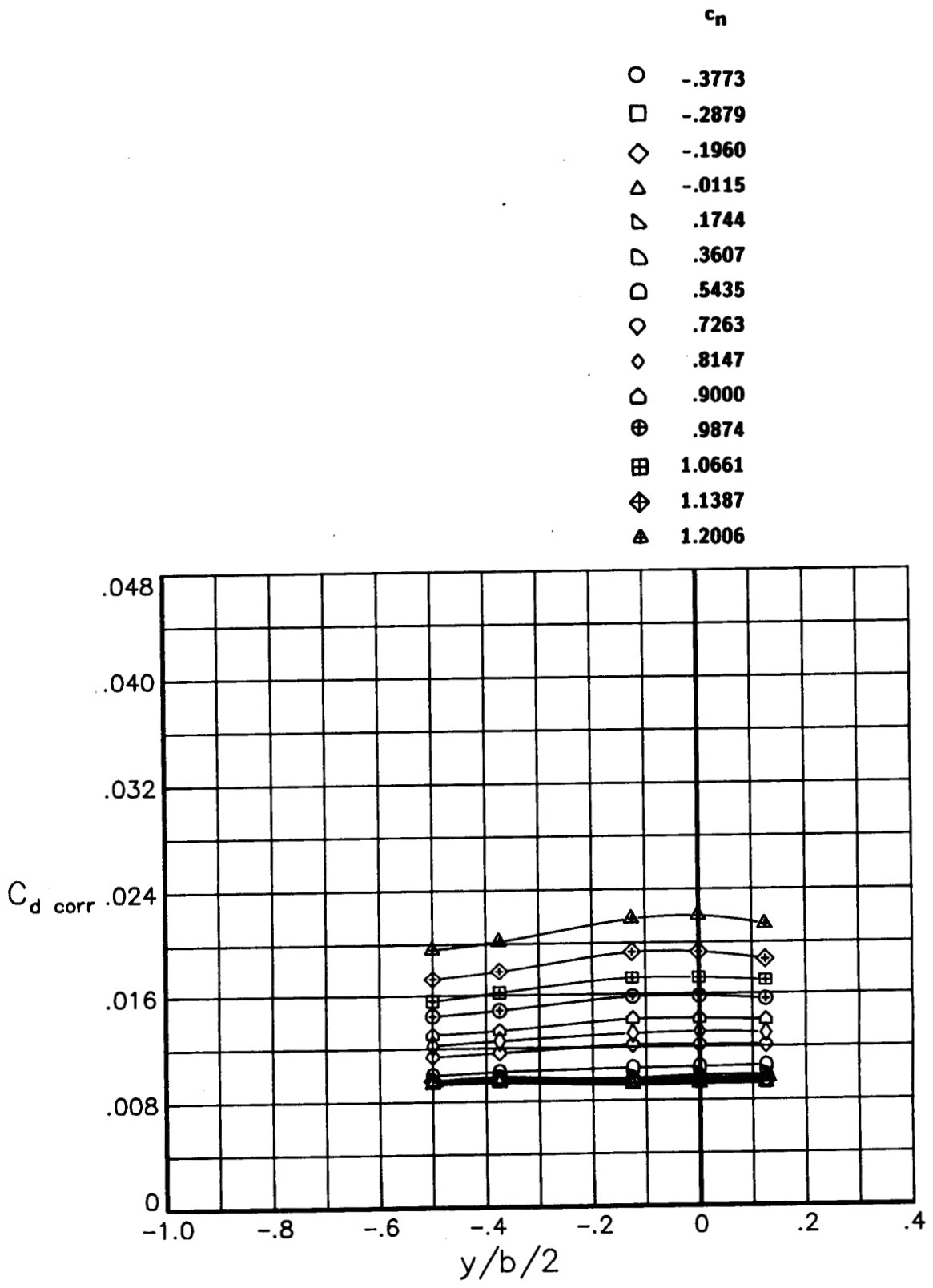

(a) R = 3.0 x 10^6

Figure 12.- Effects of normal force coefficient on the spanwise variation of drag coefficient for various Reynolds numbers at a Mach number of 0.30. Transition fixed.

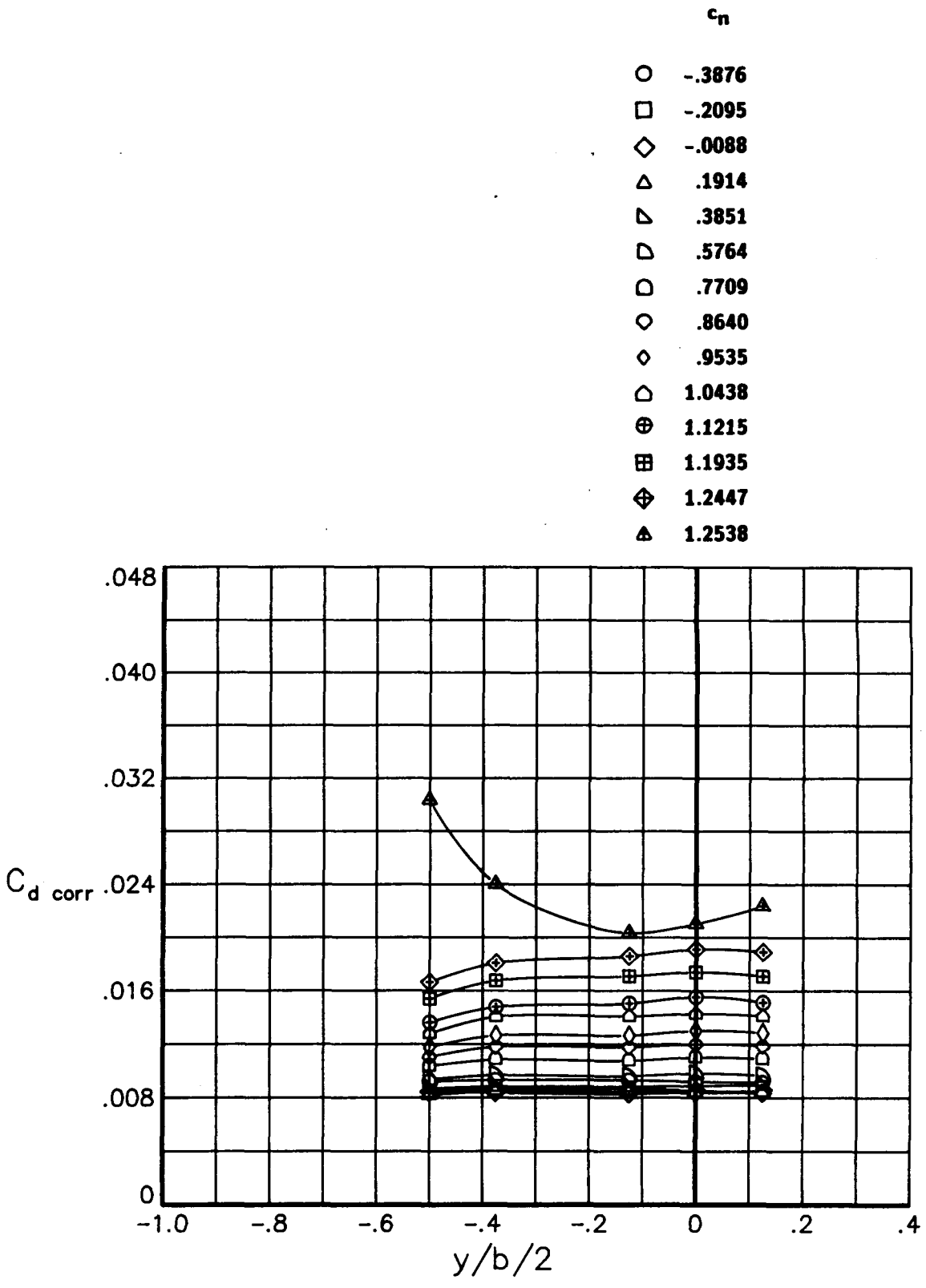

(b) R = 9.0 x 10^6

Figure 12.- Concluded.

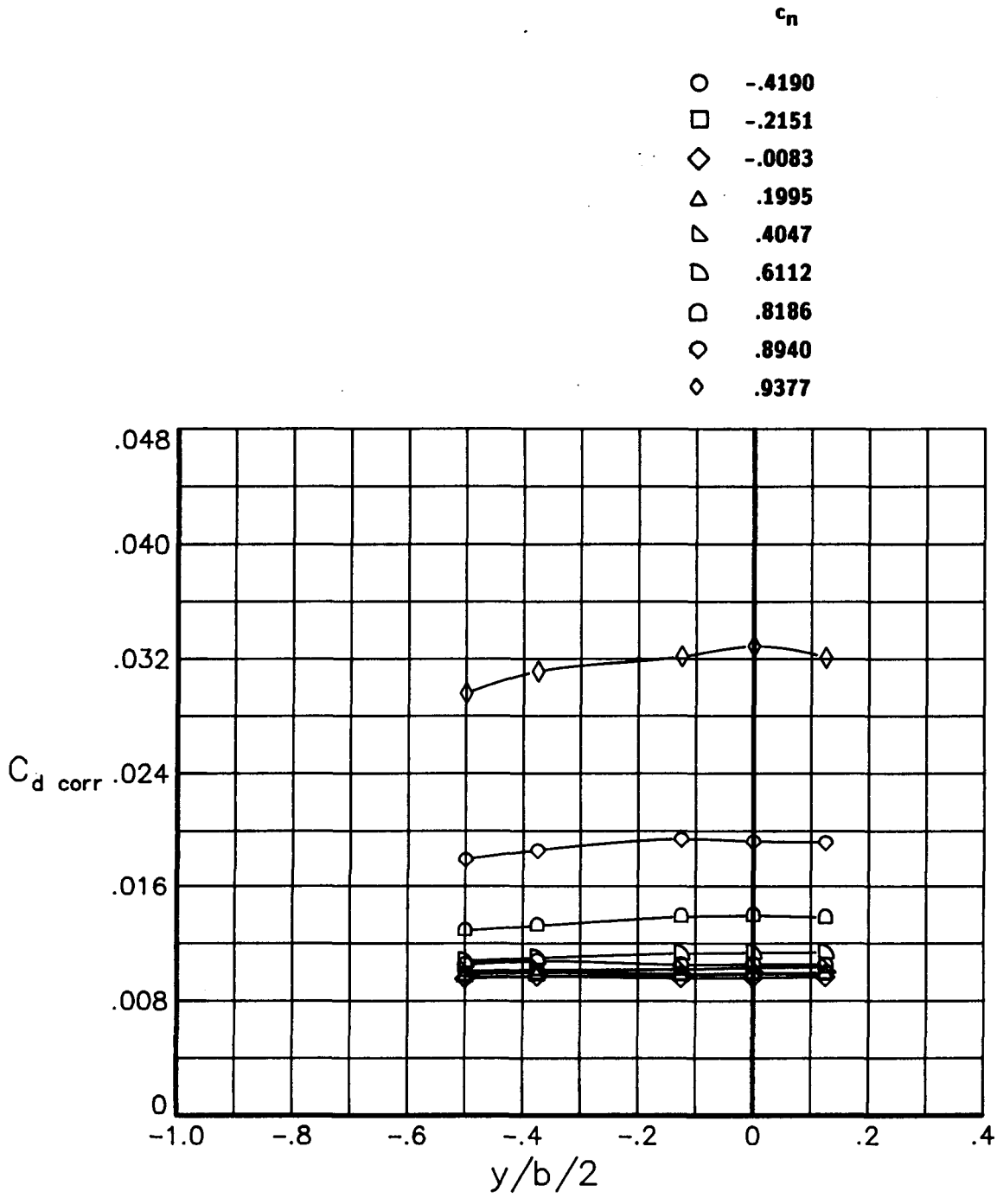

(a) $R = 3.0 \times 10^6$

Figure 13.- Effects of normal force coefficient on the spanwise variation of drag coefficient for various Reynolds numbers at a Mach number of 0.50. Transition fixed.

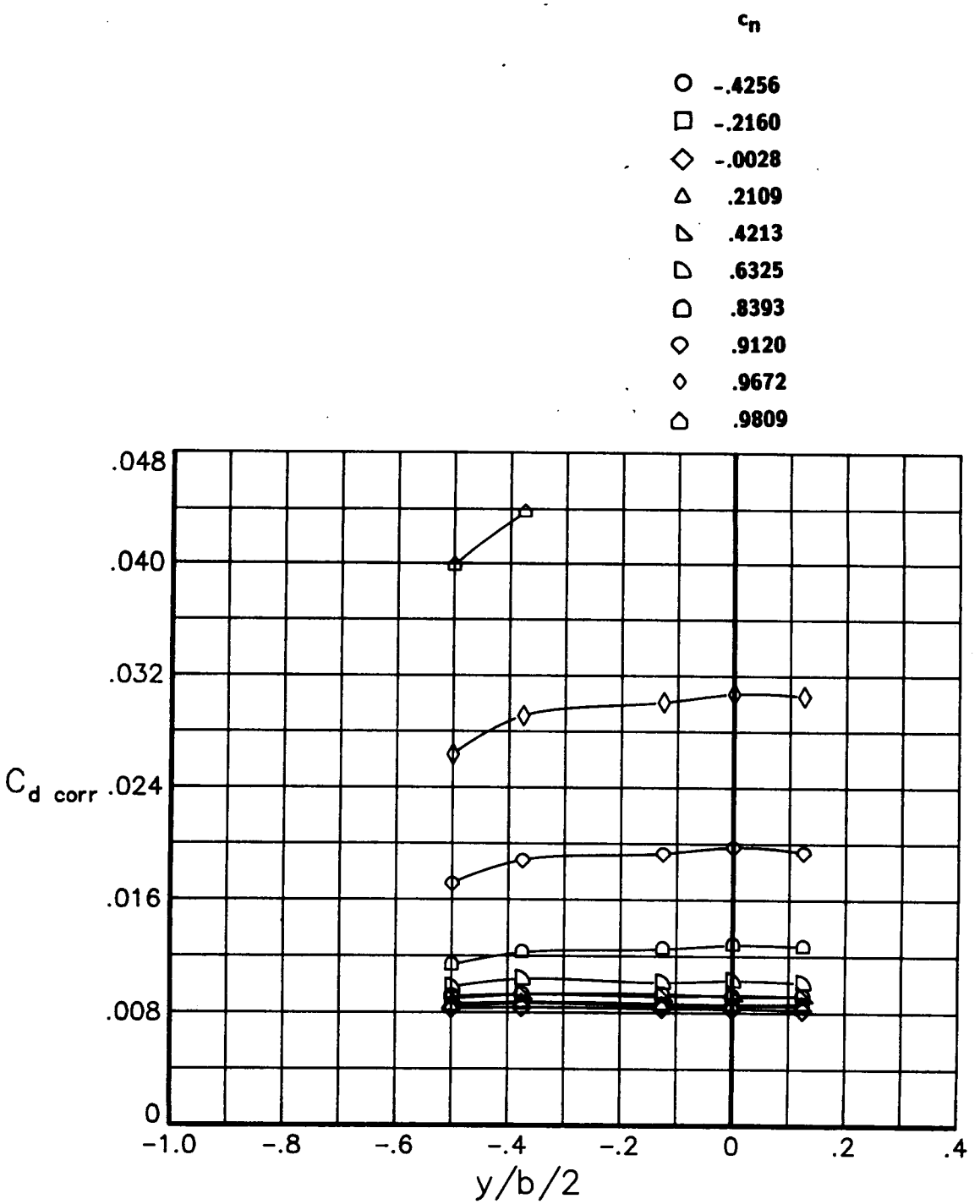

(b) R = 9.0 x 10^6

Figure 13.- Concluded.

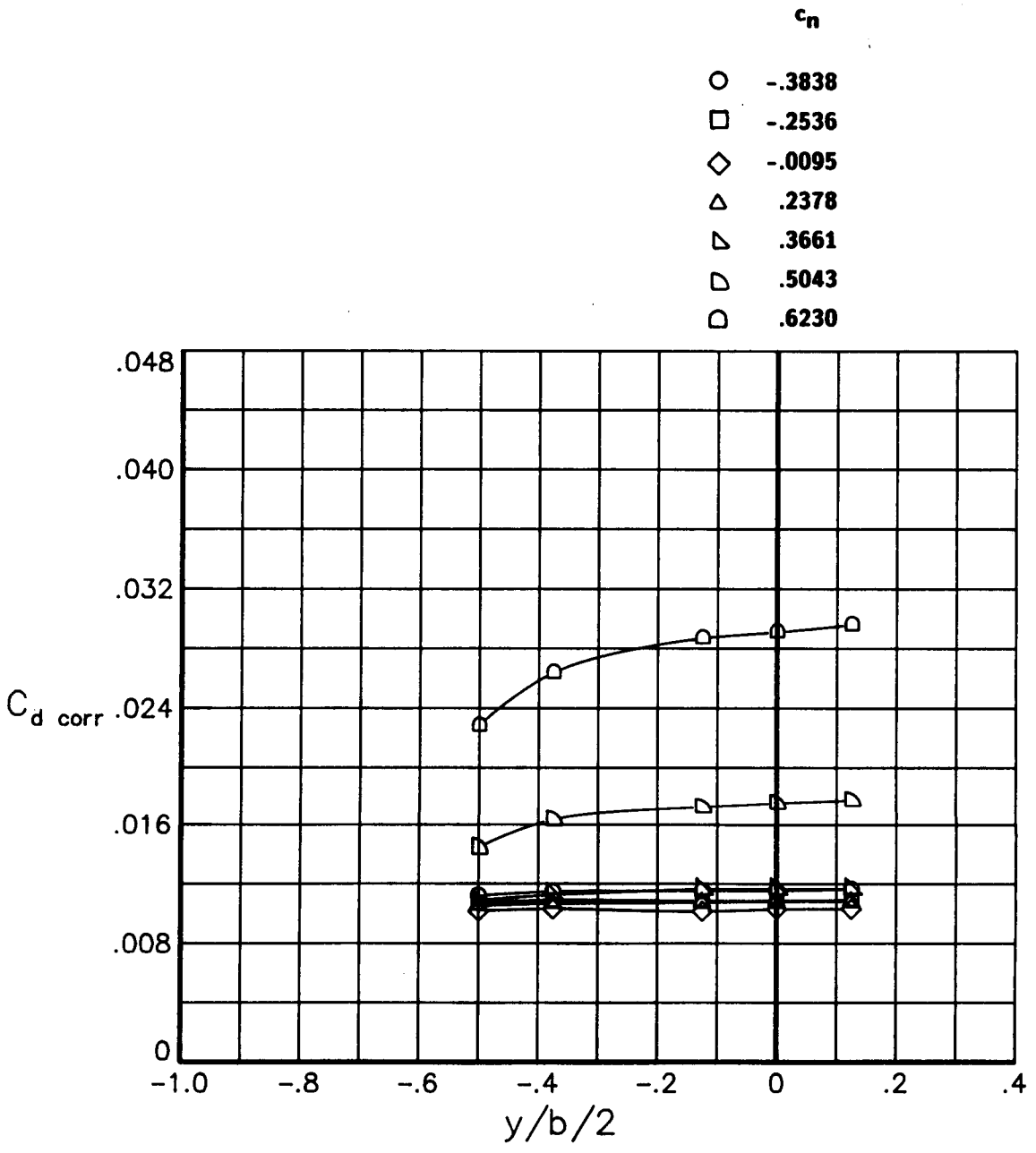

(a) R = 3.0 x 10^6

Figure 14.- Effects of normal force coefficient on the spanwise variation of drag coefficient for various Reynolds numbers at a Mach number of 0.70. Transition fixed.

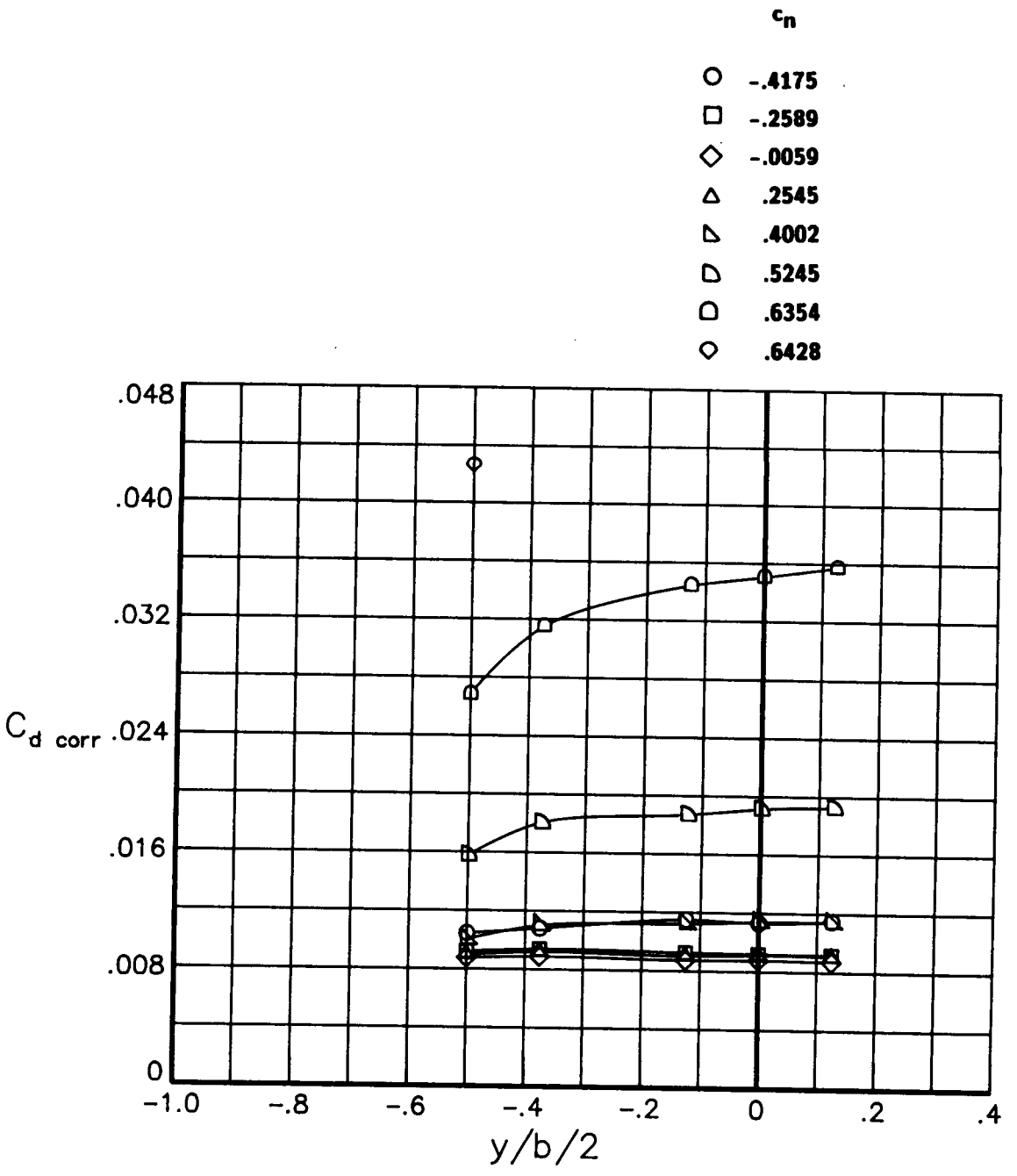

(b) R = 9.0 x 10^6

Figure 14.- Concluded.

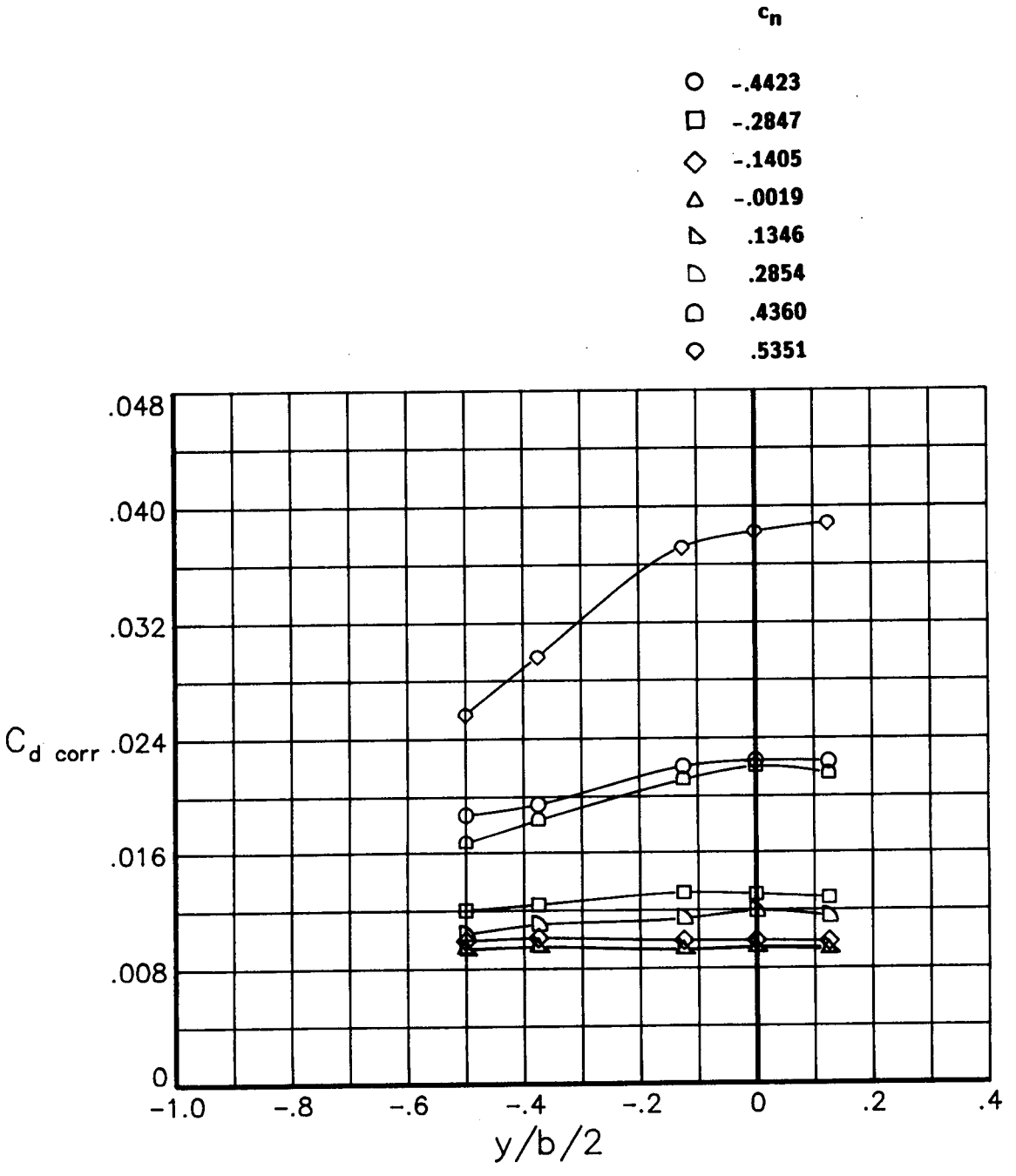

Figure 15.- Effects of normal force coefficient on the spanwise variation of drag coefficient for a Reynolds number of 9.0 x 10^6 and a Mach number of 0.74. Transition fixed.

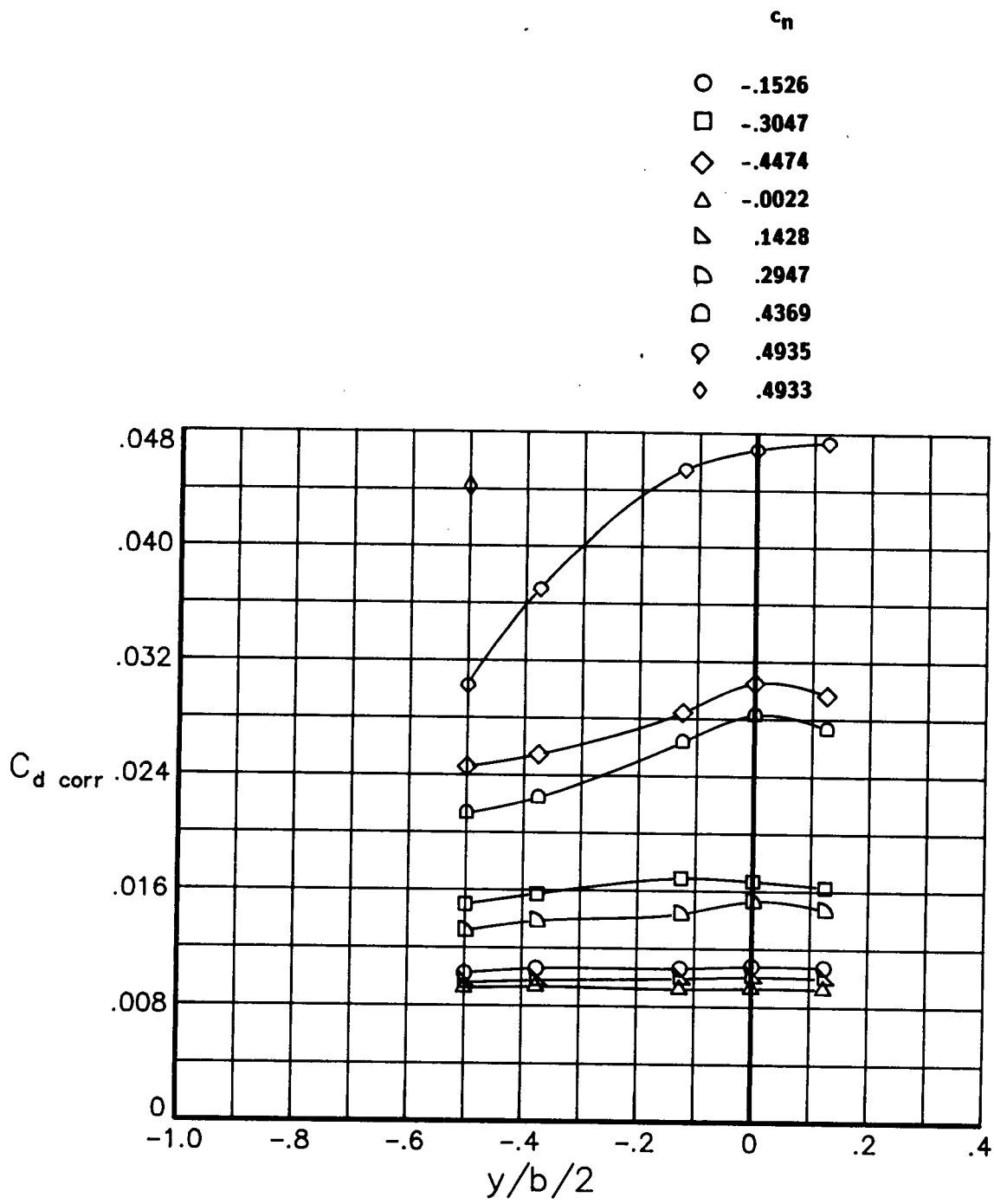

Figure 16.- Effects of normal force coefficient on the spanwise variation of drag coefficient for a Reynolds number of 9.0 x 10^6 and a Mach number of 0.76. Transition fixed.

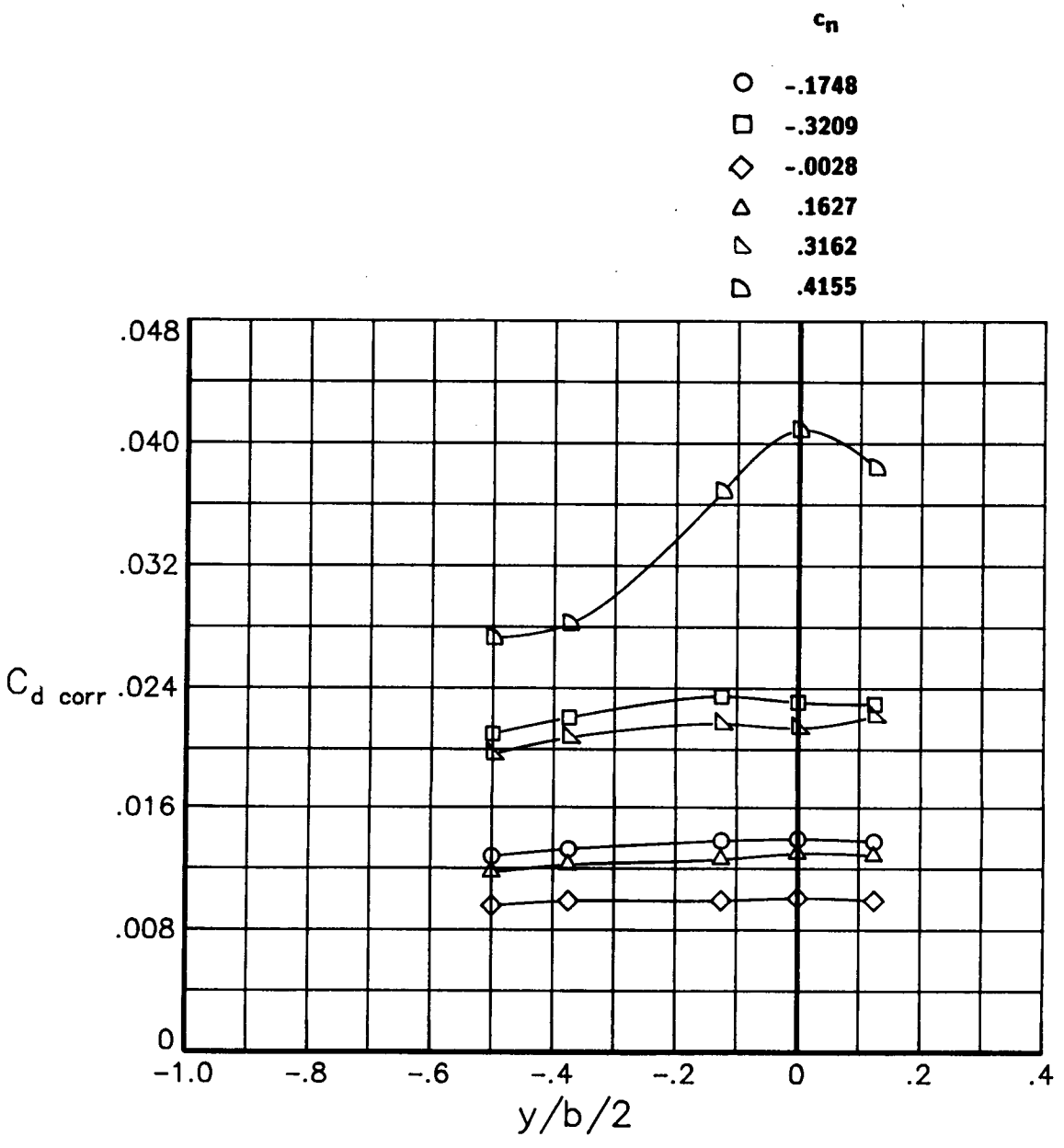

Figure 17.- Effects of normal force coefficient on the spanwise variation of drag coefficient for a Reynolds number of 9.0 x 10^6 and a Mach number of 0.78. Transition fixed.

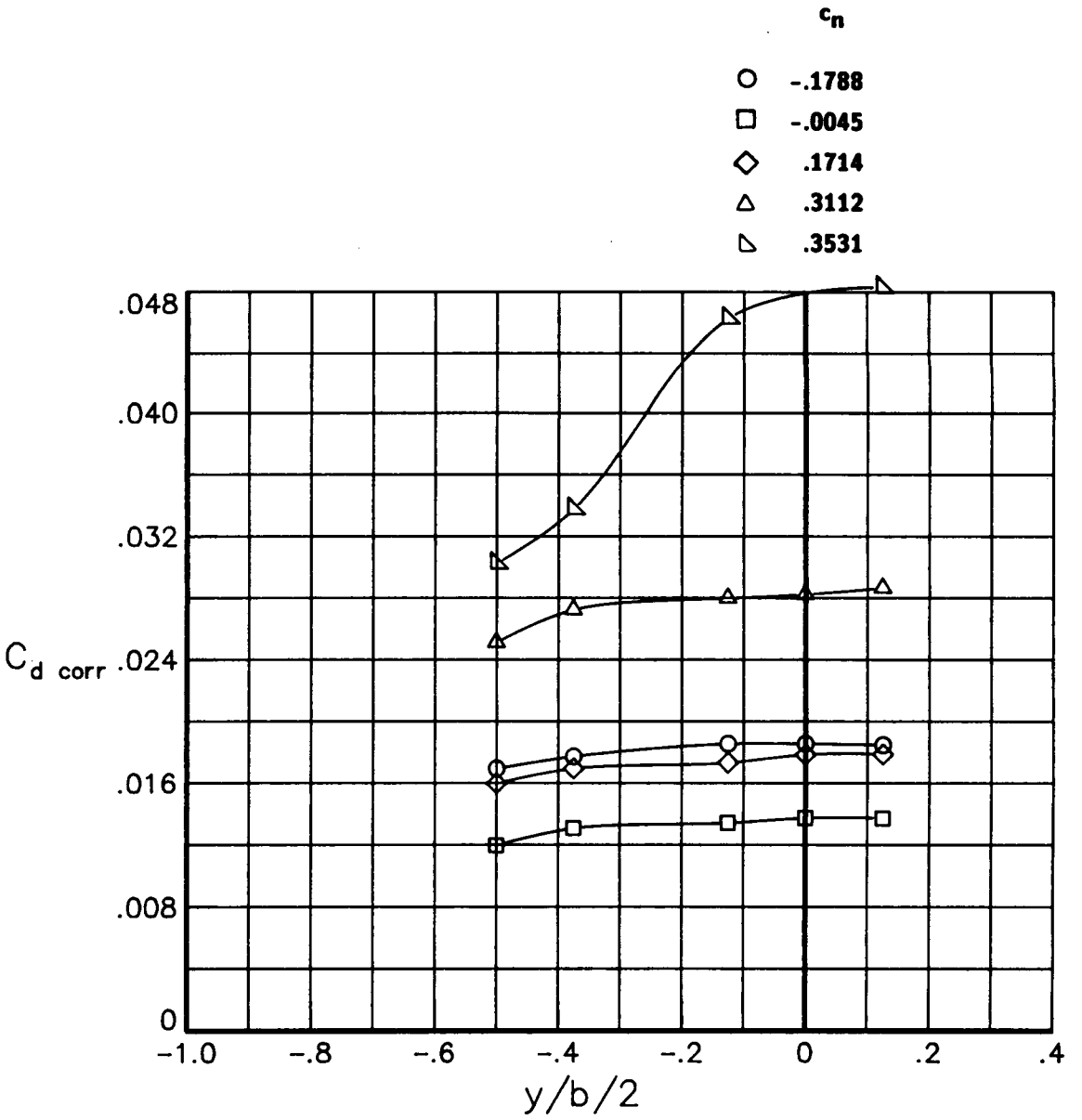

Figure 18.- Effects of normal force coefficient on the spanwise variation of drag coefficient for a Reynolds number of 9.0 x 10^6 and a Mach number of 0.80. Transition fixed.

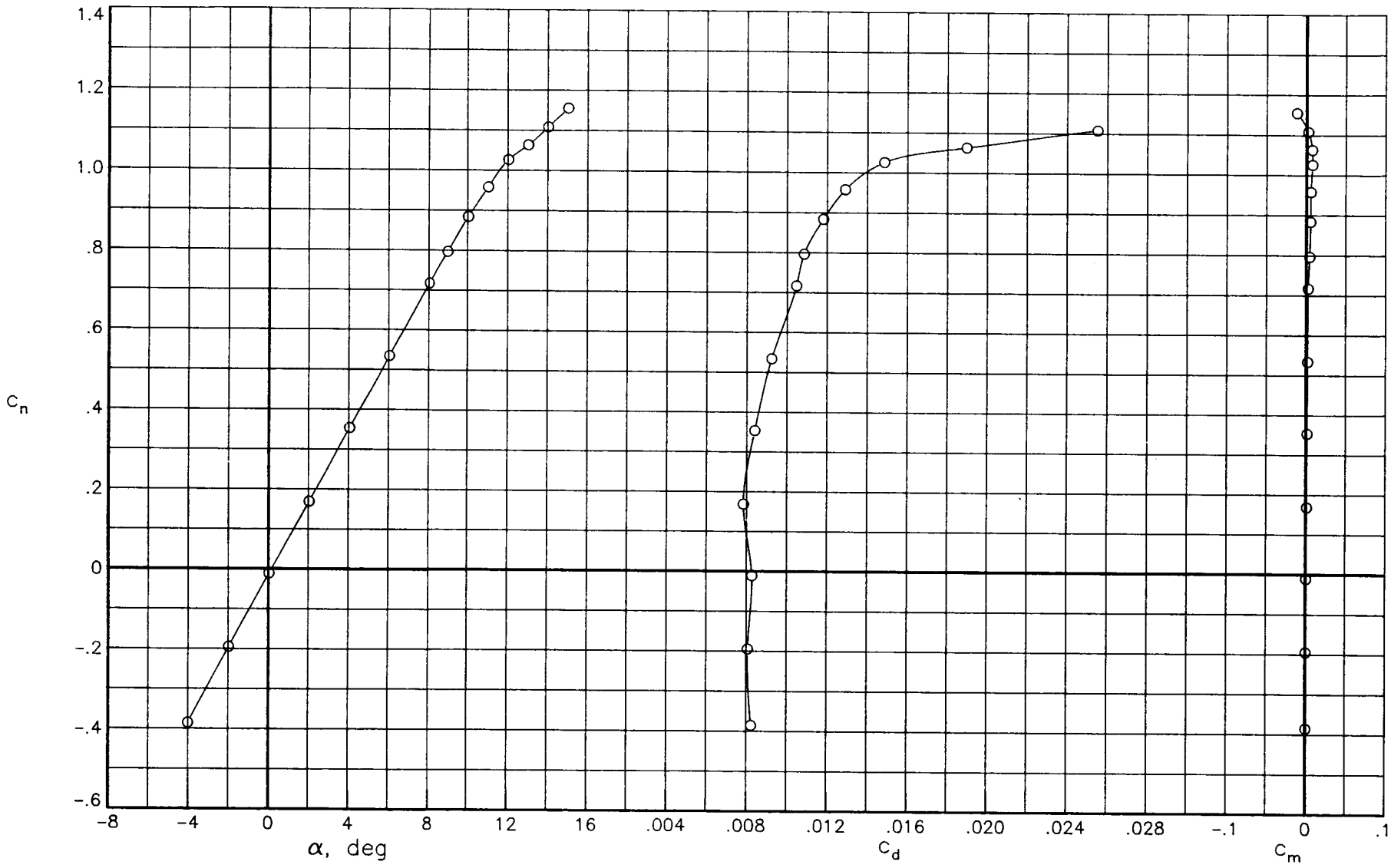

(a) R = 3.0 x 10^6

Figure 19.- Variation of basic aerodynamic data with angle of attack for various Reynolds numbers at a Mach number of 0.30. Transition free.

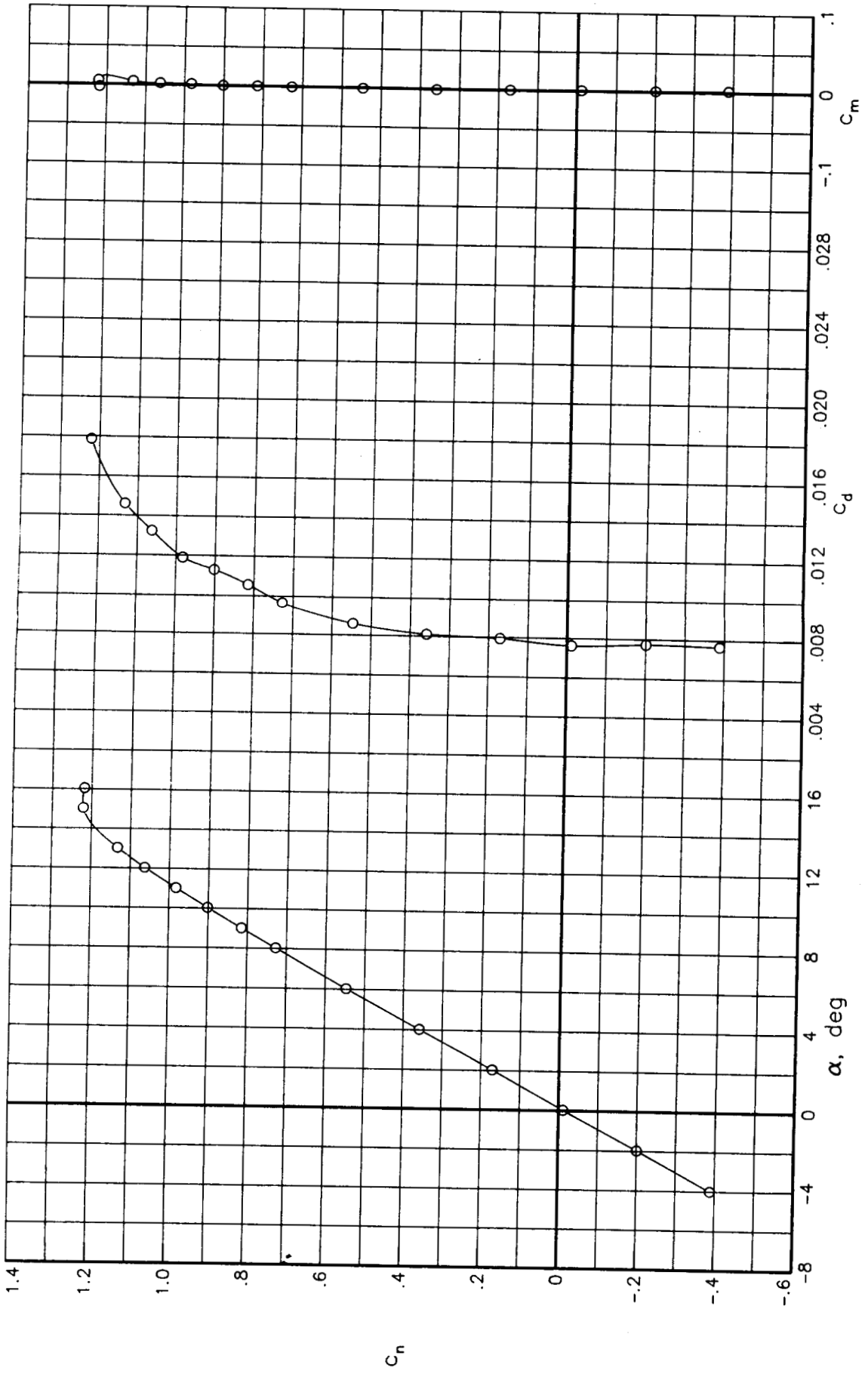

(b) R = 6.0 x 10^6

Figure 19.- Continued.

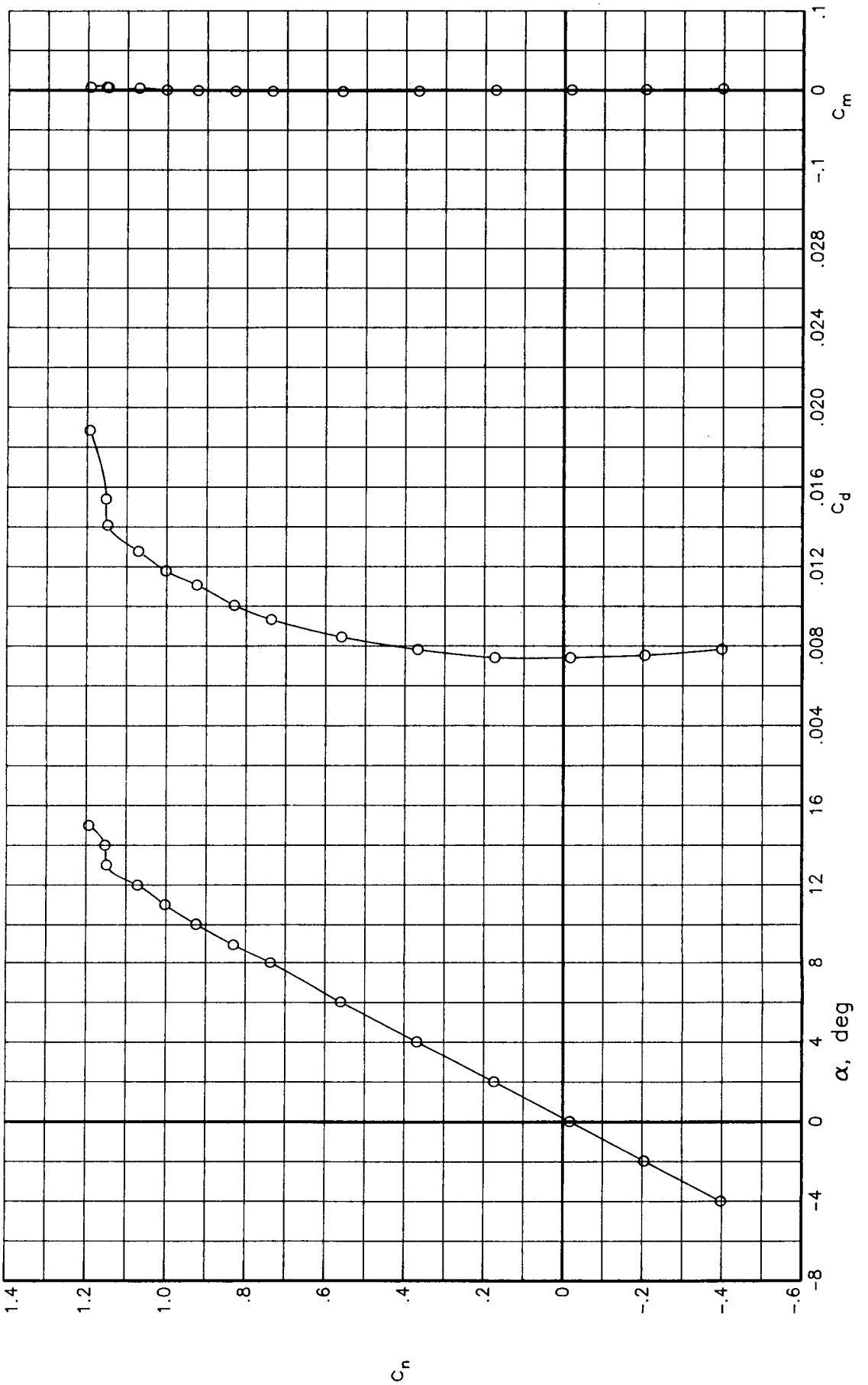

(c) R = 9.0 x 10^6

Figure 19.- Continued.

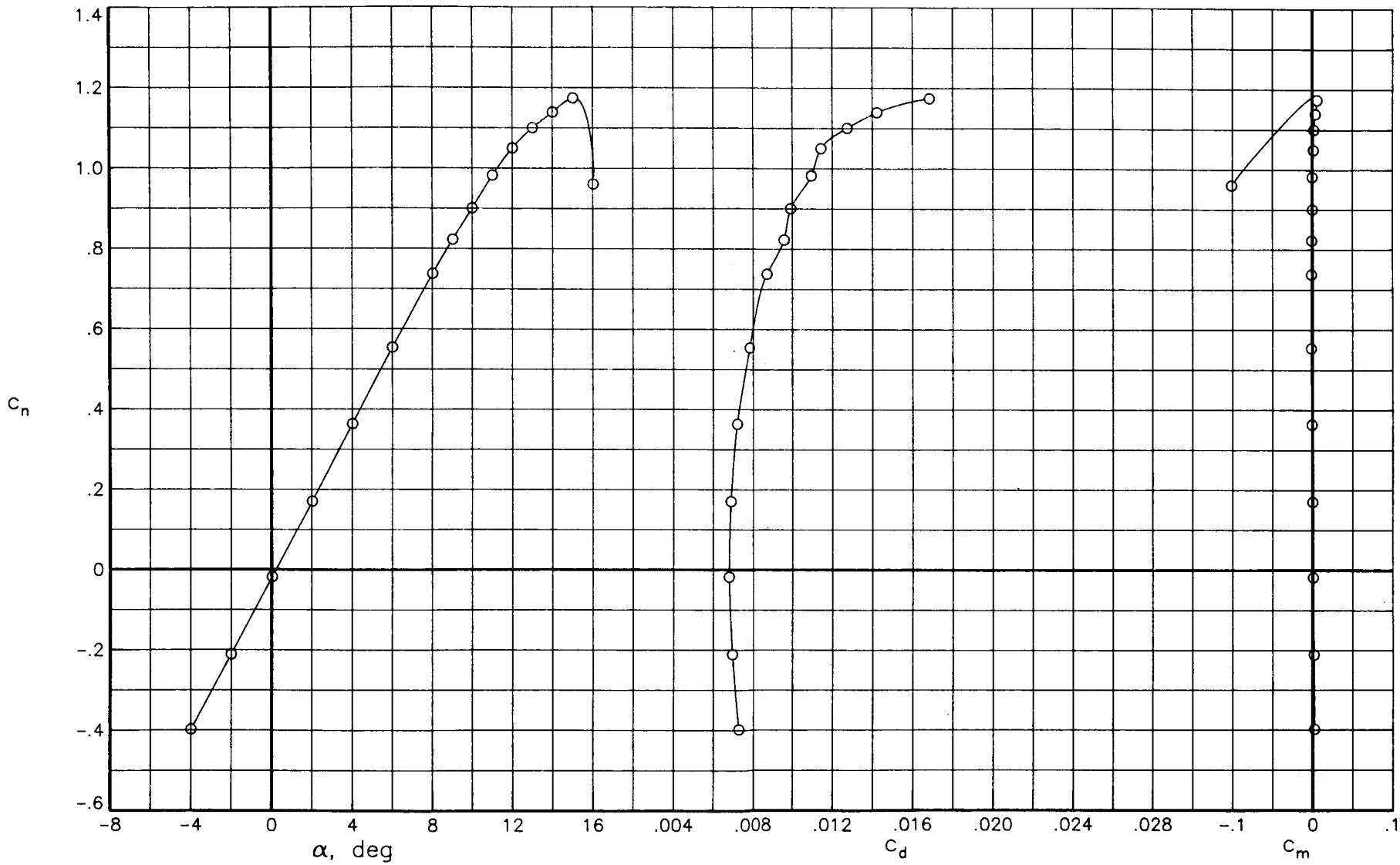

(d) R = 15.0 x 10^6

Figure 19.- Concluded.

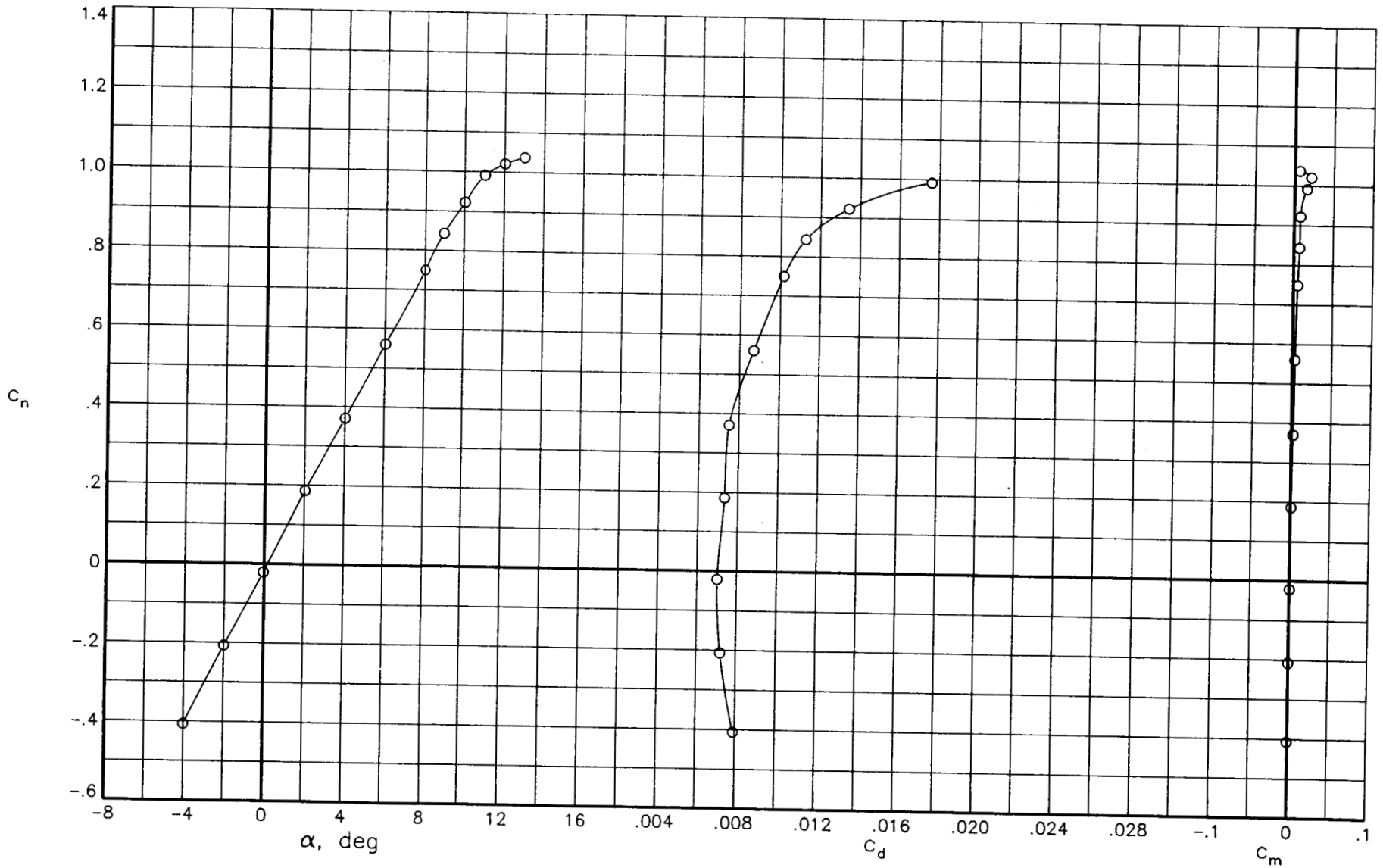

(a) R = 3.0 x 10^6

Figure 20.- Variation of basic aerodynamic data with angle of attack for various Reynolds numbers at a Mach number of 0.40. Transition free.

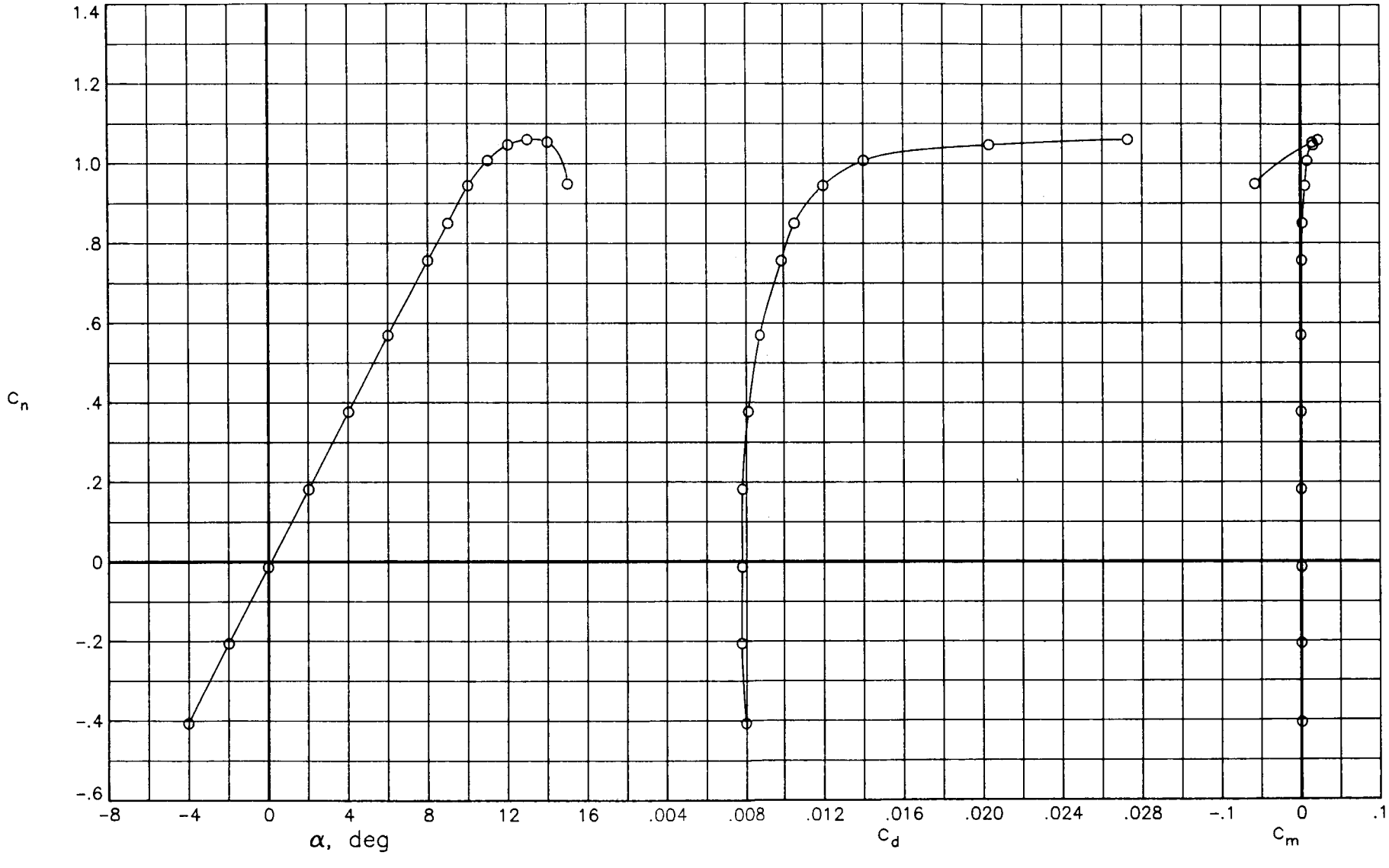

(b) R = 6.0 x 10^6

Figure 20.- Continued.

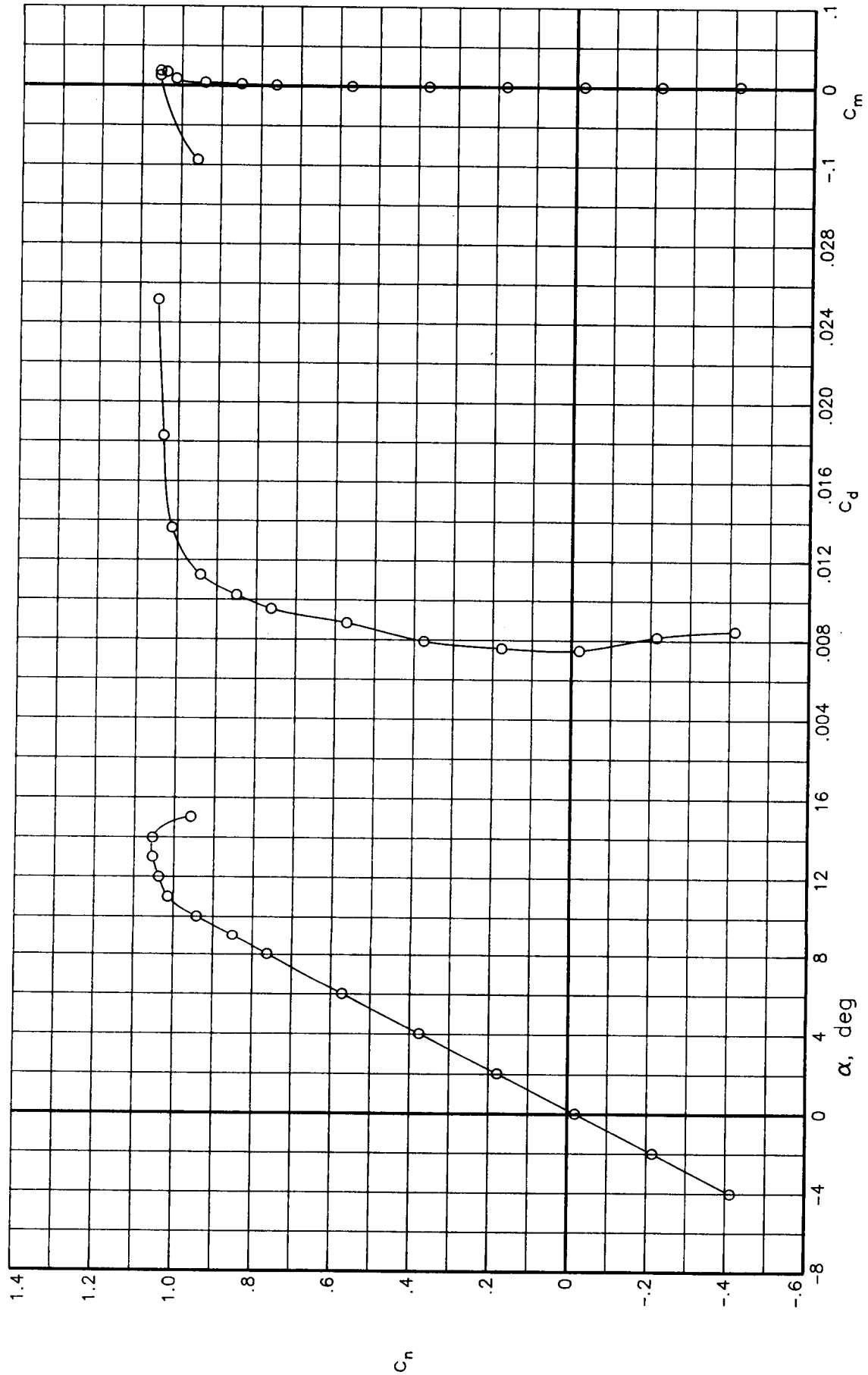

(c) R = 9.0 x 10^6

Figure 20.- Continued.

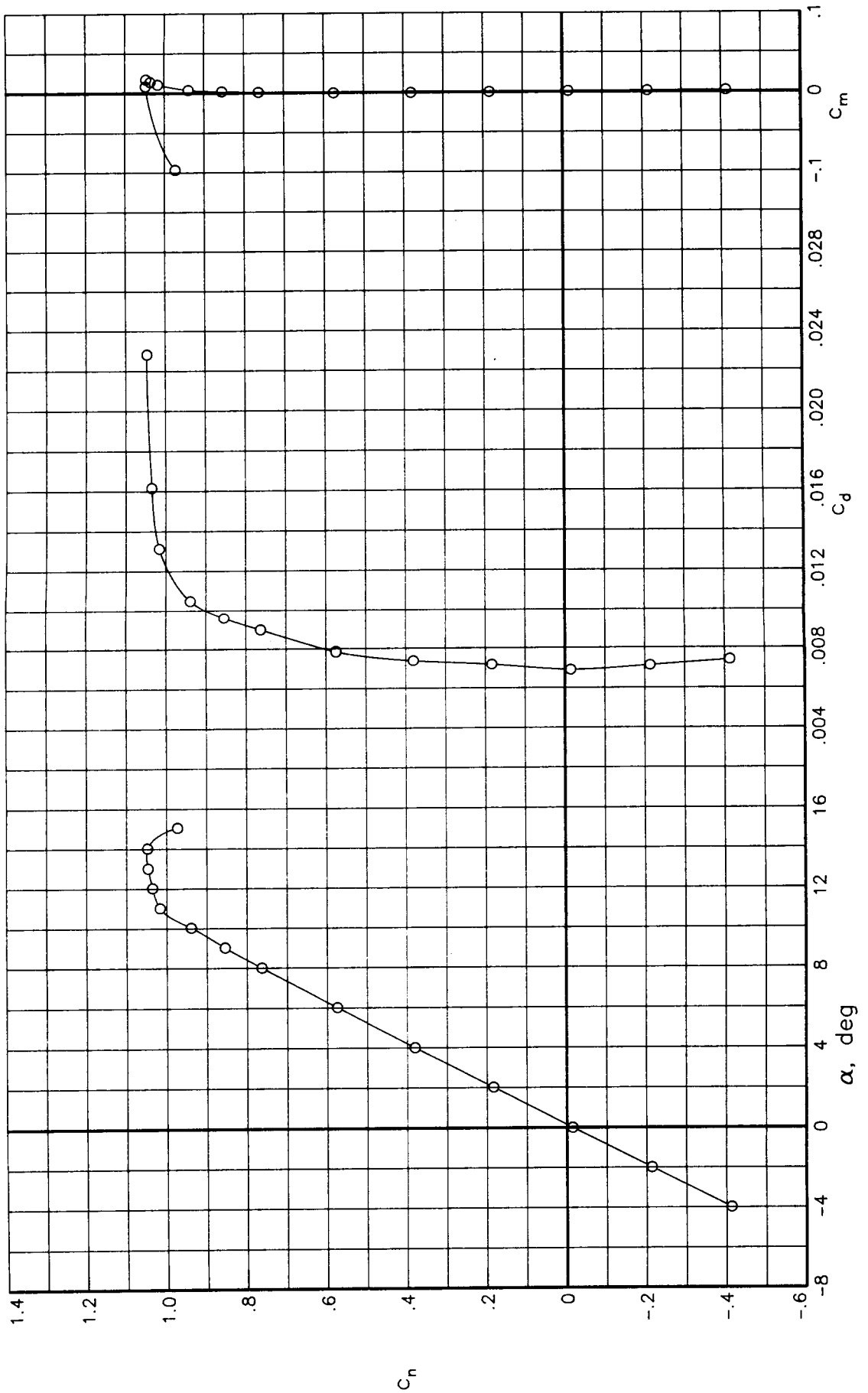

(d) R = 15.0 x 10^6

Figure 20.- Concluded.

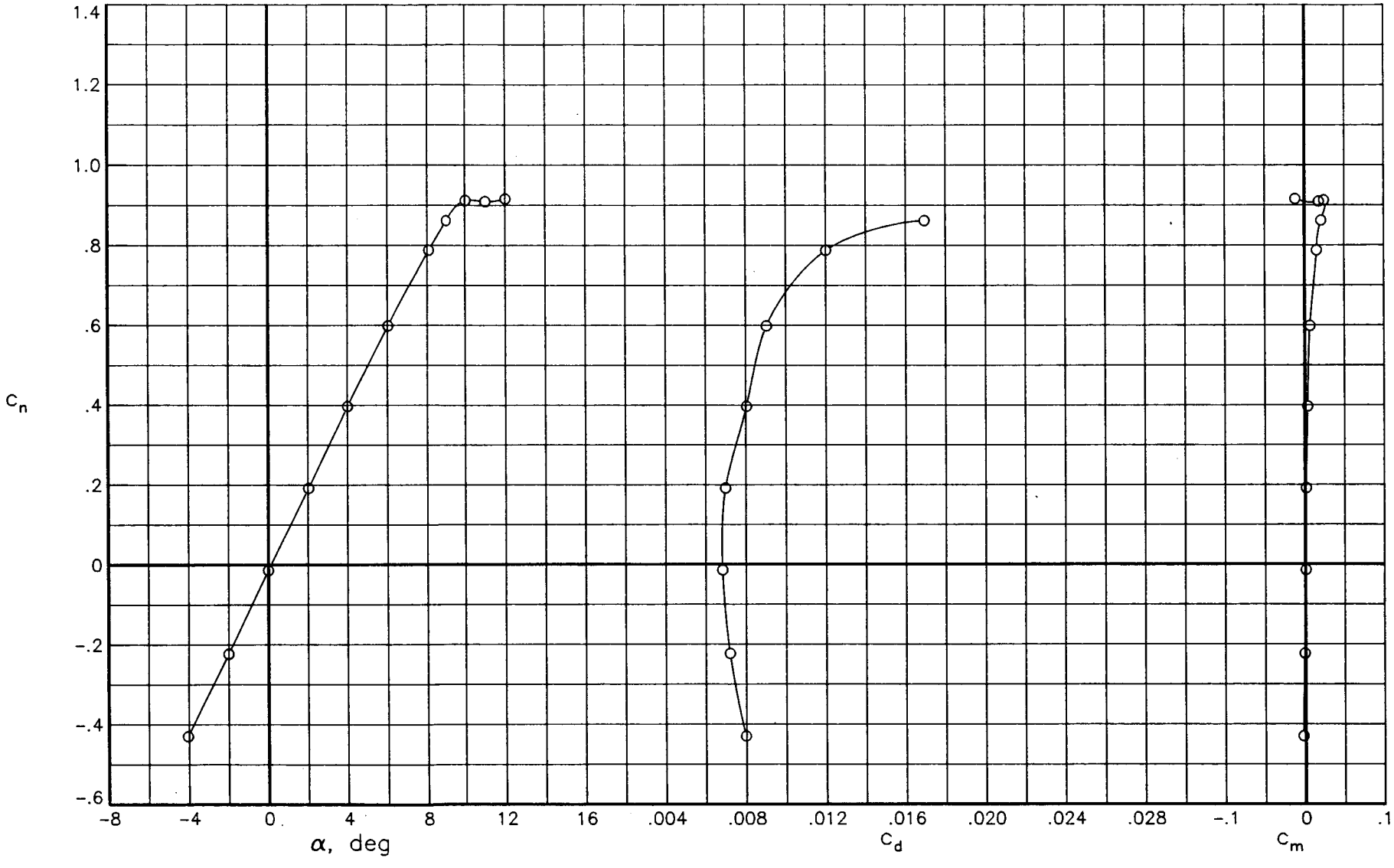

(a) R = 3.0 x 10^6

Figure 21.- Variation of basic aerodynamic data with angle of attack for various Reynolds numbers at a Mach number of 0.50. Transition free.

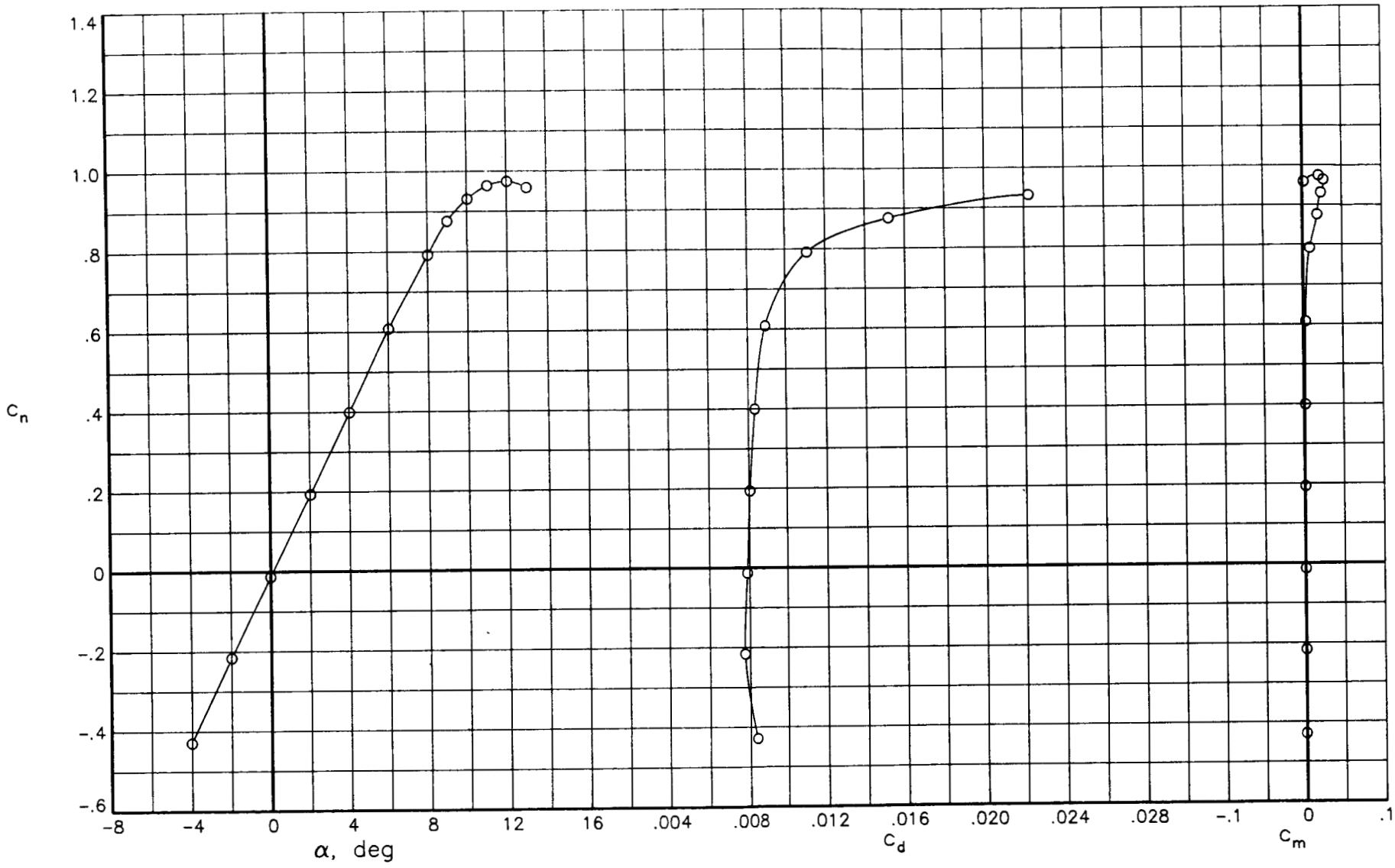

(b) R = 6.0 x 10^6

Figure 21.- Continued.

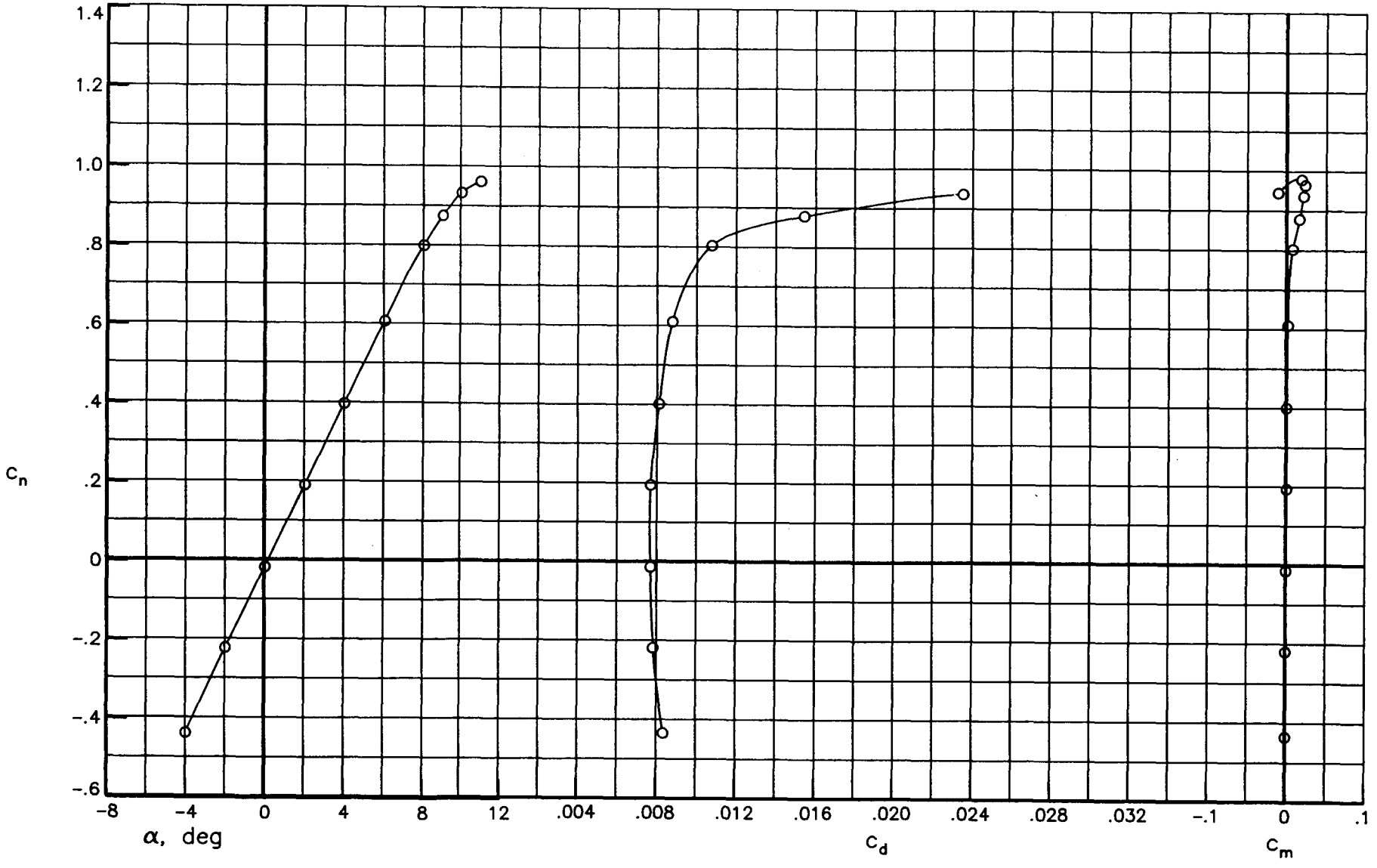

(c) R = 9.0 x 10^6

Figure 21.- Continued.

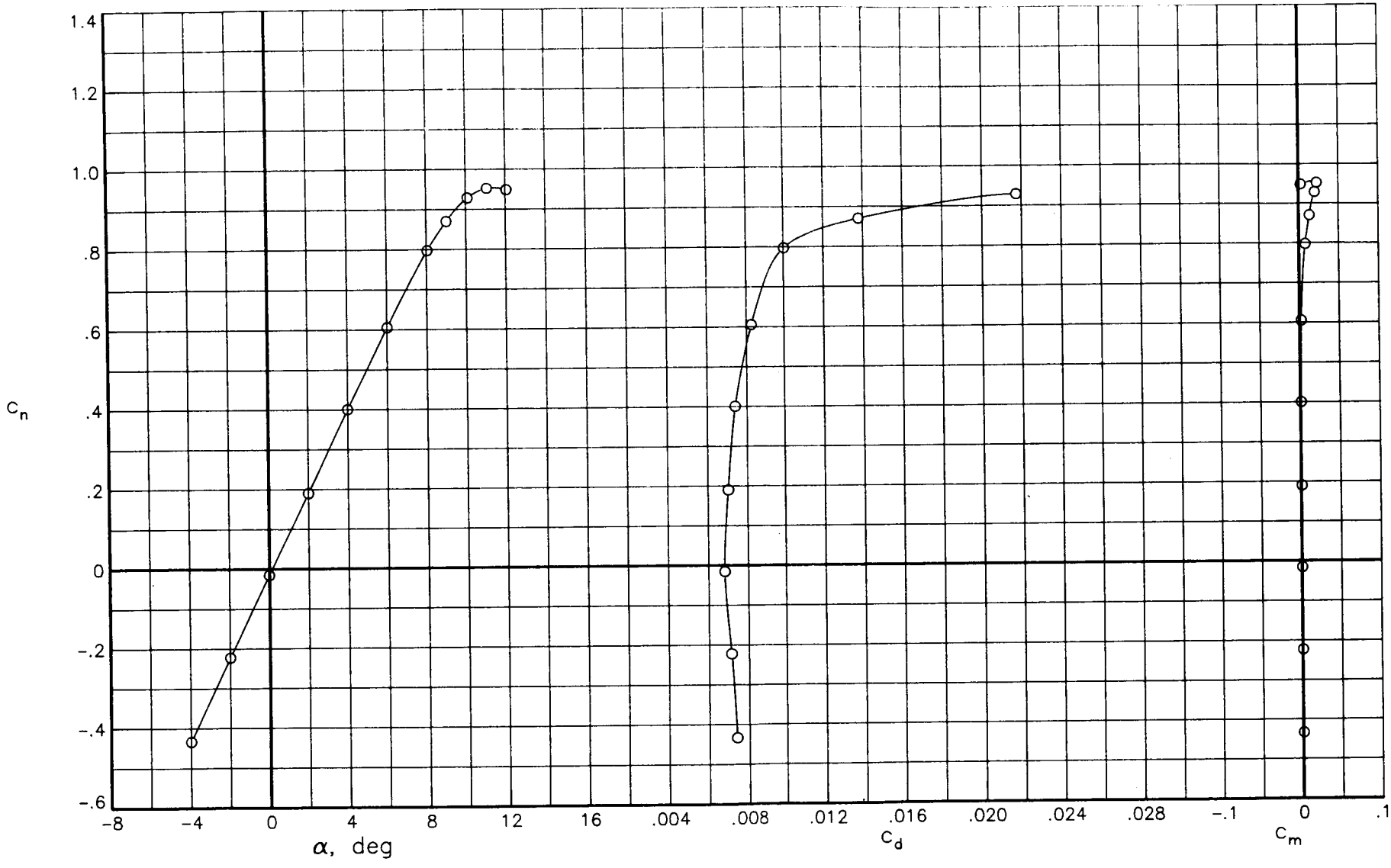

(d) R = 15.0 x 10^6

Figure 21.- Continued.

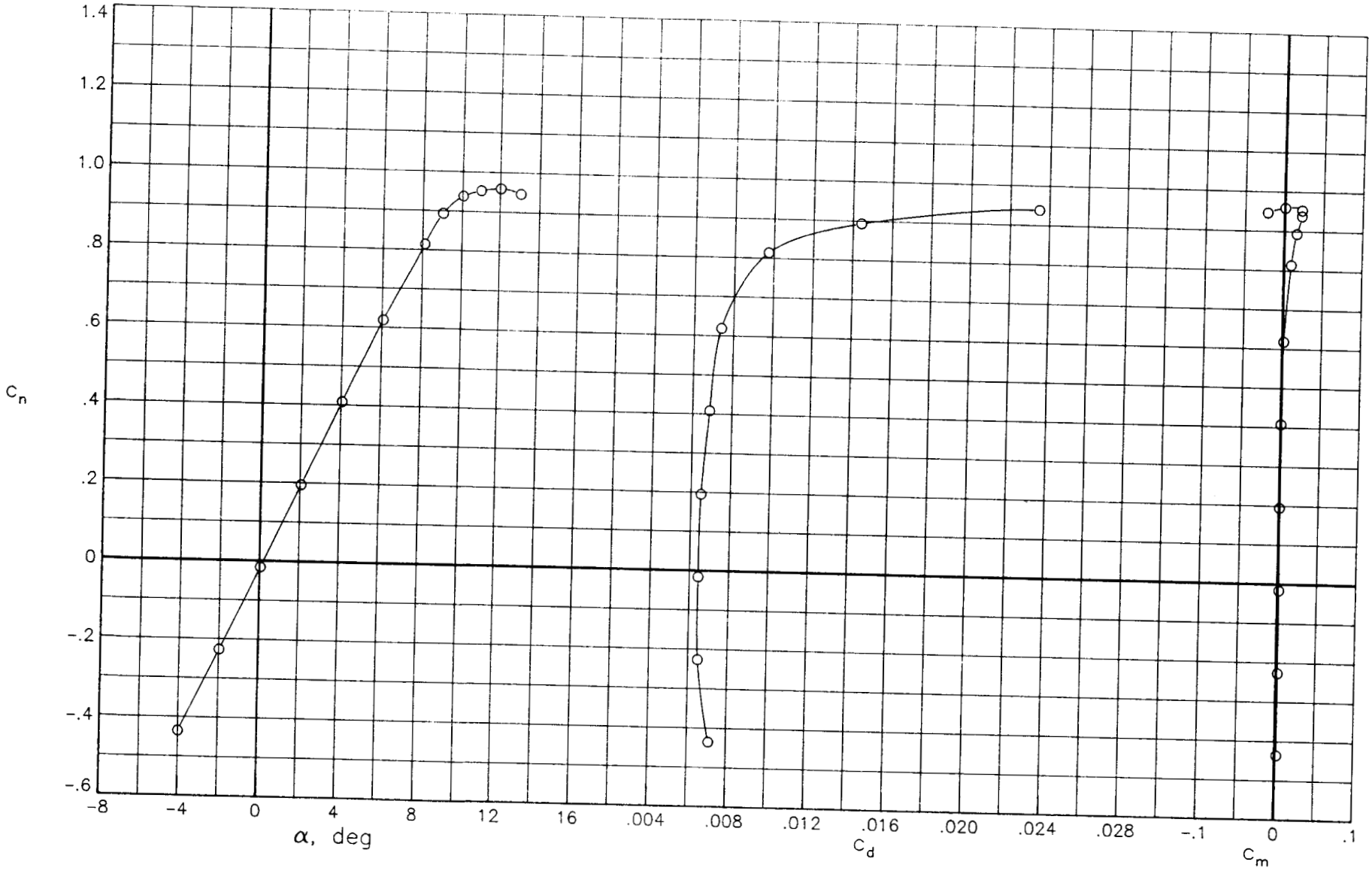

(e) R = 30.0 x 10^6

Figure 21.- Concluded.

(a) R = 3.0 x 10^6

Figure 22.- Variation of basic aerodynamic data with angle of attack for various Reynolds numbers at a Mach number of 0.60. Transition free.

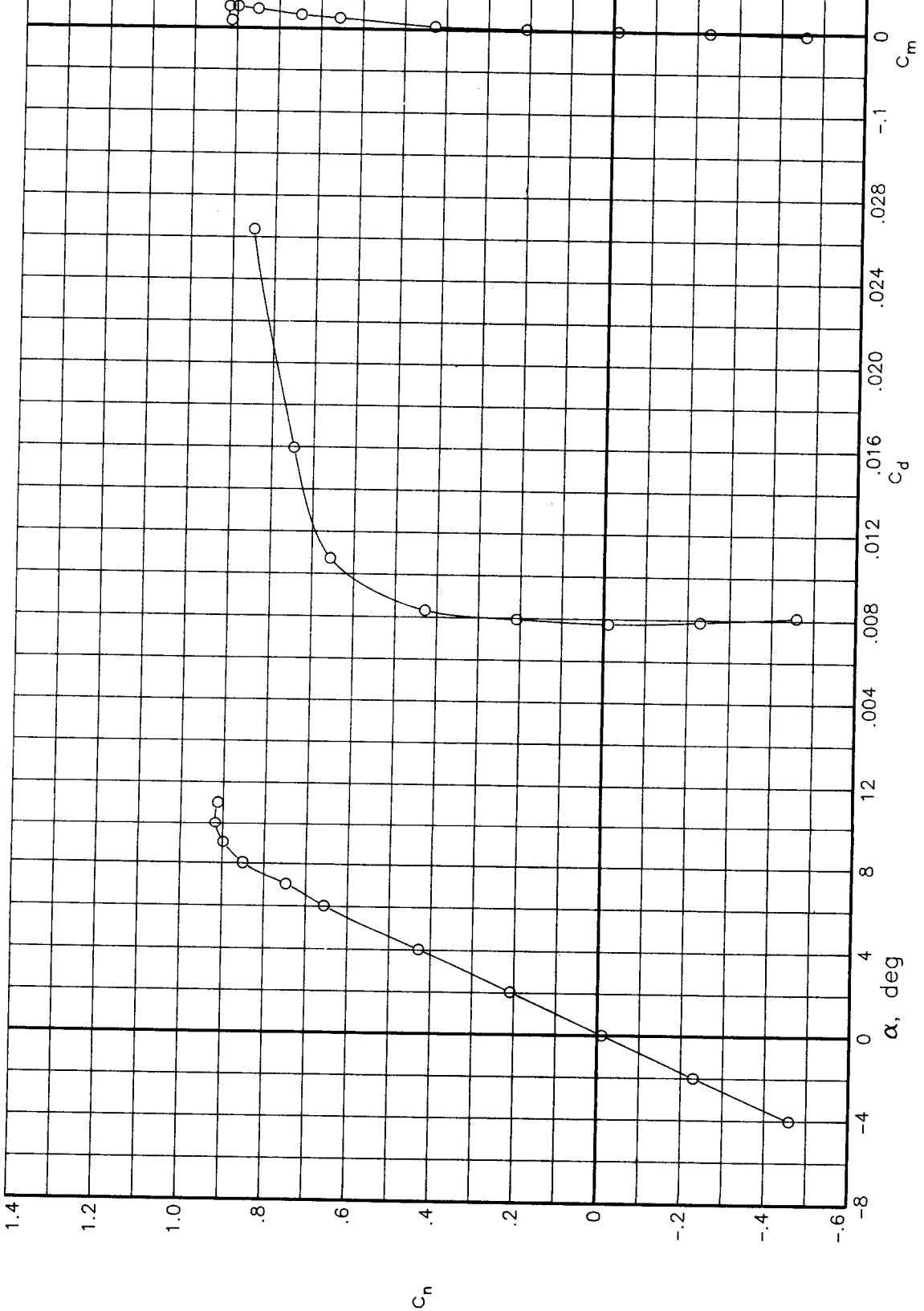

(b) R = 6.0 x 10^6

Figure 22.- Continued.

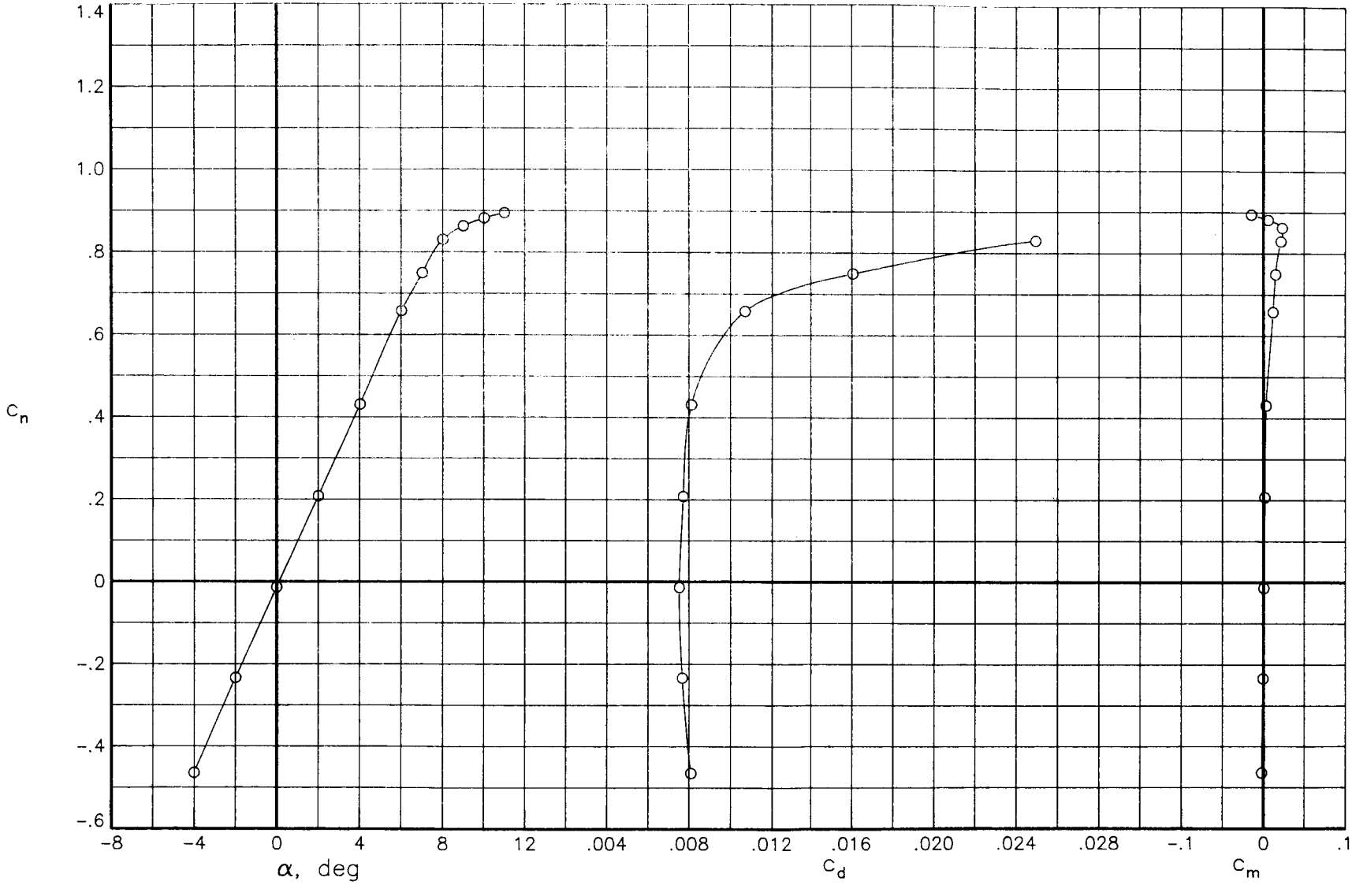

(c) R = 9.0 x 10^6

Figure 22.- Continued.

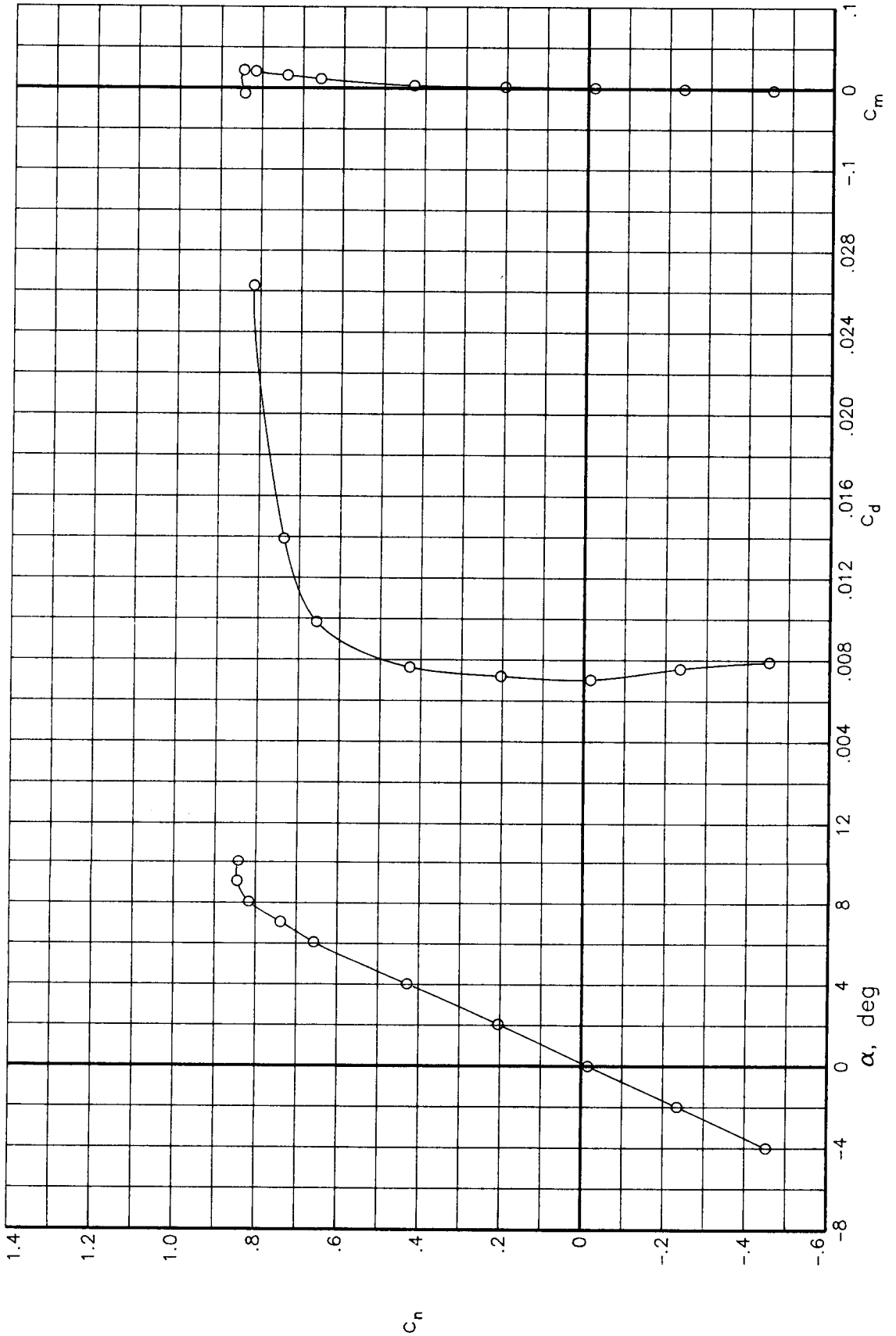

(d) R = 15.0 x 10^6

Figure 22.- Continued.

(e) R = 30.0 x 10^6

Figure 22.- Concluded.

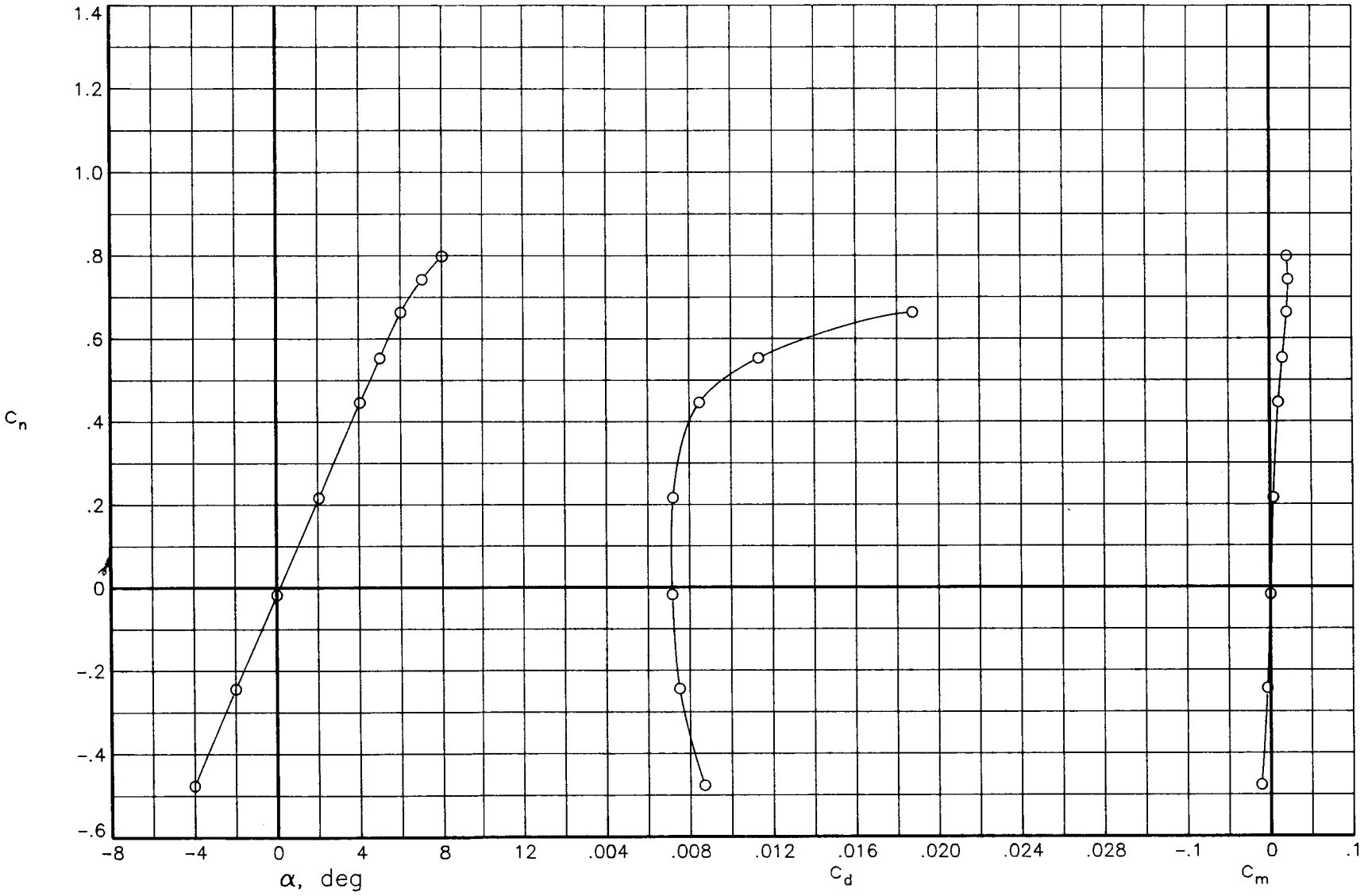

(a) R = 3.0 x 10^6

Figure 23.- Variation of basic aerodynamic data with angle of attack for various Reynolds numbers at a Mach number of 0.65. Transition free.

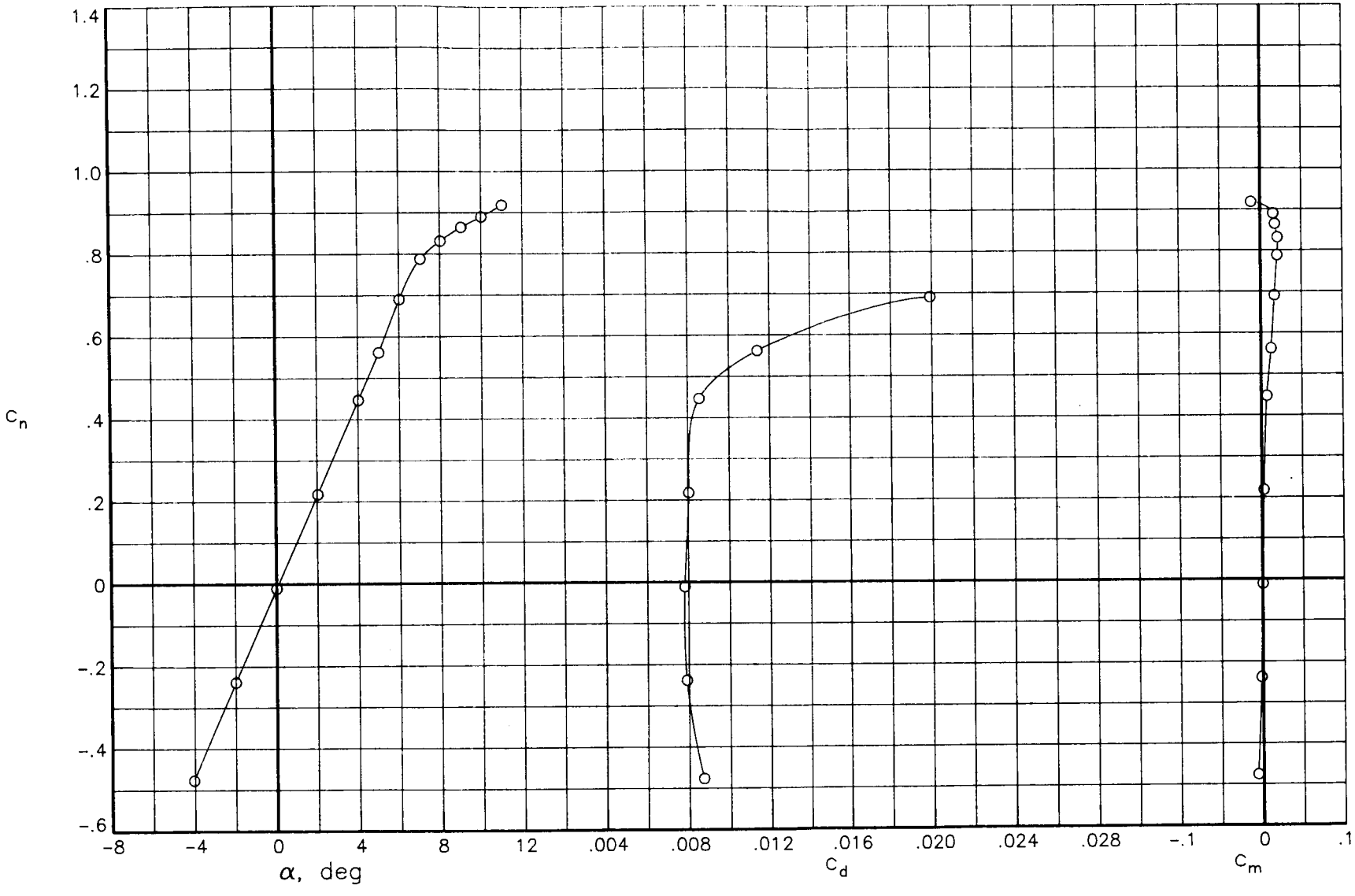

(b) R = 6.0 x 10^6

Figure 23.- Continued.

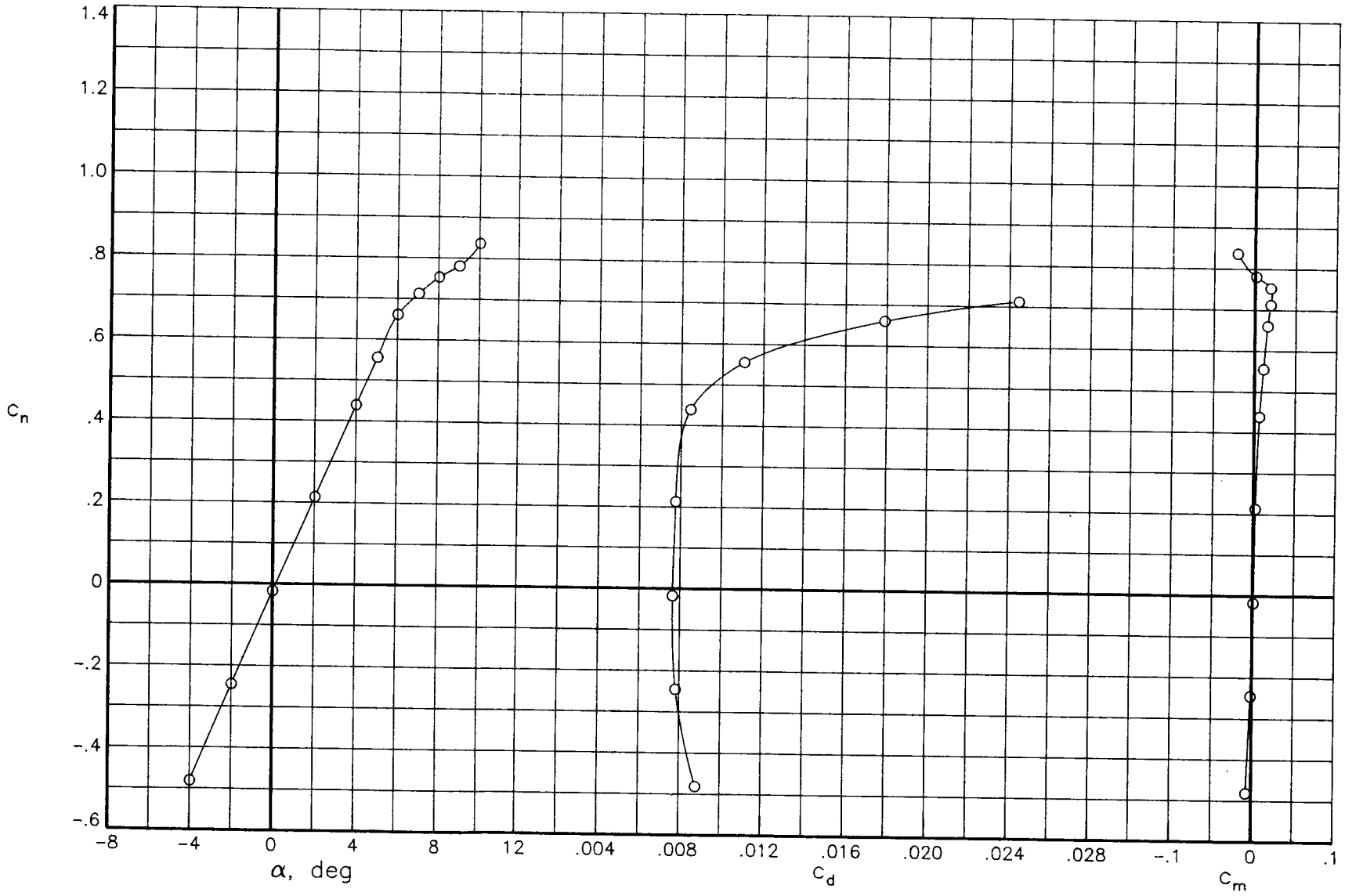

(c) R = 9.0 x 10^6

Figure 23.- Continued.

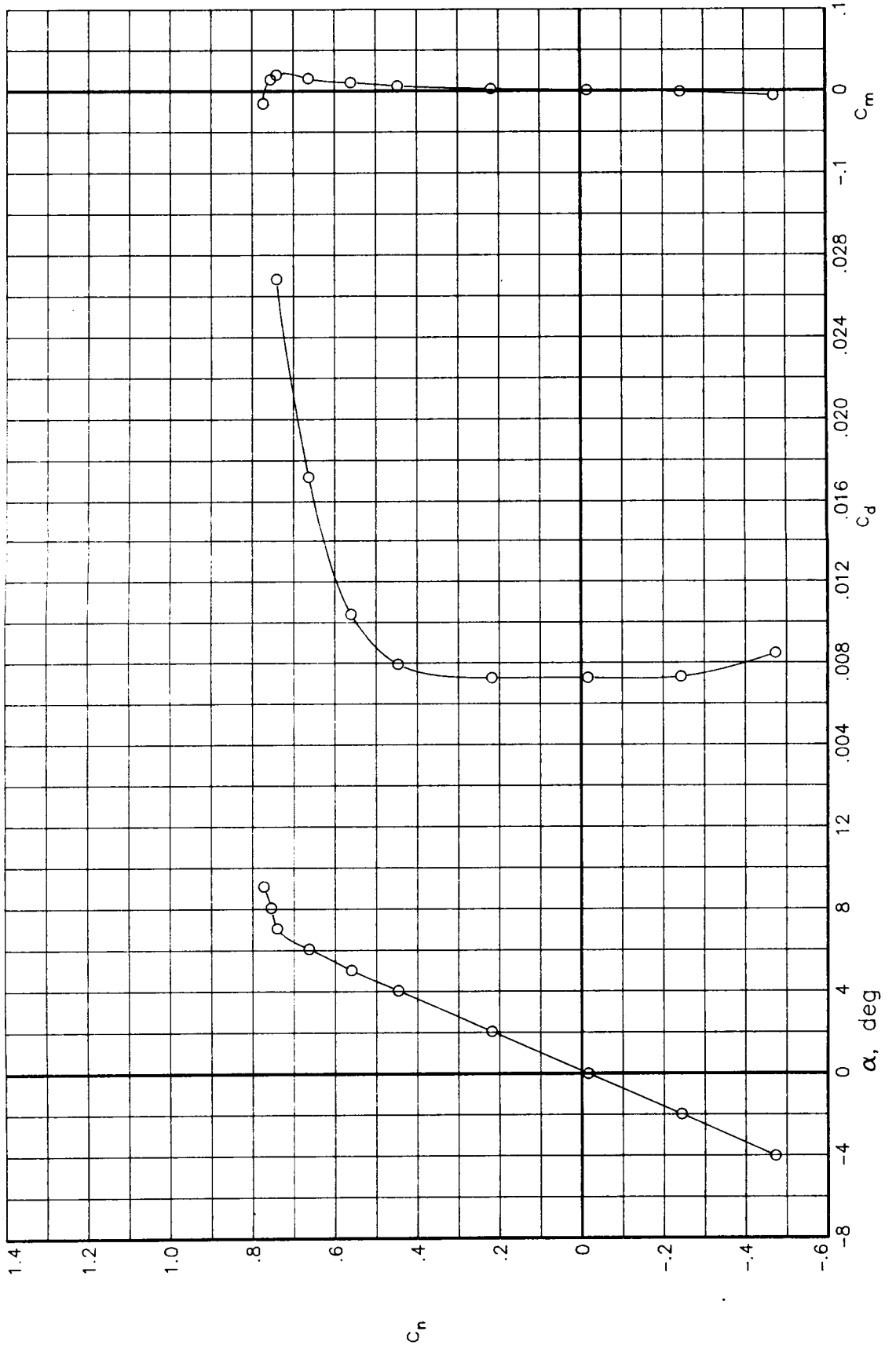

(d) R = 15.0 x 10^6

Figure 23.- Continued.

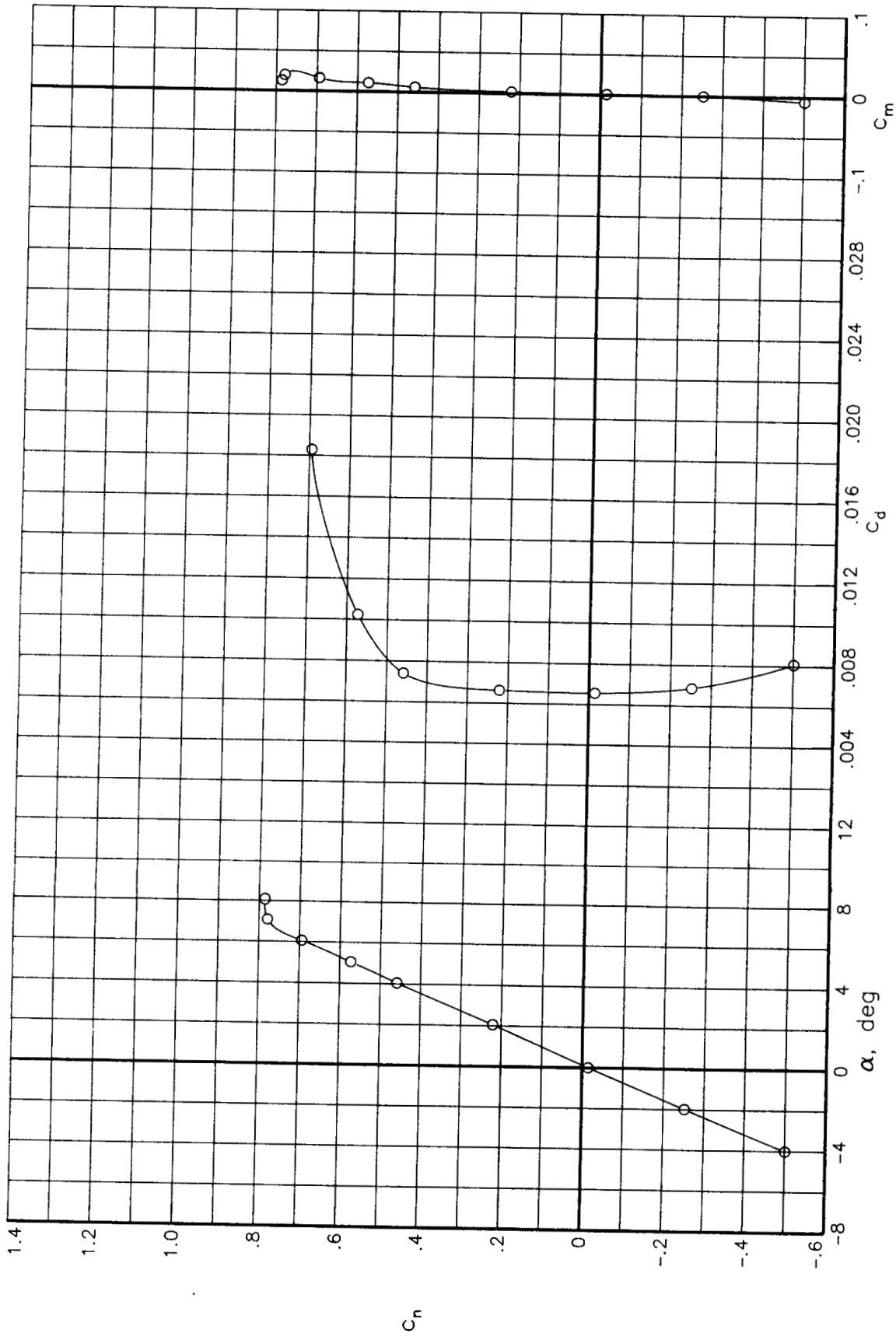

(e) R = 30.0 x 10^6

Figure 23.- Concluded.

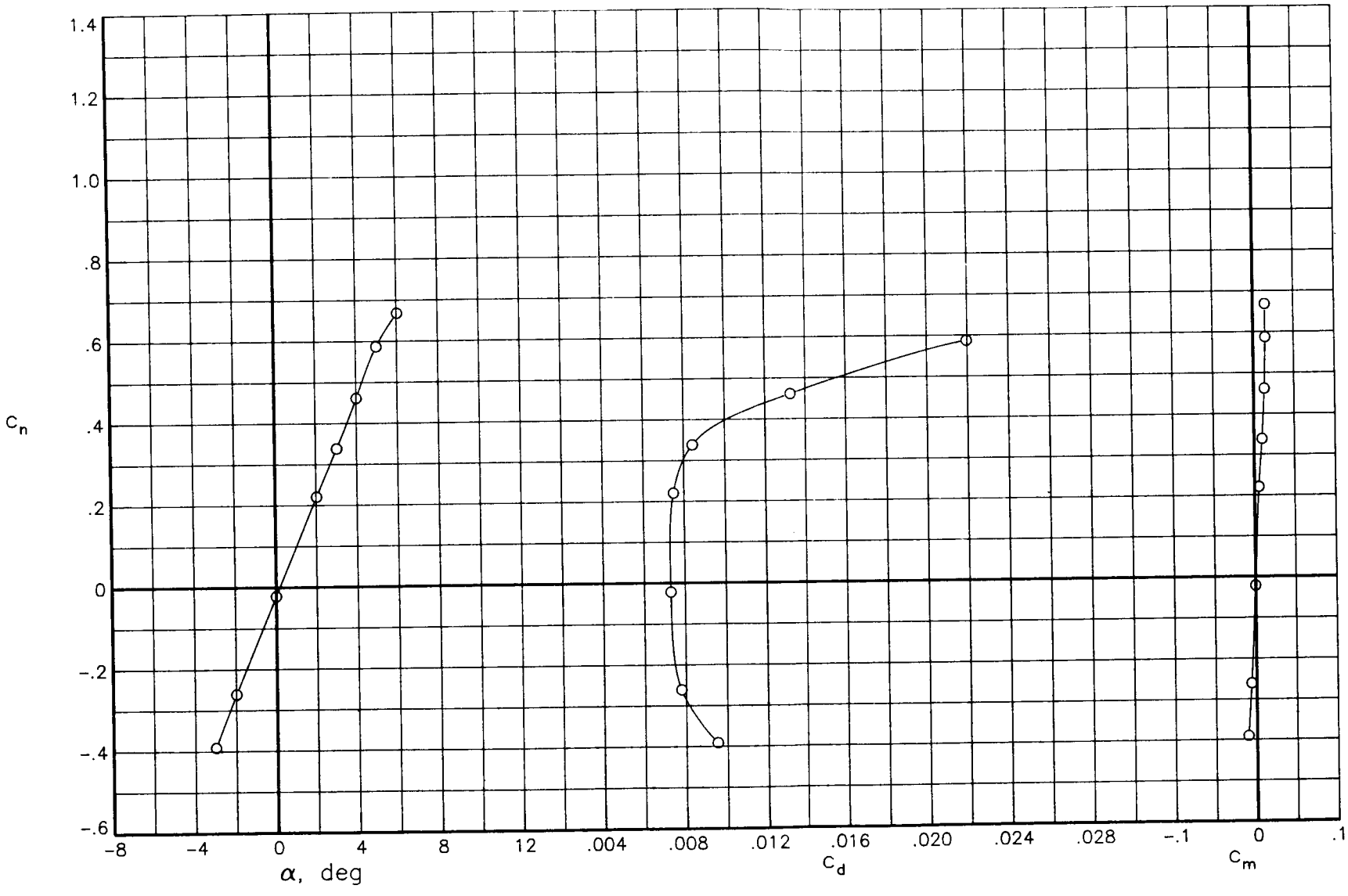

(a) R = 3.0 x 10^6

Figure 24.- Variation of basic aerodynamic data with angle of attack for various Reynolds numbers at a Mach number of 0.70. Transition free.

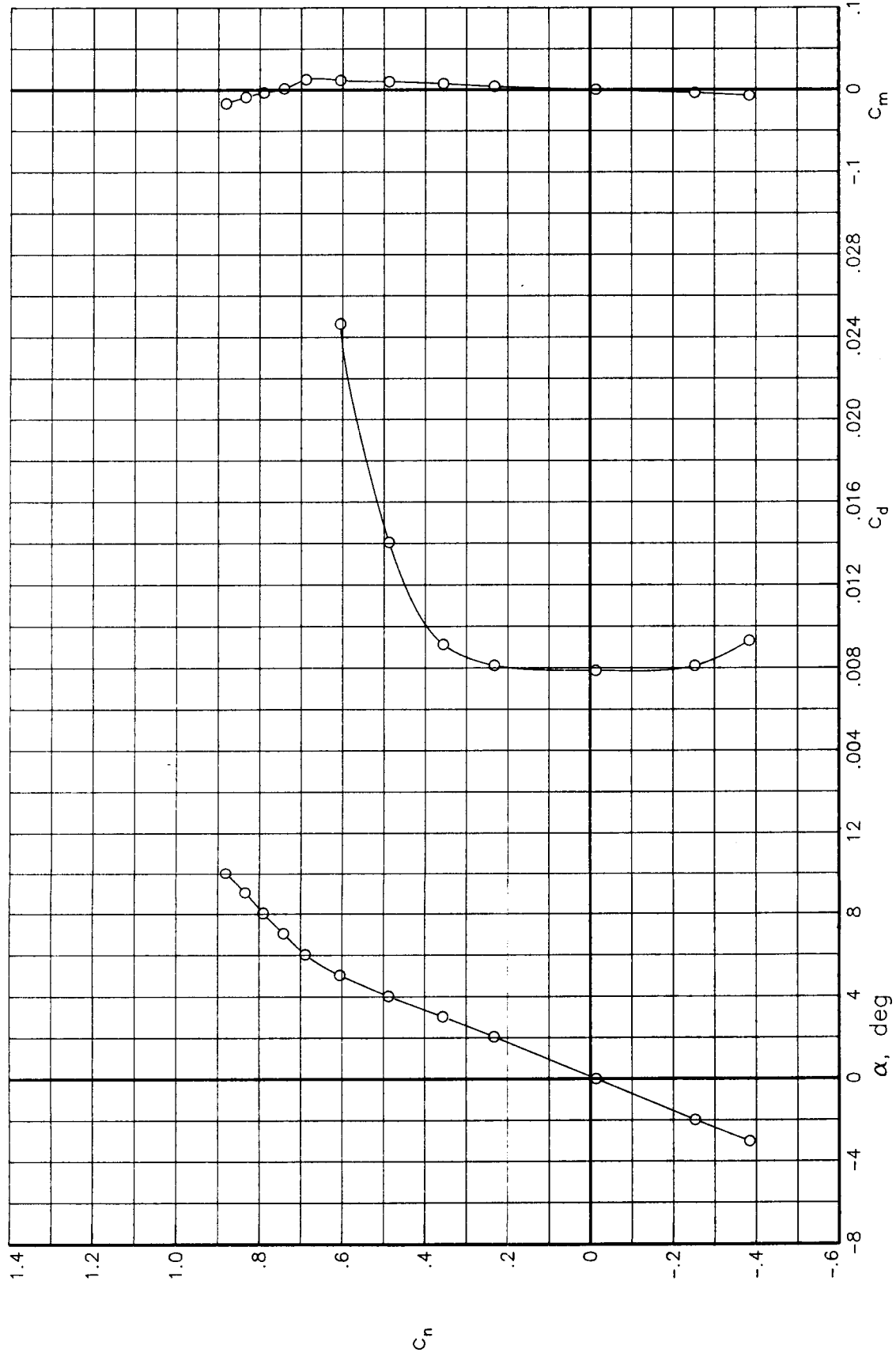

C-2

(b) R = 6.0 x 10^6

Figure 24.- Continued.

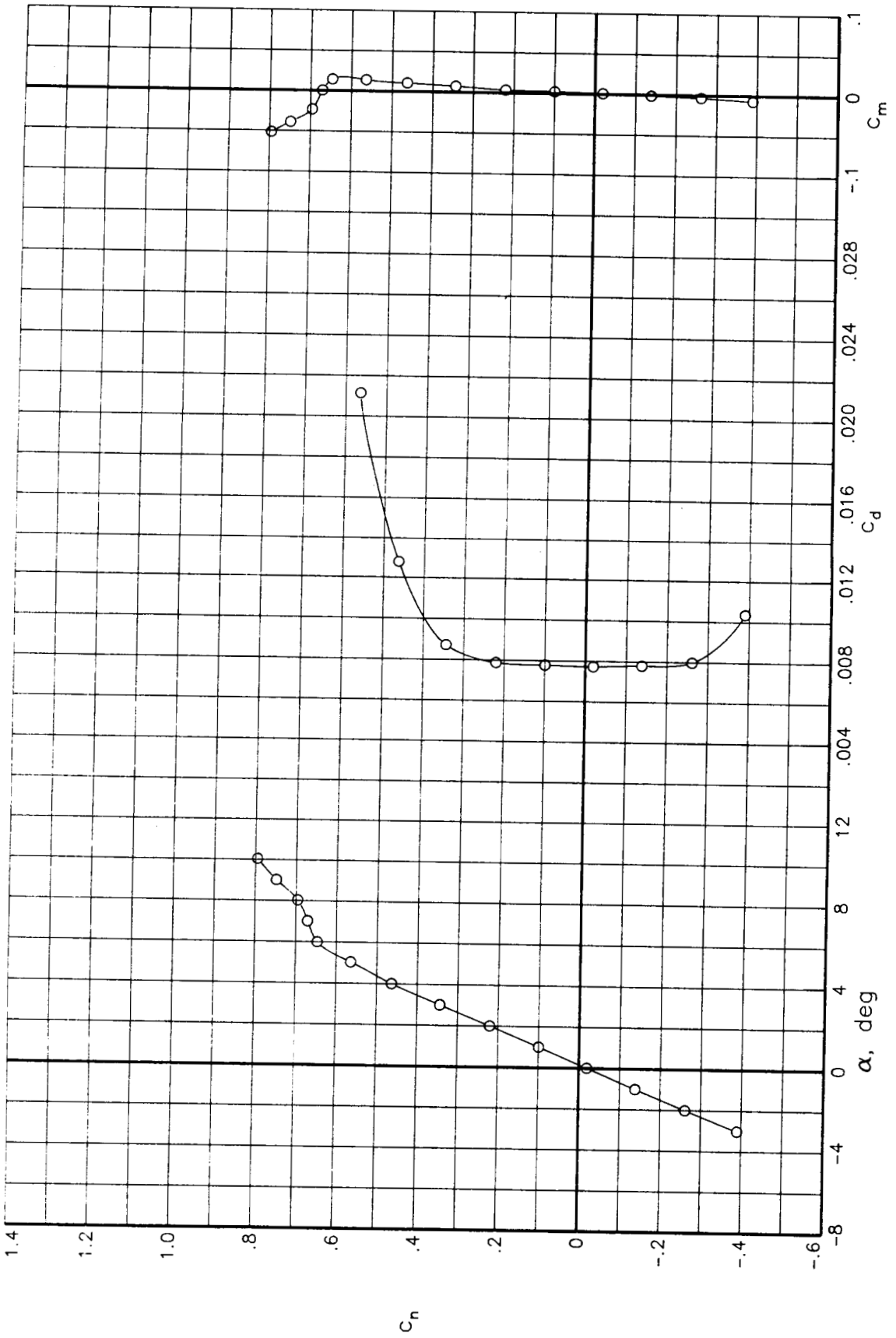

(c) R = 9.0 x 10^6

Figure 24.- Continued.

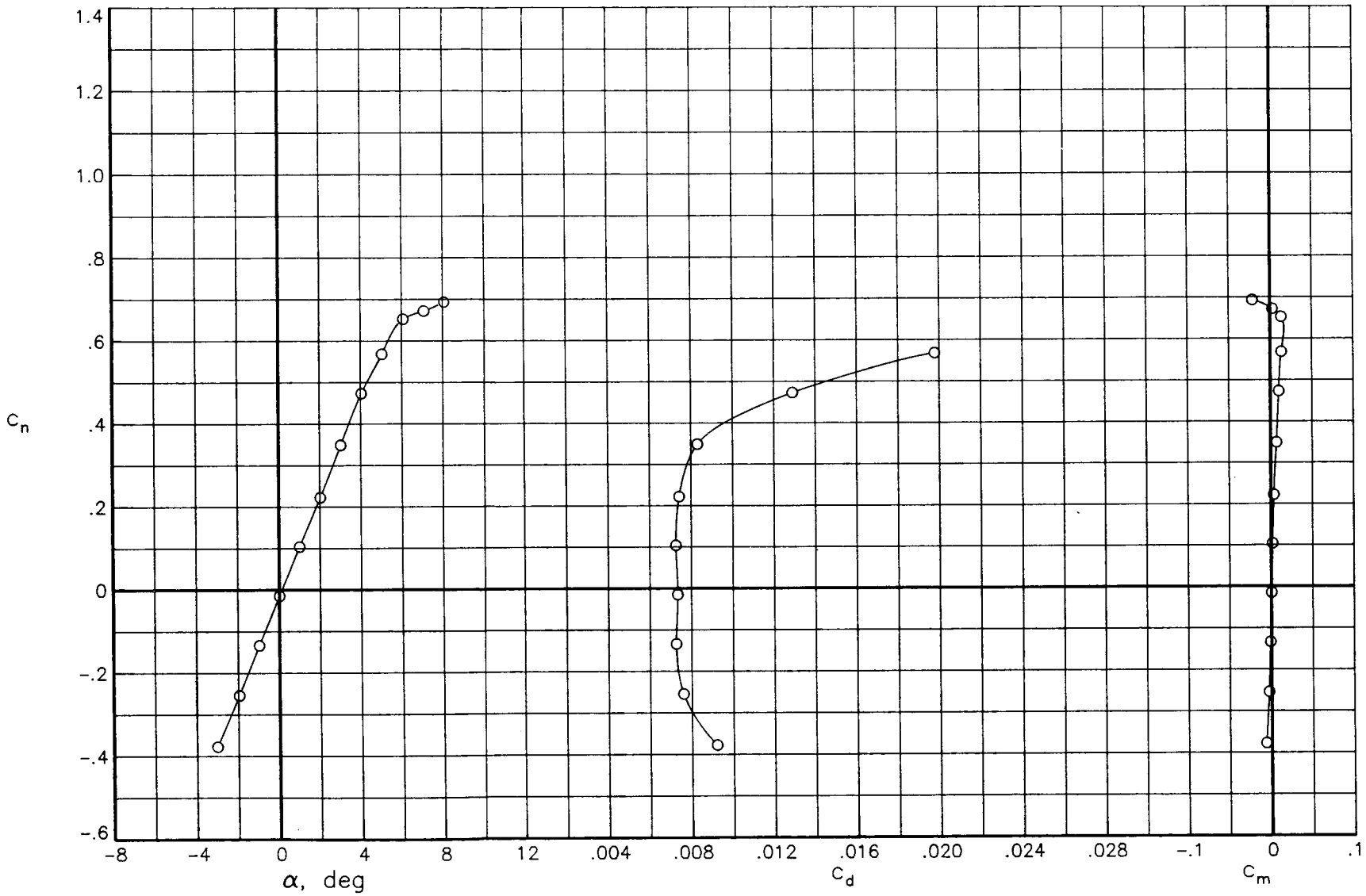

(d) R = 15.0 x 10^6

Figure 24.- Continued.

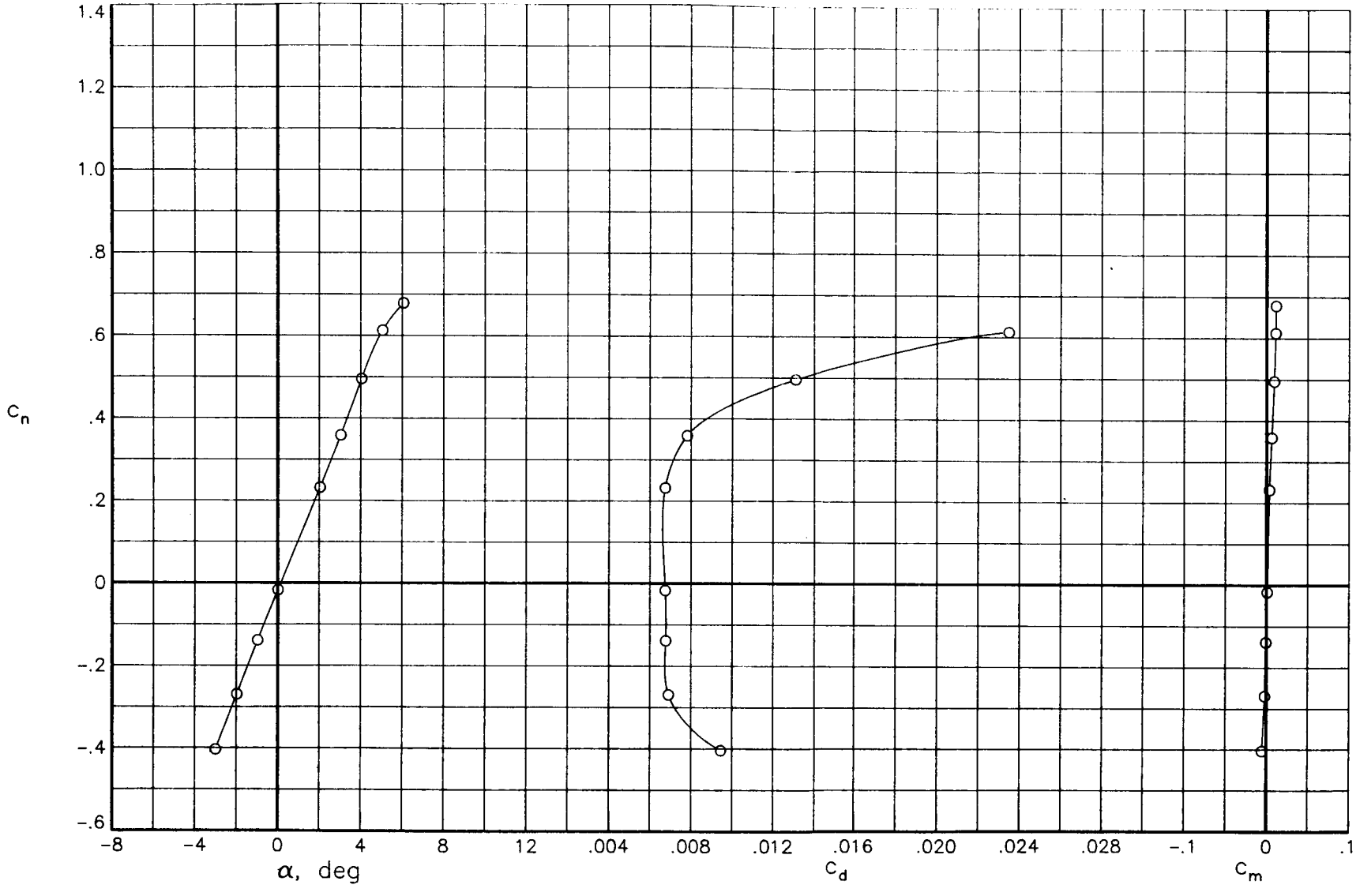

(e) R = 30.0 x 10^6

Figure 24.- Concluded.

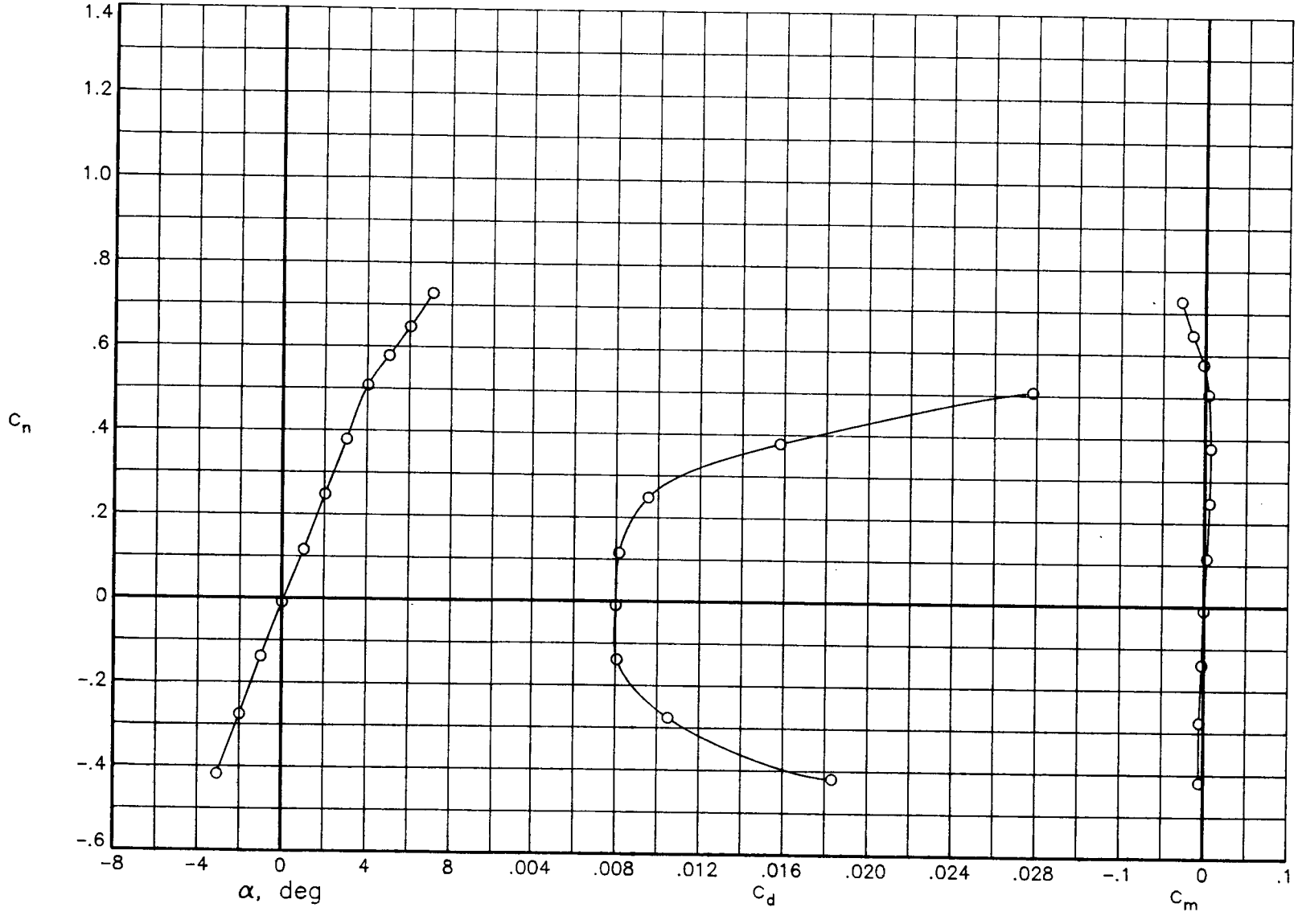

(a) R = 6.0 x 10^6

Figure 25.- Variation of basic aerodynamic data with angle of attack for various Reynolds numbers at a Mach number of 0.74. Transition free.

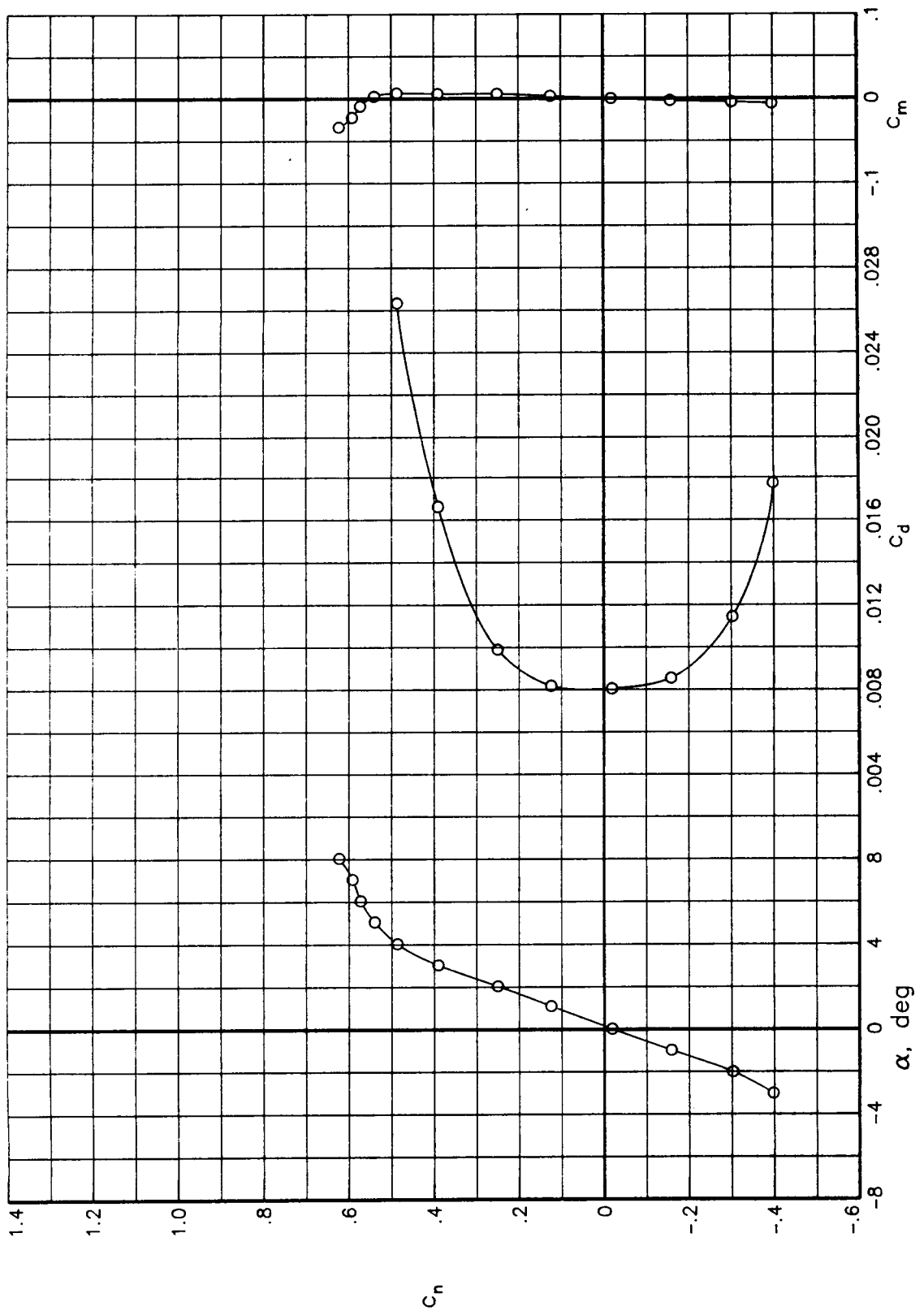

(b) R = 9.0 x 10^6

Figure 25.- Continued.

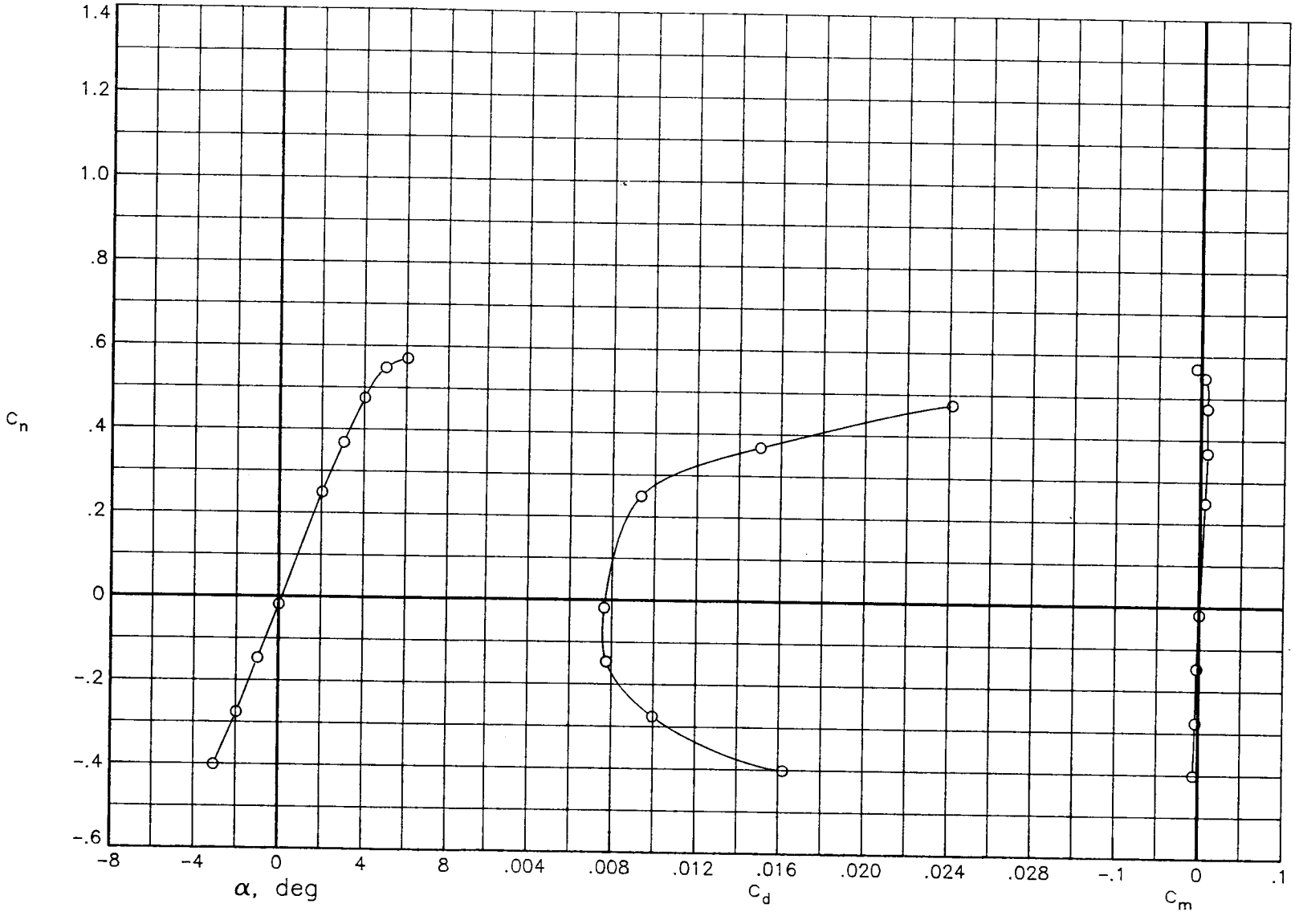

(c) R = 15.0 x 10^6

Figure 25.- Continued.

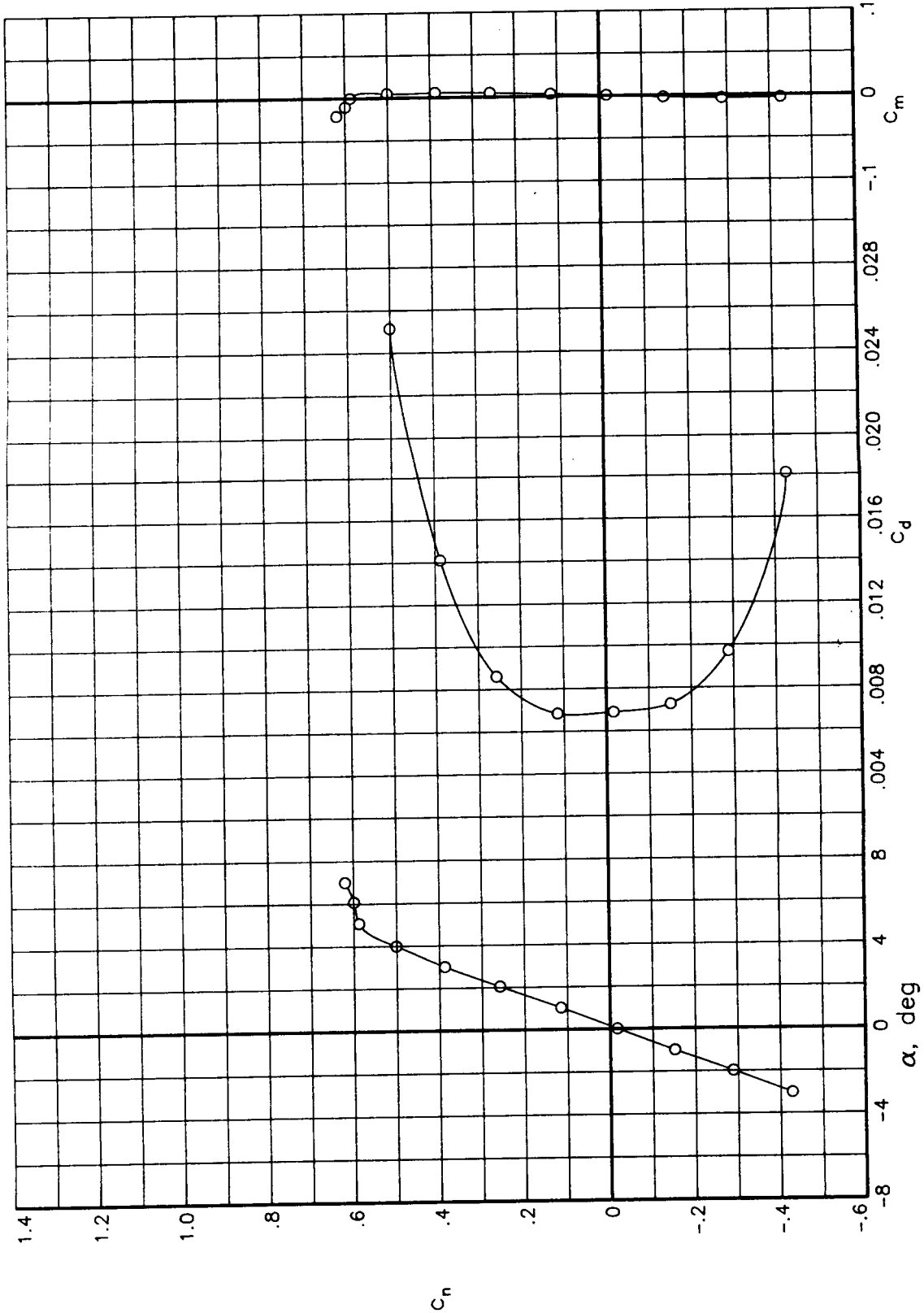

(d) R = 30.0 x 10^6

Figure 25.- Concluded.

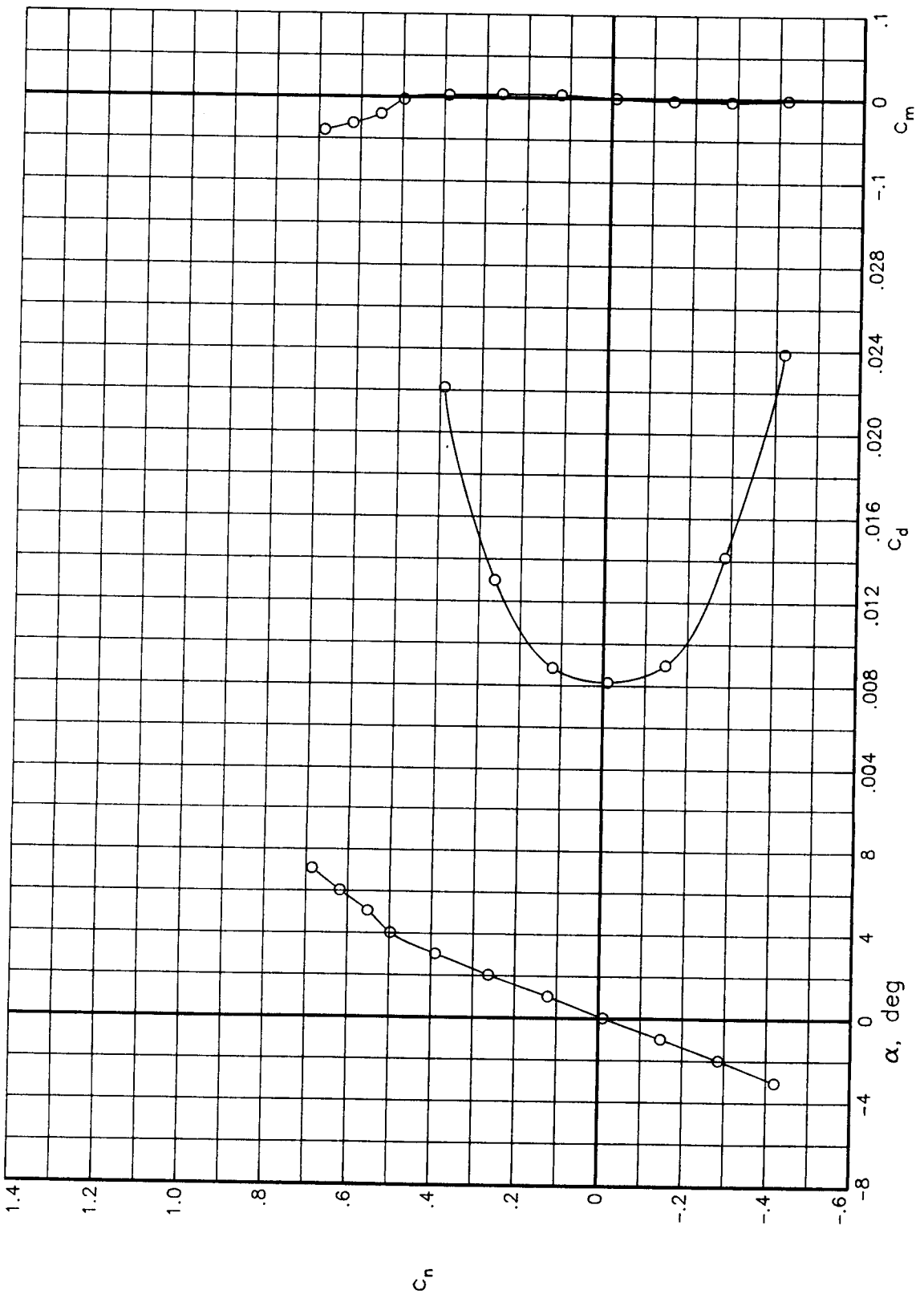

(a) R = 6.0 x 10^6

Figure 26.- Variation of basic aerodynamic data with angle of attack for various Reynolds numbers at a Mach number of 0.76. Transition free.

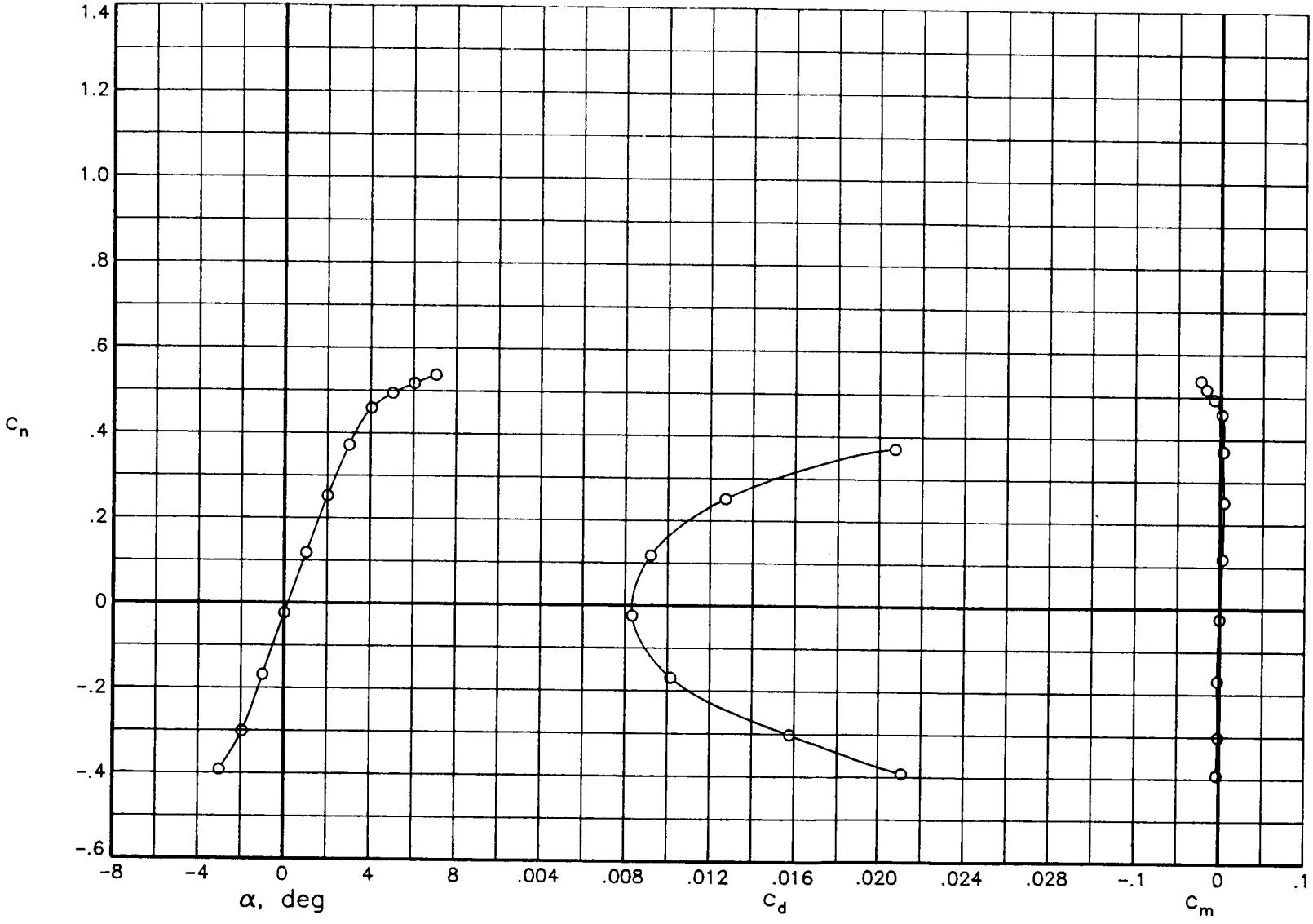

(b) R = 9.0 x 10^6

Figure 26.- Continued.

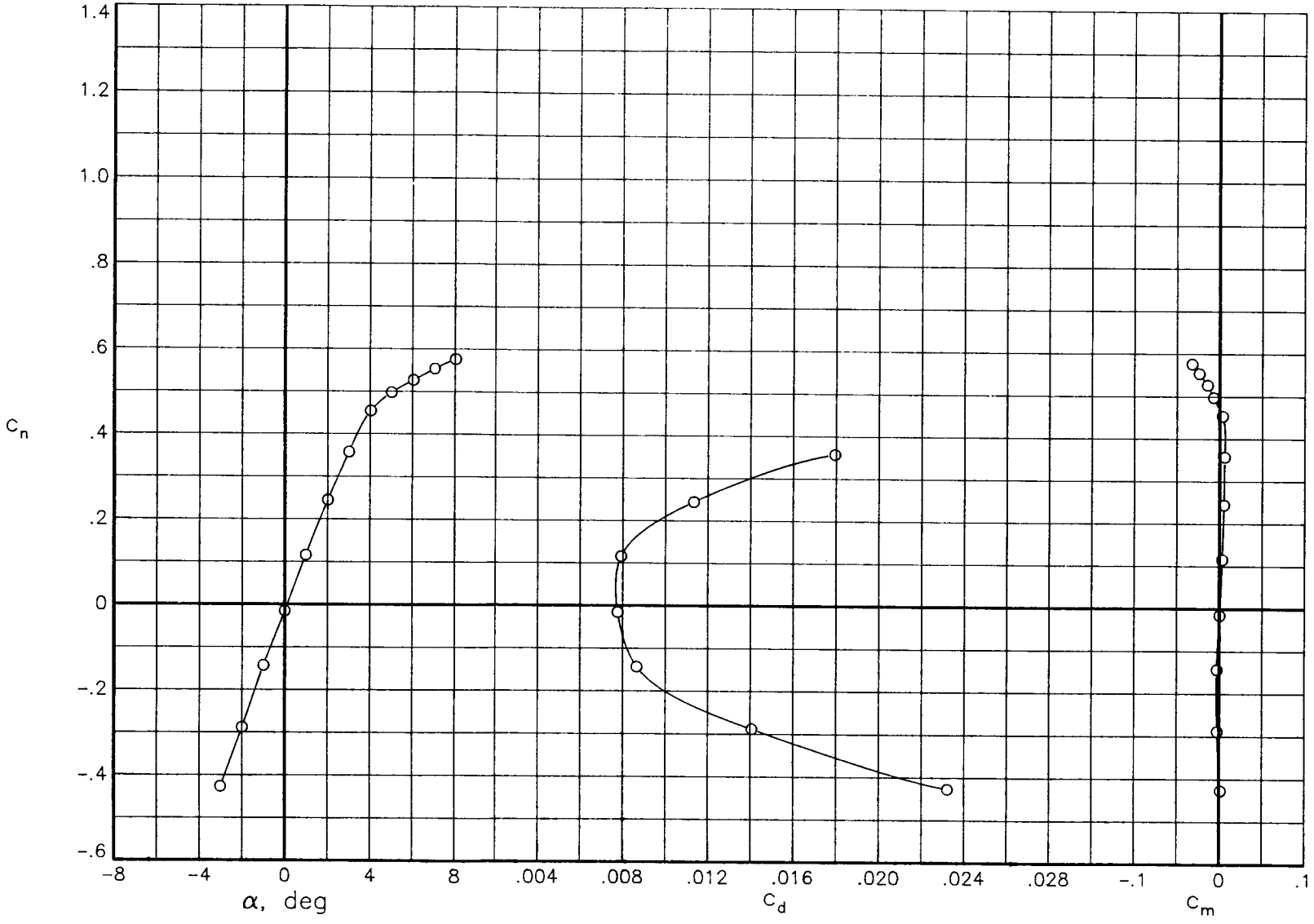

(c) R = 15.0 x 10^6

Figure 26.- Continued.

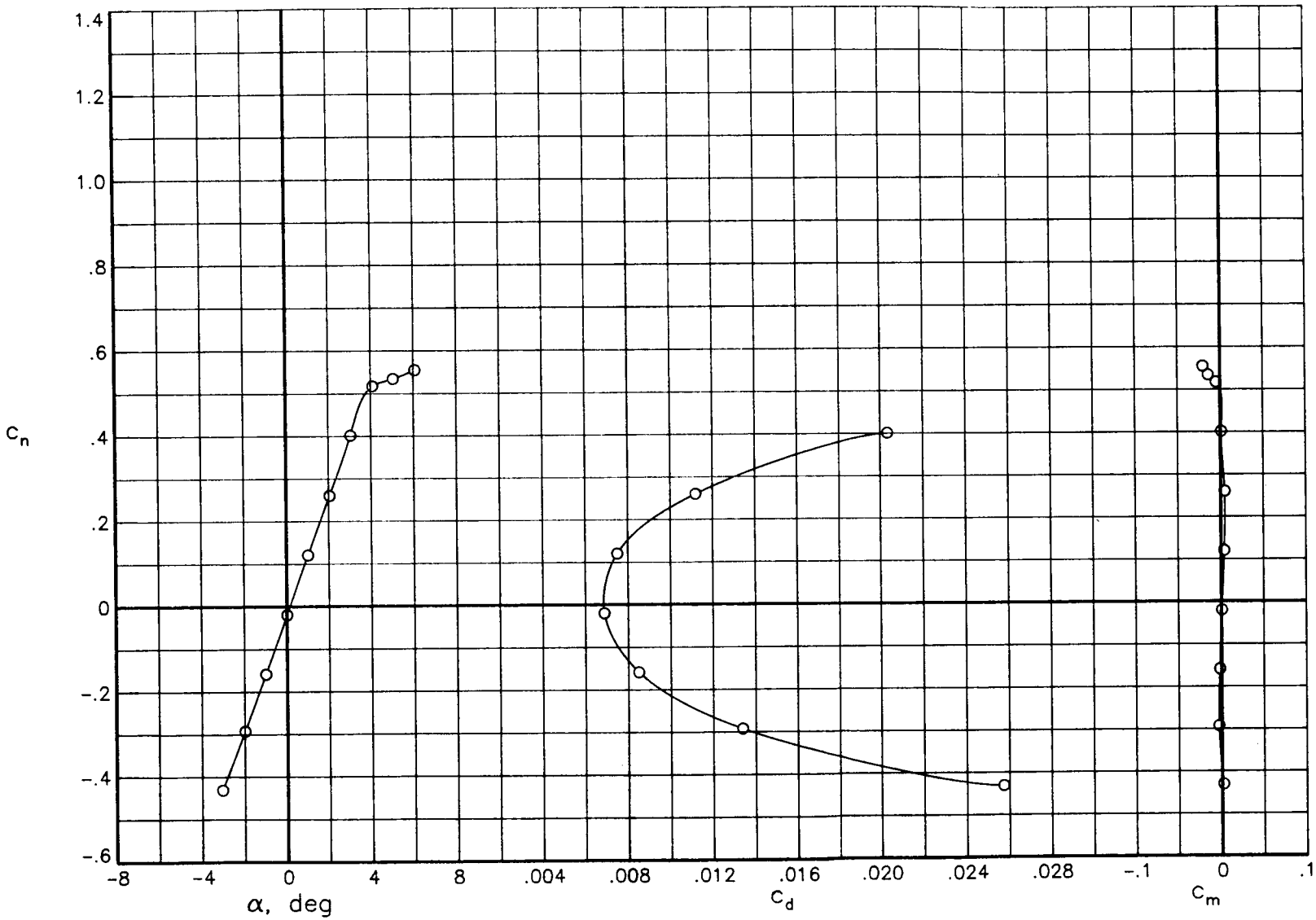

(d) R = 30.0 x 10^6

Figure 26.- Continued.

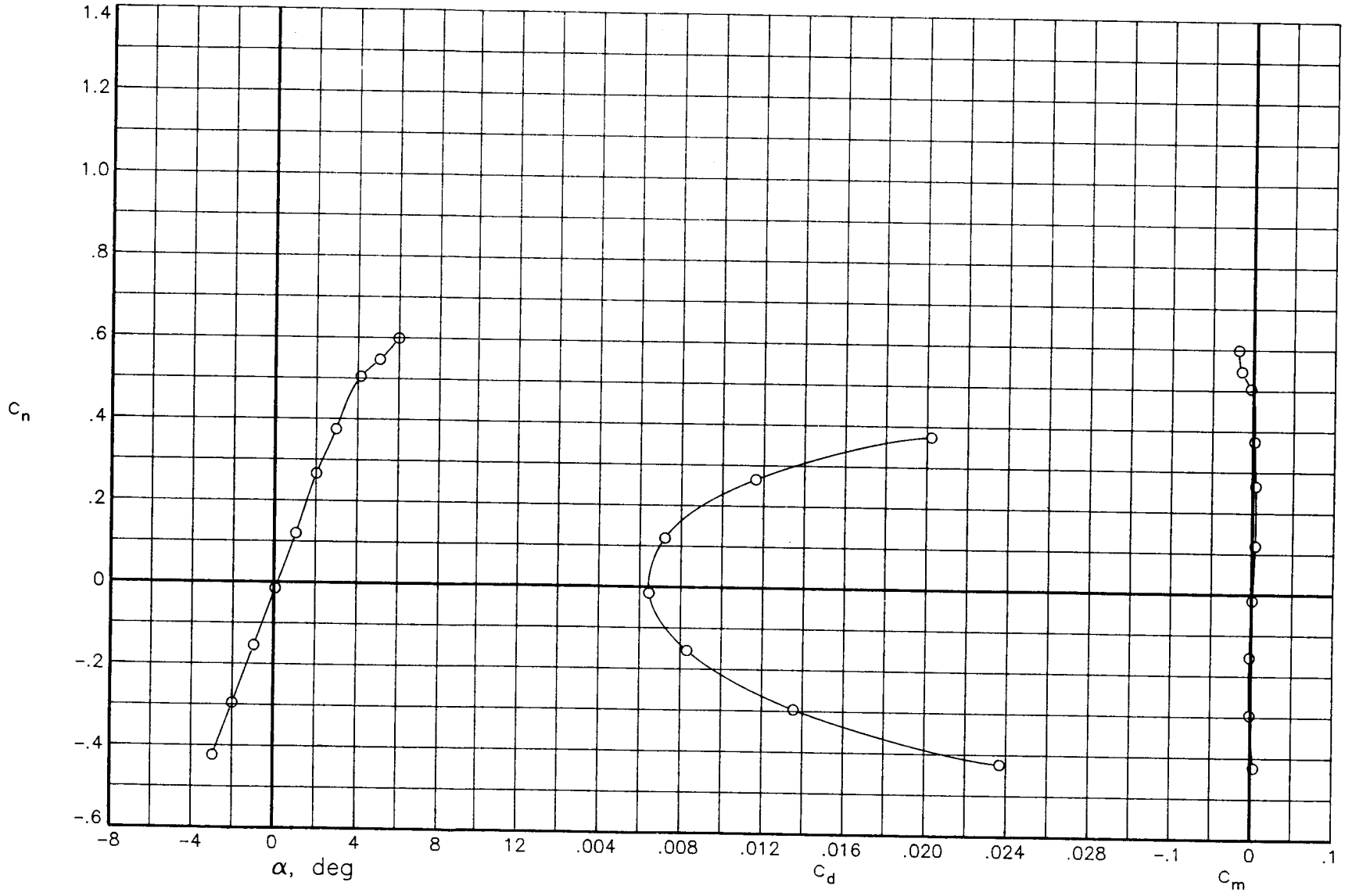

(e) R = 45.0 x 10^6

Figure 26.- Concluded.

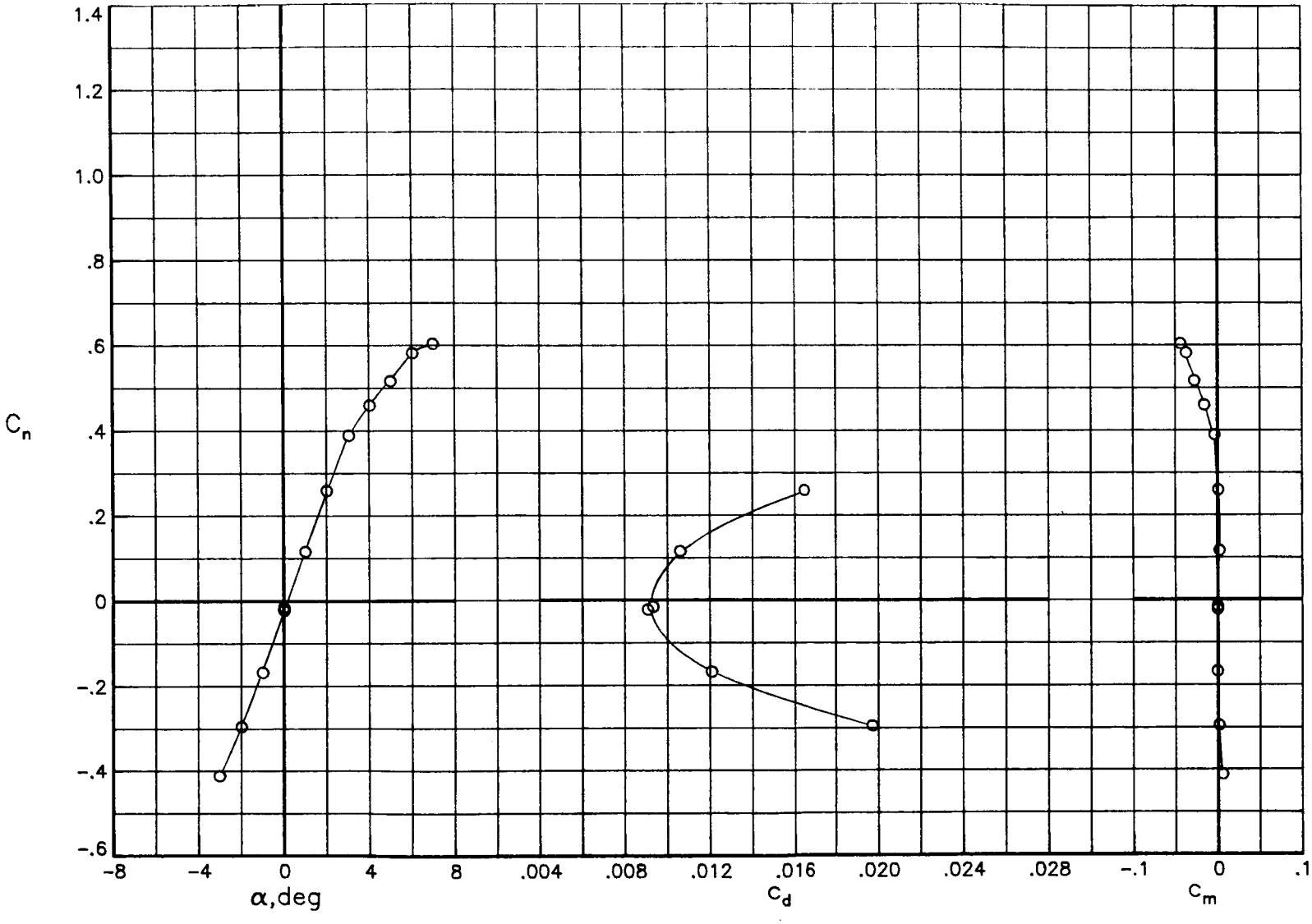

(a) R = 6.0 x 10^6

Figure 27.- Variation of basic aerodynamic data with angle of attack for various Reynolds numbers at a Mach number of 0.78. Transition free.

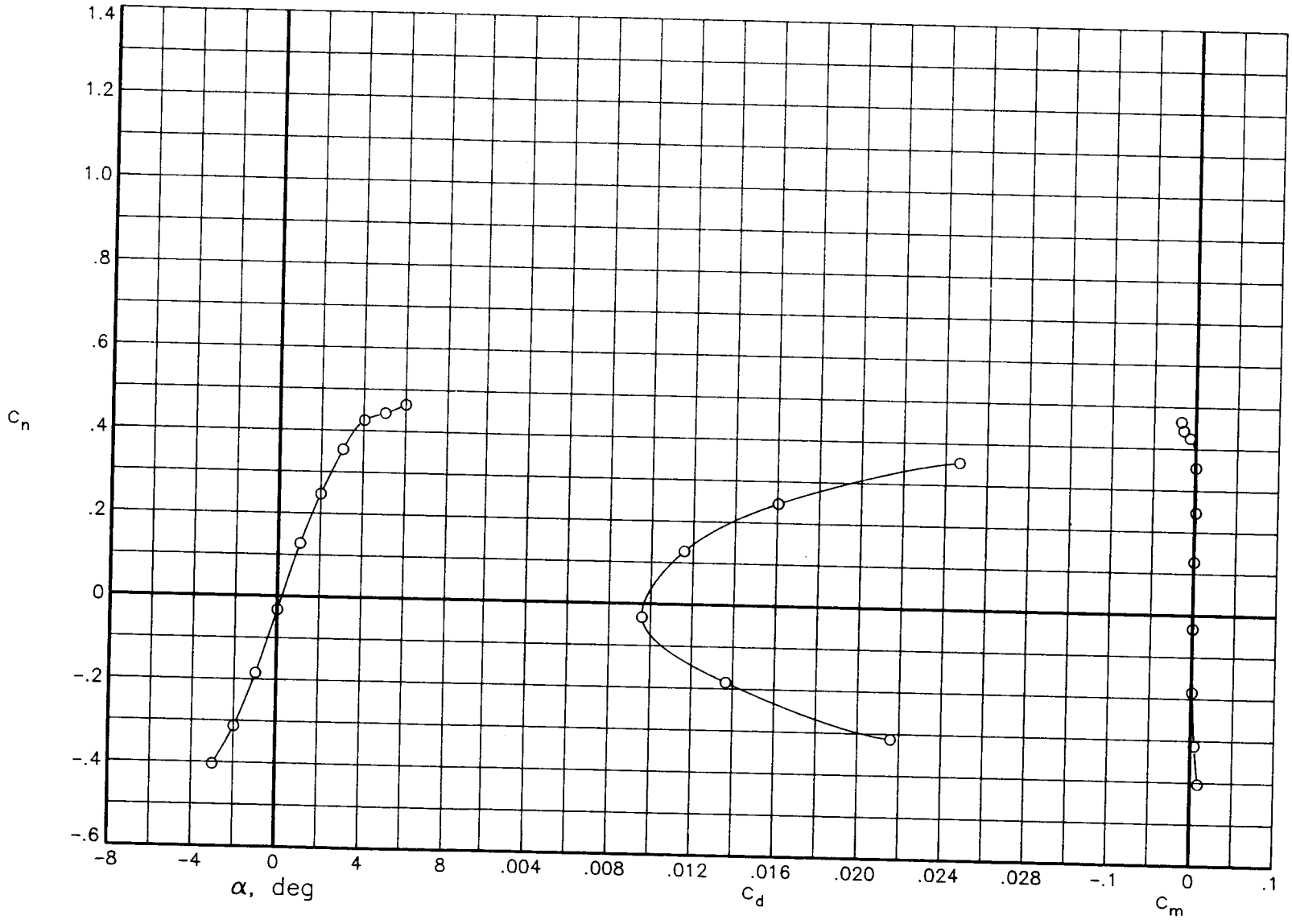

(b) R = 9.0 x 10^6

Figure 27.- Continued.

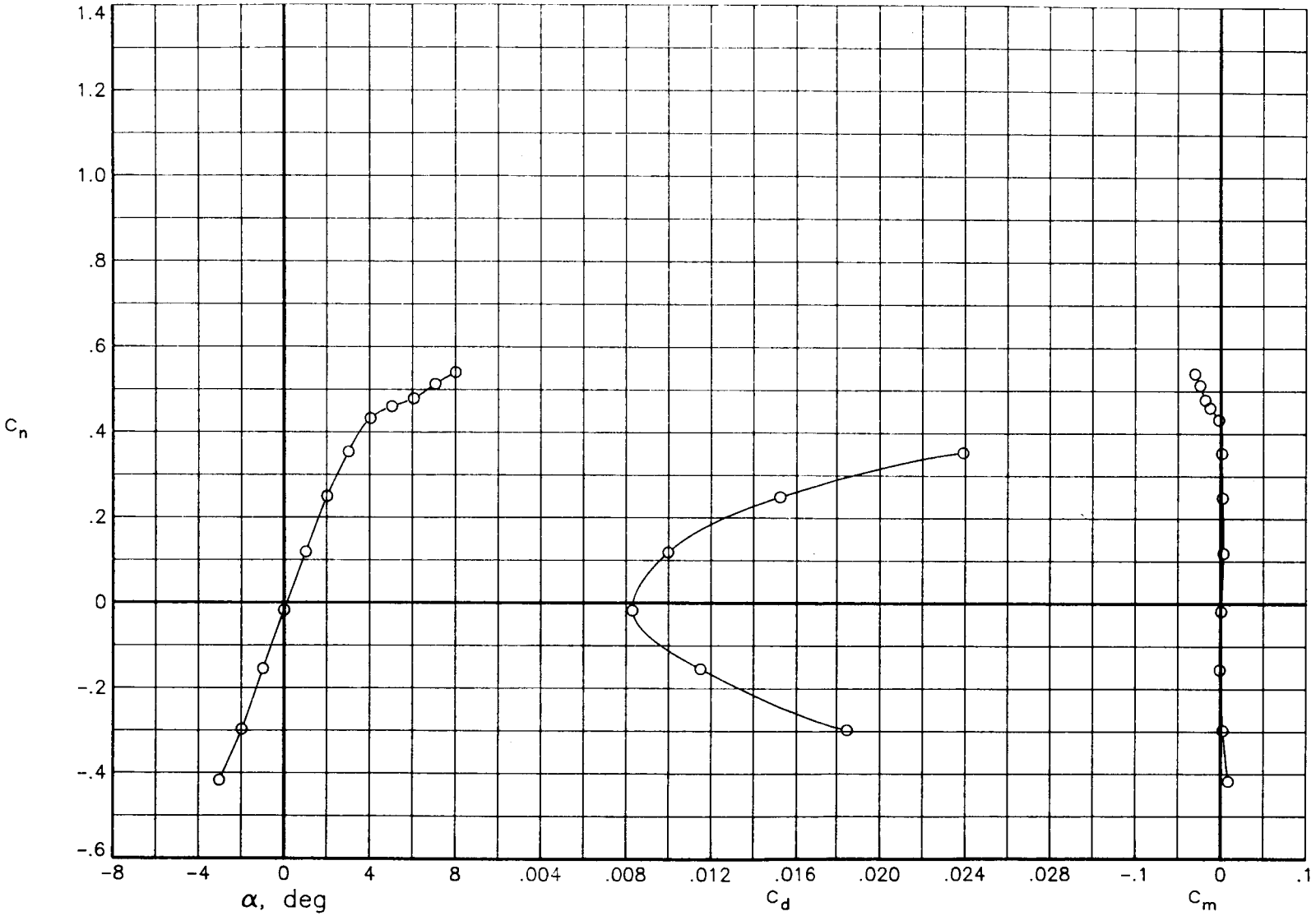

(c) R = 15.0 x 10^6

Figure 27.- Continued.

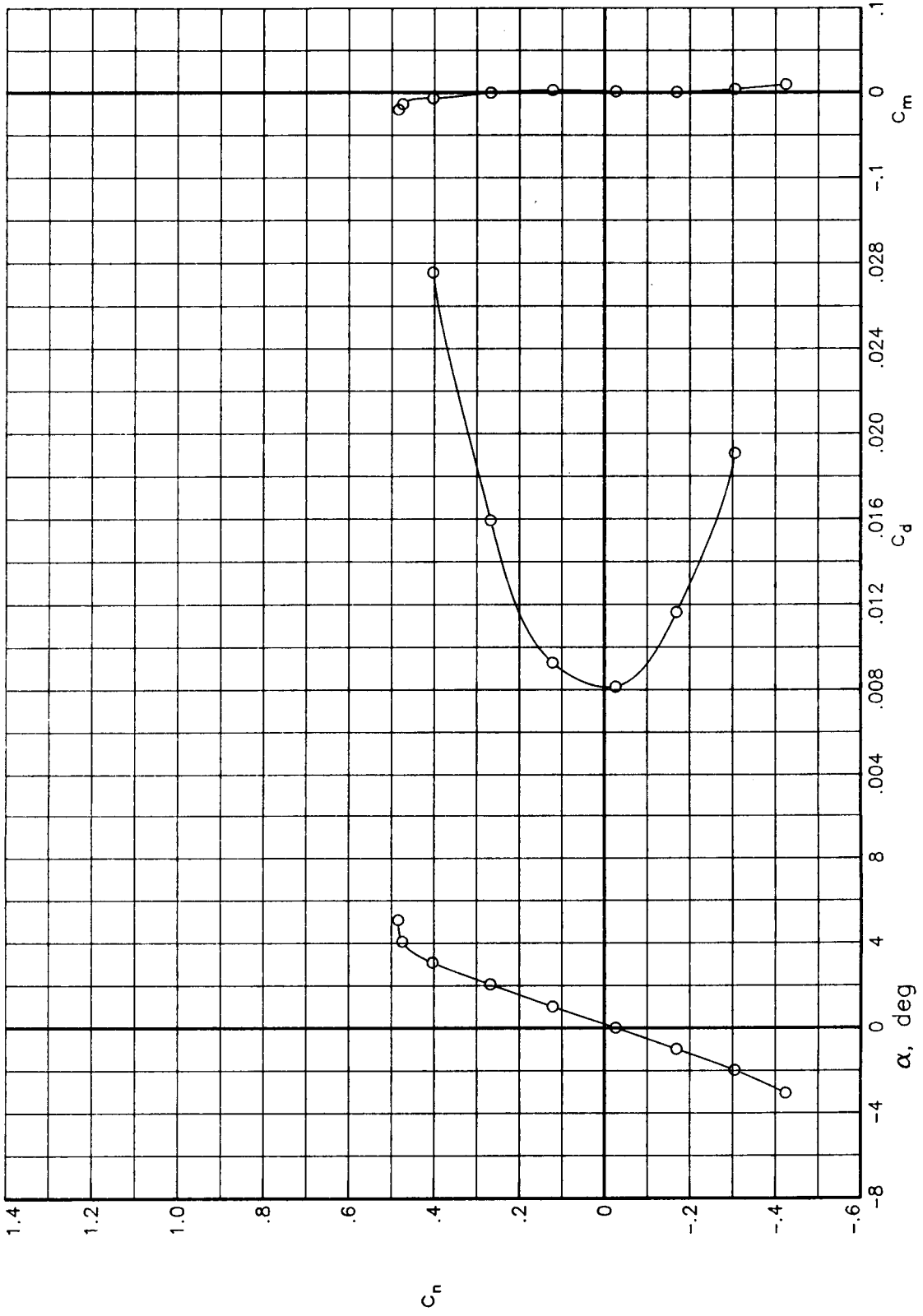

(d) R = 30.0 x 10^6

Figure 27.- Continued.

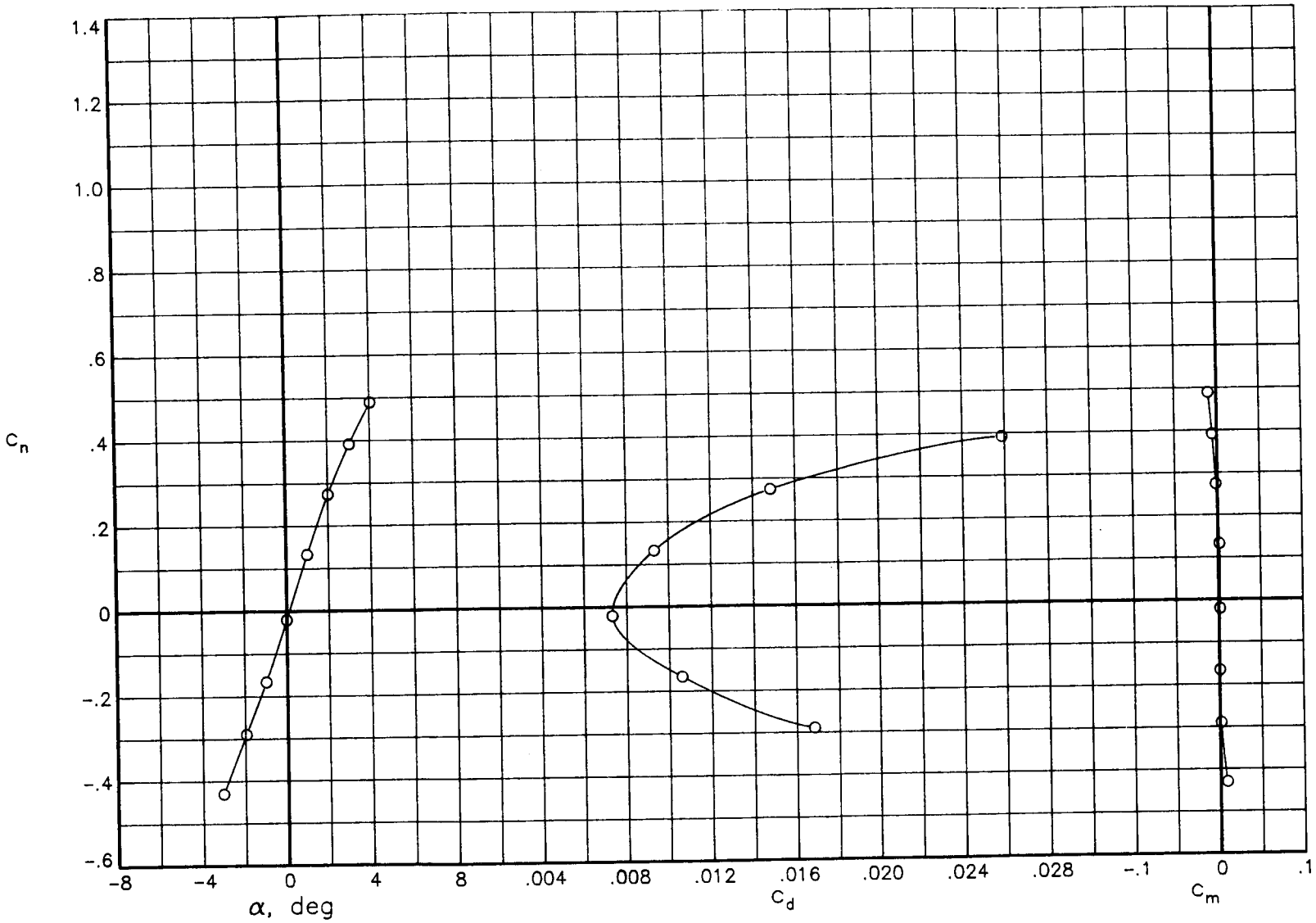

(e) R = 45.0 x 10^6

Figure 27.- Concluded.

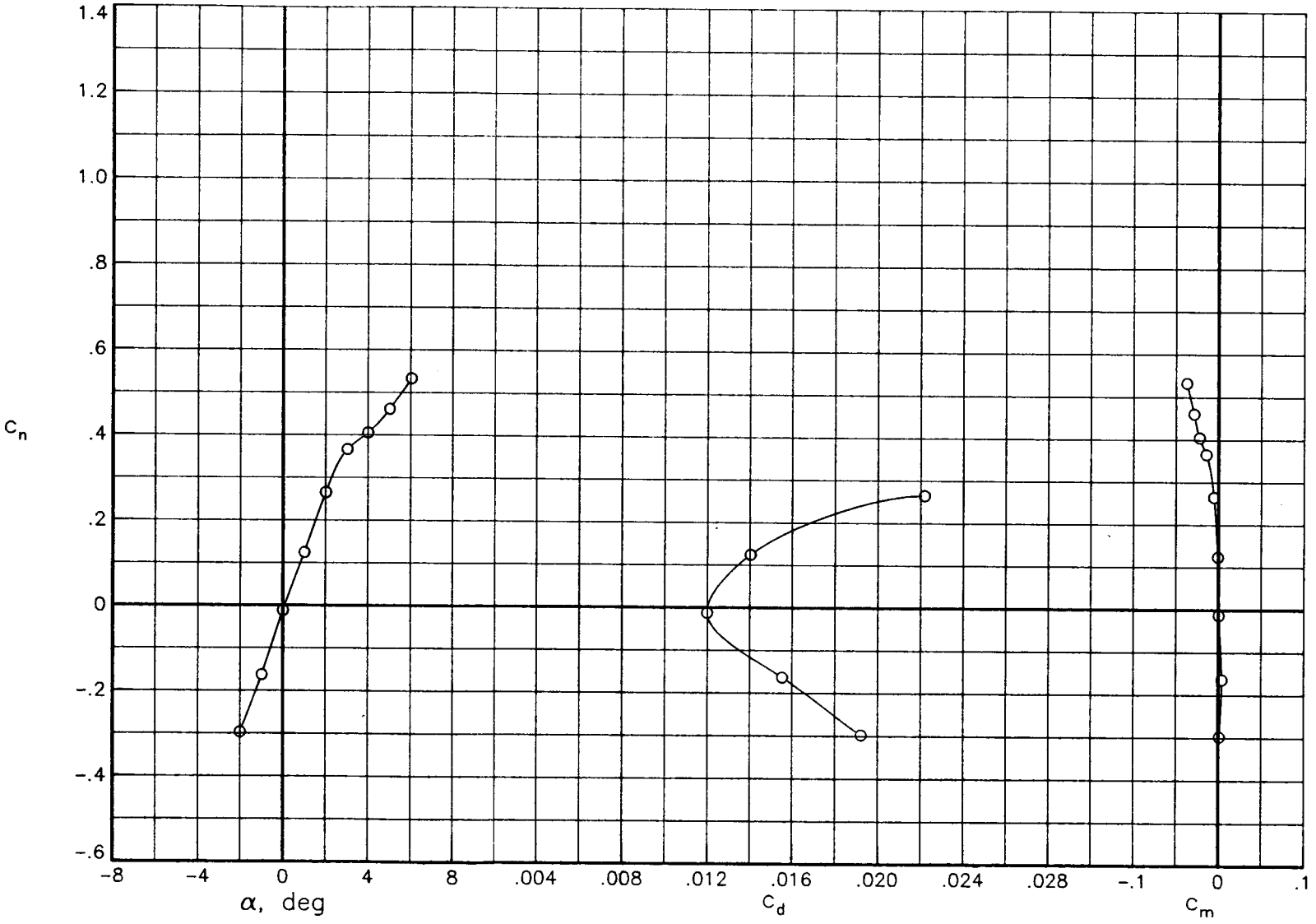

(a) R = 6.0 x 10^6

Figure 28.- Variation of basic aerodynamic data with angle of attack for various Reynolds numbers at a Mach number of 0.80. Transition free.

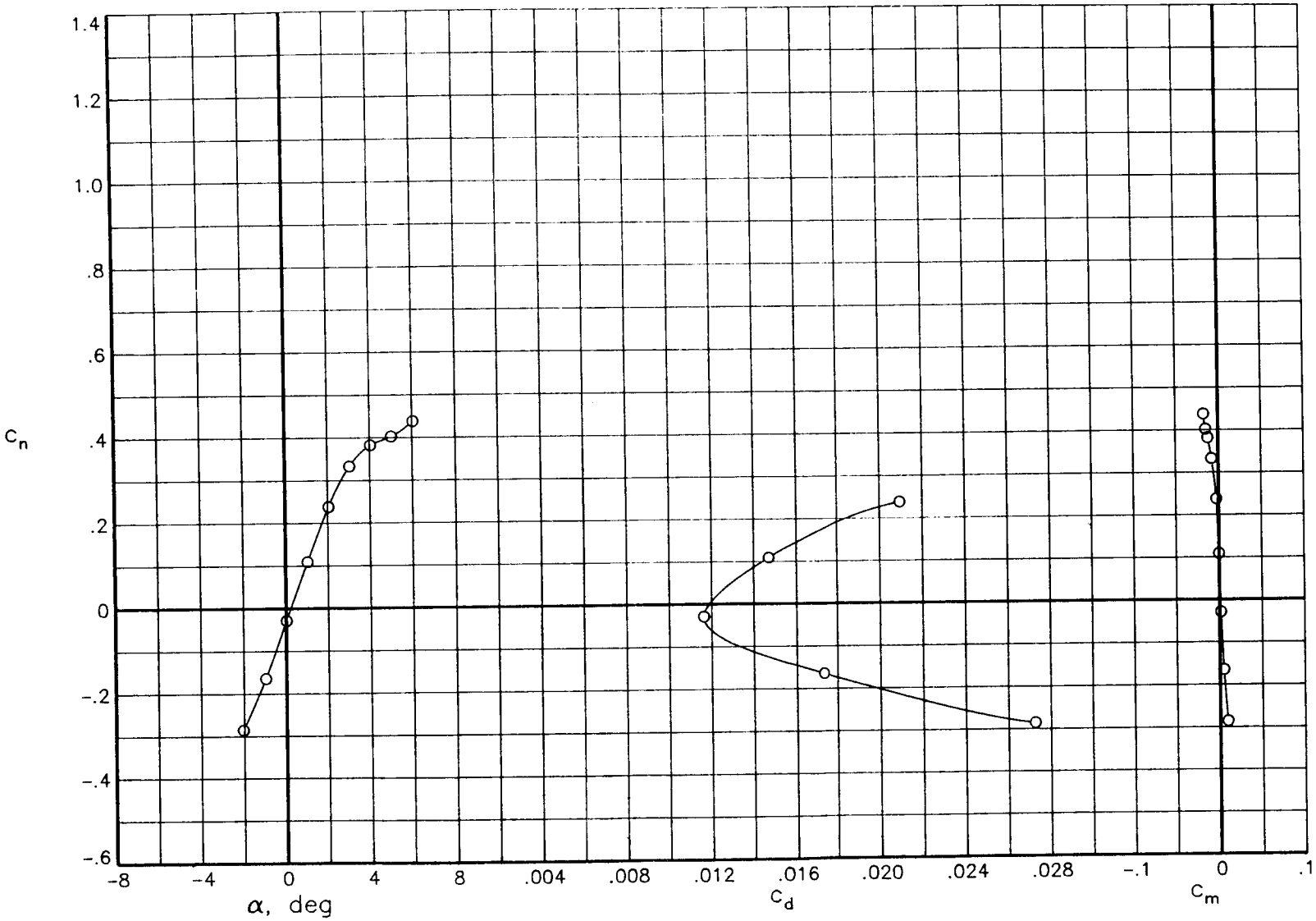

(b) R = 9.0 x 10^6

Figure 28.- Continued.

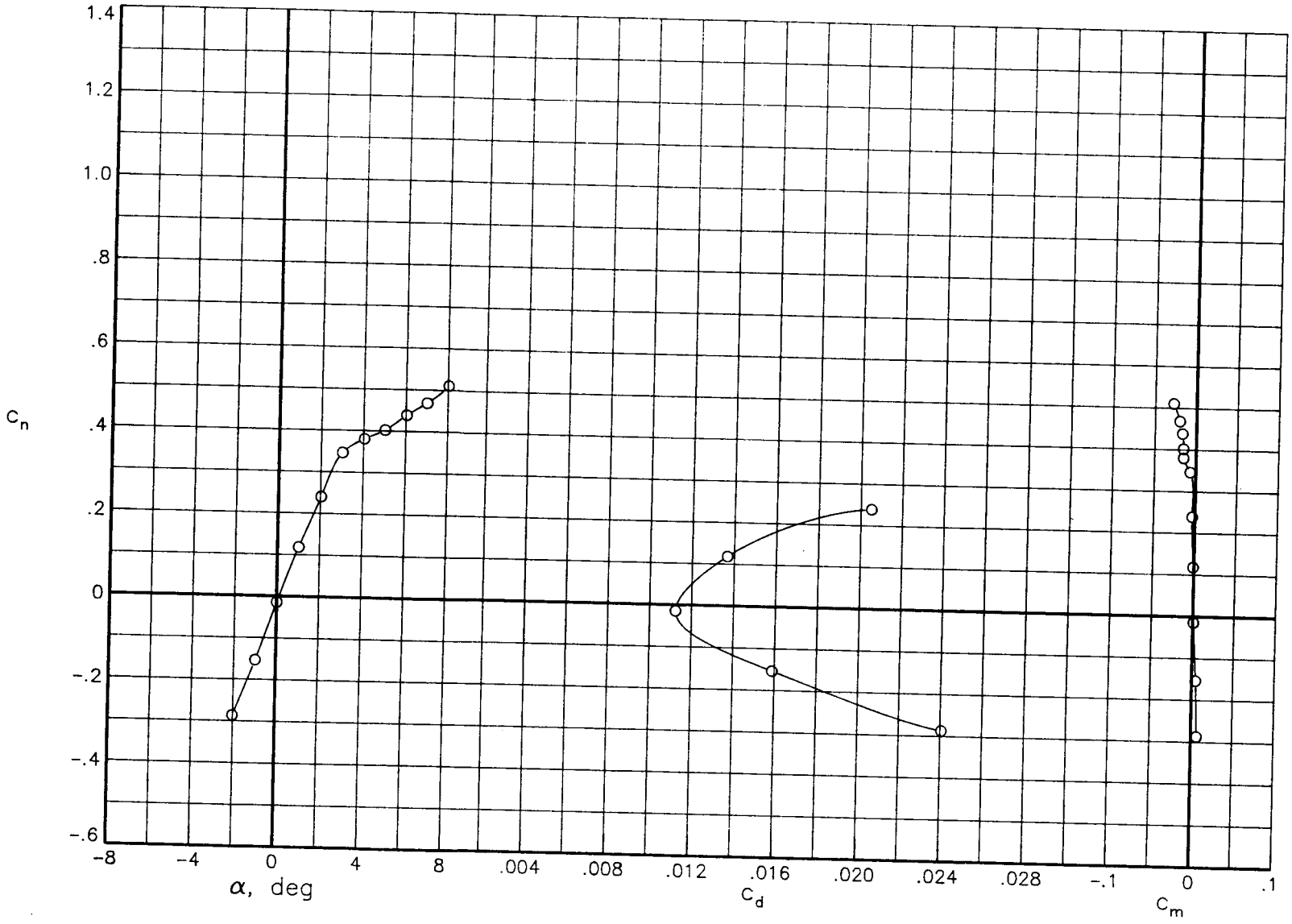

(c) R = 15.0 x 10^6

Figure 28.- Continued.

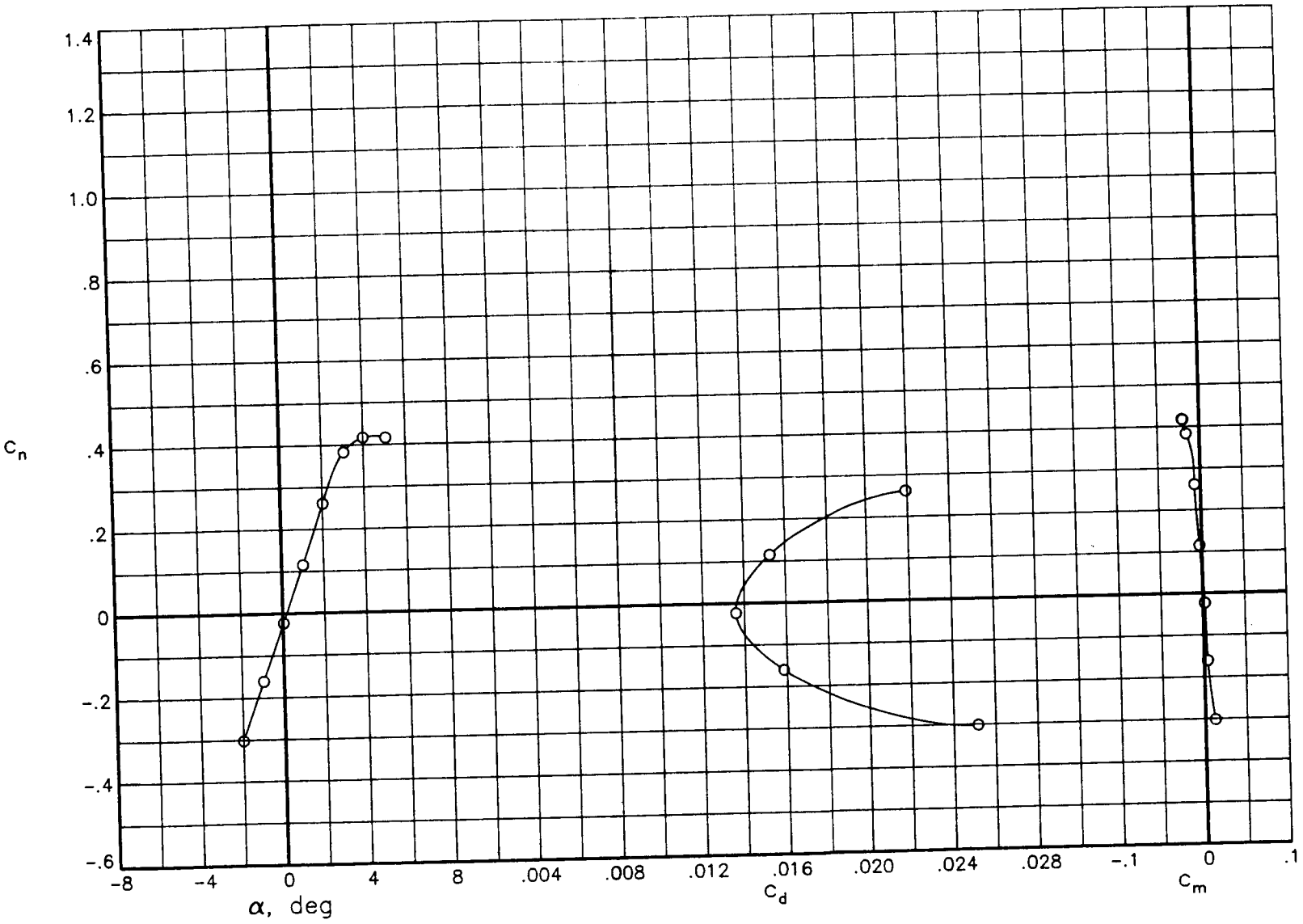

(d) R = 30.0 x 10^6

Figure 28.- Continued.

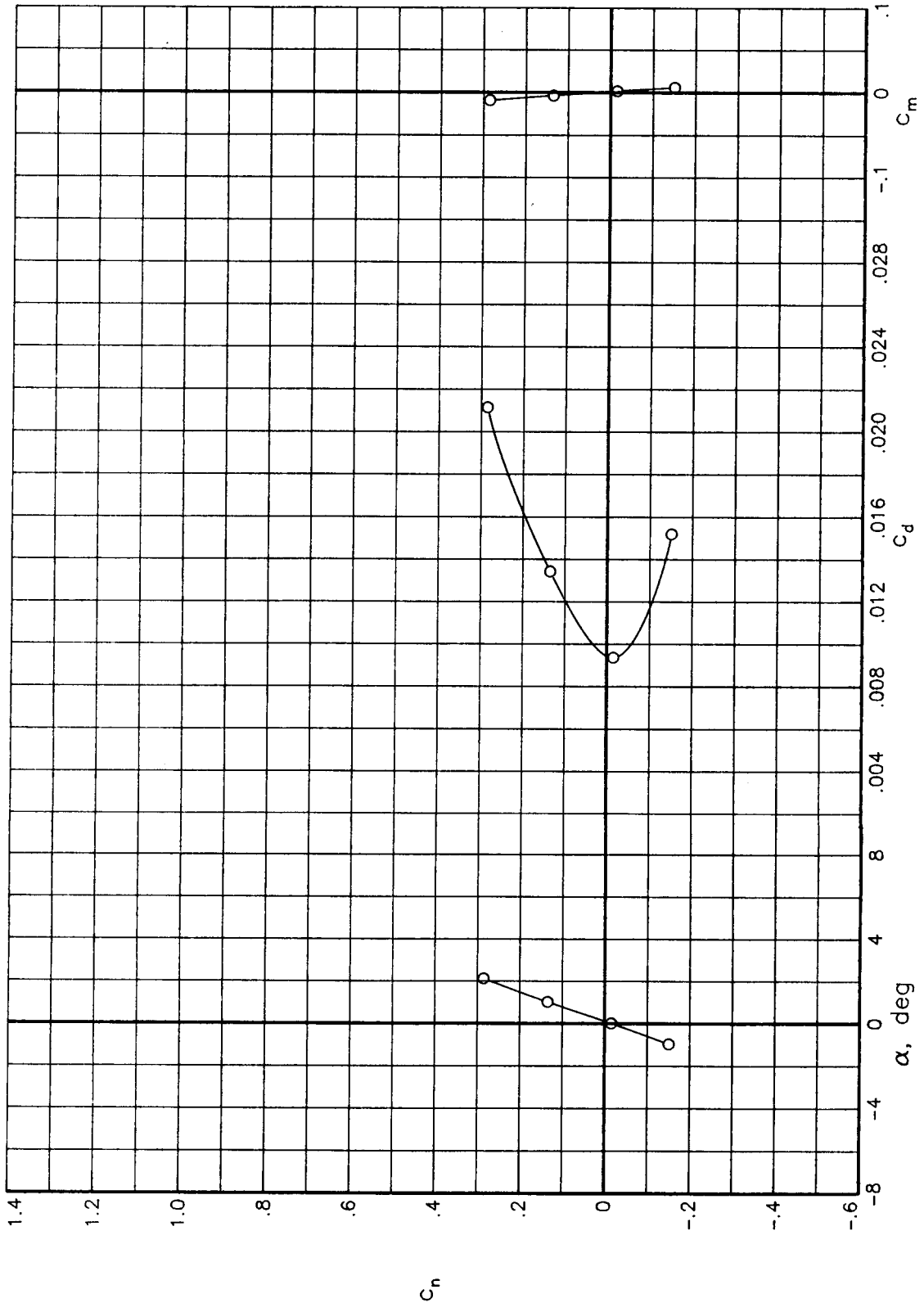

(e) R = 45.0 x 10^6

Figure 28.- Concluded.

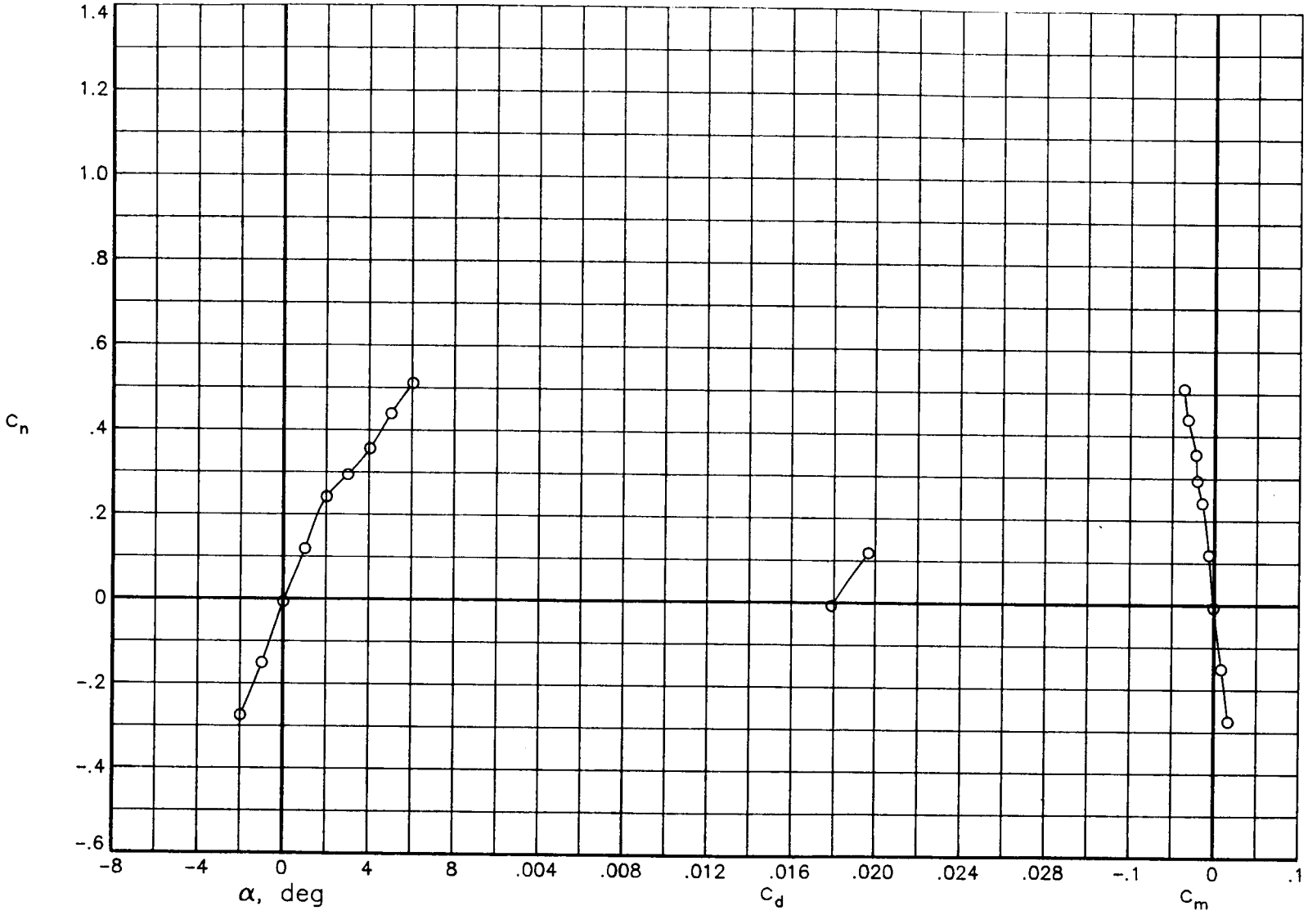

(a) R = 6.0 x 10^6

Figure 29.- Variation of basic aerodynamic data with angle of attack for various Reynolds numbers at a Mach number of 0.82. Transition free.

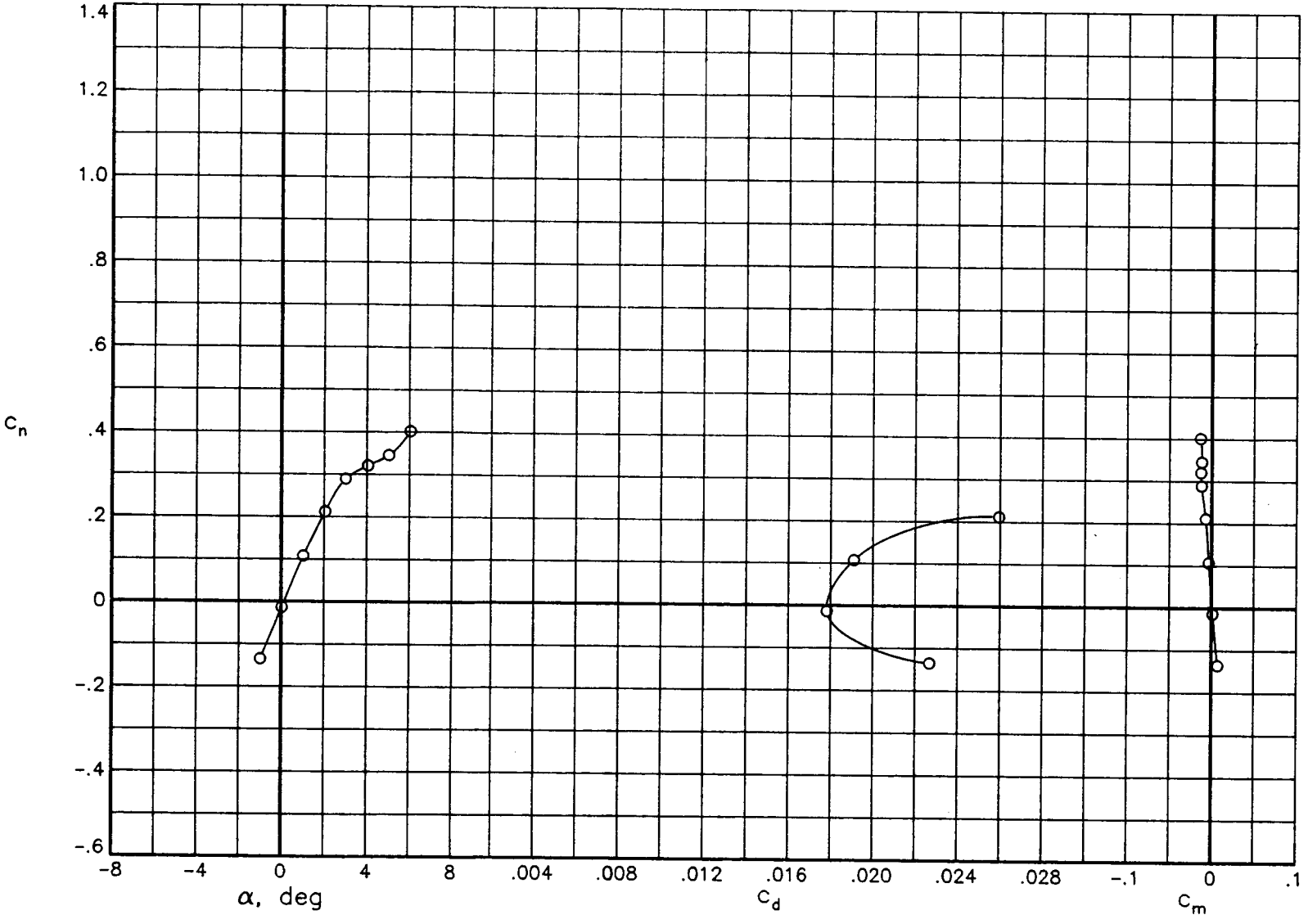

(b) R = 9.0 x 10^6

Figure 29.- Continued.

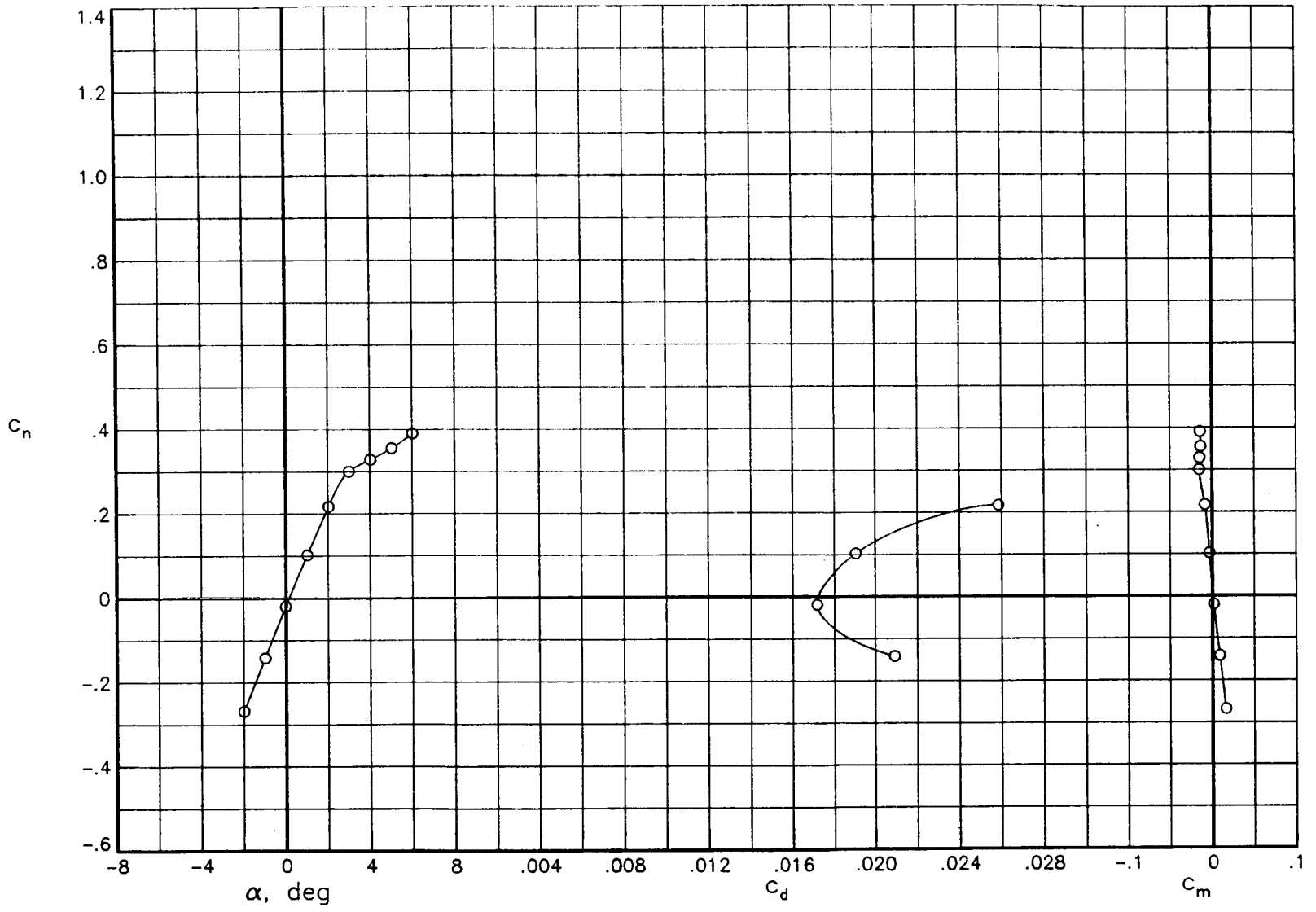

(c) R = 15.0 x 10^6

Figure 29.- Continued.

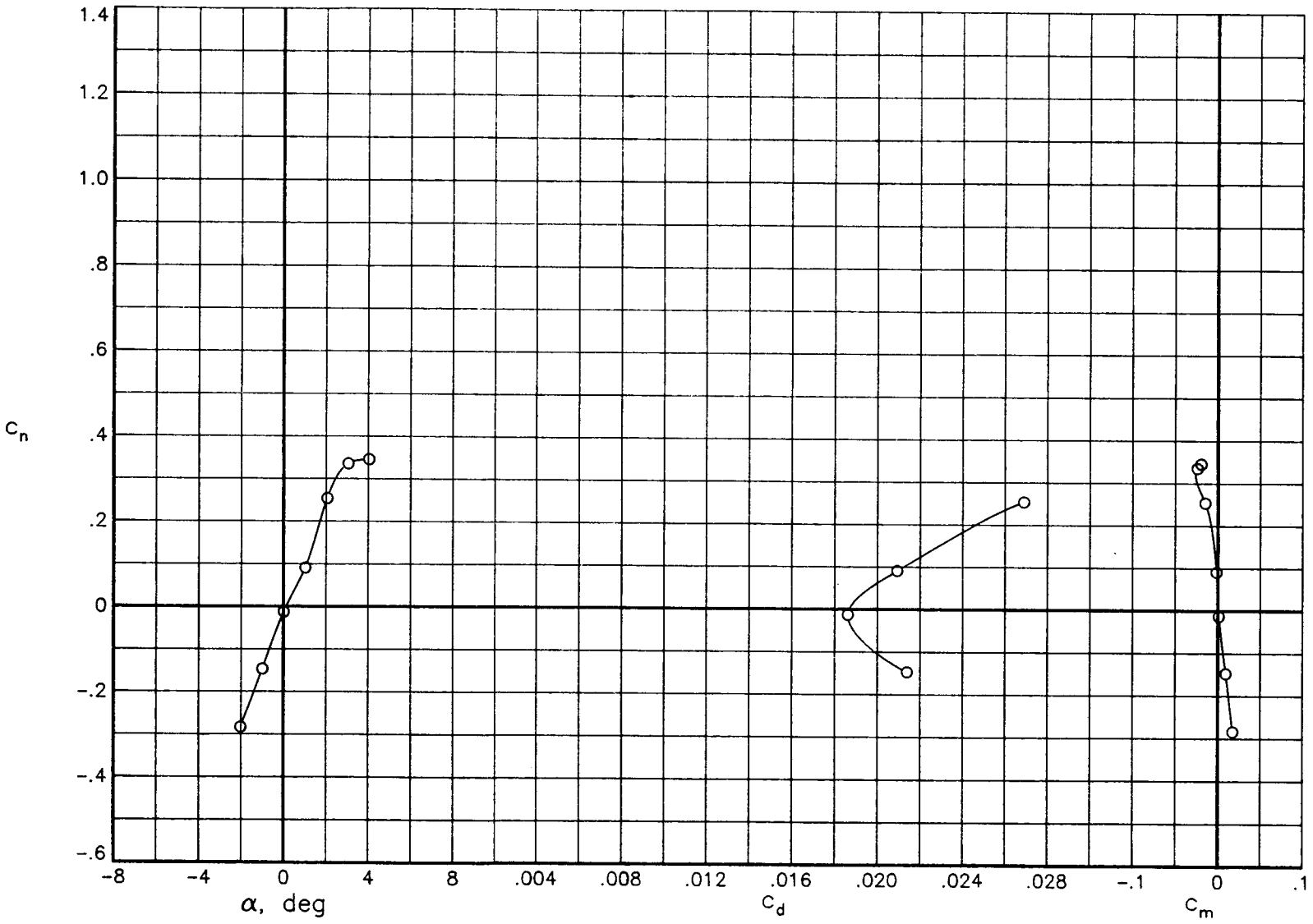

(d) R = 30.0 x 10^6

Figure 29.- Continued.

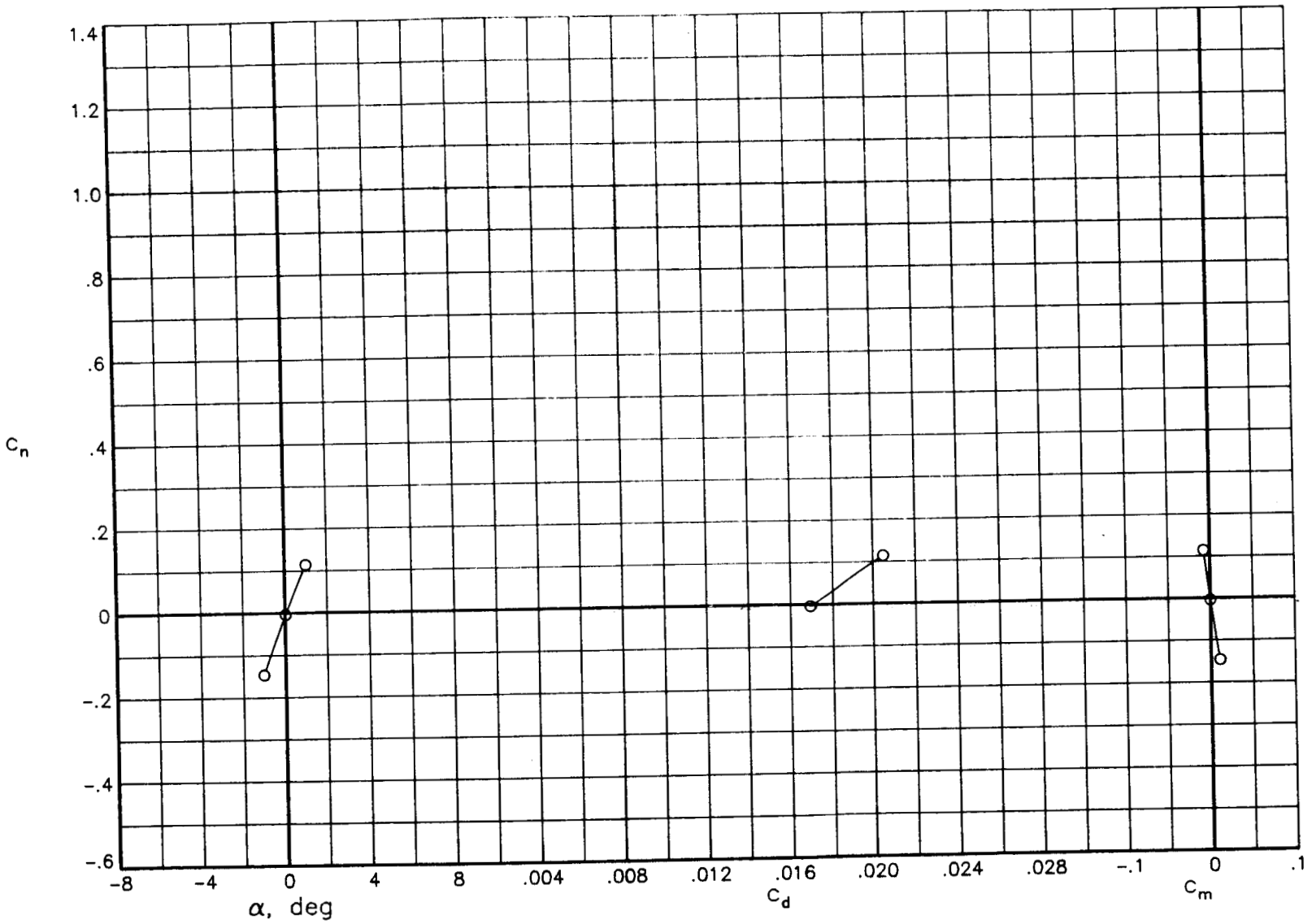

(e) R = 45.0 x 10^6

Figure 29.- Concluded.

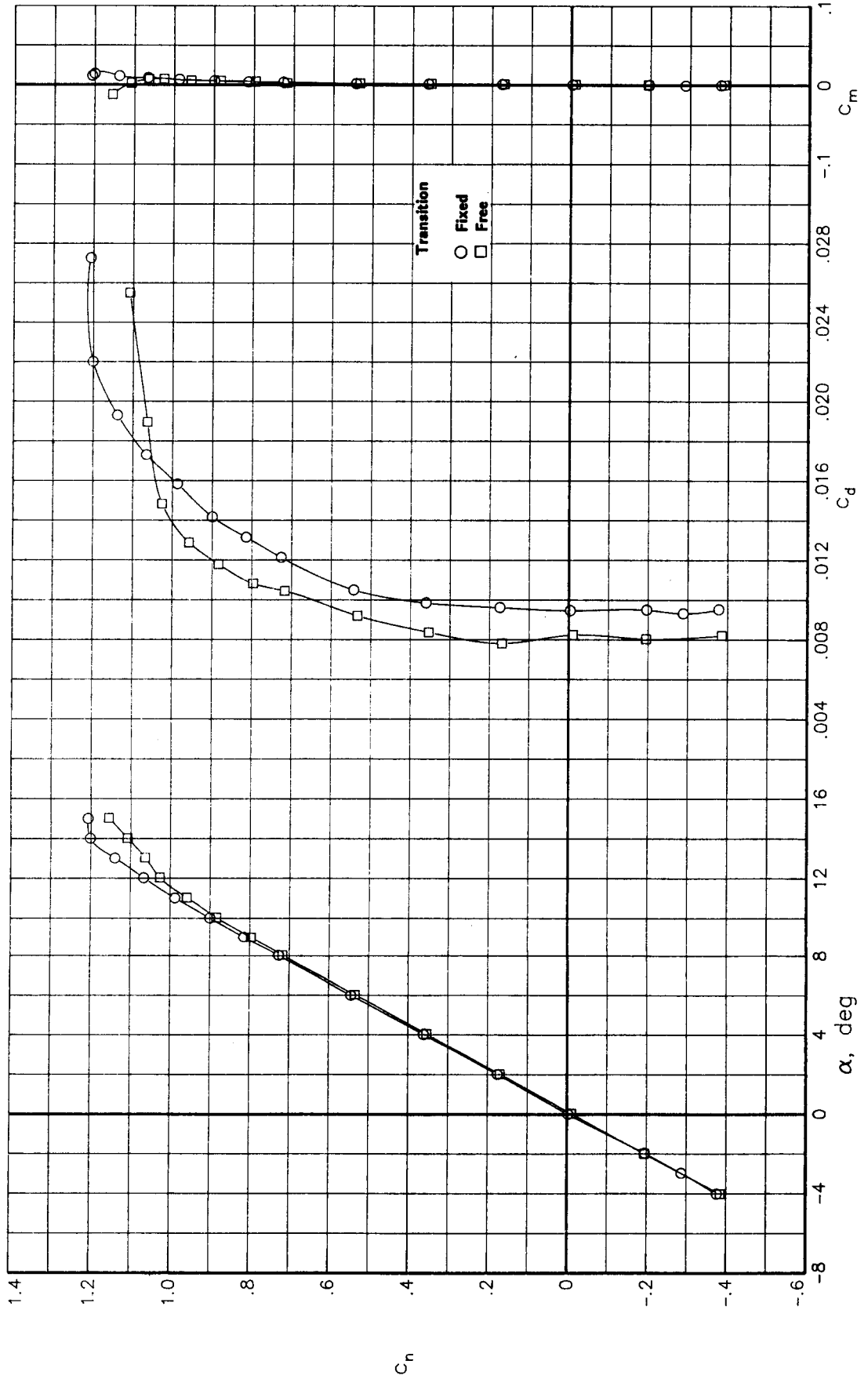

(a) R = 3.0 x 10^6

Figure 30.- Effects of fixing transition on the variation of basic aerodynamic data with angle of attack for various Reynolds numbers at a Mach number of 0.30.

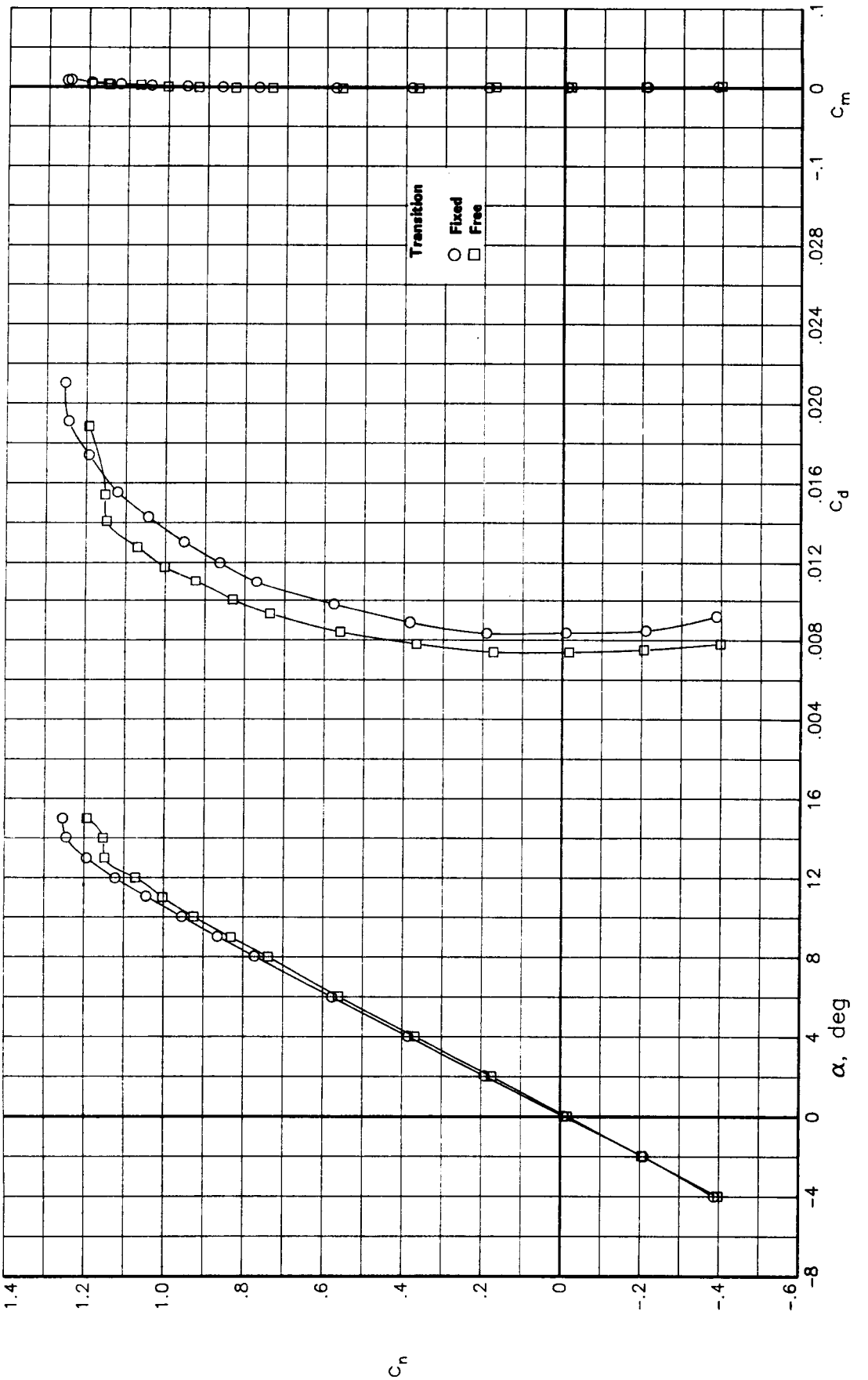

(b) R = 9.0 x 10^6

Figure 30.- Concluded.

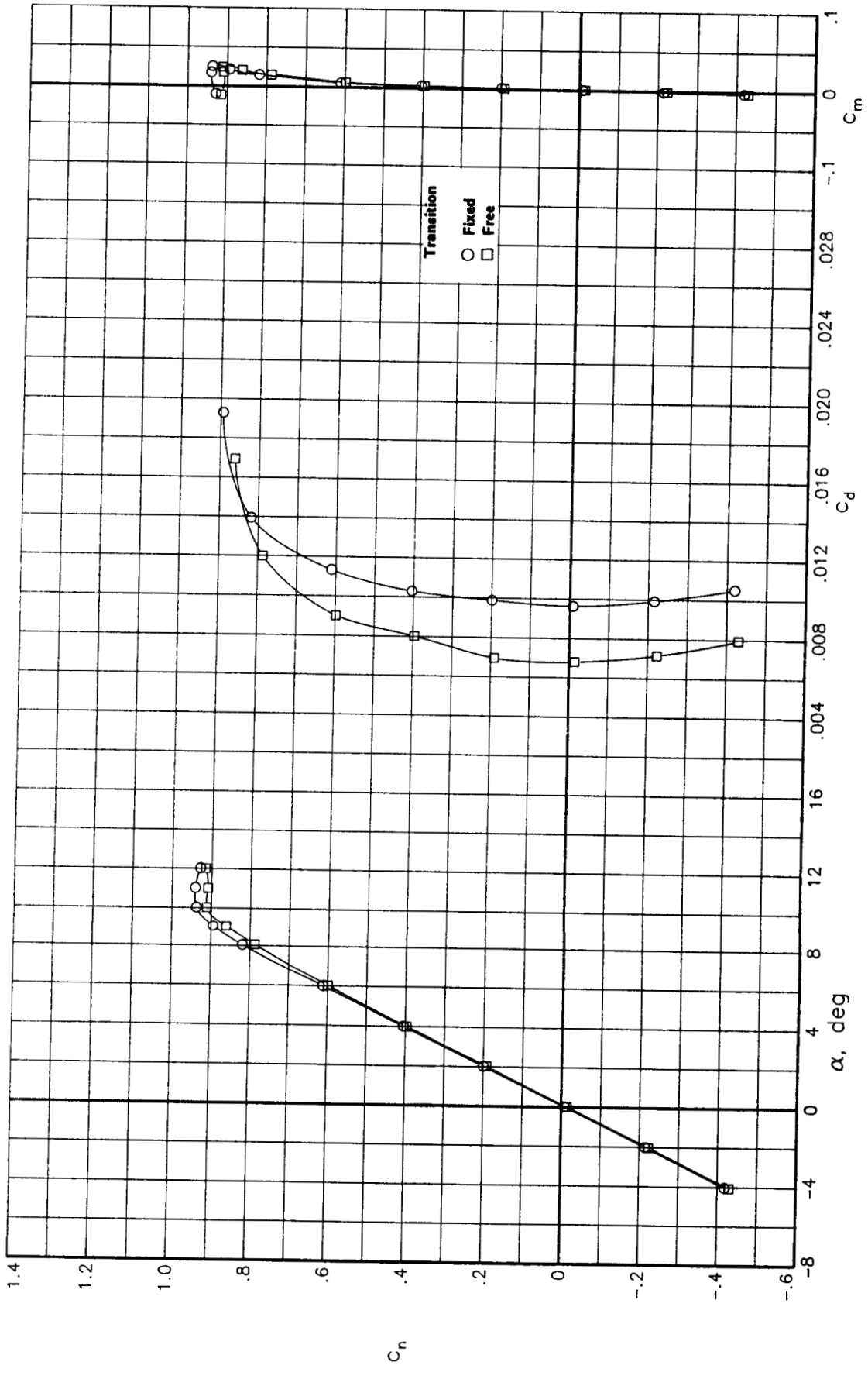

(a) R = 3.0 x 10^6

Figure 31.- Effects of fixing transition on the variation of basic aerodynamic data with angle of attack for various Reynolds numbers at a Mach number of 0.50.

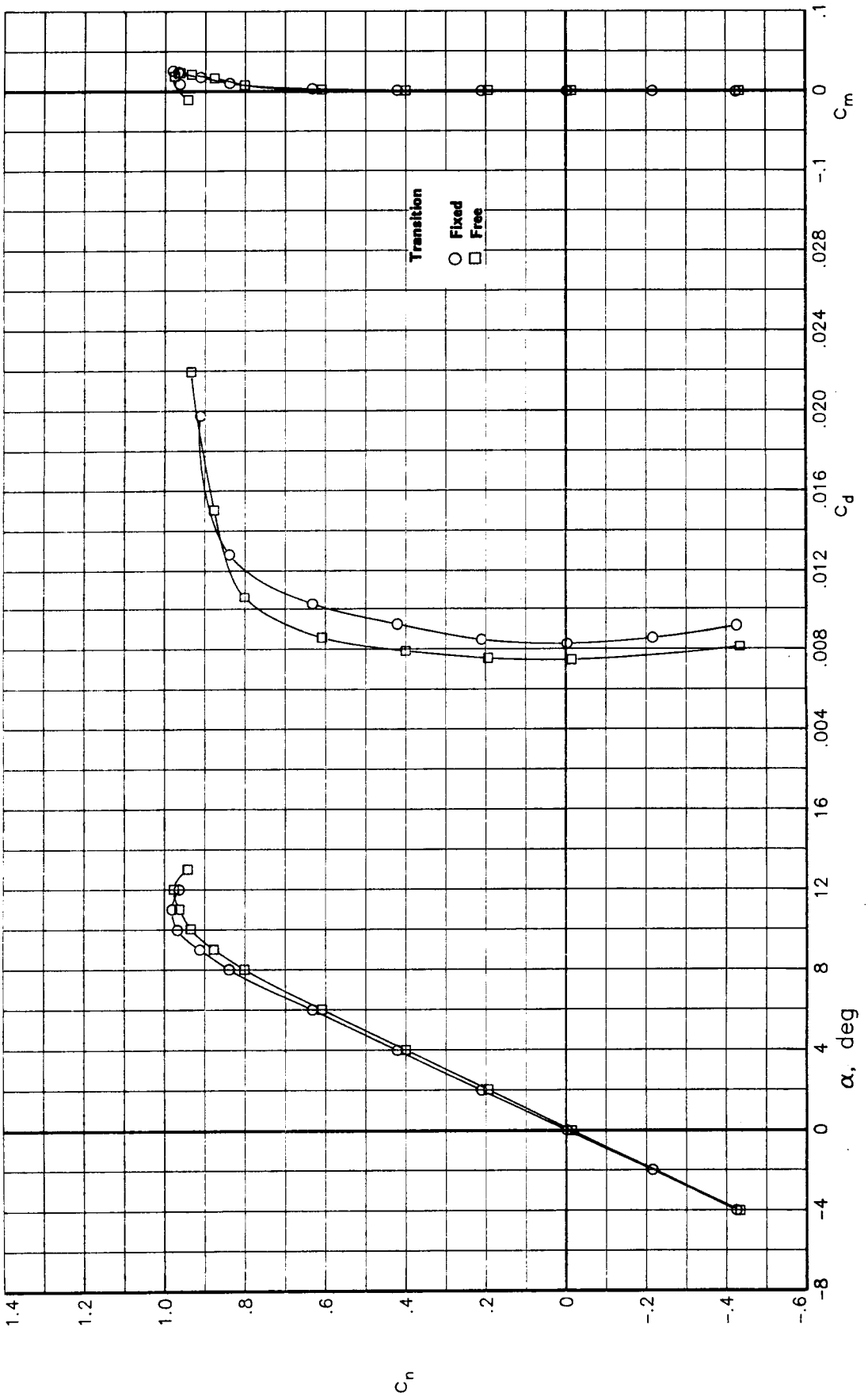

(b) R = 9.0 x 10⁶

Figure 31.- Concluded.

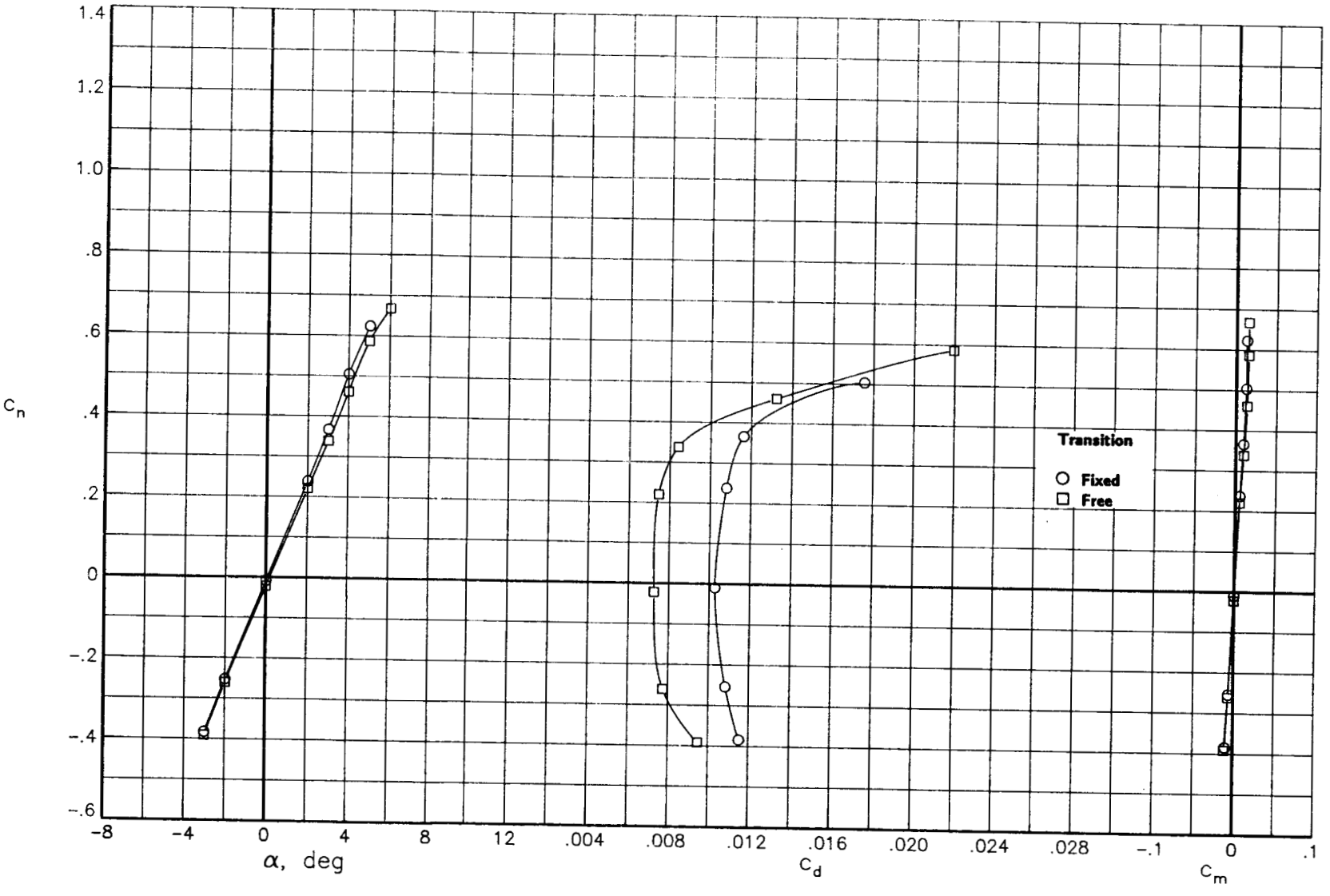

(a) R = 3.0 x 10^6

Figure 32.- Effects of fixing transition on the variation of basic aerodynamic data with angle of attack for various Reynolds numbers at a Mach number of 0.70.

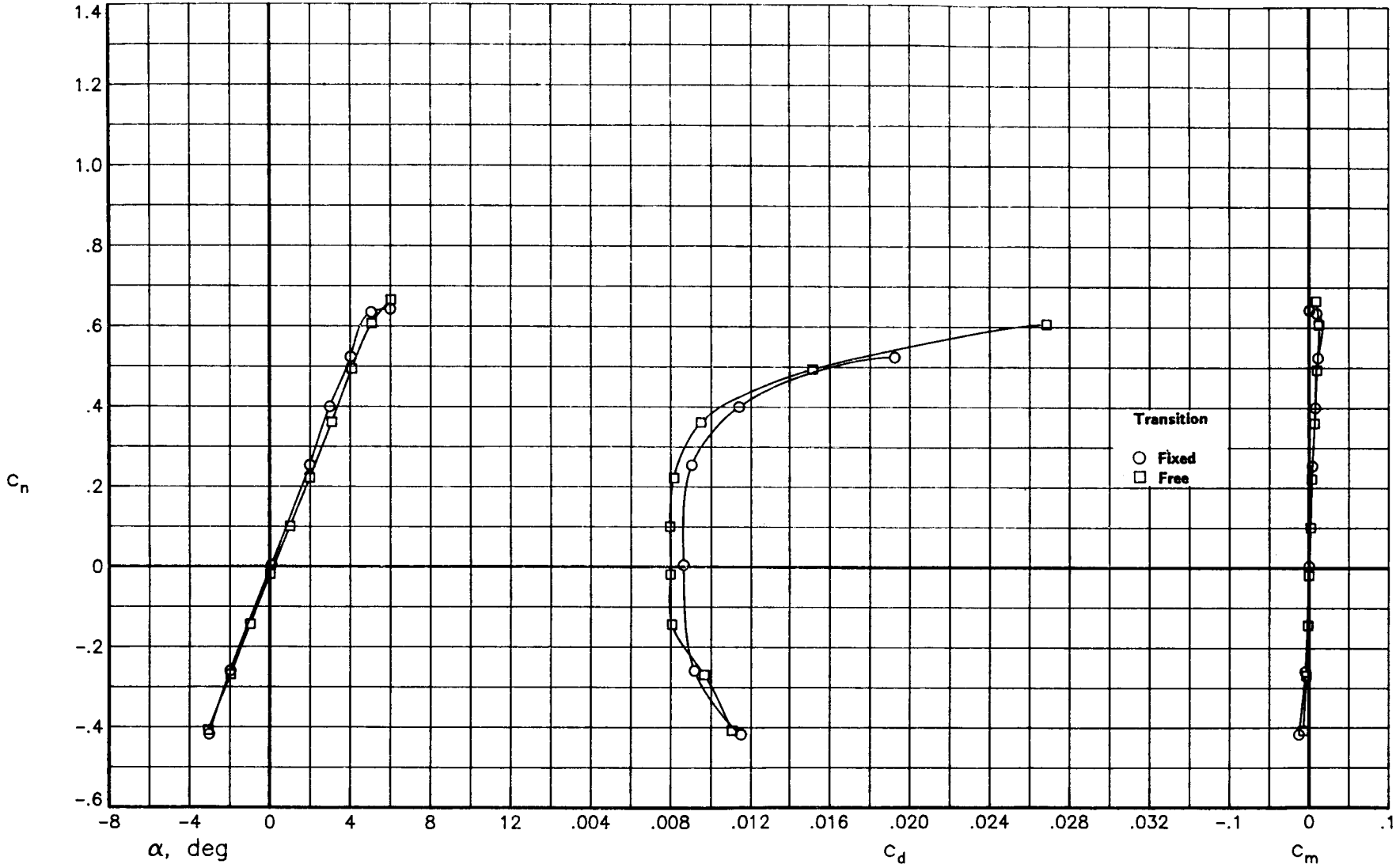

(b) R = 9.0 x 10^6

Figure 32.- Concluded.

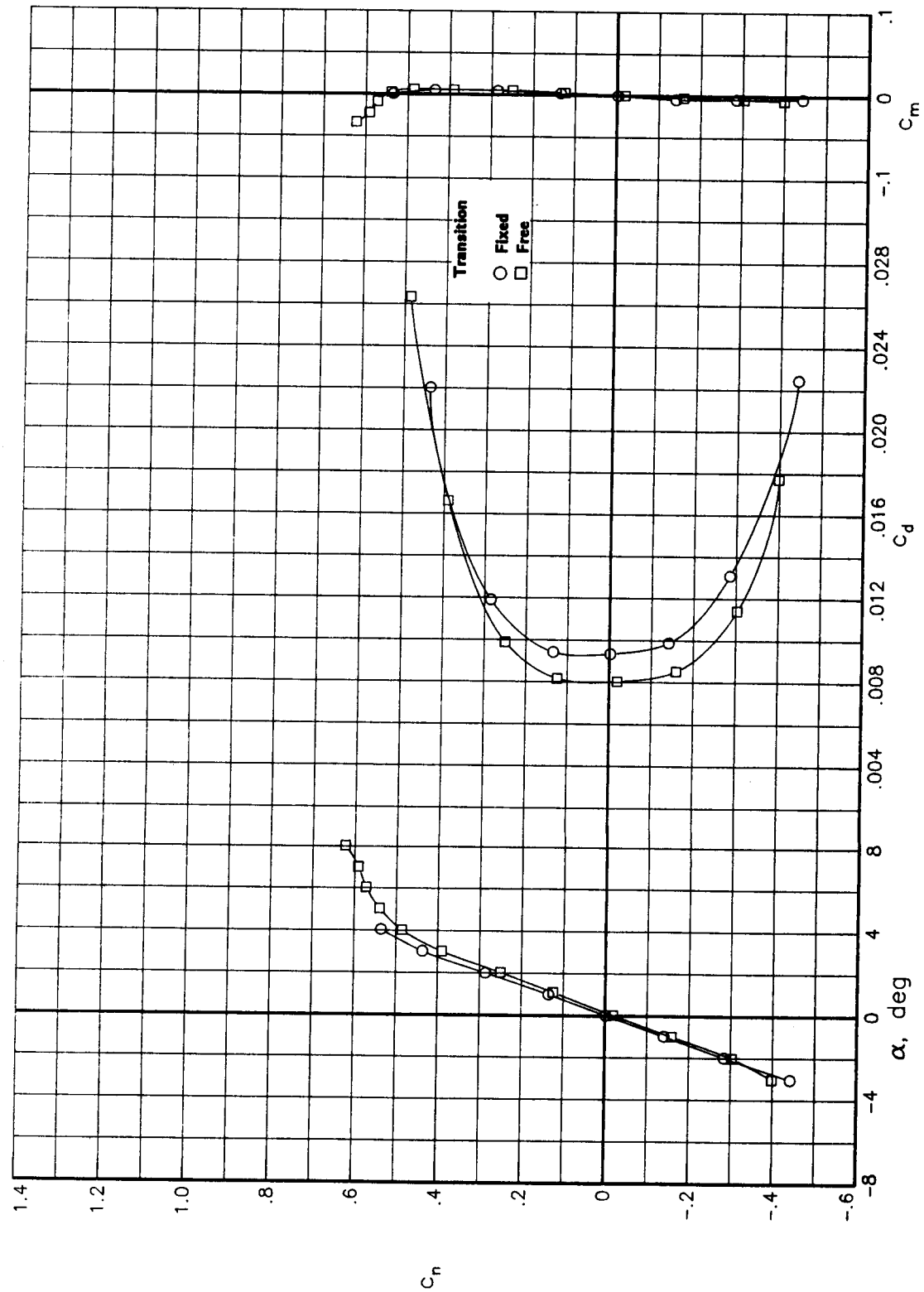

Figure 33.- Effects of fixing transition on the variation of basic aerodynamic data with angle of attack at a Reynolds number of 9.0×10^6 and a Mach number of 0.74.

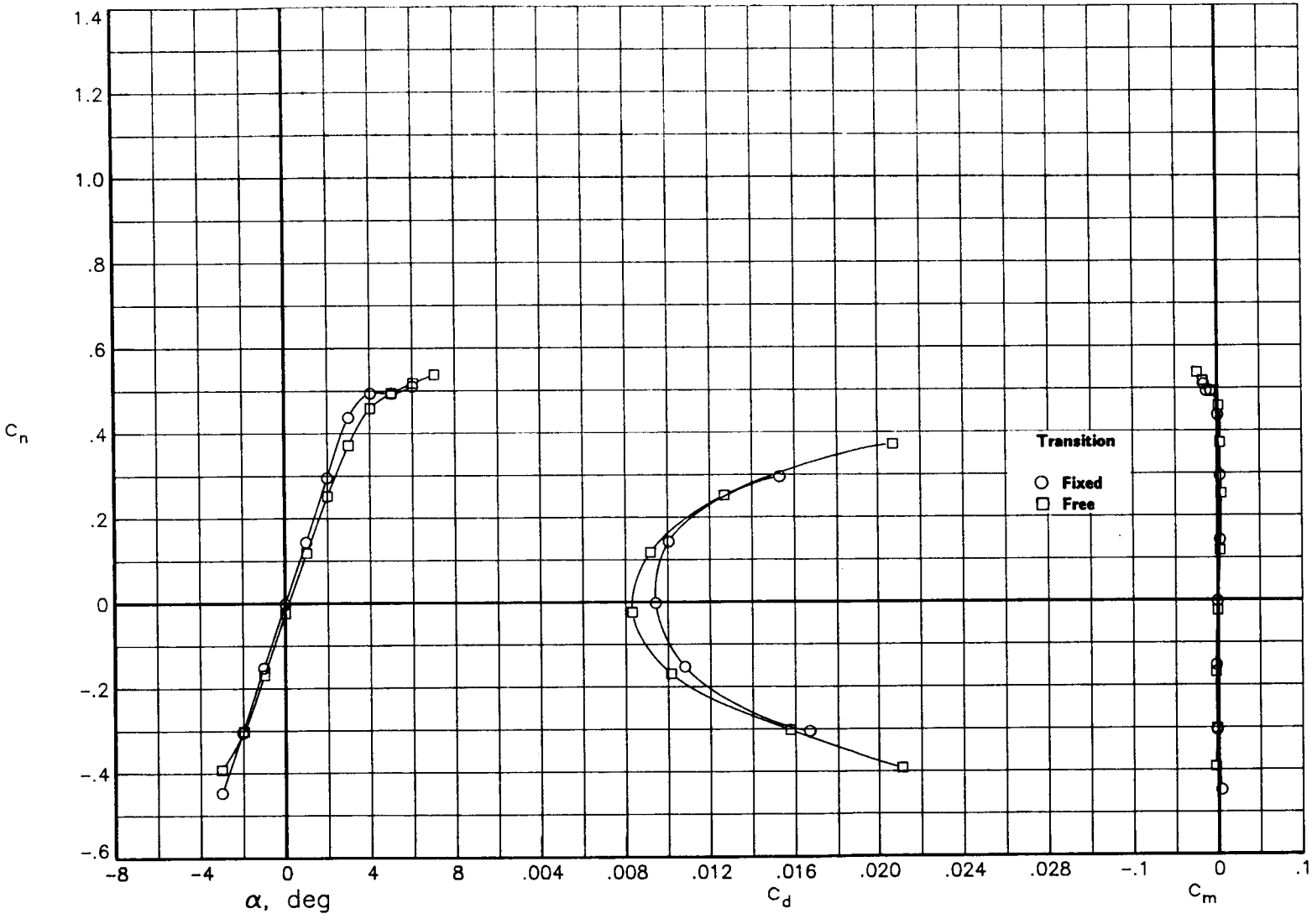

Figure 34.- Effects of fixing transition on the variation of basic aerodynamic data with angle of attack at a Reynolds number of 9.0 x 10^6 and a Mach number of 0.76.

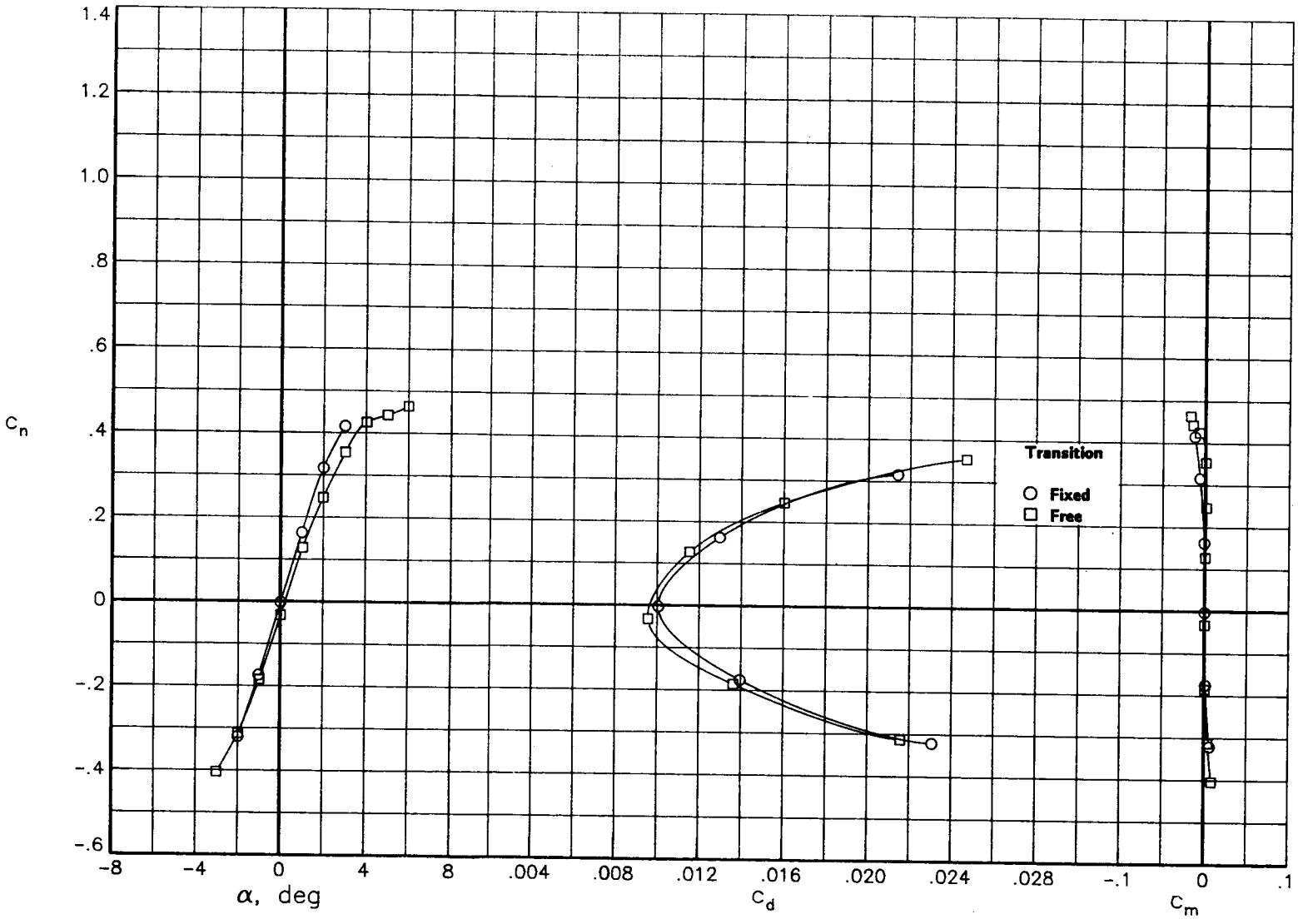

Figure 35.- Effects of fixing transition on the variation of basic aerodynamic data with angle of attack at a Reynolds number of 9.0 x 10^6 and a Mach number of 0.78.

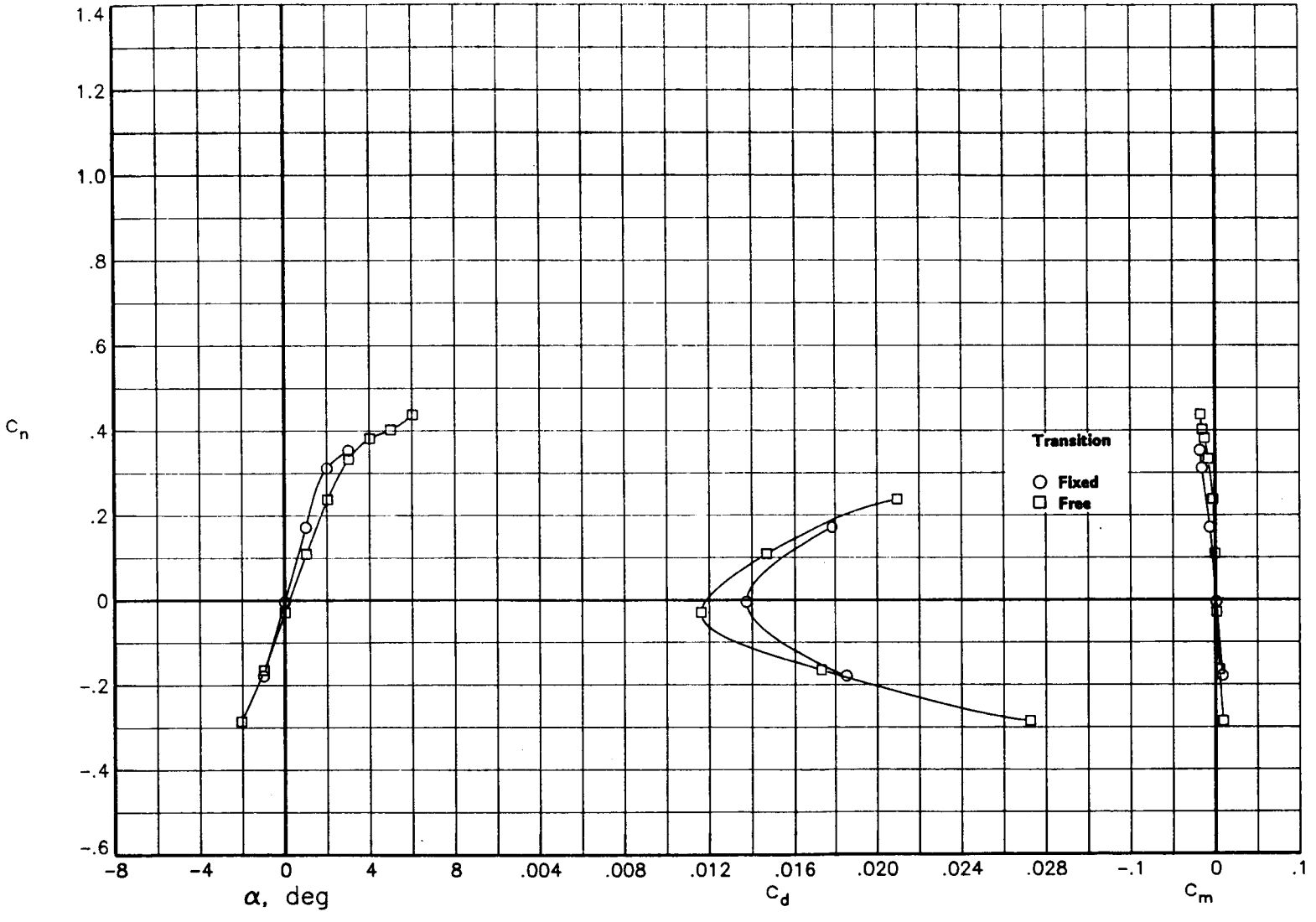

Figure 36.- Effects of fixing transition on the variation of basic aerodynamic data with angle of attack at a Reynolds number of 9.0 x 10^6 and a Mach number of 0.80.

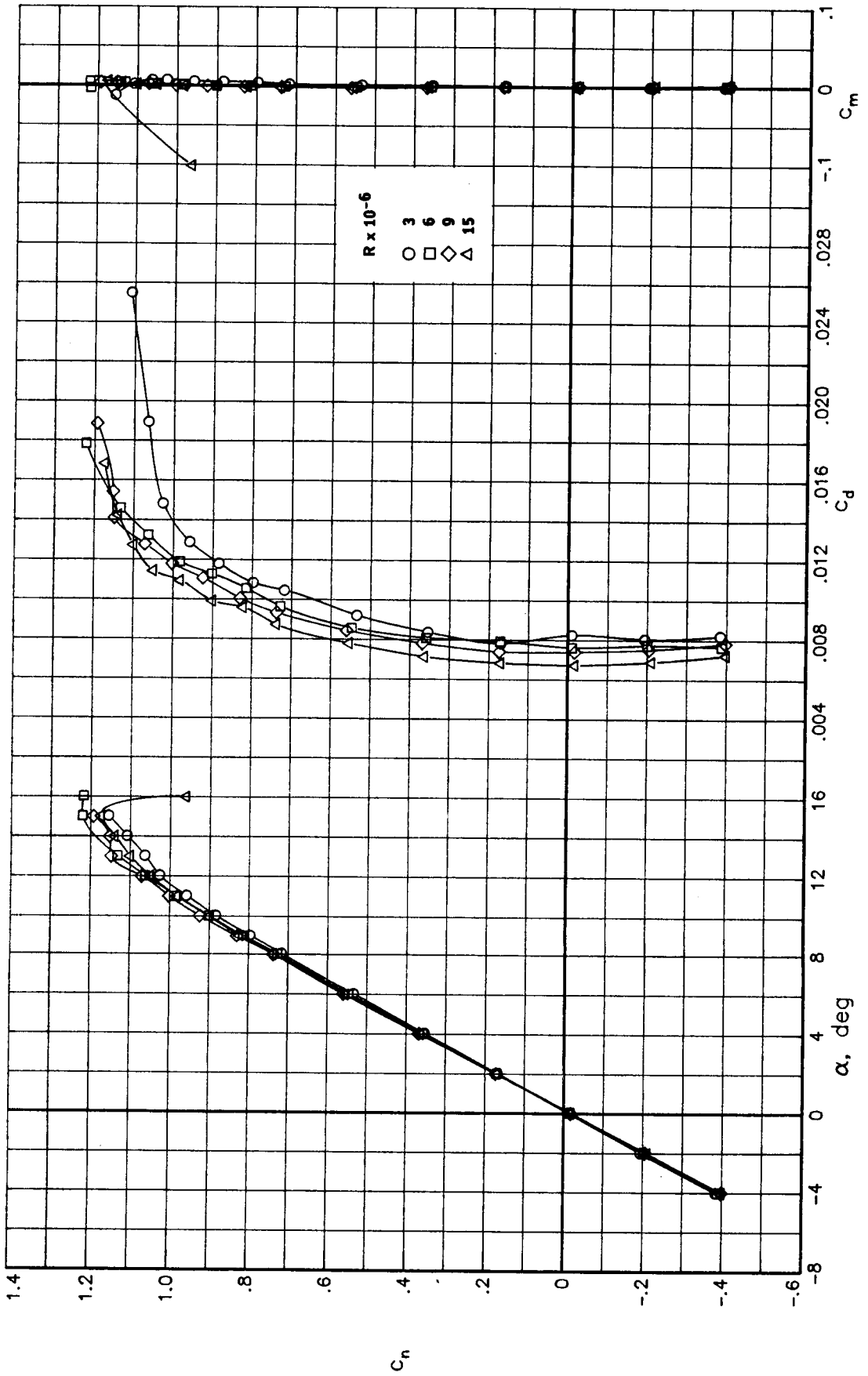

Figure 37.- Comparison of the effects of Reynolds number on the basic aerodynamic data for a Mach number of 0.30. Transition free.

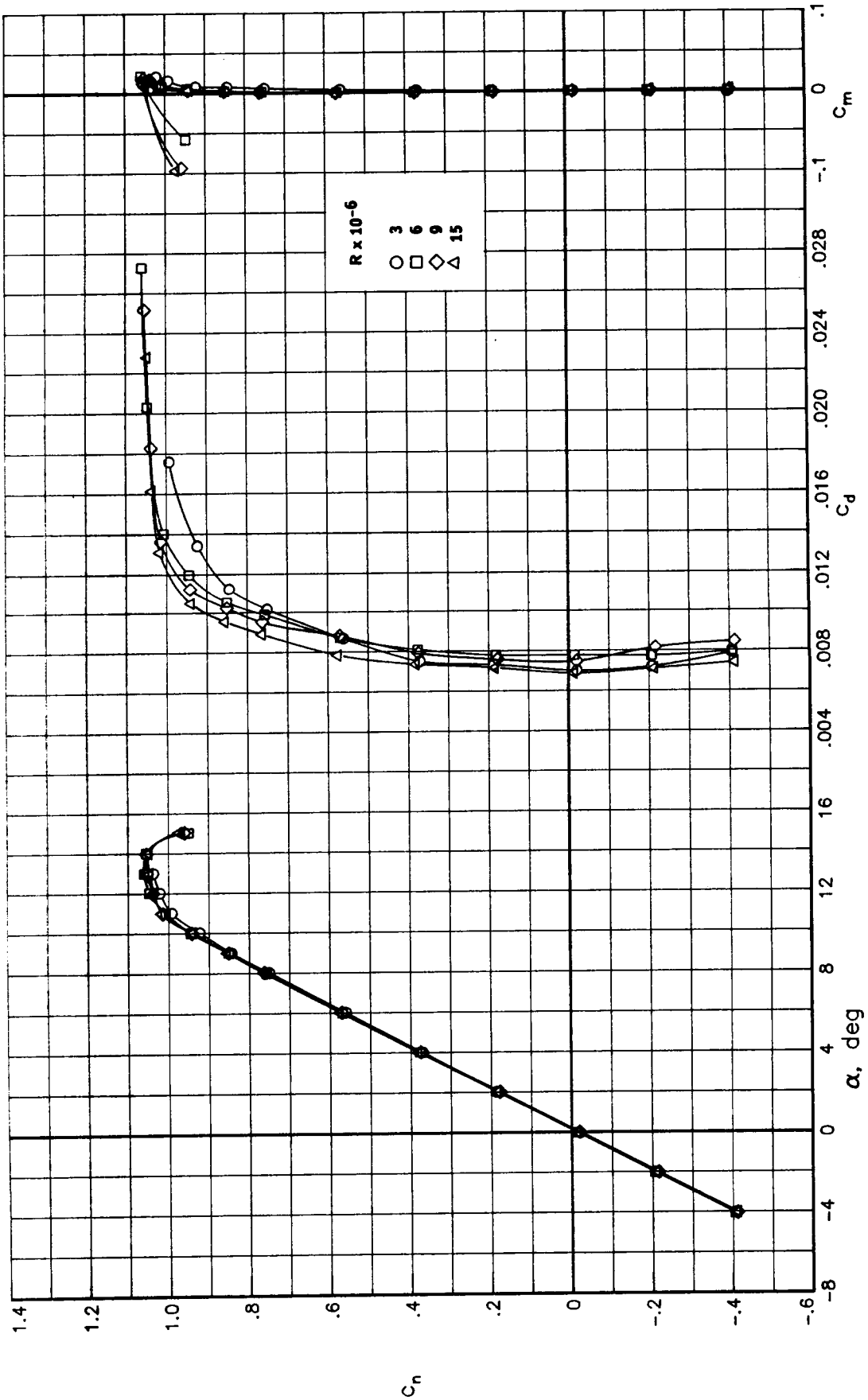

Figure 38.- Comparison of the effects of Reynolds number on the basic aerodynamic data for a Mach number of 0.40. Transition free.

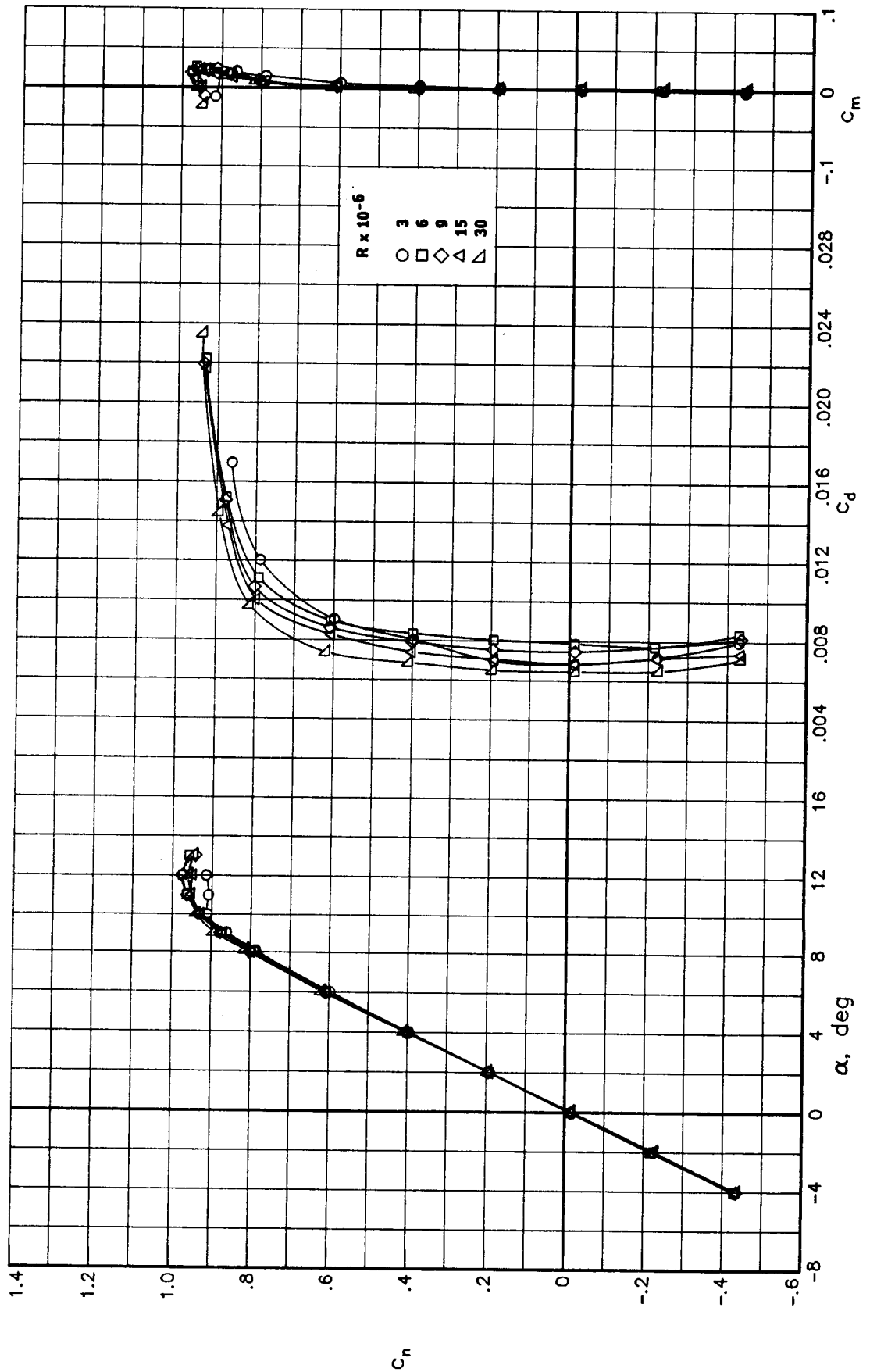

Figure 39.- Comparison of the effects of Reynolds number on the basic aerodynamic data for a Mach number of 0.50. Transition free.

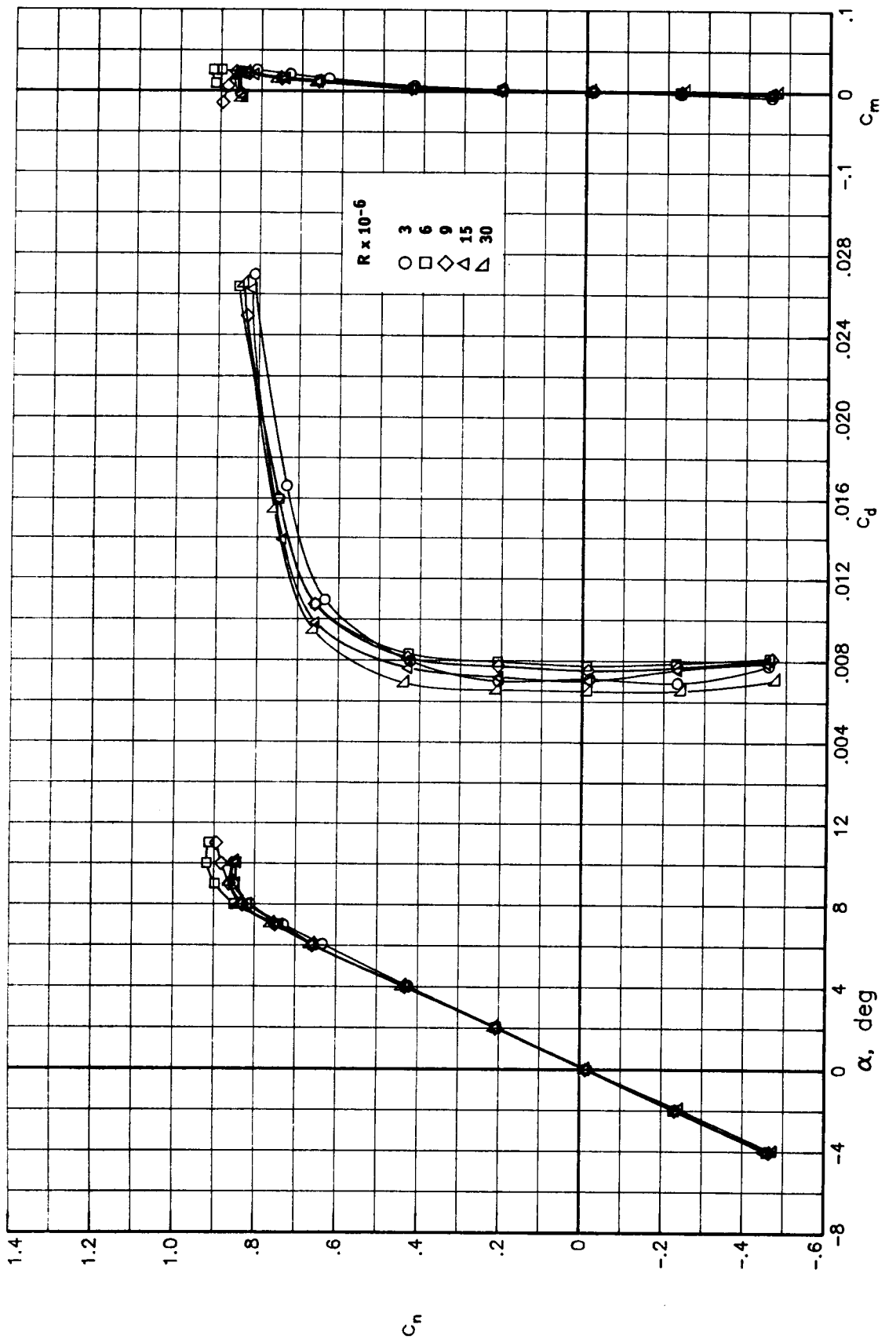

Figure 40.- Comparison of the effects of Reynolds number on the basic aerodynamic data for a Mach number of 0.60. Transition free.

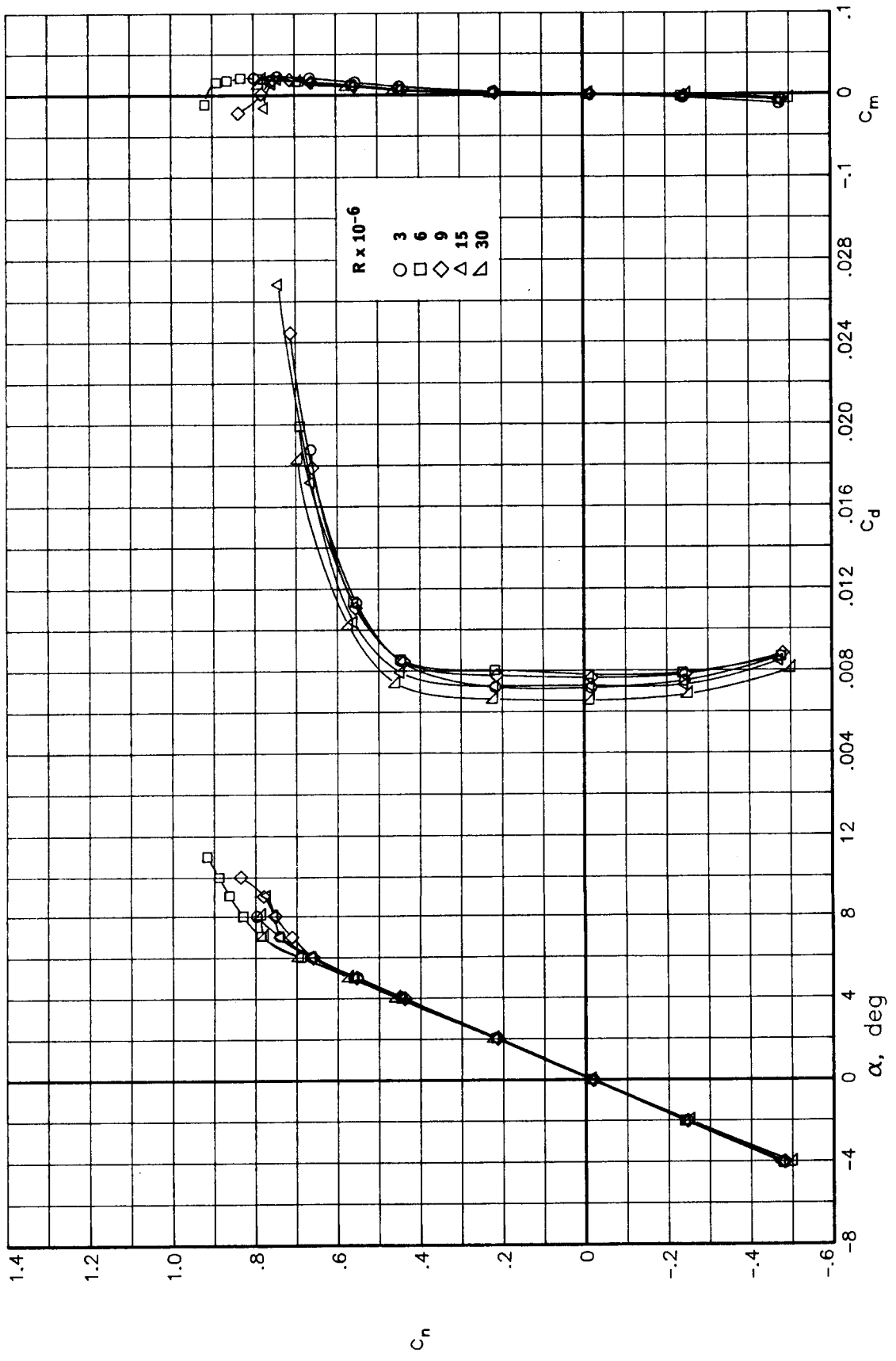

Figure 41.- Comparison of the effects of Reynolds number on the basic aerodynamic data for a Mach number of 0.65. Transition free.

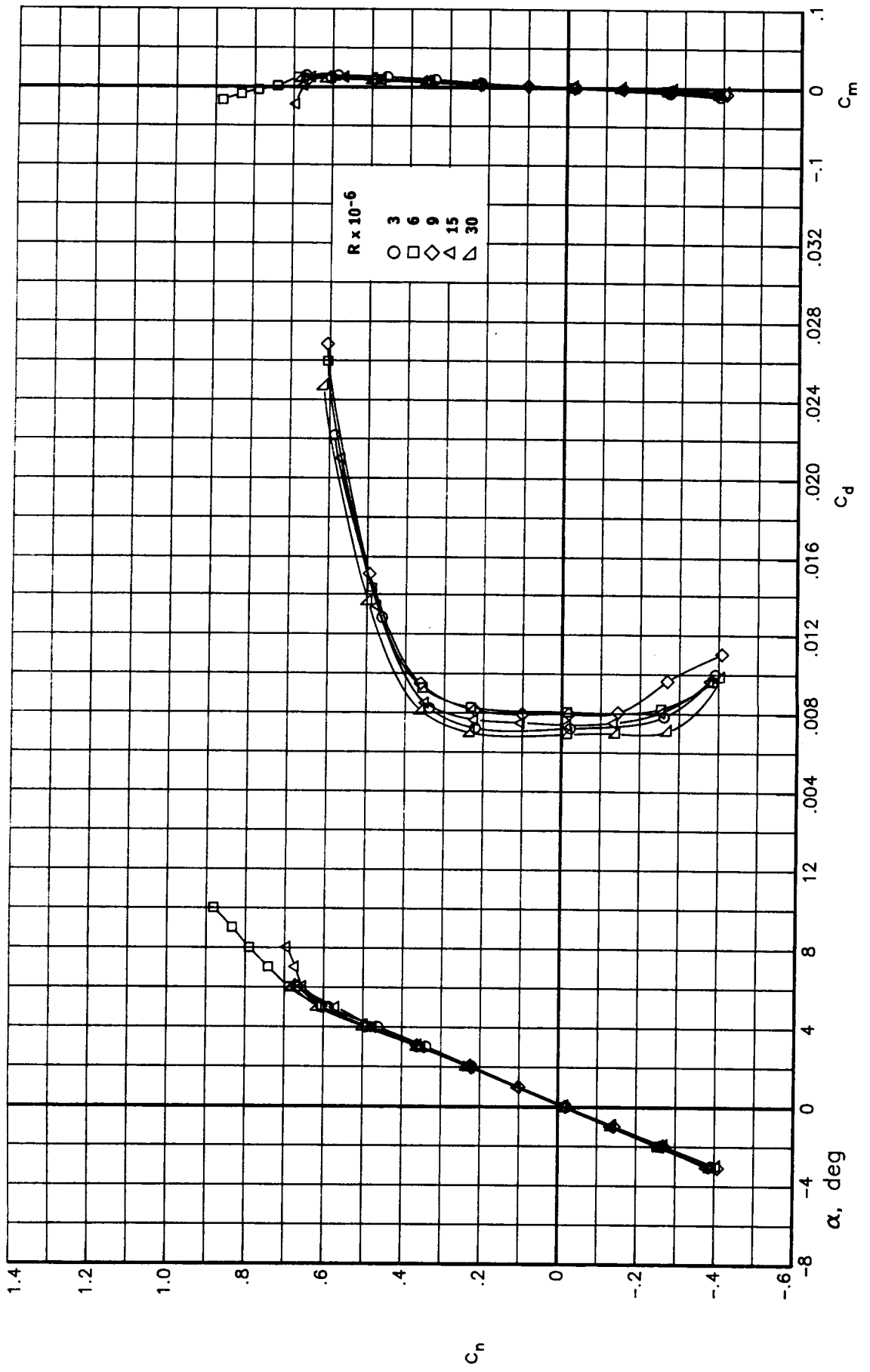

Figure 42.- Comparison of the effects of Reynolds number on the basic aerodynamic data for a Mach number of 0.70. Transition free.

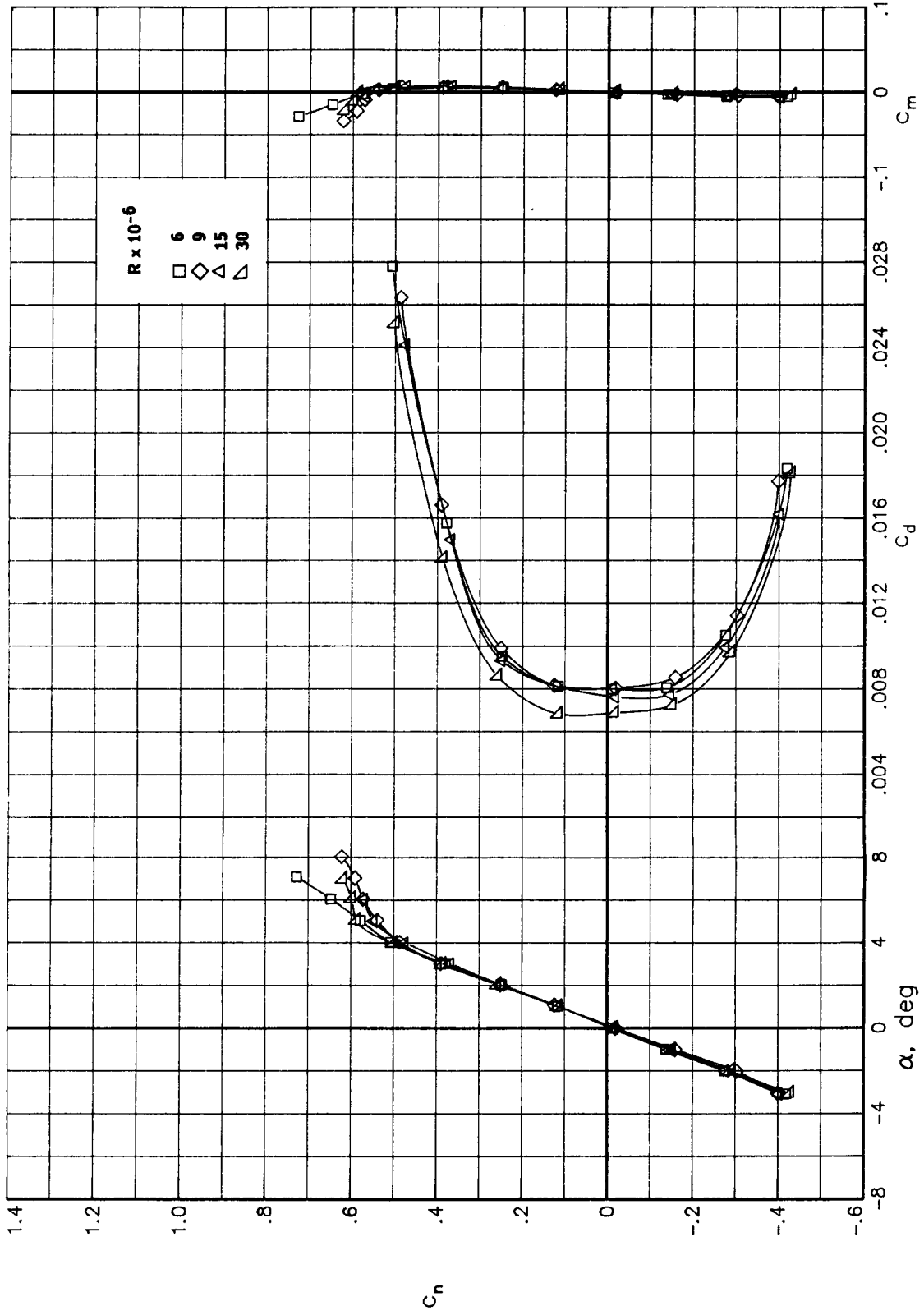

Figure 43.- Comparison of the effects of Reynolds number on the basic aerodynamic data for a Mach number of 0.74. Transition free.

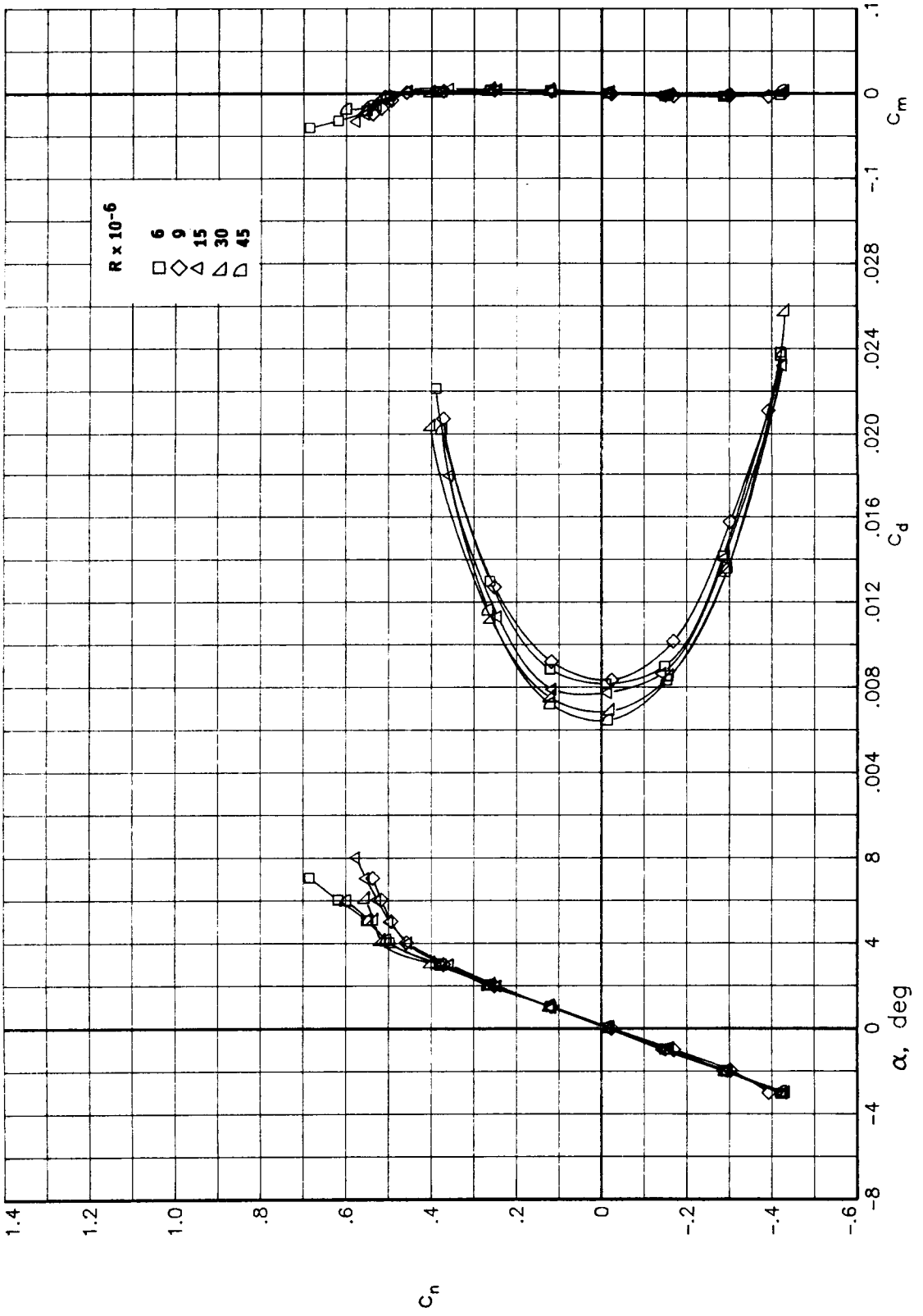

Figure 44.- Comparison of the effects of Reynolds number on the basic aerodynamic data for a Mach number of 0.76. Transition free.

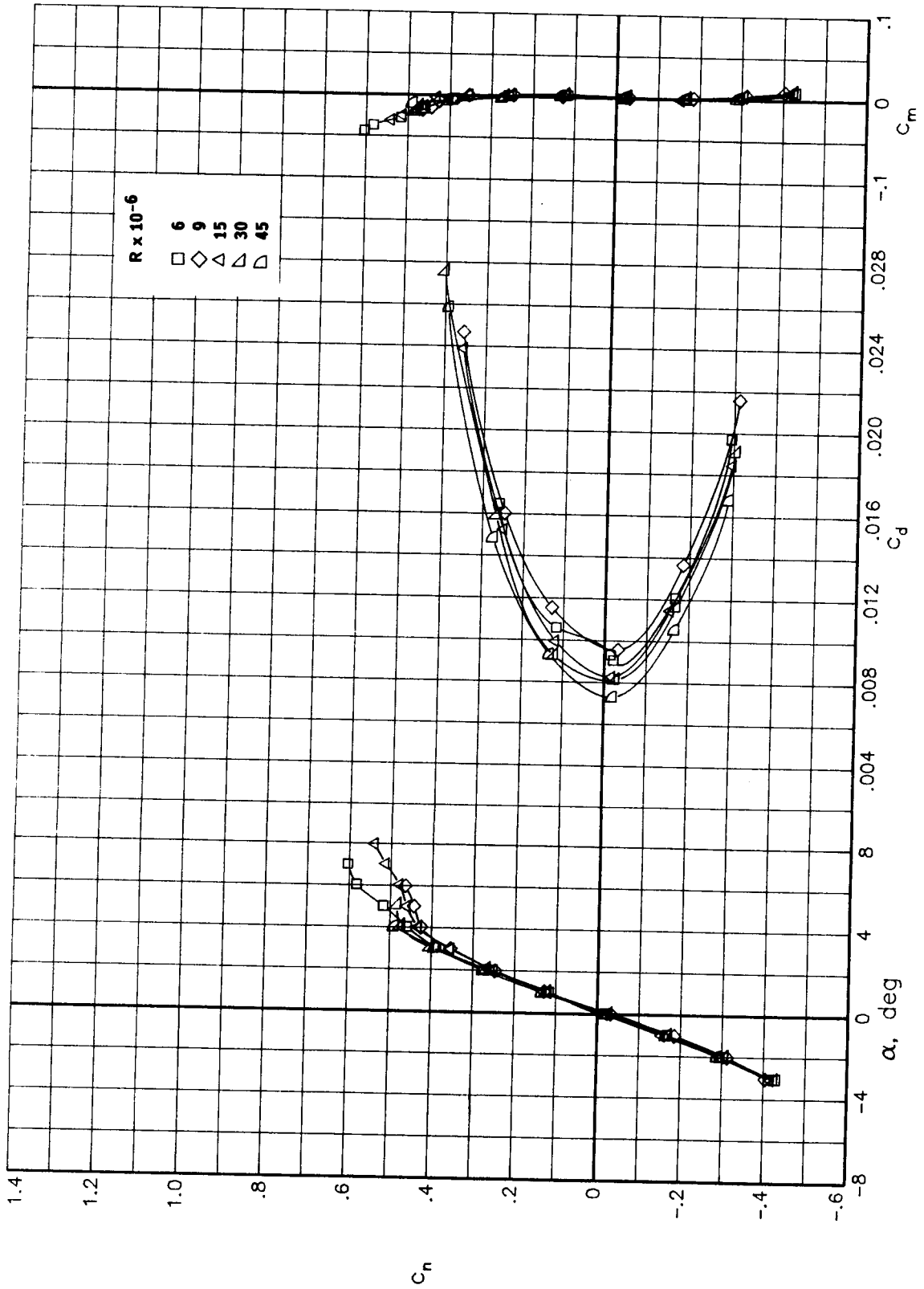

Figure 45.- Comparison of the effects of Reynolds number on the basic aerodynamic data for a Mach number of 0.78. Transition free.

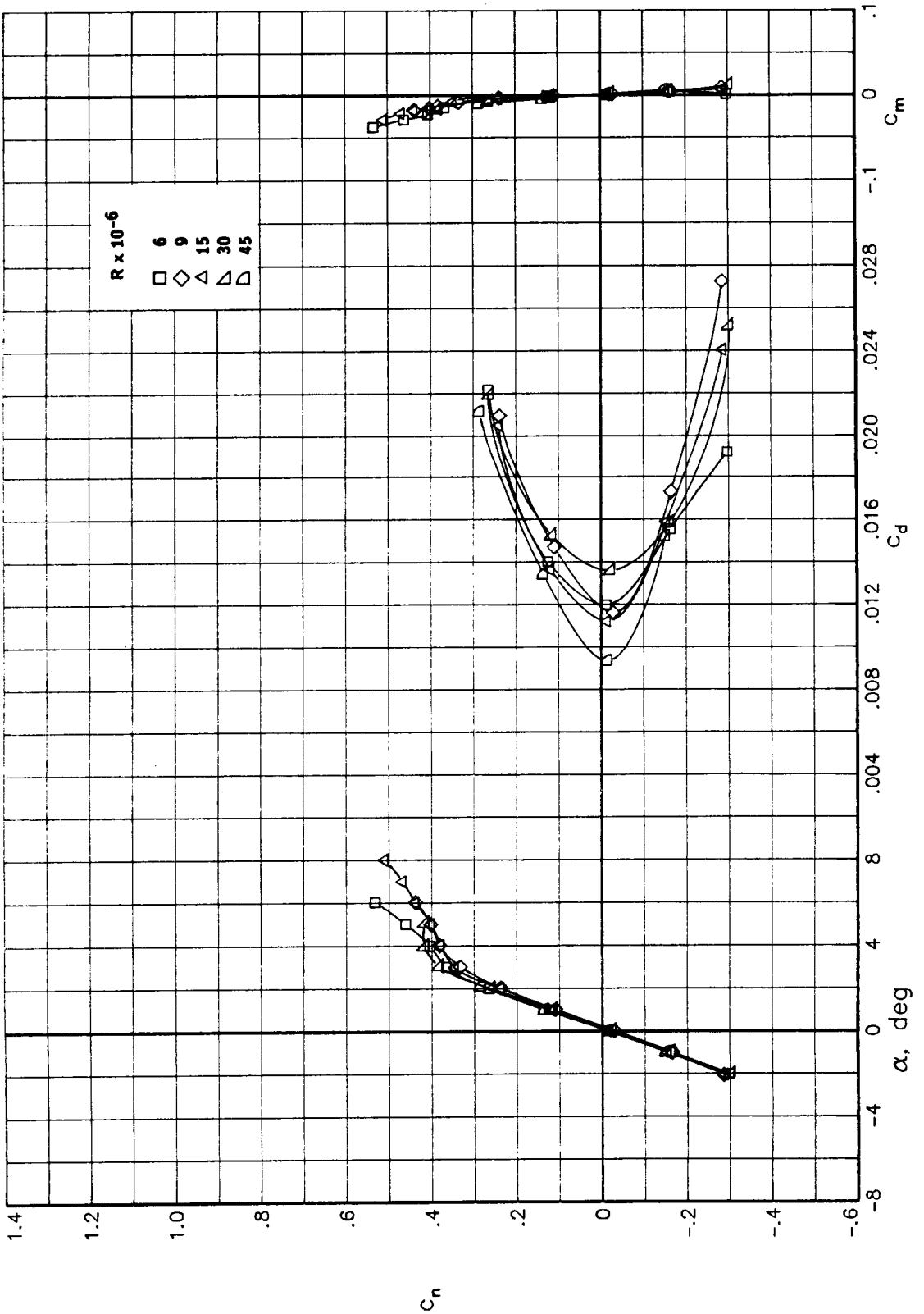

Figure 46.- Comparison of the effects of Reynolds number on the basic aerodynamic data for a Mach number of 0.80. Transition free.

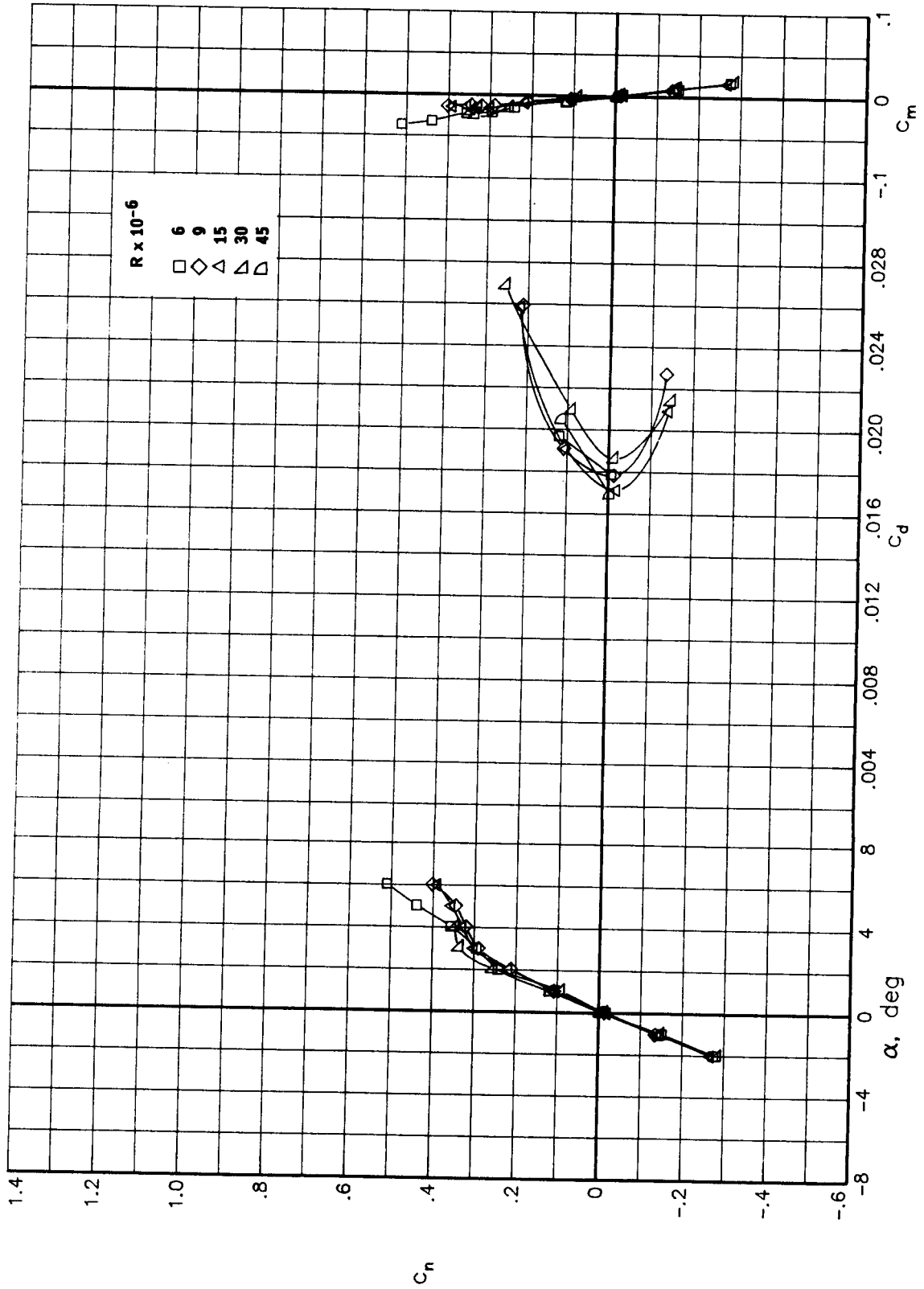

Figure 47.- Comparison of the effects of Reynolds number on the basic aerodynamic data for a Mach number of 0.82. Transition free.

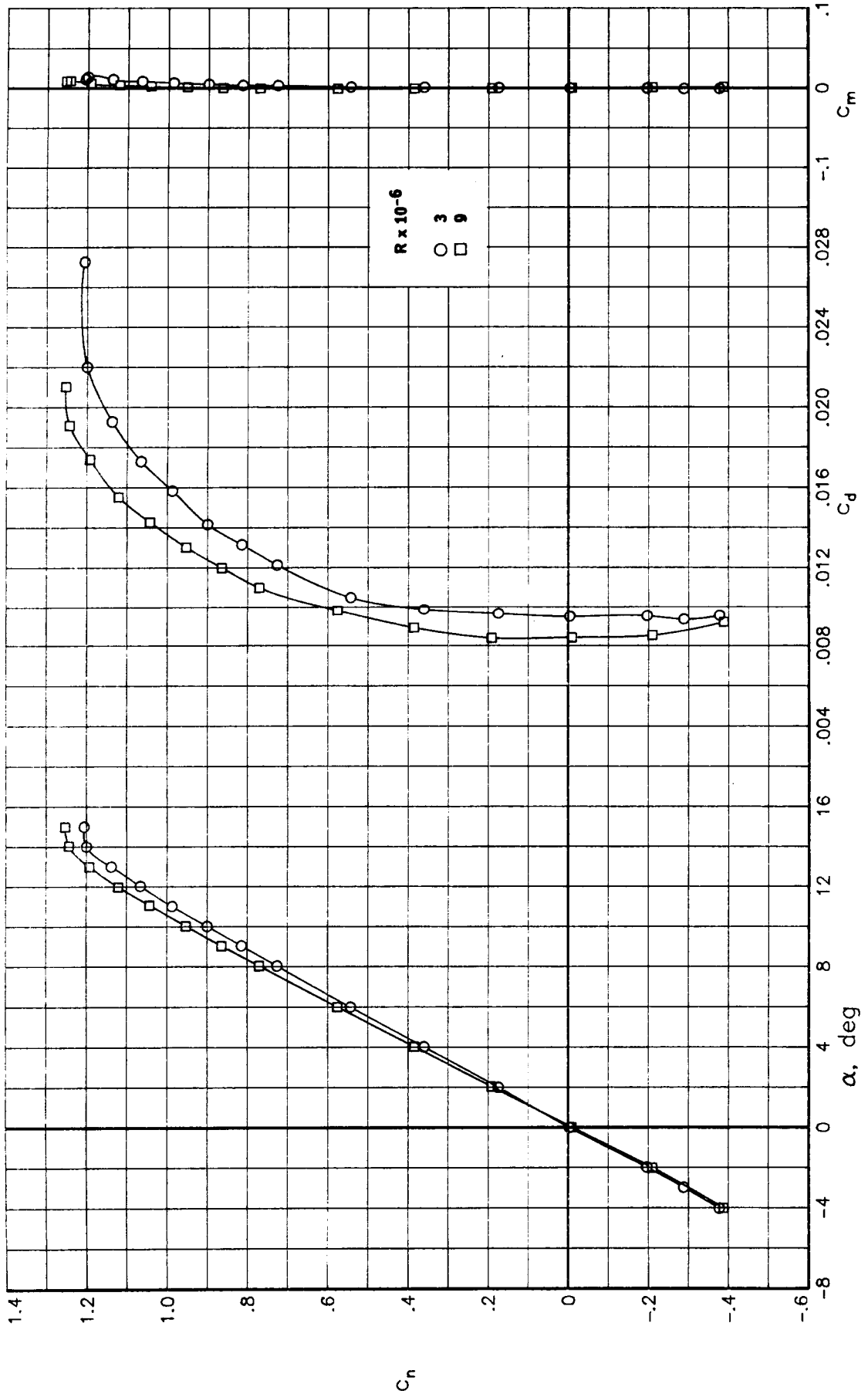

Figure 48.- Comparison of the effects of Reynolds number on the basic aerodynamic data for a Mach number of 0.30. Transition fixed.

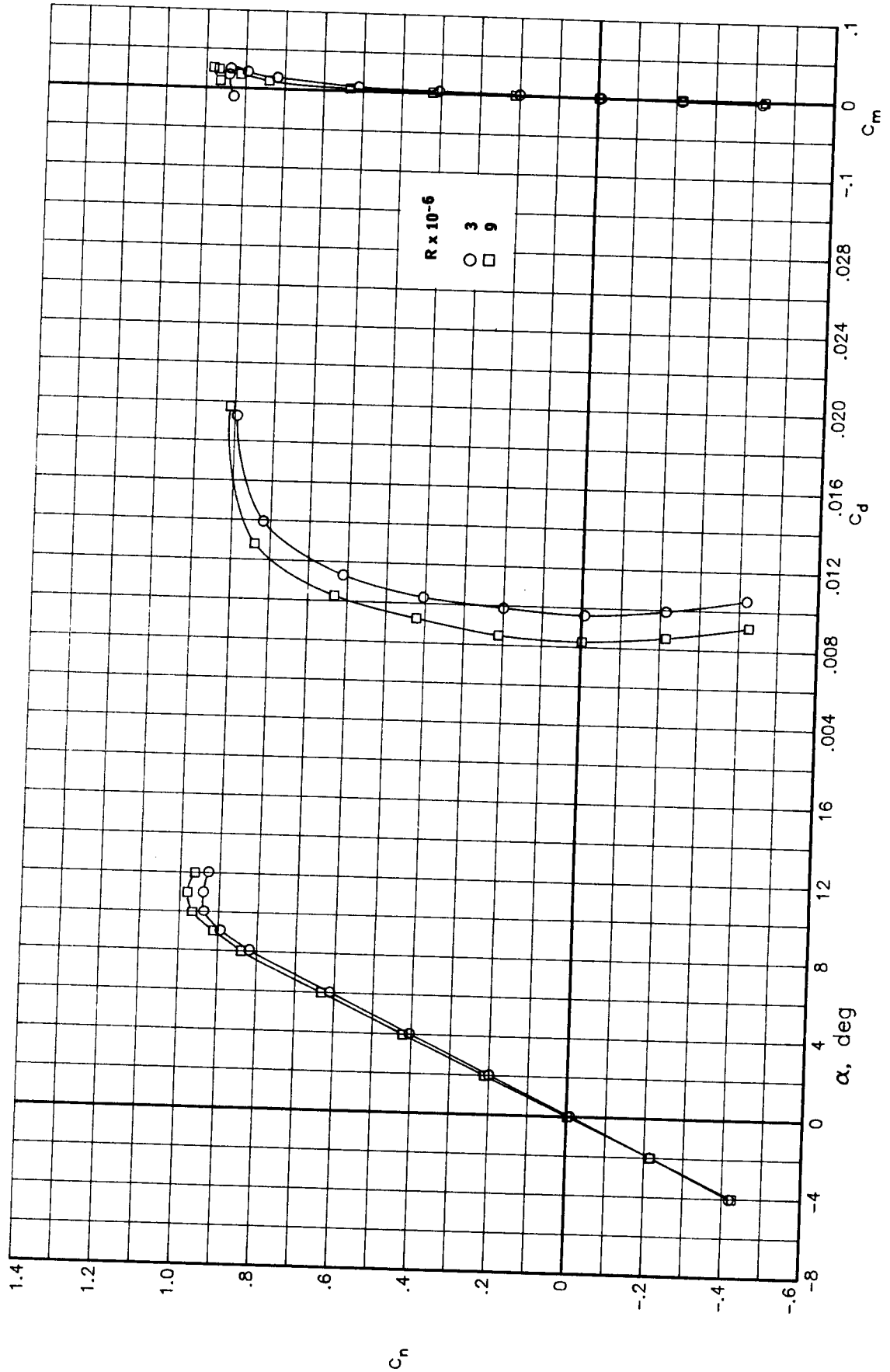

Figure 49.- Comparison of the effects of Reynolds number on the basic aerodynamic data for a Mach number of 0.50. Transition fixed.

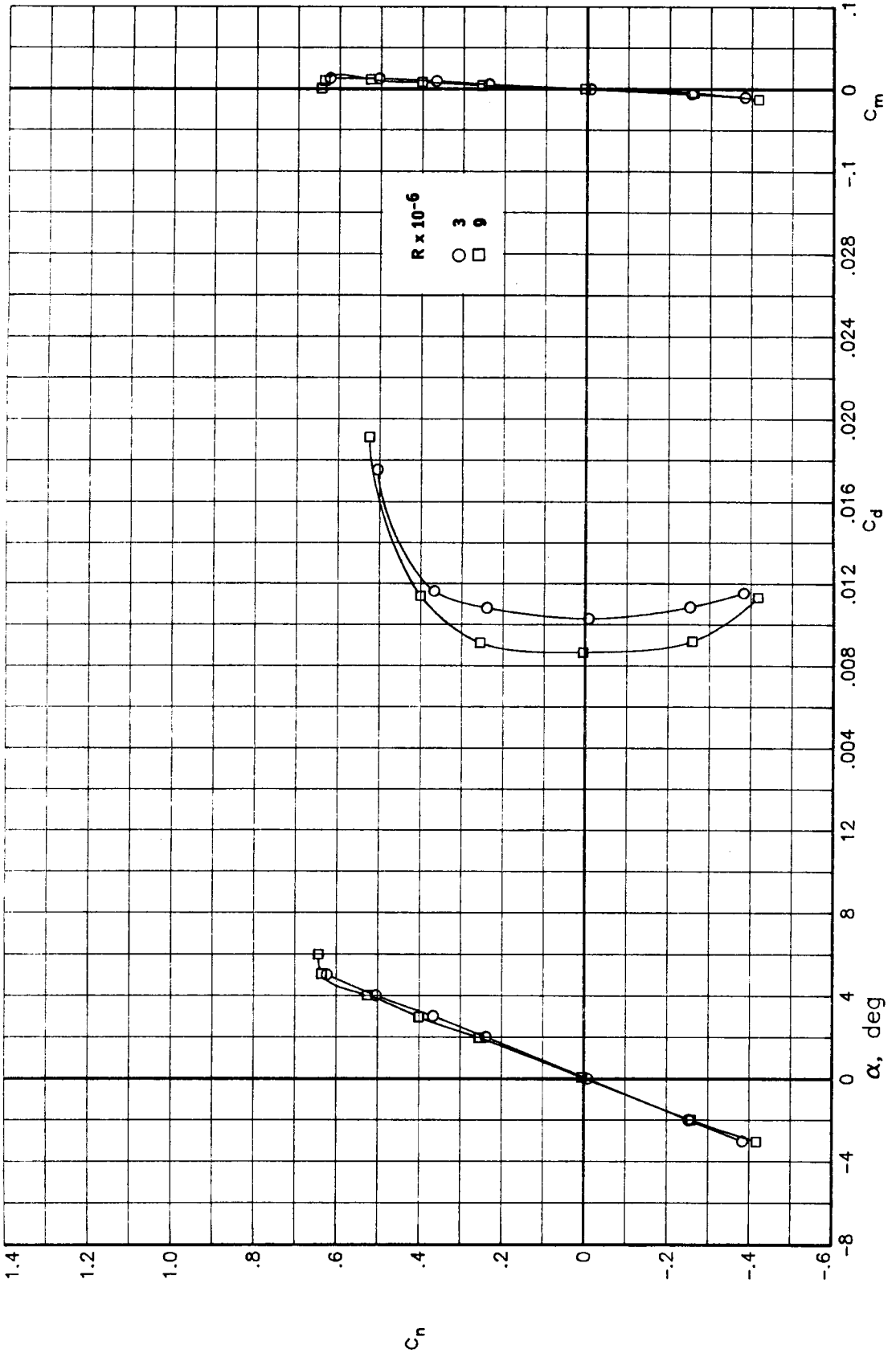

Figure 50.- Comparison of the effects of Reynolds number on the basic aerodynamic data for a Mach number of 0.70. Transition fixed.

NASA National Aeronautics and Space Administration

Report Documentation Page

1. Report No.	2. Government Accession No.	3. Recipient's Catalog No.
NASA TM-100527		

4. Title and Subtitle
High Reynolds Number Transonic Tests on an NACA 0012 Airfoil in the Langley 0.3-Meter Transonic Cryogenic Tunnel

5. Report Date
December 1987

6. Performing Organization Code

7. Author(s)
Charles L. Ladson and Acquilla S. Hill

8. Performing Organization Report No.

10. Work Unit No.
505-61-01-02

9. Performing Organization Name and Address
NASA Langley Research Center
Hampton, VA 23665-5225

11. Contract or Grant No.

13. Type of Report and Period Covered
Technical Memorandum

12. Sponsoring Agency Name and Address
National Aeronautics and Space Administration
Washington, DC 20546

14. Sponsoring Agency Code

15. Supplementary Notes

16. Abstract

Tests were conducted in the two dimensional test section of the Langley 0.3-meter Transonic Cryogenic Tunnel on an NACA 0012 airfoil to obtain aerodynamic data as a part of the Advanced Technology Airfoil Test (ATAT) program. The test program covered a Mach number range of 0.30 to 0.82 and a Reynolds number range of 3.0×10^6 to 45.0×10^6. The stagnation pressure was varied between 1.2 and 6.0 atmospheres and the stagnation temperature was varied between 300 K and 90 K to obtain these test conditions. Plots of the spanwise variation of drag coefficient as a function of normal force coefficient and the variation of the basic aerodynamic characteristics with angle of attack are shown. The data are presented uncorrected for wall interference effects and without analysis.

17. Key Words (Suggested by Author(s))	18. Distribution Statement
Airfoils High Reynolds numbers Cryogenic wind tunnels	Unclassified - Unlimited Subject Category - 02

19. Security Classif. (of this report)	20. Security Classif. (of this page)	21. No. of pages	22. Price
Unclassified	Unclassified	149	A07